Spring 2019

The Regulation of Skeletal Muscle Fatigue During the Progression of Cancer Cachexia

Brandon N. VanderVeen

The Regulation of Skeletal Muscle Fatigue During the Progression of Cancer Cachexia

by

Brandon N. VanderVeen

Bachelor of Science
Wheaton College, 2014

Submitted in Partial Fulfillment of the Requirements

For the Degree of Doctor of Philosophy in

Exercise Science

The Norman J. Arnold School of Public Health

University of South Carolina

2019

Accepted by:

James A. Carson, Major Professor

Mark A. Sarzynski, Committee Member

Ho-Jin Koh, Committee Member

E. Angela Murphy, Committee Member

Cheryl L. Addy, Vice Provost and Dean of the Graduate School

ACKNOWLEDGEMENTS

Although there are many people that have helped me throughout the past few years, I would especially like to thank Michelle for her patience and support throughout my doctoral degree. I would also like to thank my parents, Ken and Becky, and my siblings Kristen, Josh, Ryan, Courtney, and Jason for their encouragement and support over the past several years that has been instrumental for the successful completion of my doctoral degree. Next, I would like to thank my mentor, Dr. James Carson. His guidance and mentorship years in the lab and in my own professional development has set me up for a successful career in any arena that I may choose. I would also like to thank my dissertation committee members, Dr. Mark Sarzynski, Dr. Angela Murphy, and Dr. Ho-jin Koh, for their patience and guidance throughout the comprehensive exam and dissertation process. Lastly, I would like to thank all the IMB lab members (past and present), Dr. Justin Hardee, Dr. Song Gao, Dennis Fix, Brittany Counts, and Ryan Montalvo, who not only were vital for my successful completion of my degree, but also had to deal with my obscure work habits over the years.

ABSTRACT

Cachexia is the unintentional loss of body weight secondary to chronic disease and is prevalent is roughly 50% of cancer patients. The loss of body weight and skeletal muscle mass is reduced functional capacity associated with reduced life quality. The etiology of cachexia is multimodal and complex; however, cachexia has been linked to several systemic (e.g. chronic inflammation, hypogonadism, anemia, insulin resistance) and behavioral (e.g. anorexia, inactivity) changes that can compound to accelerate muscle mass and body weight loss. While several inflammatory cytokines are associated with cachexia's disease progression, our laboratory has established that Interleukin-6 (IL-6) is a key regulator of skeletal muscle mass maintenance in tumor-bearing $Apc^{Min/+}$ (MIN) mice. Additionally, we have shown that reduced volitional activity and increased skeletal muscle fatigue occurs prior to significant wasting and exercise training is able to prevent IL-6-induced cachexia in the MIN without affecting muscle inflammatory signaling. Furthermore, repeated muscle contractions were able to attenuate myofibrillar atrophy, and increase muscle oxidative metabolism without effecting the tumor environment. While the efficacy of exercise to improve skeletal muscle's metabolic health during aging and disease has been well described, the effects of volitional activity on cancer-induced skeletal muscle fatigue, oxidative metabolism, and muscle inflammatory signaling is not well understood. The overall purpose of this study is to determine the regulation of skeletal muscle fatigue by activity and muscle inflammatory signaling during the progression of cachexia. Our central hypothesis is that cancer-induced skeletal muscle fatigue develops prior to

significant weight loss concomitant with decreased muscle use and disrupted muscle oxidative metabolism which occurs through chronically activated muscle gp130 signaling. Our results suggest that the onset of skeletal muscle fatigue developed prior to significant weight loss in MIN mice. Furthermore, elevated circulating IL-6 accelerated skeletal muscle fatigue and reduced muscle oxidative metabolism through muscle gp130 signaling; however, loss of muscle gp130 signaling was unable to improve skeletal muscle fatigue in MIN mice. Last, we demonstrate that there is a direct relationship between activity and skeletal muscle fatigability in healthy and tumor-bearing mice. Together, these results suggest that fatigue develops independent of weight loss and while elevated IL-6 contributes to skeletal muscle fatigue, cancer-induced fatigue was not solely regulated by IL-6/muscle gp130 signaling.

TABLE OF CONTENTS

LIST OF TABLES

LIST OF FIGURES

LIST OF SYMBOLS

P_o	Skeletal muscle maximal tetanic force
${}_sP_o$	Skeletal muscle maximal specific force
L_o	Optimal length
L_f	Fiber Length
±	Plus or Minus
α	Alpha
β	Beta
κ	Kappa
°	Degrees
p	Probability of type 1 error
%	Percent

LIST OF ABBREVIATIONS

Akt..... Protein Kinase B

AMP.....Adenosine Monophosphate

AMPK..... AMP-activated Protein Kinase

ANOVA.....Analysis of Variance

APC..... *Adenomatous Polyposis Coli*

ATP..... Adenosine Triphosphate

BCL..... B-cell Lyphoma

Bnip..... BCL2 interacting protein

BW.....Body Weight

C..... Control

C/EBPβ..... CCAAT Enhancer Binding Protein

C-26.....Colon-26 Carcinoma

CHF..... Congestive Heart Failure

CLC.....Cardiotrophin-like Cytokine

CNTF.....Ciliary Neurotropic Factor

COPD.....Chronic Obstruction Pulmonary Disease

CSA.....Cross Sectional Area

CT-1.....Cardiotrophin 1

CX.....Cachectic

DHPR..... Dihydropyridine Receptor

DNA.....Deoxyribonucleic acid

+dP/dt.....Change in Force/Change in Time during Contraction

-dP/dt..... Change in Force/Change in Time during Relaxation

DRP.....Dynamin-Related Protein

EC ..... Excitation Contraction

ECM.....Extracellular Matrix

EDL.....Extensor Digitorum Longus

Erk 1/2..... Extracellular signal-related Kinases

FAP ..... Familial Adenomatous Polyposis

FDA..... Federal Drug Association

Fis..... Fission Protein

FOXO.....Forkhead Box O

g.....Grams

GAPDH.....Glyceraldehyde 3-phosphate dehydrogenase

gp130..... Glycoprotein 130

GRIM .....Genes Associated with Retinoid-interferon Mortality

GTP ..... Guanosine Triphosphate

H+ ..... Hydrogen ion

HA..... High Activity

HSA.....Human alpha-skeletal actin

IFN .....Interferon

iKO.....Inducible knockout

IL-6 .....Interleukin 6

iNOS .....Inducible Nitric Oxide Synthase

JAK .....Janus Kinase

kN/m^2 .....Kilonewtons/meters^2

KO.....Knockout

LA.....Low Activity

LC3.....Microtubule-associated proteins 1A/1B light chain 3B

LIF.....Leukemia Inhibitory Factor

LLC.....Lewis Lung Carcinoma

LPS.....Lipo-polysaccharide

MAPK.....Mitogen Activated Protein Kinases

Mfn.....Mitofusion

mg.....Milligrams

MHC.....Myosin Heavy Chain

MIN.....$Apc^{Min/+}$

MLC.....Myosin Light Chain

MMP.....Matrix Metalloproteinase

mN.....Millinewtons

mRNA.....Messenger Ribonucleic Acid

ms.....Milliseconds

mTORC.....Mechanistic Target of Rapamycin Complex

NFAT.....Nuclear Factor of Activated T cells

NF-κB.....Nuclear Factor κ B

NMJ.....Neuromuscular Junction

NOS.....Nitric Oxide Synthase

NRF.....Nuclear Response Factor

OPA.....Optic Atrophy Protein

OSM.....Oncostatin M

p.....Phosphorylated

PBS ..... Phosphate Buffered Saline

PCr ..... Phosphocreatine

PGC-1 ..... Peroxisome-Proliferator Gamma-Activated Receptor Coactivator

ROS ..... Reactive Oxygen Species

RT ..... Relaxation Time

RT-PCR ..... Real Time Polymerase Chain Reaction

RvR ..... Ryanodine Receptor

SD ..... Standard Deviation

SDH ..... Succinate Dehydrogenase

SEM ..... Standard Error of the Mean

SERCA ..... Sacro(endo)plasmic Reticulum Calcium ATPase

skm ..... Skeletal Muscle

Smad3 ..... Mothers Against Decapentaplegic Homolog 3

SR ..... Sarco(endo)plasmic Reticulum

STAT3 ..... Signal Transducer and Activator of Transcription 3

t ..... Total

TA ..... Tibialis Anterior

TBST ..... Tris Buffered Saline-Tween 20

TFAM ..... Mitochondrial Transcription Factor A

TGF ..... Transforming Growth Factor

TNF ..... Tumor Necrosis Factor

TPT ..... Time to Peak Twitch

WA ..... Wheel Access

WS ..... Weight Stable

CHAPTER 1

REVIEW OF THE LITERATURE

1.1 – Cancer Cachexia

Overview

Cachexia is a complex wasting disorder characterized by the unintentional loss of body weight and muscle mass secondary to chronic disease (Evans et al. 2008). While cachexia can develop in patients with renal failure, human immunodeficiency virus and acquired immune deficiency syndrome, heart failure, and chronic obstructive pulmonary disease (Dahele and Fearon 2004; Deans and Wigmore 2005; Evans et al. 2008), cachexia affects roughly 80% of cancer patients and is responsible for over 20% of all cancer-related deaths (Argiles 2012; Tisdale 2002; Fearon 2008). The prevalence and severity of cachexia is largely dependent on the cancer type, with the highest prevalence in head and neck, lung, and gastrointestinal cancers (esophageal, pancreatic, colon, etc.) and the lowest prevalence in breast cancers (Deans and Wigmore 2005; Evans et al. 2008; von Haehling and Anker 2014; Vigano et al. 2000; Fearon 2008). Additionally, the etiology and progression of cachexia are unique within different cancer types and can present differently with each patient (Monitto et al. 2001). Cancer patients that experience significant weight loss are less likely to be functionally independent, have a low tolerance to chemotherapeutic interventions, and have a low life quality, which all negatively impact disease prognosis (Vigano et al. 2000; Winningham et al. 1994; Stene et al. 2015; O'Gorman, McMillan, and McArdle 1999; Montazeri 2009; Tisdale 2002). Currently, there are no FDA approved

treatments for cachexia, likely due to the disparity across cancer types as well as the complexity and multimodal nature of the disease.

Cachexia is associated with systemic disruptions including chronic inflammation, anemia, hypogonadism, and insulin resistance (Evans et al. 2008). Cachectic patients also demonstrate behavioral changes including anorexia and physical inactivity; however, whether these behavioral changes are causal, or consequence of cachexia progression and the systemic disruptions remains inconclusive (Evans et al. 2008; Muscaritoli et al. 2010). Each of these systemic and behavioral changes can both independently and synergistically affect the mass, metabolism, and functional properties of skeletal muscle (Evans et al. 2008). The maintenance of skeletal muscle mass, metabolism, and function have established roles in physiological and pathological conditions including obesity, ageing, and chronic disease (Wolfe 2006; Romanello and Sandri 2015; Carson, Hardee, and VanderVeen 2016). While cachexia's etiology continues to be unearthed, the loss of muscle mass and functional quality are thought to develop primarily through disruptions to muscle metabolic homeostasis (Tisdale 2009). Disruptions to muscle protein turnover (i.e. accelerated muscle protein catabolism and suppressed anabolism) has been a primary target for cancer-cachexia therapeutics; however, several therapies have failed in clinical trials due to the inability to improve skeletal muscle function (al-Majid and McCarthy 2001a; Christensen et al. 2014; Aversa, Costelli, and Muscaritoli 2017; Biolo, Cederholm, and Muscaritoli 2014; Dobs et al. 2013; Ramage and Skipworth 2018).

Cachexia-induced skeletal muscle mass loss is associated with the reduced ability to perform activities of daily living which eventually leads to a loss of functional independence and markedly reduces life quality (Vigano et al. 2000; Evans et al. 2008;

Moses et al. 2004; Fearon KC 2006; Argiles 2014; Amano et al. 2017). Chronic inflammation, anemia, and hypogonadism, hallmarks of cancer-cachexia, can each lead to functional decrements without necessarily affecting muscle mass (Argiles et al. 2009; Fearon 2008; Evans et al. 2008; Tisdale 2002; Muscaritoli et al. 2010). Cancer patients, regardless of cachexia diagnosis, have increased perceived (central) fatigue and decreased functional independence which are negatively associated with life quality and survival (al-Majid and McCarthy 2001a; Stone et al. 1999; O'Gorman, McMillan, and McArdle 1999; von Haehling and Anker 2014; Christensen et al. 2014; Winningham et al. 1994; Muscaritoli et al. 2010). While there are no treatments currently approved for cancer cachexia, improving our mechanistic understanding of cachexia-induced muscle wasting, metabolic dysfunction, and more recently contractile dysfunction, should provide vital insight necessary for the development of successful therapeutic interventions (Dahele and Fearon 2004). The overall goal of this literature review is to outline our current understanding of cancer-induced skeletal muscle metabolic and contractile dysfunction and their regulatory mechanisms during the progression of cachexia. Additionally, the efficacy for exercise to prevent and/or treat cancer-induced skeletal muscle metabolic and contractile dysfunction will be discussed.

Pre-clinical Models of Cancer Cachexia

The high prevalence of cachexia in cancer patients and strong relationship between muscle mass loss and morbidity/mortality with disease progression provides significant rationale to investigate the molecular mechanisms of this complex disorder aimed at identifying successful therapeutic targets and improve patient life quality and survival

(Tisdale 2002; Fearon KC 2006). There are inherent difficulties to examining the mechanisms of a comorbidity like cachexia. Clinically, patients are treated first for the primary disease and these treatments often affect the comorbidities which serves as a consistent barrier to understanding the comorbidities underlying mechanisms alone (Penna, Busquets, and Argiles 2016). As previously stated, the development of cachexia is not ubiquitous across cancer types, nor does every patient within a certain cancer type develop cachexia in the same fashion (Fearon KC 2006). Additionally, patients often suffer from weight loss prior to cancer diagnosis, making it difficult to understand the progression of the disease (Bruera 1997; Tisdale 2002; Kritchevsky et al. 1991). Lastly, upon cancer diagnosis, patients are prescribed a specific and tightly regulated treatment regimen that often involve radiation, chemotherapy, and/or surgery, all of which can negatively impact body weight, muscle mass, and muscle function (Barreto et al. 2016; Barreiro et al. 2002). To elude these existing barriers, several preclinical models have been developed to understand the progression and underlying mechanism of cancer-induced cachexia (Deboer 2009; Penna, Busquets, and Argiles 2016). While there are inherent limitations to animal pre-clinical models, significant progress has been made in our understanding of the disease largely in part due to the development of genetic and tumor implant rodent models. Furthermore, mechanistic investigations with the use of *in vitro* strategies involving tumor cell-cultured media and specific cachectic factors further our understanding of the signaling pathways associated with muscle wasting. The following 2 sections will review the mouse and rat models that have been commonly used in cancer cachexia studies.

Tumor Implant Models of Cancer Cachexia

Over the last few decades, several mechanistic investigations of cachexia have utilized tumor-implant models (Puppa, Gao, et al. 2014; Monitto et al. 2001; Judge et al. 2014; Ekman et al. 1982; Jaweed et al. 1983; Talbert et al. 2014). These models are cost and time effective and provide several distinct advantages to understanding cancer induced muscle wasting. Two commonly used tumor cell lines that induce a cachectic phenotype are Lewis Lung Carcinoma (LLC) cells implanted into a mouse with a C57BL/6 genetic background, and the Colon-26 carcinoma (C-26) implanted into mice with either a Balb/c or CD2F1 genetic background (Talbert et al. 2014; Puppa, Gao, et al. 2014). While the LLC and C-26 are the most commonly used models, several other tumor cell lines have been developed to model cancer cachexia using a tumor implantation including the Walker 256, MAC16, AH-130, and B16 melanoma lines (Deboer 2009; Penna, Busquets, and Argiles 2016). All these implant models involve the tumor cells to be isolated and cultured *in vitro* and then injected into the flank of the mouse with the appropriate genetic background. Only a few days after tumor cell implantation, a mass is palpable at the injection site and significant wasting can be achieved within 14 days with the C-26 and 28 days with the LLC (Penna, Busquets, and Argiles 2016; Deboer 2009; Gao and Carson 2016; Puppa, Gao, et al. 2014; Seto, Kandarian, and Jackman 2015). In addition to the different rates of cachexia development between LLC and C-26, their etiologies are distinct. For example, C-26 induced muscle wasting appears to be associated with the interleukin-6 (IL-6) family of cytokine members, IL-6 and leukemia inhibitory factor (LIF), while tumor necrosis factor (TNF) and IL-6 levels have been linked to LLC induced cachexia progression (Carson and Baltgalvis 2010; Gao and Carson 2016; Seto, Kandarian,

and Jackman 2015). Several tumor implant models have also been developed for analysis in rat models of cancer induced wasting which have their own distinct advantages and disadvantages when compared to the mouse. Rat tumor implant models primarily include the methylcholanthrene sarcoma cells (Ekman et al. 1982) and Yoshida AH-130 hepatoma (Busquets et al. 2000). The rat tumor implant models demonstrate significant body weight and muscle mass loss after only seven days of tumor implantation. However, the use of rat models is advantageous for several models of exercise intervention/prevention. Additionally, there is the added benefit of significantly greater blood volume and tissue size compared to the mouse with allows for the analysis of several cachexia-associated targets within one cohort of animals.

A distinct advantage of the LLC mouse model of cancer cachexia is the ease of incorporating genetically modified knockout mice using C57BL/6 mice. This allows the investigator to examine the role of certain cachectic factors in the wasting process with relative ease (Pin et al. 2015; Puppa, Gao, et al. 2014; Zhang, Jin, and Li 2011). While rat models and the C-26 tumor implant model provides a shorter duration of cachexia progression, these models lack the ease of genetic manipulation through breeding. However, to elude these disadvantages, significant progress has been made in the developments of plasmid electroporation or an adeno-associated virus to mechanistically understand the wasting of C-26 and rat models (Cornwell et al. 2014; Seto, Kandarian, and Jackman 2015; Judge et al. 2014). Together, these tumor implant models have dramatically improved our mechanistic understanding of skeletal muscle wasting with cancer.

While preclinical models cannot perfectly mirror the human condition, LLC and C-26 tumor bearing mice exhibit body weight, muscle mass, and adipose tissue loss

associated with high levels of systemic inflammation and disrupted whole-body and muscle metabolism similar to cancer patients (Deboer 2009). While the presence of systemic inflammation remains consistent across cachexia models, their individual inflammatory cytokine profiles are distinct. While initially this may appear to be a limitation, the diversity between models is translatable as cancer patients have a similar range in inflammatory cytokine profiles depending on the cancer type and host genome (Argiles et al. 2009).

Genetically Modified Mouse Models of Cancer Cachexia

The *Apc*$^{Min/+}$ (MIN) mouse is an established model of colorectal cancer, or more specifically, familial adenomatous polyposis (FAP) (Moser, Pitot, and Dove 1990). MIN mice have a nonsense germline mutation in the *Adenomatous polyposis coli* (*Apc*) gene which predisposes mice to multiple intestinal neoplasia resulting in the development of intestinal polyps. Polyps develop at as early as 4 weeks of age and the number of polyps plateau by approximately 12 weeks of age while polyp size continues to increase (Moser, Pitot, and Dove 1990; McClellan et al. 2012). Depending on the size and number of intestinal polyps, mice will initiate body weight loss around 16 weeks and significant body weight loss is present between 18-26 weeks (Baltgalvis 2010). The MIN mouse has been commonly used in cancer/tumor-cell biology since its discovery in 1990. This model is advantageous as ~70% of FAP patients have a similar mutation to the *Apc* gene that predisposes them to several polyps in the colon which can become malignant over time (Moser, Pitot, and Dove 1990; Aihara, Kumar, and Thompson 2014). While there are inherent differences between the MIN mouse and FAP patients, our laboratory and others have demonstrated significant body weight loss, muscle and fat mass loss, high systemic

inflammation, hypogonadism, and fatigue similar to that observed in colorectal cancer patients that experience cachexia (Baltgalvis et al. 2008; Baltgalvis et al. 2009; Baltgalvis 2010; Ravasco, Monteiro-Grillo, and Camilo 2007).

The MIN mouse provides an advantage for therapeutic investigations as the onset and progression of cachexia occurs over several weeks compared to the rapid wasting that occurs with tumor-implant models (Baltgalvis 2010). As previously stated, the progression and severity of cachexia in the MIN mouse is related to the tumor number and size; however, our laboratory has demonstrated the cachexia in the MIN mouse is dependent on circulating IL-6 levels (Baltgalvis et al. 2008; White, Baltgalvis, et al. 2011). The loss of body weight over time is associated with both muscle and fat mass loss in addition to loss of testes and seminal vesicle mass in males (White JP 2013; Hardee, Counts, et al. 2018). Interestingly, the initiation and progression of cachexia in male and female MIN mice are unique. While IL-6 was sufficient to accelerate cachexia progression in the male MIN mouse, IL-6 was not correlated to wasting in the female and IL-6 over expression had no effect on body weight of muscle mass (Hetzler et al. 2015). These sex differences are an intriguing area of investigation that requires additional work. Additionally, the MIN mouse is bread on the C57BL/6 background which, similar to the LLC mouse, provides the advantage of readily available genetic knockouts.

1.2 – IL-6 Family of Cytokines, Muscle gp130 Signaling, and Cancer Cachexia

Inflammation Overview

Inflammation is broadly defined as a physiological immune response that results in the accumulation of immune cells, plasma proteins, and fluid in a target tissue; however,

chronic or pathological, often low-grade, inflammation is associated with increased morbidity and mortality with aging and disease (Abbas, Lichtman, and Pillai 2015; Franceschi et al. 2000; Franceschi and Campisi 2014). Chronically elevated systemic inflammation is one of the established drivers of cachexia development across several chronic diseases (Evans et al. 2008). While understanding broad, general inflammation provides some mechanistic insight into the cachectic condition, several inflammatory mediators, namely cytokines, have established roles in muscle mass loss in both cancer patients and pre-clinical cachexia models (Argiles et al. 2009; Belizario et al. 2016; Carson and Baltgalvis 2010). Out of the numerous pro-inflammatory cytokines that exist, the interferon (IFN), transforming growth factor (TGF), TNF, IL-1 and 6 superfamilies' have emerged as critical regulators of muscle mass and metabolism during cachexia progression (Carson and Baltgalvis 2010; Chen et al. 2016; Loumaye et al. 2015; Mueller et al. 2016; Onesti and Guttridge 2014; Patel and Patel 2017; Pal, Febbraio, and Whitham 2014; Reid and Li 2001; Rodriguez et al. 2014; Sandri 2008).

IL-6 Family of Cytokines and Muscle gp130 Signaling

Circulating pro-inflammatory cytokines affect several physiological processes through binding to either a soluble or membrane bound receptor to stimulate intracellular signaling in numerous target tissues (Argiles et al. 2009; Glass 2005; Rose-John 2018; Argiles, Busquets, and Lopez-Soriano 2005; Puigserver et al. 2001). Indeed, several inflammatory mediators, including the IL-6 family of cytokines, have been widely investigated in skeletal muscle physiology and pathophysiology for its role in the regulation of muscle mass, recovery/regeneration, and metabolic homeostasis during

exercise, aging, and disease (Carson and Baltgalvis 2010; Flint et al. 2016; Zimmers, Fishel, and Bonetto 2016; Narsale and Carson 2014; Pedersen 2012; Febbraio et al. 2004; Puigserver et al. 2001). The IL-6 family of cytokines includes IL-6, IL-11, IL-27, LIF, ciliary neurotropic factor (CNTF), oncostatin M (OSM), cardiotrophin 1 (CT-1), and cardiotrophin-like cytokine (CLC) (Rose-John 2018). Apart from the rest, elevated circulating levels of IL-6, LIF, and CNTF have been demonstrated in cancer patients and preclinical cachexia models and therefore will be the primary focus of this review (Argiles et al. 2009). It is important to note, however, that there is considerable overlap between inflammatory cytokine families as to the intracellular inflammatory signaling proteins that can be activated (Argiles et al. 2009; De Paepe and De Bleecker 2013; Spate and Schulze 2004). Therefore, when the direct role of IL-6 is not well understood, evidence garnered from other inflammatory mediators will be discussed as rationale for further investigation.

IL-6 has been described as a pleiotropic cytokine and has been implicated as a critical regulator of inflammation-induced skeletal muscle remodeling during and following exercise (Washington TA 2011; White JP 2009; Mihara M 2012; Febbraio and Pedersen 2002) as well as contributes to skeletal muscle (and fat) wasting during chronic disease (Pal, Febbraio, and Whitham 2014; Mihara M 2012; Carson and Baltgalvis 2010). The IL-6 family of cytokines bind to their respective receptors (e.g. IL-6R, LIFR, CNTFR) which allows for heterodimerization with the ubiquitously expressed glycoprotein 130 (gp130) receptor (Schwantner et al. 2004). The IL-6 and gp130 receptors are transmembrane receptors that have no protein kinase activity; however, are constitutively associated with the tyrosine kinase, Janus kinase (JAK) (Schwantner et al. 2004; Rose-John 2018). Specific to skeletal muscle, once the cytokine binds and the gp130 receptor

heterodimerizes, JAK phosphorylates immediate downstream target signal transducer and activator of transcription 3 (STAT3). Once activated, STAT3 can translocate to the nucleus and initiate the transcription of several target genes (Schwantner et al. 2004; Carson and Baltgalvis 2010). In addition to STAT3, IL-6 family of cytokines signaling through gp130 has been demonstrated to activate protein kinase B (Akt) and mitogen activated protein kinases (MAPK), which include extracellular signal-related kinases (Erk 1/2) and p38 (Bonetto A 2012; Carson and Baltgalvis 2010; Gao et al. 2017). Intracellular signaling through STAT3, Akt, and MAPK modulate skeletal muscle mass and metabolism through the regulation of protein synthesis, mitochondrial dynamics, and cell proliferation (Gao et al. 2017; Fix et al. 2018).

IL-6 Family of Cytokines, Muscle gp130 Signaling, and Cancer Cachexia

Both systemic inflammation and muscle inflammatory signaling have been extensively examined for their regulation of muscle wasting with cancer (Tisdale 2002; Evans et al. 2008; Carson and Baltgalvis 2010; VanderVeen, Fix, and Carson 2017; Argiles et al. 2009; Argiles 2014; Deans and Wigmore 2005; Sandri 2008; Onesti and Guttridge 2014). Chronic inflammation has been linked to disrupted muscle protein turnover and oxidative metabolism, which are both integral to the pathology of muscle mass loss during cachexia progression (White, Baltgalvis, et al. 2011; Carson, Hardee, and VanderVeen 2016; Argiles et al. 2009; White, Baynes, et al. 2011; Deans and Wigmore 2005; Seto, Kandarian, and Jackman 2015; Cannon TY 2007; Onesti and Guttridge 2014; Fearon, Glass, and Guttridge 2012). Although many systemic mediators of cancer cachexia appear to be associated with specific preclinical models and cancer types, IL-6 has been implicated

as a driver of cachexia in cancer patients and preclinical models including the MIN and C-26 mouse (Carson and Baltgalvis 2010). To this end, elevated circulating IL-6 can be observed in cachectic cancer patients and pre-clinical models alike and is strongly correlated to body weight and muscle mass loss (Fortunati et al. 2007; Baltgalvis et al. 2009; Seto, Kandarian, and Jackman 2015). Systemic overexpression of IL-6 in the MIN mouse is sufficient to accelerate the cachectic phenotype, while IL-6 null MIN mice had no significant muscle mass loss (Baltgalvis et al. 2008). Additionally, administration of an IL-6 receptor antibody in C-26 mice attenuated muscle mass loss associated with reduced ubiquitin-dependent proteolytic pathways (Fujita et al. 1996). Recent evidence suggests LIF, another member of the IL-6 family, modulates cachexia progression in both LLC and C-26 tumor-bearing mice (Jackman et al. 2017; Seto, Kandarian, and Jackman 2015; Mori et al. 1991; Gao and Carson 2016; Kandarian et al. 2018).

Downstream muscle gp130 signaling through STAT3 and MAPK have received significant mechanistic investigation for their roles in cancer cachexia. Loss of the muscle gp130 receptor in LLC tumor-bearing mice had suppressed muscle STAT3 and p38 activation associated with improved muscle mass. Constitutively active muscle specific STAT3 was sufficient to induce skeletal muscle mass loss in both tumor-bearing and tumor-free mice, while STAT3 inhibition attenuated body weight and muscle mass loss in tumor bearing mice (White, Baynes, et al. 2011; Bonetto A 2012; Miller et al. 2016). Furthermore, IL-6 null MIN mice did not lose body weight or muscle mass and had suppressed muscle STAT3 activation; however, STAT3 did not return to the expression level of healthy controls (Baltgalvis et al. 2008). Interestingly, elevated muscle protein degradation was still present in both gp130 loss in the LLC and the IL-6 null MIN mouse

(Puppa, Gao, et al. 2014). These results suggest that IL-6 and muscle gp130 signaling are not the sole regulators of the cachectic condition and other inflammatory mediators' compound with IL-6 to exacerbate the cachectic condition (Baltgalvis et al. 2008; Baltgalvis et al. 2009).

The role of MAPK signaling in cancer-induced muscle wasting has received significant investigation; however, the role of MAPK signaling in cancer-induced muscle wasting appears dependent on tumor type and the treatment vehicle. The induction of protein degradation through the E3 ligase, Atrogin-1, during LLC-induced cachexia is regulated by the p38-MAPK-C/EBPβ (CCAAT enhancer binding protein) signaling axis and loss of muscle C/EBPβ attenuated muscle mass loss through suppressed proteasomal proteolysis (Zhang, Jin, and Li 2011). While administration of the MAPK inhibitor, PD98059, to C-26 tumor bearing mice attenuated muscle mass loss associated with improved muscle myogenesis (Penna et al. 2010), the MAPK inhibitor, Selumetinib, had no effect on muscle mass in LLC tumor-bearing mice (Au et al. 2016). Lastly, administration of the MAPK inhibitor, MEK162, attenuated muscle mass loss concomitant with reduced atrophy associated genes (Talbert et al. 2017).

The role of muscle inflammatory signaling in cachexia-induced muscle wasting continues to be an active area of investigation. The IL-6 family of cytokines and associated muscle gp130 signaling through STAT3 and MAPK appear to regulate skeletal muscle mass during cachexia progression through modulation of muscle metabolism and protein turnover. Due to the complexity of the disease and diversity in cancer types, additional work is needed to determine the efficacy of treatments targeting these signaling pathways.

1.3 – Skeletal Muscle Metabolism

Overview

Skeletal muscle metabolism is the net chemical reactions that occur within skeletal muscle; however, the current review refers to skeletal muscle metabolism in regard to the fuel metabolism necessary to produce ATP to meet the energy demand of skeletal muscle. Holistically, skeletal muscle metabolism has a vital role in the maintenance of physiological health and metabolic homeostasis in several disease conditions including obesity, ageing, and chronic disease (Wolfe 2006; Romanello and Sandri 2015). Additionally, skeletal muscle makes up roughly 40% of total body weight in a healthy adult and accounts for 20-30% of whole-body resting energy expenditure (Zurlo et al. 1990). While skeletal muscle can serve as an amino acid reservoir during energy stress, skeletal muscle is also a glucose sink. Skeletal muscle is the primary site of insulin stimulated glucose transport and is a key regulator of whole-body glucose homeostasis (Kummitha et al. 2014; Wolfe 2006). Along with its role in glucose homeostasis, at rest and low-intensity activity skeletal muscle relies on beta-oxidation of fatty acids as a primary a fuel source (Kummitha et al. 2014). As the duration and intensity of activity increases, skeletal muscle's primary fuel source shifts towards glycolytic pathways although still account for as much as 90% of whole body oxygen uptake during high-intensity activity (Zurlo et al. 1990). The modulation and disruption of these phenomena remains an active area of investigation across several physiological and pathological conditions.

Skeletal Muscle Oxidative Metabolism

Skeletal muscle oxidative metabolism is determined by the muscle's mitochondria content and ATP production efficiency, which along with free radical production, defines mitochondrial function. In addition to oxidative metabolism, mitochondria have an established role the regulation of muscle apoptosis, autophagy, and protein turnover (Romanello and Sandri 2013). The relative content and function of the muscle's mitochondria align with the muscle's contractile phenotype and myosin heavy chain isoform expression which are described in later sections (Schiaffino and Reggiani 1996). The unique plasticity of skeletal muscle allows for mitochondrial content and function to be modulated by several different stimuli including muscle use, systemic inflammation, and circulating hormones (Holloszy and Coyle 1984; Thomason and Booth 1990). Furthermore, this plasticity involves the regulation of mitochondrial content and function through the modulation of mitochondrial dynamics, mitophagy, and biogenesis regulation, which collectively define mitochondrial quality control (Deng and Haynes 2017; Picca et al. 2017).

The regulation of mitochondrial dynamics involves the coordination of mitochondrial fission and fusion, or the addition and fragmentation of a mitochondrion to and from the mitochondrial network, respectively (Romanello and Sandri 2015; Youle and van der Bliek 2012; Iqbal et al. 2013; Drake, Wilson, and Yan 2016). Mitochondrial fusion is regulated by the GTPases Mitofusin 1 and 2 (MFN-1, MFN-2) and optic atrophy protein 1 (OPA1) (Drake, Wilson, and Yan 2016; Yan, Lira, and Greene 2012). While MFN-1 and MFN-2 have a similar structure, MFN-1 plays a greater role in the fusion of the outer mitochondrial membrane and MFN-2 regulates GTP hydrolysis required for this dynamic

process (Romanello and Sandri 2015; Iqbal and Hood 2015; Carson, Hardee, and VanderVeen 2016). Mitochondrial fission machinery is controlled by the GTPase cytosolic dynamin-related protein 1 (DRP-1) which can translocate to the outer mitochondrial membrane and develop active fission sites (Jheng et al. 2012; Romanello et al. 2010; Romanello and Sandri 2015; Wu et al. 2011; Youle and van der Bliek 2012; Iqbal and Hood 2015). Fission protein 1 (FIS1) is required for mitochondrial division by signaling DRP-1 to translocate the outer mitochondrial membrane (Iqbal and Hood 2015). Disruptions to mitochondrial dynamics through accelerated fission and/or reduced fusion results in a relative increase in isolated mitochondria from the network which reduces mitochondrial ATP production efficiency (Youle and van der Bliek 2012).

Mitochondrial biogenesis is a critical process necessary for maintaining an adequate abundance of skeletal muscle mitochondria in order to sustain the energy demands of the cell (Baar 2004; Garnier et al. 2005; Romanello and Sandri 2015; Wu et al. 1999). The peroxisome-proliferator gamma-activated receptor coactivator (PGC-1) has been extensively examined as the critical regulator of skeletal muscle mitochondrial biogenesis (Puigserver and Spiegelman 2003). PGC-1α and β isoforms have been demonstrated to regulate oxidative metabolism independently. PGC-1β can regulate myosin heavy-chain isoform expression, and increased expression by transgenic overexpression induced an oxidative muscle phenotype (Arany et al. 2007). PGC-1α can induce nuclear response factors (NRF-1,2) and mitochondrial transcription factor A (Tfam) transcription, which both transcriptionally regulate the expression of mitochondrial associated genes (Wu et al. 1999; Lin et al. 2002; Puigserver and Spiegelman 2003; Baar 2004). Moreover, the stimulation of mitochondrial biogenesis by PGC-1α can increase

mitochondrial content and the loss of PGC-1α results in decreased relative muscle mitochondrial content and suppressed muscle ATP production (Joseph et al. 2006; Lira et al. 2010; Vainshtein et al. 2015).

The autophagic removal of damaged and dysfunctional mitochondria is termed mitophagy (Jokl and Blanco 2016; Kimura et al. 2007; Carson, Hardee, and VanderVeen 2016). Autophagy can be described as both general or specific, wherein specific organelles, including mitochondria, can be targeted for degradation. The induction of p62, B-cell Lyphoma (BCL2) interacting protein 3 (Bnip3), and microtubule-associated proteins 1A/1B light chain 3B (LC3)-interacting domains are responsible for the intracellular degradation of organelles (Luo et al. 2014; Romanello and Sandri 2015; Youle and van der Bliek 2012). The autophagic removal of damaged and dysfunctional mitochondria, termed mitophagy, is critical for the maintenance of a healthy network of mitochondria (Drake and Yan 2017). Failure of these processes can lead to an accumulation of damaged mitochondria which can negatively regulate metabolism and mass (Romanello and Sandri 2015; Sandri 2010; Penna et al. 2013).

Cachectic Skeletal Muscle Oxidative Metabolism

Several chronic diseases are associated with disrupted skeletal muscle oxidative metabolism and mitochondrial dysfunction (Deng and Haynes 2017; Prasai 2017; Bordi, Nazio, and Campello 2017; Romanello and Sandri 2015; Boland, Chourasia, and Macleod 2013; Carson, Hardee, and VanderVeen 2016). Furthermore, the regulation of oxidative metabolism has emerged as a biological target of cancer-induced muscle wasting (Carson, Hardee, and VanderVeen 2016). Loss of mitochondria content and associated reductions

in ATP production have been reported in several preclinical models of cachexia (White, Baltgalvis, et al. 2011; Brown et al. 2017). Although skeletal muscle with a greater abundance of oxidative muscle fibers differ in mitochondria content and reliance on oxidative metabolism when compared to primarily glycolytic muscles, reductions in mitochondrial content is observed in both muscle types in the mouse hindlimb from severely cachectic mice (White, Baltgalvis, et al. 2011).

Increased mitochondrial fission is a hallmark of mitochondrial dysfunction in inflammatory diseases (White, Baltgalvis, et al. 2011; White et al. 2012; Wu et al. 2011; Carson, Hardee, and VanderVeen 2016); however, mitochondrial fission is required for the removal of old or damaged mitochondria and blocking these processes can result in mitochondrial dysfunction and muscle atrophy (Romanello et al. 2010; White et al. 2012; Wu et al. 2011). Furthermore, the loss of mitochondrial fusion proteins MFN1 and 2 results in reduced mitochondrial DNA and significant muscle mass loss (Lee et al. 2014). While the regulation of these processes in cachectic skeletal muscle is only beginning to be described, suppressed MFN1 and 2 in skeletal muscle has been reported early in cachexia progression in the MIN mouse (White et al. 2012). While increased FIS1 expression is observable only in severely cachectic skeletal muscle in LLC tumor bearing mice, there is a significant reduction in OPA1 prior to muscle mass loss (White, Baltgalvis, et al. 2011; Brown et al. 2017).

Aberrations of skeletal muscle mitophagy can contribute to skeletal muscle mitochondrial dysfunction leading to mass loss (Aversa et al. 2016; White et al. 2012; Penna et al. 2011). Several indices of accelerated mitophagy has been reported in skeletal muscle from cancer patients and pre-clinical models (Cosper and Leinwand 2011; Ding et

al. 2016; Fritzen et al. 2016; McClung et al. 2010; Talbert et al. 2014; White et al. 2012). Muscle mitophagy is dependent on the adenosine monophosphate (AMP) activated protein kinase (AMPK), Forkhead Box O (FOXO), and mechanistic target of rapamycin complex 1 (mTORC1) signaling axis, and when disrupted can negatively regulate muscle mass and metabolism (Fritzen et al. 2016; Sanchez et al. 2012; Sandri 2010). Additionally, increased activation of non-selective autophagy has been reported in cachectic muscle and bearing mice (Tessitore et al. 1993; Penna et al. 2013); however additional work is needed to identify the regulation of mitophagy during cachexia progression (Mayers et al. 2014).

IL-6 Family of Cytokines, Muscle gp130 Signaling, and Skeletal Muscle Oxidative Metabolism

Manipulating systemic IL-6 can affect the disruption of muscle oxidative metabolism during cancer cachexia; however, a direct mechanistic link in skeletal muscle has not been described. Systemic IL-6 over-expression can reduce protein expression of muscle mitochondrial biogenesis and dynamics proteins in tumor bearing mice (White et al. 2012), while IL-6 receptor antibody negates these disruptions and prevents the loss of muscle oxidative metabolism (White, Baltgalvis, et al. 2011; White et al. 2013; Fujita et al. 1996). Recently, mitochondrial STAT3 localization has been implicated as a regulator of basal cellular respiration, and it has been hypothesized that the accumulation of mitochondrial STAT3 disrupts efficiency of the electron transport chain and induces mitochondrial ROS production (Smith et al. 2014; Wegrzyn et al. 2009). A role for STAT3 in the disruption of skeletal muscle oxidative metabolism with cancer cachexia has yet to be established.

Inflammatory signaling has been linked to cancer-induced mitochondrial dysfunction in skeletal muscle (Carson, Hardee, and VanderVeen 2016). Specifically, activation of either nuclear factor κ B (NF-κB), STAT3, or mothers against decapentaplegic homolog 3 (Smad3) signaling have been associated with cancer-induced muscle mitochondria dysfunction in tumor bearing mice (VanderVeen, Fix, and Carson 2017). *In vivo* and *in vitro* analysis of LLC driven cachexia demonstrated decreased muscle ATP synthesis rates and decreased electron transport chain efficiency with associative increases in TNF-α (Constantinou et al. 2011; McLean, Moylan, and Andrade 2014). Furthermore, inhibiting direct TNF-α downstream target, NF-κB, improved diaphragm mitochondrial respiration in mice bearing P07 lung derived tumors (Fermoselle et al. 2013). While STAT3's role in skeletal muscle mitochondrial homeostasis has not been clearly defined, examination of liver and heart mitochondria demonstrate that STAT3 accumulation disrupts genes associated with retinoid-interferon mortality (GRIM 19) (Wegrzyn et al. 2009). Lastly, elevated Smad3 signaling was associated with reduced enzymatic activity in isolated skeletal muscle mitochondria, however, a mechanistic link requires further investigations (Padrao et al. 2013). Currently, our mechanistic understanding of mitochondrial quality control and mitochondrial respiration in skeletal muscle during cachexia progression is extremely limited due to the dearth of published studies and the heterogeneity of the preclinical cancer cachexia models used in these investigations.

1.4 – Skeletal Muscle Function

Overview

Skeletal muscle function is classically defined as the muscle's force production, fatigue properties, and twitch characteristics (Close 1972; Fitts and Holloszy 1977; Fitts et al. 1984; Brooks and Faulkner 1988; Close 1964). Examination of these functional outcomes provides a distinct physiological window into the functional quality of the muscle that may be affected by several physiological and pathological conditions (Allen, Lamb, and Westerblad 2008; Westerblad and Allen 2003). Skeletal muscle's contractile phenotype is classically categorized by its myofiber twitch rates and fatigue properties (e.g. fast-fatigable, fast-fatigue resistant, and slow-fatigue resistant) and/or their metabolic profile (e.g. fast-glycolytic, fast-oxidative/glycolytic, and slow-oxidative) (Fitts and Holloszy 1977; Close 1972; Fitts et al. 1984; Allen, Lamb, and Westerblad 2008). Each skeletal muscle has a heterogenous mix of several fiber-types, however a muscle can be categorized based on the relative abundance of a particular fiber-type (Close 1972; Fitts et al. 1980). While central, peripheral, and systemic factors can influence muscle function, this section will discuss the intrinsic properties of the muscle that directly impact force, fatigue, and contractile quality. This section will outline the functional properties of skeletal muscle and the known disruptions to skeletal muscle function in cachectic cancer patients and preclinical cachexia models.

Skeletal Muscle Function Analysis Techniques

There are several modalities of examining skeletal muscle function in both humans and preclinical models (Fitts et al. 1980; Thompson et al. 1992; Segal, White, and Faulkner

1986; Brooks and Faulkner 1988; Bonetto, Andersson, and Waning 2015; Altenburg et al. 2007; Widrick et al. 1997). While significant technological advancements have dramatically improved our understanding of skeletal muscle function in humans, mechanistic investigations of skeletal muscle function are primarily done in animal models (Bonetto, Andersson, and Waning 2015). The analysis of whole-body muscle function through grip strength, daily activity, and time to exercise-induced exhaustion provides physiological relevance; however, whole-body functional assessments are not specific to skeletal muscle as well as lacks mechanistic depth. Analysis of skeletal muscle *in vitro*, or often termed *ex vivo*, allows for analysis of a whole muscle in a highly controlled system (Brooks and Faulkner 1988). This technique provides mechanistic advantages; however, the controlled system is limited in its physiological relevance. Analysis of skeletal muscle *in situ* allows for analysis of a single muscle while maintaining the host nerve and blood supply (Murphy et al. 2012; Schiaffino and Reggiani 1996). This technique provides physiological advantages, however, limits mechanistic specificity to the muscle as changes in circulation of neural stimulation can affect force output. Additionally, *in situ* muscle function allows for analysis of larger muscles (primary movers), while *ex vivo* muscle function is primarily done in smaller muscles with 2 teasable tendons. To study the contractile properties of a single fiber-type the analysis of isolated single myofibers is the most advantageous technique (Widrick et al. 1997; Schiaffino and Reggiani 1996). Similar to *ex vivo* analysis, isolated myofibers are difficult to dissect and have lower physiological relevance, however, provides significant mechanistic insight. Lastly, skinned myofibers allow for precise mechanistic investigation into muscle contractile properties and fatigue,

specifically calcium kinetics and metabolic changes that affect fatigue (Widrick et al. 2001; Kandarian and Williams 1993).

Skeletal Muscle Contractile Properties

Examination of the skeletal muscle's contractile properties provides important information regarding skeletal muscle function and metabolic phenotype changes with aging, disease, and disuse (Fitts and Holloszy 1977; Fitts et al. 1984; Brooks and Faulkner 1988; Barreiro and Gea 2015; Berchtold, Brinkmeier, and Muntener 2000; Widrick et al. 2001; Wolfe 2006). Skeletal muscle twitch characteristics depend on neural excitation, sarcomeric structure, calcium handling, and myosin ATPase isoform expression (Close 1972; Schiaffino and Reggiani 1996; Khodabukus and Baar 2015). A fundamental characteristic of skeletal muscle is the capacity to produce force and the contractile properties of the muscle is a strong indicator of the muscle's maximal capacity to produce force (Close 1972). Skeletal muscles produce force through the interaction of contractile proteins actin and myosin. Actin and myosin are intermyofibrillar filaments which undergo tightly coordinated rapid conformation changes that result in shortening the distance between the sarcomere's z-lines (Burkholder et al. 1994).

The initiation of a single muscle contraction, or twitch, begins in the neuron where a change in the resting membrane potential above threshold results in an action potential (Schneider and Chandler 1973). During an action potential voltage gated-ion channels open allowing for the rapid exchange of sodium and potassium resulting in the propagation of the action potential down the axon until it reaches the synapse between the nerve and the muscle, termed the neuromuscular junction (NMJ) (Gonzalez-Freire et al. 2014). At the

NMJ the nerve releases acetylcholine to bind to the acetylcholine receptor to continue the action potential along the sarcolemma to initiate Excitation-Contraction (EC) coupling (Franzini-Armstrong and Jorgensen 1994; Bannister 2016; Sandow 1965). This leads to a release of calcium from the sacro(endo)plasmic reticulum (SR) into the cytosol by the interaction between the Ryanodine Receptor (RyR) and Dihydropyridine Receptor (DHPR) (Franzini-Armstrong and Jorgensen 1994; Kandarian and Williams 1993). Calcium then binds to troponin which causes a conformational shift in tropomyosin to expose the myosin binding site on actin (Winegrad 1965). Once the myosin binding site is exposed myosin binds to actin forming the crossbridge. After formation of the crossbridge, myosin ATPase causes ATP to be released from the myosin head causing a 'powerstroke' to initiate a contraction (Sweeney and Hammers 2018). After the contraction the muscle relaxes by releasing calcium binding from troponin and get sequestered back to the SR by the sacro(endo)plasmic reticulum calcium ATPase (SERCA) (MacLennan, Asahi, and Tupling 2003). A single stimulus large enough to stimulate a single action potential can stimulate a single muscle contraction, or a muscle twitch.

The rate of twitch rise and relaxation is a strong prognosticator for the muscle's contractile phenotype and contractile quality (Close 1972; Fitts and Holloszy 1977; Brooks and Faulkner 1988). The rate of contractile rise and relaxation depends primarily on the muscle's myosin heavy chain (MHC) and SERCA isoform expression, respectively (Fitts et al. 1980; Close 1964; Brooks and Faulkner 1988; Burkholder et al. 1994). Muscle fibers expressing type I MHC isoform have the slowest myosin ATPase activity resulting in the slowest contractile speed. Furthermore, the slower contractile speeds are associated with low force production (Khodabukus et al. 2015; Khodabukus and Baar 2015). Muscle fibers

expressing type II MHC isoform have faster myosin ATPase activity and thus have faster contraction speeds (Fitts et al. 1980). Type II muscle fiber however can be further divided into type IIa, IIx, or IIb, each of which have distinct metabolic profiles and increase in contraction speeds from IIa to IIx, to IIb (Fitts et al. 1984). The rate of muscle relaxation relies on the rate that calcium is sequestered back to the SR by the SERCA to release calcium binding from troponin (Khodabukus and Baar 2015). Skeletal muscle's that are primarily slow-twitch have similar expression levels of SERCA1a and SERCA2a isoforms, while skeletal muscle's that are primarily fast-twitch are almost exclusively comprised of SERCA2a (Kandarian and Williams 1993). The slow-twitch muscles have a reduced or prolonged relaxation time, while fast-twitch muscles have a rapid relaxation time.

Cachectic Skeletal Muscle Contractile Properties

Recently, specific decrements to skeletal muscle's contractile quality have been identified in cachectic patients and tumor bearing mice (Christensen et al. 2014; Gorselink et al. 2006; Murphy et al. 2012; Roberts, Frye, et al. 2013; Jaweed et al. 1983). Slower twitch rise and relaxation have been reported in AC-33 tumor bearing rats, however the effect of cachexia on the twitch properties of skeletal muscle isolated from C-26 tumor bearing mice remains inconclusive (Jaweed et al. 1983; Murphy et al. 2012; Roberts, Frye, et al. 2013). Roberts et. al showed slower 1/2 relaxation time (RT) and time to peak twitch (TPT) in the extensor digitorum longus (EDL) and soleus (Roberts, Frye, et al. 2013); however, both Murphy et. al and Gorselink et. al report no change in twitch rates in the tibialis anterior (TA) and EDL, respectively (Murphy et al. 2012; Gorselink et al. 2006). One potential explanation for the slower twitch properties could be a shift in fiber-type

distribution (Toth et al. 2016). It is generally accepted that preferential atrophy of type II muscle fibers occurs during cachexia, particularly at the early stages of wasting. Interestingly, muscle mass loss is associated with reduced myofiber cross sectional area (CSA) in all fiber-types (IIb, IIx, and IIa) from the TA, EDL, and soleus in cachectic mice (Hardee et al. 2016). Thus, the loss of fiber atrophy and metabolic dysfunction could contribute to the disrupted contractile phenotype during severe cachexia and should be explored in future investigations.

Classically, twitch relaxation is dependent on the rate of calcium reuptake by SERCA after stimulation (Close 1972; Berchtold, Brinkmeier, and Muntener 2000). Modifications to SERCA expression and function by cachexia remains a largely untapped area of study. Previous reports have shown increased expression of SERCA1 and SERCA2 in the gastrocnemius and EDL, respectively, which was hypothesized to be indicative of leaky calcium channels resulting in aberrant calcium handling thought to contribute to mitochondrial dysfunction, EC uncoupling, and fatigue (Debold 2016; Fontes-Oliveira et al. 2013; Carson, Hardee, and VanderVeen 2016). Consistent with this notion, 1/2 RT is increased in the EDL and soleus in tumor-bearing mice (Roberts, Frye, et al. 2013; Jaweed et al. 1983). These results provide a strong rationale for investigating calcium release and reuptake by the SR in cachectic muscle and its role in disrupted muscle function.

IL-6 Family of Cytokines, Muscle gp130 Signaling, and Skeletal Muscle Contractile Properties

While the mechanisms regulating cachexia-induced skeletal muscle contractile dysfunction have not been well described, skeletal muscle contractile dysfunction is

commonly reported across several inflammatory diseases including Chronic Obstruction Pulmonary Disease (COPD), Congestive Heart Failure (CHF), sepsis, and cancer (Hussain 1998; Hussain and Sandri 2013; Pieske et al. 1996). Injection of lipo-polysaccharide (LPS) is a preclinical model of sepsis and induces a robust inflammatory response. Administration of LPS markedly reduces force and contractile function through disrupting sarcolemma function, EC coupling, and disruptions to the contractile machinery (Comtois et al. 2001; Lin et al. 1998). One prevailing hypothesis is that high levels of inflammation and/or inflammatory cytokines induce oxidative stress which disrupts skeletal muscle contractility (Barreiro et al. 2002; Reid, Lannergren, and Westerblad 2002). While elevated levels of the IL-6 family of cytokines have been reported with LPS, results from these studies have led investigators to understand the role of TNFα in contractile dysfunction.

Interestingly, the deleterious effects of TNFα on skeletal muscle contractility have been demonstrated to occur through the induction of oxidative stress, namely nitrous oxide systems (NOS) and reactive oxygen species (ROS) (Hardin et al. 2008; Reid, Lannergren, and Westerblad 2002). Recently, IL-6 has been shown to regulate nitric oxide synthase dependent signaling associated with a reduction in cardiac myocyte post-rest potentiation indicative of disrupted calcium transiency (Yu, Kennedy, and Liu 2003; Yu et al. 2005). Increased inducible NOS (iNOS) with IL-6 was associated with increases in STAT3 and Erk 1/2 signaling; however, inhibition of STAT3, not Erk 1/2, mitigated the IL-6 induction of iNOS and was sufficient to rescue myocyte contractility (Yu, Kennedy, and Liu 2003). IL-6 alone has also been demonstrated to reduce caffeine stimulated calcium release from the SR further demonstrating a role for IL-6 in the disruption of calcium transiency and muscle contractile quality (Yu et al. 2005).

Skeletal Muscle Force Production

The mechanisms of muscle force production during an isolated muscle twitch were previously described in the *Skeletal Muscle Contractile Properties* section. While the twitch characteristics provide insight into the force producing capabilities of the muscle, analysis of maximal skeletal muscle force production provides greater physiological relevance. The 'all or none' principal of skeletal muscle contraction describes the phenomena that if the motor neuron membrane potential exceeds threshold, a single action potential will occur regardless of the strength of the stimulus (Fitts et al. 1980). As previously described, this single action potential will elicit a muscle twitch and if the muscle is able to completely reach relaxation, a second stimulus will simply induce a second twitch. If the frequency of the stimulus is great enough, where complete relaxation does not occur, the second stimulus will increase muscle force greater than observed with a single twitch (Bannister 2016; Schneider and Chandler 1973; Gonzalez-Freire et al. 2014). This property of skeletal muscle function is termed 'summation' and the loss of muscle relaxation time is termed 'tetanus'. To this end, there is a positive sigmoidal relationship between the stimulation frequency and muscle force production. Based on the summation principle of skeletal muscle, it is simple to surmise that muscles that are predominately made up of slow-twitch muscle fibers (slow 1/2 RT and TPT) will reach maximal tetanic force (P_o) at a lower simulation frequency than muscles with a greater abundance of fast-twitch fibers (fast 1/2 RT and TPT). Furthermore, in association with reaching P_o earlier, analysis of isolated slow-twitch muscle fibers identified muscles that are predominately made up of slow-twitch muscle fibers produce significantly less force when compared to muscles with a greater abundance of fast-twitch fibers.

While analysis of isolated muscle fibers is mechanistically advantageous, the key contributors to force production by whole muscles are the size of the muscle fibers innervated by the motor neuron, the number of muscle fibers within the motor unit, the muscle fiber-type distribution, and relative amount of non-contractile tissue within the muscle (Close 1972; Bodine et al. 1987; Brooks and Faulkner 1988; Bonetto, Andersson, and Waning 2015). Intrinsic to the muscle, skeletal muscle force can be modulated by myofiber CSA (sarcomeres in parallel), percent non-contractile tissue (fibrosis), and relative myosin heavy chain isoform expression (fiber-type). Changes in any of these structural or biochemical aspects of skeletal muscle will alter its functional properties (Brooks and Faulkner 1988; Fitts et al. 1984; Friden and Lieber 1992; Holloszy and Booth 1976; Segal, White, and Faulkner 1986).

Cachectic Skeletal Muscle Force Production

Skeletal muscle specific tetanic force ($_sP_o$), or force produced per unit area, has been a principal parameter for establishing muscle's structural integrity with aging and disease (Burkholder et al. 1994; Brooks and Faulkner 1988; Barreiro and Gea 2015). Often skeletal muscle weakness can be explained by a loss of muscle weight and muscle CSA; however, if the structural integrity of the muscle is compromised, or there is increased fibrosis/non-contractile tissue, the loss of muscle strength will be compounded (Siegel 1989). While decreased P_o has been demonstrated in cancer patients and preclinical models, whether there is a decrease in $_sP_o$ with cachexia remains inconclusive. The disparity in results is likely related to the muscle tested, degree and duration of cachexia, and heterogeneity of the disease related to the animal model and tumor type. Interestingly,

reductions in absolute (grams of force) and relative (grams of force/kilograms of body weight) grip strength was demonstrated in C-26 mice with both mild and severe body weight loss (Murphy et al. 2012). While *ex vivo* diaphragm $_sP_o$ was reduced in cachectic C-26 mice, there was not a significant reduction of *in situ* TA $_sP_o$ (Murphy et al. 2012). These results were supplemented with reductions in muscle mass and CSA. *Ex vivo* examination of the soleus and EDL from C-26 mice showed reductions in both absolute and specific tension concomitant with decreased myofiber CSA and a shift towards a more glycolytic phenotype with increased percentage of type IIb/x in the EDL and an increased type IIa and IIb/x in the soleus (Roberts, Frye, et al. 2013).

Specific tension can be negatively impacted by expansion of the extracellular matrix (ECM), which involves connective tissue deposition and/or edema. Our lab has previously reported increased non-contractile tissue in cachectic MIN mice, which did not appear to be associated with regeneration or degeneration (Hardee et al. 2016). Matrix metalloproteinases (MMP) are key ECM remodeling proteins that degrade the collagen in the ECM, as well as play a role in the synthesis and deposition of new collagen (Spinale 2007). MMP-2, MMP-3, and MMP-9 are the primary isoforms in skeletal muscle and when elevated can indicate increased ECM remodeling (Zhang et al. 2014; Mehan et al. 2011). Elevated expression of MMP-2 and MMP-3 has been reported in the diaphragm, EDL, and soleus from C-26 tumor bearing mice (Devine et al. 2015). The regulation of ECM remodeling with cachexia and its contribution to skeletal muscle weakness is not well understood, however several inflammatory cytokines and immune cells have direct roles in ECM remodeling and the stimulation of fibroblast proliferation.

IL-6 Family of Cytokines, Muscle gp130 Signaling, and Skeletal Muscle Force Production

As previously outlined, systemic inflammation and muscle inflammatory signaling play critical roles in cachexia development. While understanding the biochemical regulation that drives skeletal muscle wasting is of great importance, decrements in muscle force directly impact cancer patient quality of life and health status (Argiles 2012; Christensen et al. 2014). Several proposed cancer cachexia therapeutics have failed in clinical trials due to their inability to improve overall functional capabilities (Saitoh et al. 2017; Ramage and Skipworth 2018). Furthermore, our mechanistic understanding of cachexia induced muscle weakness is limited and is often left to speculation based on changes to muscle mass and CSA. Critical gaps in our knowledge of this regulation are likely related to the dearth of studies examining both muscle function and cachectic factors in the same cohort of tumor bearing mice. This lack of cohesive integration with these measurements has likely contributed to the plethora of unsuccessful cancer cachexia treatment paradigms (al-Majid and McCarthy 2001a; Baltgalvis 2010; Christensen et al. 2014; Murphy et al. 2012; Roberts, Frye, et al. 2013; White, Baltgalvis, et al. 2011; White et al. 2012). Our current understanding of cachexia-induced muscle weakness has been developed as an extension of mechanistic examinations of muscular dystrophy and cardiac dysfunction.

TNF-α overexpression alone has been eloquently demonstrated to decrease absolute and specific muscle force. Reductions in diaphragm $_sP_o$ can be observed as early as 1 hour following TNF administration and last up to 24 hours post treatment (Hardin et al. 2008). These effects were mediated through the TNFR1, not TNFR2, as TNF had no effect on muscle force in muscle lacking TNFR1 (Hardin et al. 2008). Additionally, pre-

treatment with an antioxidant, Trolox, prevented the TNF induction of muscle weakness, implicating a potential role for ROS to induce muscle weakness (Hardin et al. 2008). Further investigations into the mechanism of TNF induced muscle weakness demonstrated that the activation of MuRF1 through NFκB was required (Adams et al. 2008). Increased ROS and elevated expression of MurF1 and NFκB have been reported across several preclinical cachexia models and cancer patients alike and can be induced by several inflammatory cytokines including the IL-6 family of cytokines; however, additional work is needed to elucidate their role in cachexia induced muscle weakness (Mehl KA 2005; Williams et al. 1999; Khal et al. 2005; Bossola et al. 2003; Guttridge et al. 2000; Sandri 2008).

While the effects of TNF and TNFR signaling on skeletal muscle force are well understood, the effect of elevated circulating IL-6 on muscle weakness has not been well described. IL-6 overexpression in sedentary MIN demonstrated reduced relative grip strength compared to vector and wildtype controls; however, IL-6 overexpression in wildtype mice demonstrated an increase in relative grip strength (Puppa et al. 2012). Interestingly, in aging and heart failure patients there is an inverse relationship between circulating IL-6 and muscle strength (Toth et al. 2006). Cardiac myocytes treated with IL-6 had decreased contractile function associated with elevated iNOS, which was mediated by STAT3 and not Erk1/2 (Yu, Kennedy, and Liu 2003). However, neither systemic IL-6 nor muscle inflammatory signaling have been directly associated with skeletal muscle function decrements during the progression of cancer cachexia.

Skeletal Muscle Fatigability

Skeletal muscle fatigue is a key component of skeletal muscle function and has been studied for over 100 years, yet mechanistic investigations of muscle fatigue are still in their infancy (Allen, Lamb, and Westerblad 2008). While there is significant overlap with force production regulation, skeletal muscle's fatigability is regulated by several physiological processes including the muscle's blood and nutrient supply, metabolic profile, fiber-type distribution, and structural integrity (Holloszy and Booth 1976; Fitts and Holloszy 1977; Munkvik, Lunde, and Sejersted 2009; Thompson et al. 1992; Fitts 1994; Rutherford, Manning, and Newton 2016). Skeletal muscle fatigue is defined as the inability to maintain a given force output over time and is distinct from central or perceived fatigue which can contribute to skeletal muscle fatigue independent of the muscle fatigue properties (Fitts 1994; Allen, Lamb, and Westerblad 2008). While activity/exercise-induced fatigue has been studied extensively, difficulty identifying the direct role of several contributing factors has served as a significant barrier to understanding fatigue (Westerblad and Allen 2003). Additionally, depending on the exercise modality, fatigue may present differently (Fitts and Holloszy 1977; Munkvik, Lunde, and Sejersted 2009; Altenburg et al. 2007; Coyle et al. 1985; Hagberg et al. 1984; Hagberg et al. 1980; Hargreaves 2000; Hurley et al. 1984; Kim et al. 2015). For example, high-intensity exercise recruits each fiber-type and relies primarily on anaerobic metabolism; high intensity exercise-induced fatigue develops early and is thought to be driven through disruptions to EC coupling, disrupted calcium kinetics, and increased intracellular pH (Thompson, Balog, and Fitts 1992; Murphy and Clausen 2007). In contrast to high-intensity exercise, low-intensity endurance exercise primarily recruits type I and type IIa fiber types; the onset of fatigue

during low-intensity exercise occurs much later due to its reliance on the high efficiency of aerobic metabolism (Fitts 1994). There is considerable debate over the key regulators of low-intensity exercised-induced fatigue, however nutrient availability appears to be a key contributor.

To maintain a given force output over time, the muscle's metabolic demand must be met. Since the regulation of circulating and muscle ATP levels is so tightly monitored, fatigue develops prior to significant reductions in ATP concentrations, thought to be as a protective feedback loop (Fitts 1994). Once the initial ATP stores are used during the first few moments of activity causing an increase in ADP/ATP ratio, the phosphocreatine (PCr) system supplies enough inorganic phosphate to prop-up ATP levels to maintain force. However, the PCr system is not sustainable and at low-intensity exercises skeletal muscle recruits the slow twitch fibers and rely primarily on oxidative metabolism as the primary fuel source. As intensity and/or duration increases the faster more glycolytic fibers are recruited. Therefore, depletion of muscle glycogen is a key indicator of fatigue, however as previously stated it is not the only contributor/indicator. It is important to note that muscles with a high mitochondrial content, or a slow oxidative contractile phenotype, are more fatigue resistant as they are able to rely on oxidative metabolism for a greater duration compared to fast glycolytic muscles (Murphy and Clausen 2007). In addition to the depletion of fuel sources, the duration of calcium transient, muscle temperature, and build-up of metabolic byproducts, most notably Hydrogen ions (H+), can induce fatigue (Murphy and Clausen 2007).

In addition to reduced absolute force, fatigue presents with significantly reduced peak twitch, slower relaxation (1/2 RT), and slower contraction velocity, TPT (Thompson

et al. 1992; Fitts and Holloszy 1978). Interestingly, the slowing of contraction rates occurs prior to the increase in metabolic byproducts; however, their causal relationship remains unknown (Thompson et al. 1992; Westerblad and Allen 2003). These contractile dysfunctions are thought to develop by decreased amplitude of calcium transient; however, disrupted calcium kinetics can occur through several mechanisms (Debold 2016; Allen, Lamb, and Westerblad 2008). Whether this dysfunction occurs at the NMJ, t-tubule, or SERCA, it is clear that calcium release and reuptake contribute to fatigue demonstrated by direct release of calcium by caffeine returns force to its pre-fatigued levels.

Historically, the root causes of fatigue were thought to be attributed to the accumulation of lactate and H+ in the blood, as at physiological pH, lactic acid disassociates rapidly (Fitts 1994). The production of lactate and H+ occurs in anaerobic catabolism of glucose and/or glycogen and both lactate and H+ have strong inverse relationships with force in a fatiguing muscle (Westerblad and Allen 2003; Thompson, Balog, and Fitts 1992). Administration of lactate to an isolated muscle fiber had no effect on muscle force, demonstrating that lactate does not directly induce fatigue, but rather it is H+ that depresses force (Westerblad and Allen 2003). With high intensity exercise the pH of skeletal muscle can fall from physiological 7.0 to 6.2 which can be attributed to both increased H+ production and a reduction in cell buffer capacity (Allen, Lamb, and Westerblad 2008). Interestingly, lactate transporter inhibition accelerated fatigue and reduced pH, indicating that lactate serves as an H+ buffer to prevent fatigue rather than cause it. In addition to H+, the metabolic byproduct inorganic phosphate, can depress force through disrupting cross bridge formation and the power stroke, as well as disrupt calcium binding to troponin (Fitts 1994; Westerblad and Allen 2003).

While biochemical changes that occur during activity can result in fatigue, ultrastructural changes and muscle damage during contraction can negatively impact force production over time (Cooke 2007). While isometric and concentric muscle contractions do not typically induce muscle damage, extreme exercise durations as well as extremely high intensities can induce muscle damage and depress force (Choi and Widrick 2009). Whether the damage occurs to the myofibrils, mitochondrial membrane, T-tubule, or SR depends on the exercise modality and severity of the muscle damage; however, changes in the ultrastructure of any of these aspects can negatively impact muscle force during exercise.

Cachectic Skeletal Muscle Fatigability

Cancer patients with decreased functional ability and increased fatigue, regardless of cachexia diagnosis, experience decreased quality of life and a poorer prognosis (O'Gorman, McMillan, and McArdle 1999; al-Majid and McCarthy 2001a). Fatigue is the most frequently reported symptom by cancer patients (al-Majid and McCarthy 2001a). Cachectic patients and preclinical cachexia models exhibit decreased volitional activity and increased fatigue that precedes significant weight loss (Baltgalvis 2010; Murphy et al. 2012; Roberts, Frye, et al. 2013; Toth et al. 2016; Puppa, Gao, et al. 2014). Determining whether this fatigue is due to neural, humoral, or musculoskeletal alterations remains a consistent barrier in cancer and cachexia research. Recently, specific decrements to skeletal muscle's contractile quality have been identified in cachectic patients and tumor bearing mice (Christensen et al. 2014; Gorselink et al. 2006; Murphy et al. 2012; Roberts, Frye, et al. 2013; Jaweed et al. 1983); however, the drivers of these functional deficits in skeletal

muscle have not been clearly defined (Op den Kamp et al. 2012; Christensen et al. 2014; Biolo, Cederholm, and Muscaritoli 2014).

Along with muscle mass, fatigue is a strong predictor of survival in cancer patients (Vigano et al. 2000; Christensen et al. 2014). Cachectic skeletal muscle has been reported to have disrupted metabolic homeostasis, specifically disrupted oxidative metabolism and decreased mitochondrial content which directly impact muscle fatigue resistance. Additionally, disrupted mitochondrial quality control (decreased content and biogenesis, disrupted dynamics, etc.) and increased ROS in cachectic muscle (White et al. 2012; Carson, Hardee, and VanderVeen 2016) coincides with decreased physical activity (Baltgalvis 2010). Decrements in mitochondrial biogenesis and mitochondrial content have been strongly associated with increased fatigue in skeletal muscle (Lin et al. 2002; Brown et al. 2017), however a direct mechanistic link with cachexia-induced fatigue has not been identified. *Ex vivo* muscle function has also demonstrated increased fatigability in C-26 mice in the soleus (Roberts, Frye, et al. 2013), but the fatigue properties of the EDL and the relationship with weight loss or established indices of cachexia was not determined. The functional and metabolic impairments that occur in cachectic C-26 mice was well described and demonstrated reduced volitional activity and reductions in carbohydrate and fat oxidation concomitant with reduced energy expenditure (Murphy et al. 2012). Interestingly, while disrupted oxidative metabolism has been reported with C-26 induced cachexia, mild and severely cachectic C-26 tumor bearing mice had a greater reliance on fat oxidation relative to total body energy expenditure associated with reduced TA and diaphragm force output throughout the duration of an intermittent fatigue protocol (Murphy et al. 2012).

The current understanding of cancer induced fatigue is limited and has been excluded from several studies examining cancer- and cachexia-induced metabolic dysfunction. Substantial work is needed to determine if several contributing factors of fatigue are altered with cancer and cancer-cachexia. Additionally, further work is needed to determine the contribution of alterations to the NMJ and muscle blood flow to functional decrements with cachexia, as these can also occur with aging and chronic disease (Rudolf, Deschenes, and Sandri 2016).

IL-6 Family of Cytokines, Muscle gp130 Signaling, and Skeletal Muscle Fatigability

While the role of IL-6 and muscle gp130 signaling in skeletal muscle fatigue during chronic disease remains largely unknown, the role of systemic IL-6 and muscle inflammatory signaling during exercise and activity has been well described (Pedersen 2012; Munoz-Canoves et al. 2013; Pedersen, Steensberg, and Schjerling 2001). While there is a marked induction of plasma IL-6 with both endurance and high intensity exercise, there is evidence to suggest that the elevation of circulating IL-6 depends on the exercise intensity/duration and muscle mass recruited to perform the activity (Pedersen and Fischer 2007; Pedersen 2012). In contrast to plasma IL-6, IL-6 mRNA transcription is rapidly induced after the onset of exercise (Fischer 2006). Interestingly, there is significant evidence that suggests the induction of IL-6 transcription occurs through intracellular calcium following muscle contraction. It is well established that intracellular calcium regulates a myriad of cellular signaling; however, it has been hypothesized that calcium stimulation of nuclear factor of activated T cells (NFAT) regulates IL-6 transcription (Febbraio and Pedersen 2002). While the role of calcium and NFAT signaling in muscle

fatigue has received significant attention, the link between IL-6 and calcium regulated fatigue has not been well established.

While IL-6 transcription is initiated early during exercise, it appears IL-6 remains in the muscle until energy sources become depleted (Febbraio and Pedersen 2002). The role of oxidative metabolism, muscle glycogen, and glycogen depletion during exercise-induced fatigue was described above. Interestingly, there was a strong association with the release of IL-6 into circulation and muscle glycogen depletion during exercise. Moreover, skeletal muscles with low glycogen content had increased IL-6 transcription compared to high-glycogen muscle. IL-6 transcription may be regulated by calcium in the low glycogen state; however, it has been hypothesized that IL-6 is release in the plasma due to energy stress to activate liver glycogenolysis in order to restore muscle glycogen. In this hypothesis, IL-6 would serve to trigger a negative feedback loop to reduce muscle contraction and allow glucose uptake by the muscle and subsequent glycogen storage. If this were to occur, high levels of IL-6, during physiological exercise or pathological disease, could induce systemic and intramuscular alterations that directly impact skeletal muscle fatigability.

1.5 – Skeletal Muscle Use and Cancer Cachexia

Skeletal Muscle Use and Skeletal Muscle Function

Several aspects of skeletal muscle force production are affected by increased and decreased muscle use with exercise and unloading, respectively (Fitts et al. 1984; Holloszy and Booth 1976; Holloszy and Coyle 1984; Fitts and Holloszy 1977; Thomason and Booth 1990; Widrick et al. 2001). The nature of skeletal muscle plasticity allows for adaptations

to both metabolic and structural aspects of muscle to occur in response to increased and decreased use (Fitts and Holloszy 1977; Holloszy and Booth 1976; Holloszy and Coyle 1984; Hargreaves 2000). A shift to a slower, more oxidative, contractile phenotype is an established adaptation to exercise training (Fitts and Holloszy 1977). This contractile phenotype is associated with a shift to a slower fiber type as well as an increase in mitochondrial content (Holloszy and Coyle 1984; Kandarian and Williams 1993). The effect of exercise training on force production largely depends on the exercise modality. Endurance exercise training will have little effect on muscle force in healthy adults; however, endurance exercise may prevent the loss of strength with aging and disease (Coyle et al. 1985). Contrary to endurance exercise, resistance exercise has potent effects on absolute and relative force concomitant with increased muscle protein synthesis and increased muscle CSA (Kandarian and Williams 1993). While resistance and endurance exercise have similar effects on muscle's contractile phenotype and fiber type, resistance exercise results in increased sarcomeres in parallel which improve overall force production capacity.

Muscle Use and Cancer Cachexia

Both endurance and resistance exercise have been proposed as promising preventative and therapeutic interventions for skeletal muscle mass and strength loss with cancer cachexia (Cheema et al. 2008; Peddle-McIntyre et al. 2012; McNeely et al. 2015; Lonbro et al. 2013; Alves et al. 2015; Lira et al. 2015; al-Majid and McCarthy 2001a; Argiles 2012). Whether the plasticity of skeletal muscle remains intact in cancer patients is an active area of investigation, however cancer patients that underwent an endurance

exercise training regimen displayed increased oxygen consumption and improved life quality scores compared to baseline and sedentary controls. These results have been recapitulated by rodent models of cachexia showing endurance exercise training can improve muscle protein synthesis and muscle to body weight ratio, however skeletal muscle function was not directly measured in these studies (al-Majid and McCarthy 2001a; Puppa et al. 2012). Consequent of severe disease, exercise intolerance serves as a critical barrier to understanding the effects of endurance exercise as a therapeutic in preclinical cancer cachexia models. Cachectic muscle was, however, able to respond to an acute bout of low-frequency induced concentric muscle contractions, shown by increased transcription of several oxidative metabolism genes (Puppa, Murphy, et al. 2014). Additionally, endurance exercise prior to the onset of cachexia prevented significant body weight and muscle mass loss, however skeletal muscle strength was not directly measured (Puppa et al. 2012). Our lab has previously demonstrated that repeated bouts of eccentric muscle contraction, a model of resistance exercise, can attenuate the loss of muscle mass and myofiber CSA as well as prevent the induction of muscle non-contractile tissue in MIN mice that had initiated wasting (Hardee et al. 2016). Interestingly, cachectic muscle was able to stimulate protein synthesis and activate anabolic signaling in response to an acute bout of eccentric muscle contraction demonstrating that skeletal muscle plasticity remains intact (Hardee, Counts, et al. 2018). The culmination of these studies provides significant rationale to investigate the effect of exercise on skeletal muscle function prior to and after the onset of cachexia.

The capacity to regenerate from injury and adapt to altered use are defining features of skeletal muscle that also provide optimism for therapeutic interventions for cachectic

muscle. Exercise has been shown to be beneficial in diabetes, COPD, CHF, and continues to show beneficial results in cancer patients as well (Grande et al. 2014; Booth, Roberts, and Laye 2012). Volitional activity level in addition to regimented exercise paradigms can dramatically impact skeletal muscle mass and metabolism (Holloszy and Coyle 1984; Yan, Lira, and Greene 2012). Increased muscle activity induced a more oxidative muscle phenotype by increasing mitochondria content and function (Drake, Wilson, and Yan 2016; Holloszy 2004; Holloszy 1982; Hood 2001). Increased muscle use can positively impact muscle mass, and the extent of this change is dependent on the exercise type, intensity, duration, and frequency (al-Majid and McCarthy 2001a, 2001b). The metabolic plasticity of muscle is reinforced by the dramatic alterations that occur to skeletal muscle after an acute bout of exercise (Holloszy 2004; Holloszy and Coyle 1984; Yan, Lira, and Greene 2012). Increasing the muscle metabolic demand with exercise can stimulate mitochondrial biogenesis to increase mitochondrial content and function (Lira et al. 2010; Vainshtein et al. 2015; Wright et al. 2007). Cachectic muscle from tumor bearing mice subjected to an acute bout of low frequency electrical stimulation maintained the capacity to activate genes responsible for mitochondrial biogenesis, PGC-1α, NRF-1, and Tfam (Puppa, Murphy, et al. 2014). However, cachectic muscle had deficits in the acute activation of protein expression after a single bout of stimulated concentric contractions, which could be rescued by systemic inhibition of inflammatory signaling (Puppa, Murphy, et al. 2014).

Decreased muscle use, either by unloading or extreme sedentary behavior, can induce a shift to a more glycolytic phenotype, coinciding with decreased mitochondrial content and function, and muscle atrophy (Booth, Roberts, and Laye 2012). Cancer patients commonly suffer from excessive fatigue prior to and during chemotherapeutic treatments

(al-Majid and McCarthy 2001a; Stewart, Skipworth, and Fearon 2006; Stone et al. 1999). This fatigue is accompanied by a dramatic decrease in volitional activity and the reduced ability to perform activities of daily living (Ferriolli et al. 2012; al-Majid and McCarthy 2001a; Farkas J 2013; Montazeri 2009). Preclinical cancer models also have shown that cachectic mice undergo limited volitional activity as disease progression worsens (Murphy et al. 2012; Baltgalvis 2010). However, minimizing sedentary time and using alternative muscle contraction methods may serve as a first line of action to attenuate cachexia-induced decrements to muscle mitochondria (Booth and Chakravarthy 2006; Dahele et al. 2007; Gratas-Delamarche et al. 2014; Thyfault and Booth 2011). To this end, IL-6 over-expression in tumor bearing mice was not able to induce muscle mass loss and metabolic changes in mice that were regularly exercised on a treadmill (Puppa et al. 2012). It is interesting to speculate if disuse alters the muscle sensitivity to the cachectic environment, causing a more rapid decline in muscle metabolic function and mass. Conversely, research is needed to determine if muscle contraction or exercise serves to desensitize the muscle to the cachectic environment.

Muscle Use and Cachectic Skeletal Muscle Metabolism

Exercise also regulates mitochondrial dynamics, increasing both fission and fusion. This is thought to aid in mitochondrial turnover and improve ATP production efficiency. Endurance exercise pre-training was protective again IL-6 induced muscle mass loss and metabolic dysfunction in the MIN mouse (Puppa et al. 2012). Additionally, cachectic muscle retains the capacity to respond to repeated bouts of stimulated eccentric contractions. Cachectic muscle in MIN mice that underwent 7 bouts of eccentric

contractions increased muscle succinate dehydrogenase (SDH) activity and decreased AMPK signaling (Hardee et al. 2016). Exercise training is implicated as a potential therapeutic to either prevent or reverse muscle wasting. It is evident from preclinical studies that cachectic muscle maintains the ability to robustly respond to an acute bout of exercise or contraction. Further work is needed to determine if repeated bouts of exercise can confer the metabolic health benefits of exercise after the development of cancer cachexia (Vainshtein et al. 2015; Sheldon, Booth, and Kirby 1993).

Physical activity and contraction has been established as a potent regulator of mitophagy and may possess the potential to correct or attenuate dysfunction mitophagy processes in cachectic muscle (Lira et al. 2013; Sanchez 2016; Sanchez et al. 2014; Schwalm et al. 2015; Vainshtein et al. 2014; Yan, Lira, and Greene 2012; Pigna et al. 2016). In C-26 tumor implanted mice, voluntary wheel running attenuated cachexia induced p62 and LC3 II/I accumulation indicating improved mitophagy (Pigna et al. 2016). Additionally, AMPK activation via AICAR suppressed p62 accumulation through promotion of mitophagy and accelerating the turnover of p62 accumulation in cachectic muscle (Pigna et al. 2016). While there is growing evidence for mitophagic processes in the regulation of cancer cachexia, additional studies are warranted to establish a direct role for inflammation in the regulation of these processes. Additionally, the role of exercise and/or muscle contraction in the regulation of mitophagy in diseased or chronically inflamed muscle may prove to be a powerful therapeutic for the restoration of mitophagic balance in cachectic muscle. Clearly, further research is warranted to examine the complex interaction between cancer-induced inflammation, muscle contraction, and muscle disuse for maintenance or improvement of cachectic muscle oxidative metabolism.

CHAPTER 2

THE IMPACT OF CACHEXIA PROGRESSION ON THE DEVELOPMENT OF SKELETAL MUSCLE FATIGUE IN TUMOR-BEARING MICE

2.1 – Abstract

While cancer-induced skeletal muscle wasting has been widely investigated, the drivers of cancer-induced muscle functional decrements are only beginning to be understood. Decreased muscle function impacts cancer patient quality of life and health status, and several potential therapeutics have failed in clinical trials due to a lack of functional improvement. Furthermore, systemic inflammation and intrinsic inflammatory signaling's role in the cachectic disruption of muscle function requires further investigation. We examined skeletal muscle functional properties during cancer cachexia and determined their relationship to systemic and intrinsic cachexia indices. Male *Apc*$^{Min/+}$ (MIN) mice were stratified by percent body weight loss into weight stable (WS; <5% loss) or cachectic (CX; >5% loss). Age-matched C57BL/6 (WT) littermates served as controls. Tibialis anterior (TA) twitch properties, tetanic force, and fatigability were examined *in situ*. TA protein and mRNA expression were examined in the non-stimulated leg. CX decreased muscle mass, tetanic force (P_o), and specific tetanic force ($_sP_o$). Whole body and muscle fatigability were increased in WS and CX. CX had slower contraction rates, +dP/dt and –dP/dt, which were inversely associated to muscle STAT3 and P65 activation. STAT3 and P65 activation were also inversely associated with P_o. However, STAT3 was not related to $_sP_o$ or fatigue. Muscle SOCS3 mRNA expression was negatively associated with

TA weight, P_o, and $_sP_o$, but not fatigue. Our study demonstrates that multiple functional deficits that occur with cancer cachexia are associated with increased muscle inflammatory signaling. Notably, muscle fatigability is increased in the MIN mouse before cachexia development.

2.2 – Introduction

Cachexia is a complex wasting disorder characterized by unintentional body weight loss secondary to chronic disease (Dahele and Fearon 2004; Deans and Wigmore 2005; Evans et al. 2008). Cachexia affects roughly 80% of cancer patients and is responsible for over 20% of all cancer-related deaths (Argiles 2012; Tisdale 2002). Cachexia-induced skeletal muscle mass loss is associated with reduced ability to perform basic daily tasks leading to a loss of functional independence (Vigano et al. 2000; Evans et al. 2008; Moses et al. 2004; Fearon KC 2006; Argiles 2014; Amano et al. 2017). More clinically relevant, cancer patients with decreased functional ability and increased fatigue, regardless of cachexia diagnosis, experience decreased quality of life and a poorer prognosis (O'Gorman, McMillan, and McArdle 1999; al-Majid and McCarthy 2001a). Cachectic patients and preclinical cachexia models exhibit decreased volitional activity, whole body weakness, and fatigue (Baltgalvis 2010; Puppa 2014; Murphy et al. 2012; Roberts, Frye, et al. 2013; Toth et al. 2016). Recently, specific decrements to skeletal muscle's contractile quality have been identified in cachectic patients and tumor bearing mice (Christensen et al. 2014; Gorselink et al. 2006; Murphy et al. 2012; Roberts, Frye, et al. 2013; Jaweed et al. 1983). However, the drivers of these functional deficits in skeletal muscle have not been clearly defined (Op den Kamp et al. 2012; Christensen et al. 2014; Biolo, Cederholm, and

Muscaritoli 2014). To this end, several proposed cancer cachexia therapeutics have failed in clinical trials due to their inability to improve overall patient function (Dobs et al. 2013; Aversa, Costelli, and Muscaritoli 2017; Biolo, Cederholm, and Muscaritoli 2014). This inability of potential therapeutics to improve muscle function illustrates our lack of understanding related to the cachectic factors that induce these deficits. Critical gaps in our knowledge of this regulation are likely related to the dearth of studies examining both muscle function and cachectic factors in the same cohort of tumor bearing mice. This lack of cohesive integration with these measurements has likely contributed to the plethora of unsuccessful cancer cachexia treatment paradigms (al-Majid and McCarthy 2001a; Baltgalvis 2010; Christensen et al. 2014; Murphy et al. 2012; Roberts, Frye, et al. 2013; White, Baltgalvis, et al. 2011; White et al. 2012).

Disrupted proteostasis and oxidative metabolism, linked to chronic inflammation, are integral to the pathology of cachectic skeletal muscle (White, Baltgalvis, et al. 2011; Carson, Hardee, and VanderVeen 2016; Argiles et al. 2009). Both systemic and muscle inflammation have been extensively examined for their regulation of muscle wasting with cancer (Tisdale 2002; Evans et al. 2008; Carson and Baltgalvis 2010; VanderVeen, Fix, and Carson 2017; Argiles et al. 2009; Argiles 2014; Deans and Wigmore 2005; Sandri 2008; Onesti and Guttridge 2014). Widely examined systemic mediators of muscle wasting include pro-inflammatory cytokines Interleukin-6 (IL-6), Tumor Necrosis Factor-α (TNFα), Transforming Growth Factor β, (TGFβ), Interferon γ (IFNγ), and others (VanderVeen, Fix, and Carson 2017; Carson and Baltgalvis 2010; Kumar, Bhatnagar, and Paul 2012; Loumaye et al. 2015; Patel and Patel 2017; Onesti and Guttridge 2014). Although many systemic mediators of cancer cachexia appear to be associated with

specific preclinical models, IL-6 has been implicated as a driver of cachexia in cancer patients and preclinical models (Carson and Baltgalvis 2010). Interestingly, there is a significant inverse relationship between circulating IL-6 and muscle strength in heart failure patients and sarcopenia (Toth et al. 2006). Disrupted protein turnover and metabolic homeostasis in the $Apc^{Min/+}$ (MIN) mouse, an established cancer cachexia model, is dependent on elevated circulating IL-6 (Carson and Baltgalvis 2010; White, Baynes, et al. 2011; van Hall et al. 2008; White et al. 2012; White, Baltgalvis, et al. 2011; White et al. 2013). Muscle inflammatory signaling has also be investigated for the disruption of protein turnover and metabolism induced by cancer (Zhou et al. 2016; Acharyya and Guttridge 2007; Argiles et al. 2005; Sandri 2008). Chronic activation of signal transducer and activator of transcription (STAT3), nuclear factor κB (P65), mitogen activated protein kinases (P38 and Erk1/2), and protein kinase B (Akt) signaling in skeletal muscle are all associated with muscle wasting (Bonetto A 2012; Carson and Baltgalvis 2010; Argiles et al. 2009; Zhou et al. 2016; Klasing and Johnstone 1991). Interestingly, each of these signaling pathways can regulate muscle mass in healthy and atrophic conditions (Bonetto A 2012; Guttridge et al. 2000; Zhang, Jin, and Li 2011; White et al. 2013). Moreover, STAT3 can disrupt cardiac myocyte contractility (Yu, Kennedy, and Liu 2003; Yu et al. 2005). However, neither systemic IL-6 nor muscle inflammatory signaling have been directly associated with skeletal muscle function decrements during the progression of cancer cachexia.

Muscle force production, fatigue, and twitch characteristics are functional properties that define skeletal muscle quality. Life quality associated with aging, muscular dystrophy, COPD, and cancer patients is directly related to these muscle parameters (Wolfe

2006; Siegel 1989; Winningham et al. 1994; Barreiro and Gea 2015; al-Majid and McCarthy 2001a). Furthermore, muscle fatigability (distinct from central fatigue), myofibrillar protein expression, and calcium handling characteristics are used to define a muscle's phenotype (Close 1972; Schiaffino and Reggiani 1996; Khodabukus and Baar 2015). A myofibers response to catabolic stimuli have been shown to be regulated by phenotype; slow-oxidative fibers are more susceptible to disuse atrophy, while fast-glycolytic muscles are more sensitive to cachectic stimuli (Widrick et al. 2001; Brooks and Faulkner 1988; Roberts, Frye, et al. 2013; Acharyya and Guttridge 2007). While understanding the biochemical regulation that drives skeletal muscle wasting is of great importance, decrements in muscle function directly impact cancer patient quality of life and health status (Argiles 2012; Christensen et al. 2014), and several proposed cancer cachexia therapeutics have failed in clinical trials due to their inability to improve muscle function (Saitoh et al. 2017). Therefore, determining the regulation of impaired muscle function during cancer cachexia progression is imperative to understanding this complex wasting disorder. We have found that $Apc^{Min/+}$ (MIN) mice, an established preclinical model of cancer cachexia, demonstrate decreased voluntary wheel running and cage activity prior to significant weight loss (Baltgalvis 2010). However, it is not known if this decreased volitional activity is associated with decrements in skeletal muscle function. To this end, we examined skeletal muscle functional properties during cancer cachexia and determined their relationship to systemic and intrinsic cachexia indices. We hypothesized that cachectic skeletal muscle would exhibit decreased strength and increased fatigability when compared to weight stable and healthy controls, and that these decrements would be inversely related to increased muscle inflammatory signaling. To test this hypothesis, male

MIN mice were stratified by percent body weight loss into weight stable (MIN-WS; <5% BW loss) or cachectic (MIN-CX; >5% BW loss). Age-matched male C57BL/6 (WT) littermates served as controls. The tibialis anterior (TA) was stimulated *in situ* and analyzed for properties of muscle function. Protein and mRNA expression related to the cachectic phenotype were determined from the contra-lateral TA to determine relationships to muscle function.

2.3 – Methods

Animals

Male WT and MIN mice were purchased from Jackson Laboratories and were bred at the University of South Carolina's Animal Resources Facility. All animals were group housed and kept on a 12:12-h light-dark cycle. Body weights were measured weekly, and animals were monitored for signs of distress. Animals were given food and water *ad libitum* throughout the duration of the study. All animals were fasted 5 hours prior to tissue collection. Mice were anesthetized with a ketamine-xylazine-acepromazine cocktail, and hindlimb muscles and select organs were carefully dissected and snap frozen in liquid nitrogen and stored at -80ºC until further analysis. All animal experiments were approved by the University of South Carolina's Institutional Animal Care and Use Committee.

Analysis of Muscle Function

At ~20 weeks of age, mice were anesthetized with 2% isoflurane inhalation and kept anesthetized at 1.5 % isoflurane throughout the duration of the procedure (~1 hour). Muscle function analysis of the TA *in situ*, which maintains the host nerve and blood supply, has been previously described (Murphy et al. 2012; Bonetto, Andersson, and

Waning 2015; Dellorusso et al. 2001). Briefly, the distal tendon of the right TA was isolated and tied to a force transducer (Aurora Scientific, Ontario, Canada) using 5-0 silk sutures. The mouse was place on the apparatus maintained at 37°C throughout the entirety of the procedure (Bonetto, Andersson, and Waning 2015). The sciatic nerve was exposed proximal to the knee and maintained using warmed mineral oil. The sciatic nerve was then subjected to a single stimulus to determine the optimal length (L_o). Once L_o was obtained, a force-frequency curve was generated, and maximal tetanic force was determined. After a 5-minute rest the TA was subjected to a 4-minute intermittent fatigue protocol consisting of 1 second maximal stimulation every 4 seconds (Murphy et al. 2012). Maximal tension was again measured 5 and 10 minutes after completion of the fatigue protocol. Specific tension was determined using TA muscle CSA calculated by muscle mass/(L_f x 1.06), where L_f represents fiber length determined by multiplying L_o by 0.6, the predetermined TA muscle length to fiber length ratio, and 1.06 represents the skeletal muscle density (Brooks and Faulkner 1988).

Western blot analysis

Western blot analysis was performed as described previously (Puppa 2014). Briefly, the left proximal TA was homogenized, and protein concentration was determined using the standard Bradford protein assay. Homogenates were fractionated on 7-10% SDS-polyacrylamide gels and transferred to a polyvinylidene difluoride membrane. Primary antibodies for phosphorylated (p) and total (t) P65, STAT3, P38, and Erk1/2 (Cell Signaling Technology) were incubated 1:1000 overnight at 4ºC in 5% TBST milk. Anti-rabbit IgG-conjugated secondary antibodies (cell signaling) were incubated 1:2000 for 1 hour at room temperature in 5% TBST milk. Enhanced Chemiluminescence was used to

visualize antibody-antigen interaction and captured using the Syngene: G-Box. Blots were analyzed by determining the integrated optical density of each band using ImageJ (NIH software).

RNA isolation and RT-PCR

RNA isolation, cDNA synthesis, and real-time PCR were performed as previously described (Narsale et al. 2016) using reagents from Applied Biosystems (Foster City, CA, USA). Primers for GAPDH, IL-6, IL-1β, TNF-α, SOCS3, SERCA1, RyR1, and Calsequestrin were purchased from IDT (Coralville, Iowa, USA) and run using SYBR green PCR buffer (Narsale et al. 2016). Data were analyzed using the $2^{-\Delta\Delta CT}$ method.

Cytochrome C Oxidase Activity

Extensor Digitorum Longus (EDL) muscle samples were homogenized in extraction buffer (0.1 M KH2P04/Na2HP04, 2 mM EDTA, pH 7.2). Cytochrome-c oxidase (COX) activity was determined by measuring the rate of oxidation of fully reduced cytochrome c at 550nm using (CYTOCOX1) Sigma Aldrich Kit and spectrophotometer (Eppendorf) (Iqbal and Hood 2015).

Treadmill Run to Fatigue

A separate cohort of WT (n=6) and MIN (n=15) mice was run on a treadmill to examine time to exhaustion as a measure of whole body fatigue, as previously described (Velazquez et al. 2014). Three days prior to the fatigue test, mice were acclimated to the treadmill by running at a 5% grade for a total of 20 minutes, with 5 m/min incremental increases in speed starting at 5m/min and finishing at 20m/min. After acclimation, the mice were run on a treadmill until complete exhaustion, determined by 2 minutes of resistance

to hand prodding. The fatigue test consisted of 5 minutes at 5m/min, 10 m/min, 15 m/min, and 30 minutes at 20 m/min and then increased to the final speed of 25 m/min.

Statistical analysis

Values are presented as means ± standard error of the mean (SEM). Student t-tests were performed to determine differences between genotypes. A one-way ANOVA was used to determine differences in muscle function and inflammatory signaling when MIN mice were stratified by age or body weight loss. Post hoc analyses were performed with student Newman-Keuls methods. A Bartlett's test was used to determine significantly different standard deviations ($p<0.05$). If a significant difference was observed between group standard deviations, a non-parametric Kruskal-Wallis one-way ANOVA was used. A Pearson correlation was used to determine correlations between inflammatory genes and proteins with muscle function properties in MIN mice. Stepwise linear regression models were used to identify predictors (cachexia indices) of the 8 measured outcomes related to skeletal muscle function. Significance was set at $p<0.05$.

2.4 – Results

MIN-CX had increased plasma IL-6 levels compared to MIN-WS and WT mice (Figure 2.1a). MIN-CX had significantly reduced TA weight (35%) compared to MIN-WS (Figure 2.1b). We then examined intrinsic muscle inflammatory signaling proteins in the non-stimulated TA (Figure 2.1c, d). Activation of signaling proteins was determined from the phosphorylated to total ratio of the expressed protein in muscle. STAT3 activation increased 24-fold in MIN-CX compared to MIN-WS and 19-fold compared to WT. P65 activation increased 1.5-fold in MIN-CX compared to MIN-WS and 1.6-fold compared to

WT. Erk1/2 activation increased 3.4-fold in MIN-CX compared to MIN-WS and 3.3-fold compared to WT. P38 activation was increased 2.2-fold in MIN-CX compared to MIN-WS and 2.0-fold compared to WT. We then examined muscle inflammatory gene expression in the non-stimulated TA (Figure 2.1e). IL-6 mRNA was increased in MIN-CX 9.1-fold compared to MIN-WS and 9.0-fold compared to WT. SOCS3 mRNA was increased in MIN-CX 15-fold compared to MIN-WS and 16-fold compared to WT. IL-1β mRNA was increased in MIN-CX 7.1-fold compared to MIN-WS and 4.8-fold compared to WT. Lastly, TNF-α mRNA was increased in MIN-CX 1.3-fold compared to MIN-WS, but was not different from WT. Extensor digitorum longus (EDL) cytochrome C oxidase (COX) enzyme activity was reduced 50% in MIN-CX compared to MIN-WS and 52% compared to WT (Figure 2.1f). There was a negative relationship between STAT3 activation and TA weight in all MIN mice (Figure 2.1g). Similarly, a negative relationship was observed with SOCS3 mRNA and TA weight (Figure 2.1h). Many indices of cachexia had a negative relationship with body weight loss in all MIN mice (Table 2.3); SOCS3 expression and STAT3 activation exhibited strong negative relationships with percent body weight loss. Interestingly, only P38 activation and COX activity were related to muscle mass in all MIN mice.

Whole-body fatigability in tumor-bearing mice

We have previously reported decreased voluntary wheel running and grip strength throughout the progression of cachexia in MIN mice (Baltgalvis 2010). We have extended these prior findings by measuring time to exhaustion as a measure of whole-body fatigability using a graded treadmill exercise test in MIN and age matched WT mice. Both MIN-CX (>5% BW loss, n=7) and MIN-WS (<5% BW loss, n=5) had decreased (77% and

43%, respectively) exercise capacity compared to WT controls (Figure 2.2a). There was no difference between 12-week *Apc*$^{Min/+}$ (MIN-12) mice and age-matched WT, indicating the deficit in fatigue was not inherent to the genotype (Figure 2.2a).

Skeletal muscle fatigability in tumor-bearing mice

TA muscle fatigability was determined using an intermittent fatigue protocol *in situ*. TA fatigability was increased in the MIN compared to WT (Figure 2.2b). Interestingly, when MIN mice were stratified by body weight loss no difference was observed in muscle fatigability between MIN-CX and MIN-WS mice (Figure 2.2b). We also observed no difference in muscle fatigability between MIN-12 and age-matched WT, indicating the deficit in muscle fatigability was not to the genotype. Plasma IL-6 demonstrated a trend ($p=0.07$) for a relationship with muscle fatigue in all MIN mice; however, muscle fatigability was not significantly related to any other measured cachexia indices (Table 2.4, 2.5). Interestingly, COX activity, a surrogate for oxidative metabolism, was not related to skeletal muscle fatigability indicating fatigue may be present prior to decrements in muscle oxidative metabolism. However, it should be noted that COX activity analysis was performed in the EDL instead of the TA.

Skeletal muscle force through the progression of cachexia

TA maximal tension (P_o) was reduced 41% in MIN-CX compared to MIN-WS and 42% compared to WT (Figure 2.3c). Interestingly, a loss in force production was observed at lower frequencies (e.g., 80 Hz) (Figure 2.3a). Furthermore, there was an increase in the percent maximal tetanic force at 10, 30 and 50 Hz, which is indicative of a slower contractile phenotype in MIN-CX (Figure 2.3b). The reduction in P_o was related strongly to STAT3 activation in MIN mice (Figure 2.3d). P_o also had a strong relationship with

SOCS3 mRNA in MIN mice (Figure 2.3e). Due to the loss of muscle mass, we examined specific tension ($_sP_o$) to correct for alterations in muscle size. $_sP_o$ was reduced 14% in MIN-CX compared to MIN-WS and 21% compared to WT (Figure 2.4c). MIN-CX also displayed alterations in $_sP_o$ at both low (50 Hz) and higher stimulation frequencies (200-300 Hz) (Figure 2.4a). Similar to P_o, % of maximal specific tetanic force was increased at 10, 30 and 50Hz in MIN-CX (Figure 2.4b). The negative relationship between STAT3 activation and P_o was not present when adjusted for muscle CSA (Figure 2.4d); however, the negative relationship between SOCS3 and P_o remained when adjusting for muscle CSA (Figure 2.4e).

We then examined the relationship between indices of cachexia and maximal force (Table 2.4). We observed a strong relationship between body weight loss and both P_o and $_sP_o$, as well as a strong relationship between testes mass (White JP 2013) and P_o, but this was lost when we corrected for muscle CSA. In addition to the relationships between P_o with STAT3 activation and SOCS3 mRNA, P_o was negatively related to P65 and P38 activation, TNF-α mRNA, and EDL COX activity (Table 2.4). Notably, the negative correlation between P65 activation and $_sP_o$ was strengthened when corrected for muscle CSA (Table 2.4). While several indices of cachexia had strong relationships to reduced P_o (Table 2.4), stepwise regression analysis determined that percentage body weight loss and the relative TA mass were both significant predictors of reduced P_o in MIN mice (Table 2.5). Interestingly, stepwise regression analysis also identified P65 activation as a significant predictor for reduced $_sP_o$ in MIN mice (Table 2.5).

Cachectic skeletal muscle contractile properties

Twitch and tetanic contractile characteristics were examined to better determine cachectic skeletal muscle contractile phenotype. One-half (1/2) relaxation time (1/2 RT) was increased 19% in Min-CX compared to MIN-WS and 19% compared to WT (Figure 2.5a). Furthermore, the rate of relaxation from tetanus, -dP/dt, was reduced 49% in MIN-CX compared to MIN-WS and 67% compared to WT (Figure 2.5c). There was a trend for a relationship between ½ RT and STAT3 activation ($p=0.07$) in all MIN mice (Table 2.6). Interestingly, SOCS3 mRNA expression was not related to ½ RT (Table 2.6). Stepwise regression analysis demonstrated that percent body weight loss and SOCS3 mRNA expression were significant predictors of reduced ½ RT in MIN mice. There was a strong negative relationship with –dP/dt and STAT3 as well as SOCS3 (Table 2.4); however, percent body weight loss was the only significant predictor of reduced –dP/dt (Table 2.5). Time to peak twitch (TPT) was increased 15% in MIN-CX compared to MIN-WS and 15% compared to WT (Figure 2.5b). TPT was related to STAT3 activation (Table 2.6); however, only TNF-α emerged as the only predictor for the decrements to TPT (Table 2.7). The rate of rise to tetanus, +dP/dt, was reduced 35% in MIN-CX compared to MIN-WS and 55% compared to WT (Figure 2.5d). A negative relationship existed between +dP/dt and STAT3 activation (Table 2.4) as well as SOCS3 mRNA expression (Table 2.4). Stepwise regression analysis identified TA weight as a significant predictor of reduced +dP/dt in MIN mice (Table 2.5). We found no difference in twitch tension ($_tP_o$) between any groups (Figure 2.7a). Similarly, neither STAT3 activation nor SOCS3 mRNA was related to $_tP_o$ (Table 2.6).

Calcium handling gene expression

Based on the observations demonstrating a slower contractile phenotype (Figures 2.3c, 2.4c, 2.5a, 2.5b, 2.6a, and 2.6b), we investigated the gene expression of key calcium handling proteins, Sarco(endo)plasmic Reticulum Calcium ATPase (SERCA) 1, Ryanodine Receptor (RyR) 1, and Calsequestrin (Figure 2.6). SERCA1 gene expression was increased 1.4-fold in MIN-CX muscle compared to both MIN-WS and WT. RyR1 gene expression was increased 1.3-fold in MIN-CX compared to MIN-WS and 1.6-fold compared to WT. Lastly, Calsequestrin gene expression was increased in MIN-CX (3.1-fold) and MIN-WS (2.2-fold) compared to WT; however, no significant difference between MIN-CX and MIN-WS was found.

2.5 – Discussion

The current study aimed to improve our understanding of cachectic muscle's functional decrements and illuminate potential contributing factors. While cachectic skeletal muscle force, fatigability, and inflammatory signaling have all been studied, the lack of a cohesive integration of these measurements has limited the possible conclusions to a role in the pathogenesis of muscle dysfunction with cancer (al-Majid and McCarthy 2001a; Baltgalvis 2010; Christensen et al. 2014; Murphy et al. 2012; Roberts, Frye, et al. 2013; White, Baltgalvis, et al. 2011; White et al. 2012). Therefore, the primary goal of this study was to examine the functional properties of skeletal muscle during the development of cachexia and determine their relationship to the systemic and intrinsic regulators of the cachectic muscle phenotype. This study demonstrates that a slow-fatigable contractile phenotype develops during the progression of cachexia similar to what has been previously

reported in other cachexia models (Jaweed et al. 1983; Murphy et al. 2012; Roberts, Frye, et al. 2013; Gorselink et al. 2006). However, we have extended these findings by demonstrating functional changes have a strong relationship with intrinsic muscle inflammatory signaling. We also report the novel finding that muscle fatigability was increased before significant cachexia development. Unexpectedly, we found no relationship between increased muscle fatigability and systemic IL-6 levels in male MIN mice.

Along with muscle mass, fatigue is a strong predictor of survival in cancer patients (Vigano et al. 2000; Christensen et al. 2014). Determining whether this fatigue is due to neural, humoral, or musculoskeletal alterations remains a consistent barrier in cancer and cachexia research. The present study provides evidence to support a direct role for skeletal muscle in cancer fatigue development before the onset of cachexia. Cachectic skeletal muscle has been reported to have disrupted metabolic homeostasis, which may contribute to muscle-specific fatigue. Our lab has previously found disrupted mitochondrial quality control (decreased content and biogenesis, disrupted dynamics, etc.) in MIN muscle (White et al. 2012; Carson, Hardee, and VanderVeen 2016), which coincides with decreased physical activity (Baltgalvis 2010). Decrements in mitochondrial biogenesis and mitochondrial content have been strongly associated with increased fatigue in skeletal muscle (Lin et al. 2002; Brown et al. 2017). The results of this study further extend this work by showing decreased COX activity in cachectic MIN muscle. Unexpectedly, MIN mice that were not cachectic exhibited increased whole body and muscle fatigue that preceded elevated inflammatory signaling. *Ex vivo* muscle function has also demonstrated increased fatigability in C26 mice (Roberts, Frye, et al. 2013), but the relationship with

weight loss or inflammation was not determined. However, additional research is needed to determine the contribution of alterations in the neuromuscular junction and muscle blood flow to functional decrements with cachexia, as these can occur with aging and chronic disease (Rudolf, Deschenes, and Sandri 2016). To this end, we demonstrated that tumor-bearing mice, independent of weight loss, experienced increased fatigue measured by whole body exercise and *in situ* muscle function, which was not related to elevated circulating IL-6, activated muscle inflammatory signaling, or COX activity.

Examining skeletal muscle's contractile properties provides important information on alterations to muscle function and phenotype with aging, disease, and disuse (Fitts and Holloszy 1977; Fitts et al. 1984; Brooks and Faulkner 1988; Barreiro and Gea 2015; Berchtold, Brinkmeier, and Muntener 2000; Widrick et al. 2001; Wolfe 2006). Skeletal muscle twitch characteristics depend on neural excitation, sarcomeric structure, calcium handling, and myosin isoform expression (Close 1972; Schiaffino and Reggiani 1996; Khodabukus and Baar 2015). One potential explanation for the slower twitch properties could be a shift in fiber-type distribution. It is generally accepted that preferential atrophy of type II occurs during cachexia, particularly at the early stages of wasting. Interestingly, we have previously demonstrated a loss of fiber-types (IIB , IIX, and IIA) in the TA of cachectic MIN mice, which coincided with the percent of myofibers with high succinate dehydrogenase enzyme activity (Hardee et al. 2016). Thus, the loss of fiber atrophy and metabolic dysfunction could contribute to the disrupted contractile phenotype during severe cachexia and should be explored in future investigations. Classically, twitch relaxation is dependent on the rate of calcium reuptake by the Sarcoplasmic Reticulum Calcium ATPase (SERCA) after stimulation (Close 1972; Berchtold, Brinkmeier, and

Muntener 2000). The modifications of SERCA expression and function by cachexia remain a largely untapped area of study. Previous reports have shown increased expression of SERCA1 and SERCA2 in the gastrocnemius and EDL, respectively, which was hypothesized to be indicative of leaky calcium channels resulting in aberrant calcium handling thought to contribute to mitochondrial dysfunction, EC uncoupling, and fatigue (Debold 2016; Fontes-Oliveira et al. 2013; Carson, Hardee, and VanderVeen 2016). Consistent with this notion, ½ relaxation time (RT) is increased in the EDL and soleus in tumor-bearing mice (Roberts, Frye, et al. 2013; Jaweed et al. 1983). We extend these findings by demonstrating that the decreased rate of relaxation (-dP/dt) was related to the development of cachexia. Moreover, the decline in -dP/dt was associated with body weight loss, muscle mass, and the activation of STAT3 and P38. Lastly, we also found disrupted expression of key proteins related to skeletal muscle calcium release and uptake. The results from this study identify a strong rationale for investigating calcium release and reuptake by the SR in cachectic muscle and its role in disrupted muscle function.

A fundamental characteristic of skeletal muscle is the capacity to produce force, which is related to muscle size and cross-sectional area (Close 1972; Bodine et al. 1987; Brooks and Faulkner 1988). The specific tension produced by muscle, force per unit area, has been a principal parameter for establishing muscle structural integrity (Burkholder et al. 1994; Brooks and Faulkner 1988; Barreiro and Gea 2015). While reduced specific tension has been reported previously in cachectic muscle from LLC tumor-bearing mice (Roberts, Frye, et al. 2013), others have reported no change in C-26 tumor-bearing mice (Murphy et al. 2012). These equivocal results are likely related to the muscle tested, degree and duration of cachexia, and heterogeneity related to the model and tumor type. Specific

tension can be negatively impacted by expansion of the extracellular matrix, which involves connective tissue deposition and/or edema. We have previously reported increased non-contractile tissue in MIN-CX, which did not appear to be associated with regeneration or degeneration (Hardee et al. 2016). Additionally, edema serves to decrease muscle protein concentration, which has not been found in MIN-CX mice (Mehl KA 2005). However, we found that indices of muscle inflammation were associated with reduced specific tension in cachectic muscle. Circulating inflammatory factors are widely investigated for their role in cancer cachexia; however, in non-tumor-bearing mice TNF-α overexpression was demonstrated to decrease muscle force through the activation of MuRF1 through P65 (Adams et al. 2008). While elevated MurF1 and P65 have been reported, elevated circulating TNF-α has not been shown in the MIN (Mehl KA 2005). Furthermore, we have previously demonstrated that repeated bouts of eccentric muscle contraction can attenuate the induction of muscle non-contractile tissue in MIN mice that have initiated wasting (Hardee et al. 2016). There is a strong justification for further examination of muscle inflammatory signaling's role in the induction of non-contractile tissue to decrease force independent of mass in the cachectic muscle and to further understand the beneficial effects of muscle contractions or physical activity on these processes.

In summary, our study demonstrates that multiple functional deficits that occur with cancer cachexia are associated with increased muscle inflammatory signaling, and this includes the development of a slow-fatigable contractile phenotype. Although the mechanistic regulators of this phenotype require further investigation, our findings provide a rationale for examining specific inflammatory signaling pathway regulation of muscle

function. Notably, muscle fatigability is increased in the MIN mouse before cachexia development. Additional research extending our mechanistic understanding of the underpinnings of cachectic muscle's functional decrements should provide valuable information for the development of efficacious treatments for this wasting syndrome.

Table 2.1. Characteristic data of ~20-week-old male MIN and WT mice.

	WT	MIN
n	10	16
Age	20.3 ± 0.8	20.9 ± 0.5
Peak Body Weight (g)	26.7 ± 0.5	25.4 ± 0.5
Final Body Weight (g)	26.7 ± 0.5	22.8 ± 1.0
BW Change from Peak (%)	0.0 ± 0.0	-10.6 ± 2.3^
Hindlimb Muscle (mg)	206 ± 5	161 ± 11^
Testes (mg)	196 ± 5.0	152 ± 12^
Epididymal Fat (mg)	396 ± 18	93 ± 29^
Spleen (mg)	67 ± 3	423 ± 34^
Tibia Length (mm)	16.8 ± 0.1	16.9 ± 0.0

Values are means ± SE. Body weights given in grams (g). Percent (%) loss determined from peak weight to weight prior to sacrifice. All tissue weights expressed in milligrams (mg). C57BL/6 (WT). *Apc*$^{Min/+}$ (MIN). ^Significant from WT. $p<0.05$ (t-test).

Table 2.2. Characteristic data of male MIN mice stratified by body weight loss.

	MIN-WS	MIN-CX
n	7	9
Age	21.8 ± 0.6	20.0 ± 0.6
Peak Body Weight (g)	27.0 ± 0.6	24.1 ± 0.4*
Final Body Weight (g)	26.8 ± 0.6	19.7 ± 0.4*
BW Change from Peak (%)	-0.9 ± 0.4	-18.3 ± 0.9*
Hindlimb Muscle (mg)	201 ± 5	127 ± 9*
Testes (mg)	194 ± 5	118 ± 13*
Epididymal Fat (mg)	212 ± 20	0 ± 0*
Spleen (mg)	384 ± 65	453 ± 21
Tibia Length (mm)	16.9 ± 0.0	16.8 ± 0.1

Values are means ± SE. Body weights given in grams (g). % loss determined from Peak weight to weight prior to sacrifice. All tissue weights expressed in milligrams (mg). Male *Apc*$^{Min/+}$ mice were stratified by weight loss, 0-5% loss (MIN-WS), 5-20% loss (MIN-CX). *Significant from MIN-WS. $p<0.05$ (t-test).

Table 2.3. Relationship between body weight loss, muscle mass, and cachexia indices in ~20-week-old male MIN mice.

Cachexia Indices	**TA weight**	**BW loss**
Plasma IL-6	-0.53	-0.46
STAT3	-	-0.78*
P65	-0.44	-0.55*
Erk 1/2	-0.49	-0.47*
P38	-0.77*	-0.74*
SOCS3 mRNA	-	-0.76*
IL-6 mRNA	-0.28	-0.44
IL-1β mRNA	-0.41	-0.42
TNF-α mRNA	-0.37	-0.52*
COX Activity^	0.68*	0.64*

Values are Pearson's correlation (R). Values used for STAT3, P65, Erk 1/2, and P38 are ratios of phosphorylated to total protein expression. †analysis done in the Extensor Digitorum Longus *Significant correlation $p<0.05$. Tibialis anterior (TA). Body weight (BW).

Table 2.4. Relationship between the force and fatigability of the tibialis anterior and indices of cachexia in ~20-week-old male MIN mice.

Cachexia Indices	**Fatigue**	**P_o**	**$_sP_o$**	**-dP/dt**	**+dP/dt**
Plasma IL-6	-0.56	-0.48	-0.10	-0.39	-0.33
BW Loss	0.01	0.93*	0.60*	0.86*	0.87*
Spleen/BW	0.26	-0.62*	-0.36	-0.48	-0.64*
TA/BW	-0.18	0.72*	0.01	0.63	0.66*
Testes	0.11	0.85*	0.21	0.75*	0.85*
Cachexia Indices in Skeletal Muscle					
STAT3	-	-	-	-0.64*	-0.73*
P65	0.28	-0.62*	-0.71*	-0.66*	-0.51*
Erk 1/2	-0.48	-0.44	-0.09	-0.35	-0.42
P38	0.05	-0.73*	-0.34	-0.62*	-0.73*
IL-6 mRNA	-0.08	-0.41	-0.48	-0.41	-0.26
SOCS3 mRNA	-	-	-	-0.72*	-0.58*
IL-1β mRNA	0.01	-0.41	-0.14	-0.43	-0.20
TNF-α mRNA	-0.03	-0.47*	-0.41	-0.47	-0.46*
COX Activity†	-0.08	0.65*	0.20	0.54*	0.63*

Values are Pearson's correlation (R). Values used for STAT3, P65, Erk 1/2, and P38 are ratios of phosphorylated to total protein expression. †analysis done in the Extensor Digitorum Longus *Significant correlation $p<0.05$. Absolute Force (P_o). Specific Force ($_sP_o$). Rate of Relaxation (-dP/dt). Rate of Rise (+dP/dt). Tibialis anterior (TA). Body weight (BW).

Table 2.5. Regression analysis of force and fatigability of the tibialis anterior and indices of cachexia in ~20-week old male MIN mice.

	β	SE	Partial R^2	Model R^2	*P value*
Fatigue (%)					
-	-	-	-	-	-
P_o (mN)					
BW Loss (%)	2850	340.8	0.87	0.87	<0.001
TA/ BW (mg/g)	498	158.1	0.06	0.93	0.008
$_sP_o$ (kN/m^2)					
P65	-51.2	13.5	0.51	0.51	0.002
-dP/dt (mN/ms)					
BW Loss (%)	38462	6189	0.73	0.73	<0.001
+dP/dt (mN/ms)					
TA Weight (mg)	324	47.9	0.77	0.77	<0.001

β is the estimated regression coefficient. Standard Error of β (SE). Body weight (BW). Tibialis anterior (TA). Phosphorylated to total ratio of P65 (P65). Absolute force (P_o). Specific force ($_sP_o$). Rate of relaxation (-dP/dt). Rate of rise (+dP/dt). Functional outcomes (dependent variable) are italicized. Significant ($p<0.05$) predictors (independent variables) obtained from stepwise linear regression models that included 16 variables are shown in bold for each functional outcome. Other variables that were not significant were removed from the model

Table 2.6. Relationship between the twitch properties of the tibialis anterior and indices of cachexia in ~20-week-old male MIN mice.

Cachexia Indices	**1/2 RT**	**TPT**	**$_tP_o$**
Plasma IL-6	0.27	0.44	0.27
BW Loss	-0.52*	-0.63*	-0.52*
Spleen/BW	0.34	0.49*	0.34
TA/BW	-.22	-0.18	-0.22
Testes	-0.44	-0.43	0.24
Cachexia Indices in Skeletal Muscle			
STAT3	0.45	0.57*	-0.35
P65	0.22	0.43	0.22
Erk 1/2	0.26	0.32	0.26
P38	0.37	0.48	0.37
IL-6 mRNA	-0.25	-0.15	-0.25
SOCS3 mRNA	0.02	0.19	-0.44
IL-1β mRNA	-0.13	0.04	-0.13
TNF-α mRNA	0.38	0.64*	0.38
COX Activity†	-0.04	-0.23	0.51*

Values are Pearson's correlation (R). Values used for STAT3, P65, Erk 1/2, and P38 are ratios of phosphorylated to total protein expression. †analysis done in the Extensor Digitorum Longus *Significant correlation $p<0.05$. 1/2 Relaxation Time (1/2 RT). Time to Peak Twitch (TPT). Peak twitch ($_tP_o$) Tibialis anterior (TA). Body weight (BW).

Table 2.7. Regression analysis of twitch properties of the tibialis anterior and indices of cachexia in ~20-week old male MIN mice.

	β	SE	Partial R^2	Model R^2	*P value*
1/2 RT (ms)					
BW Loss (%)	-27.8	5.89	0.29	0.29	0.033
SOCS3 mRNA	-0.19	0.05	0.35	0.63	0.004
TPT (ms)					
TNF-α mRNA	6.90	2.20	0.41	0.41	0.007
$_tP_o$ *(mN)*					
COX Activity	17.9	7.99	0.26	0.26	0.042

β is the estimated regression coefficient. Standard Error of β (SE). Body weight (BW). 1/2 Relaxation time (1/2 RT). Time to peak twitch (TPT). Peak twitch ($_tP_o$). Functional outcomes (dependent variable) are italicized. Significant ($p<0.05$) predictors (independent variables) obtained from stepwise linear regression models that included 16 variables are shown in bold for each functional outcome.

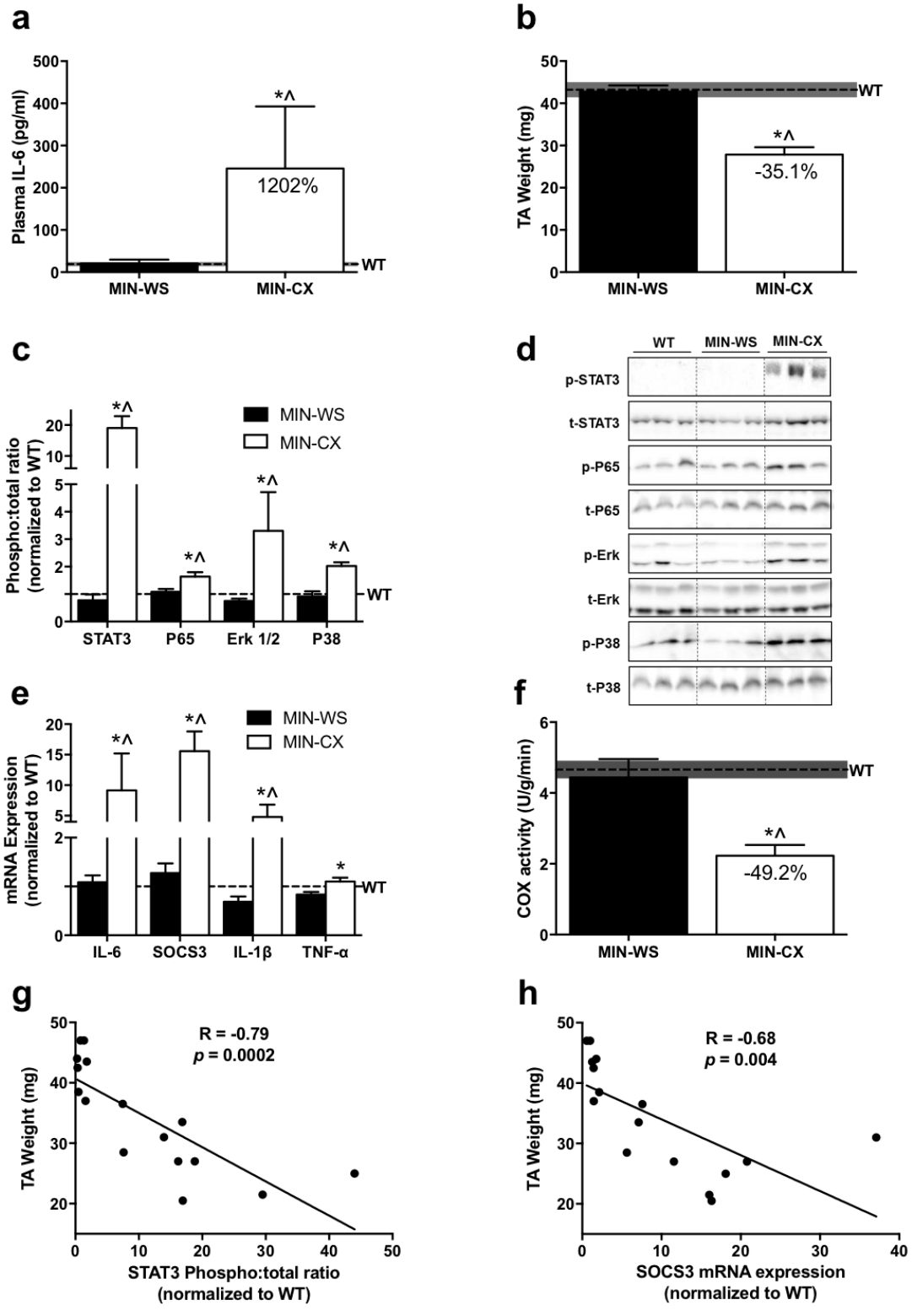

Figure 2.1 Indices of cachexia in MIN mice. (A) Plasma levels of IL-6 in picograms per milliliter (pg/mL). B) Tibialis Anterior (TA) weight in milligrams (mg). Grey shading represents the SE of WT. C) The ratio of phosphorylated to total protein expression of key inflammatory signaling proteins STAT, P65, Erk 1/2, and P38 in the TA from MIN-WS and MIN-CX normalized to WT. D) Representative western blot images of phosphorylated (p) and total (t) protein expression of inflammatory proteins in the TA. Dotted lines indicate where blots were cropped for representation. (E) mRNA expression of IL-6, SOCS3, IL-1β, and TNF-α in the TA from MIN-WS and MIN-CX normalized to WT. F) Cytochrome C oxidase (COX) activity assay in the Extensor Digitorum Longus. Grey shading represents the SE of WT. G) Pearson's correlation between TA weight and STAT3 activation in all MIN mice. H) Pearson's correlation between TA weight and SOCS3 mRNA in all MIN mice. Values are means ± SE. *Significant from MIN-WS. ^Significant from WT. Significance was set at $p<0.05$

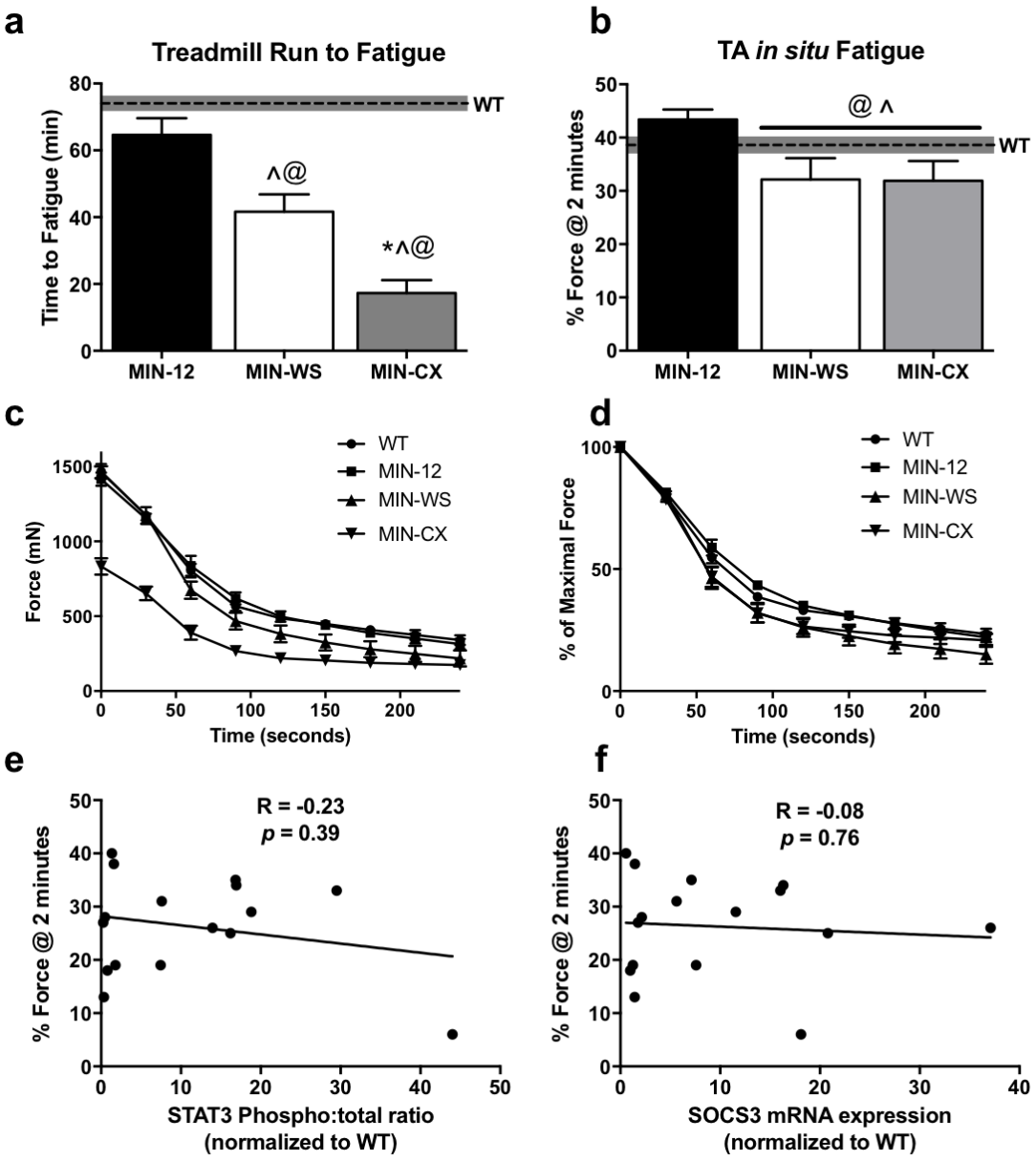

Figure 2.2 The effect of cachexia on whole body and muscle specific fatigue. (A) Treadmill time to fatigue in MIN-WS, MIN-CX, and MIN-12 compared to WT. (B) *In situ* muscle fatigability shown as % of maximal tension after 2 minutes of an intermittent fatigue protocol. (C) Absolute force over the duration of the intermittent fatigue protocol. (D) Relative (%) force over the duration of the intermittent fatigue protocol. (E) Pearson's correlation between muscle fatigability and STAT3 activation in all ~20-week-old MIN mice. (F) Pearson's correlation between muscle fatigability and SOCS3 mRNA in all ~20-week-old MIN mice. Values are means ± SE. *Significant from MIN-WS. ^Significant from WT. [@]Significant from MIN-12. Significance was set at $p<0.05$

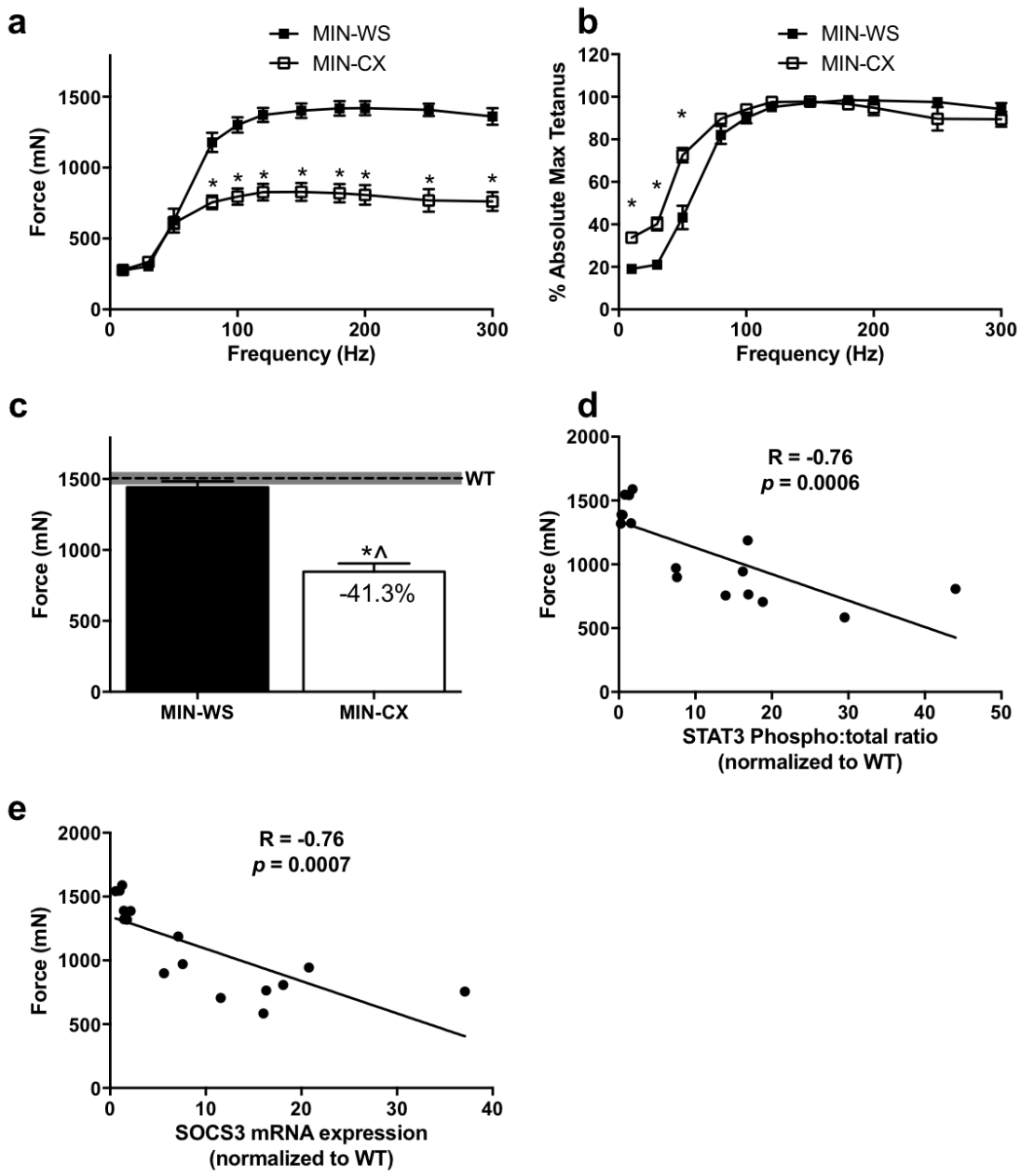

Figure 2.3 The effect of cachexia on maximal tetanic force. (A) *In situ* force-frequency curve of the TA in MIN-WS and MIN-CX. (B) Force-frequency curve relative to maximal force. (C) Absolute maximal tetanic force (P_o) of the TA in MIN-WS and MIN-CX. (D) Pearson's correlation between P_o and STAT3 activation in all ~20-week-old MIN mice. (E) Pearson's correlation between P_o and SOCS3 mRNA in all ~20-week-old MIN mice. Values are means ± SE. *Significant from MIN-WS. ^Significant from WT. Significance was set at $p<0.05$

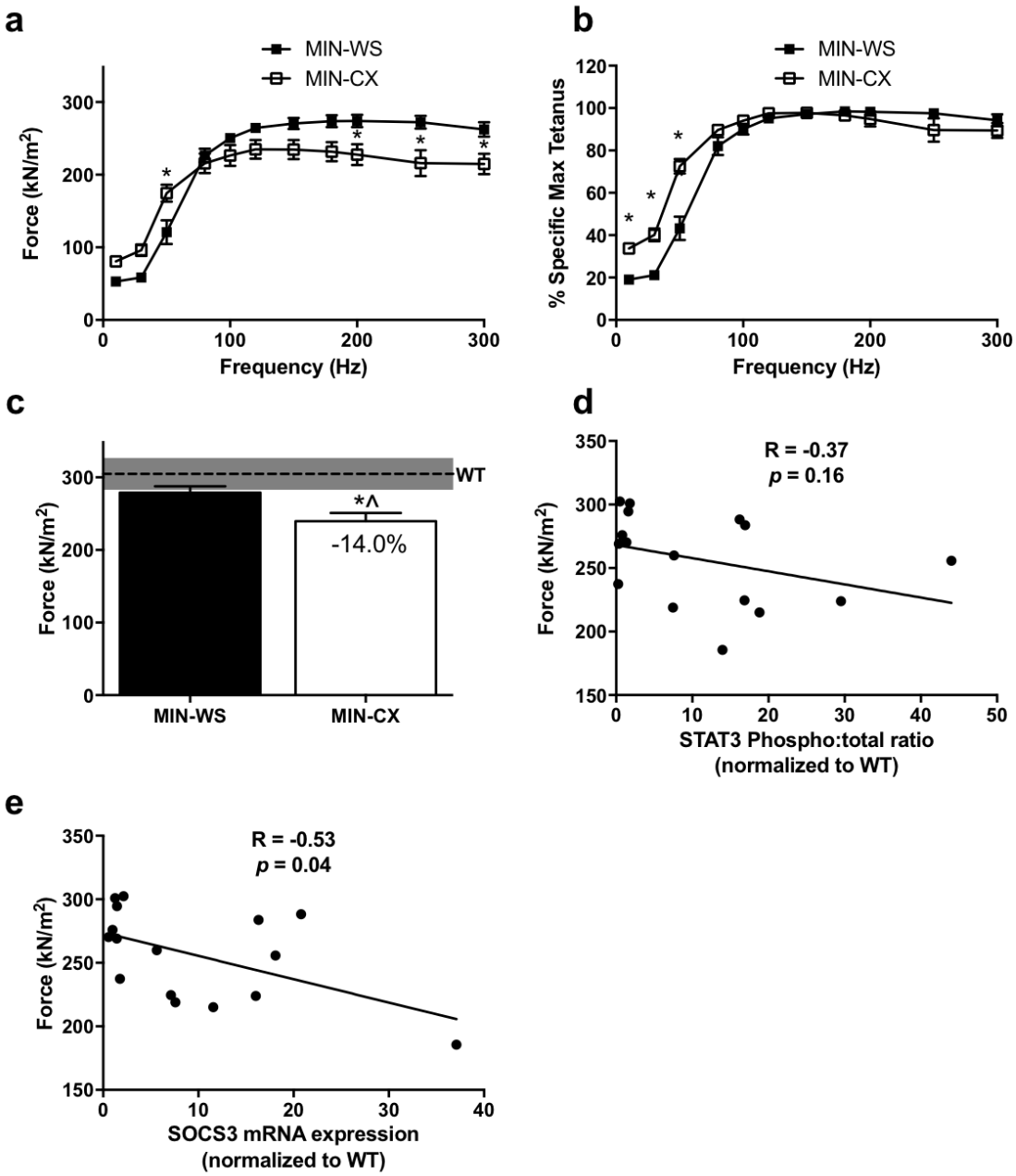

Figure 2.4 The effect of cachexia on specific tetanic force. (A) *In situ* force-frequency curve of the TA corrected for TA cross-sectional area (CSA) in MIN-WS and MIN-CX (kN/m^2). (B) Force-frequency curve relative to maximal force. (C) Specific tetanic force ($_sP_o$) of the TA in MIN-WS and MIN-CX. (D) Pearson's correlation between $_sP_o$ and STAT3 activation in all ~20-week-old MIN mice. (E) Pearson's correlation between $_sP_o$ and SOCS3 mRNA in all ~20-week-old MIN mice. Values are means ± SE. *Significant from MIN-WS. ^Significant from WT. Significance was set at $p<0.05$

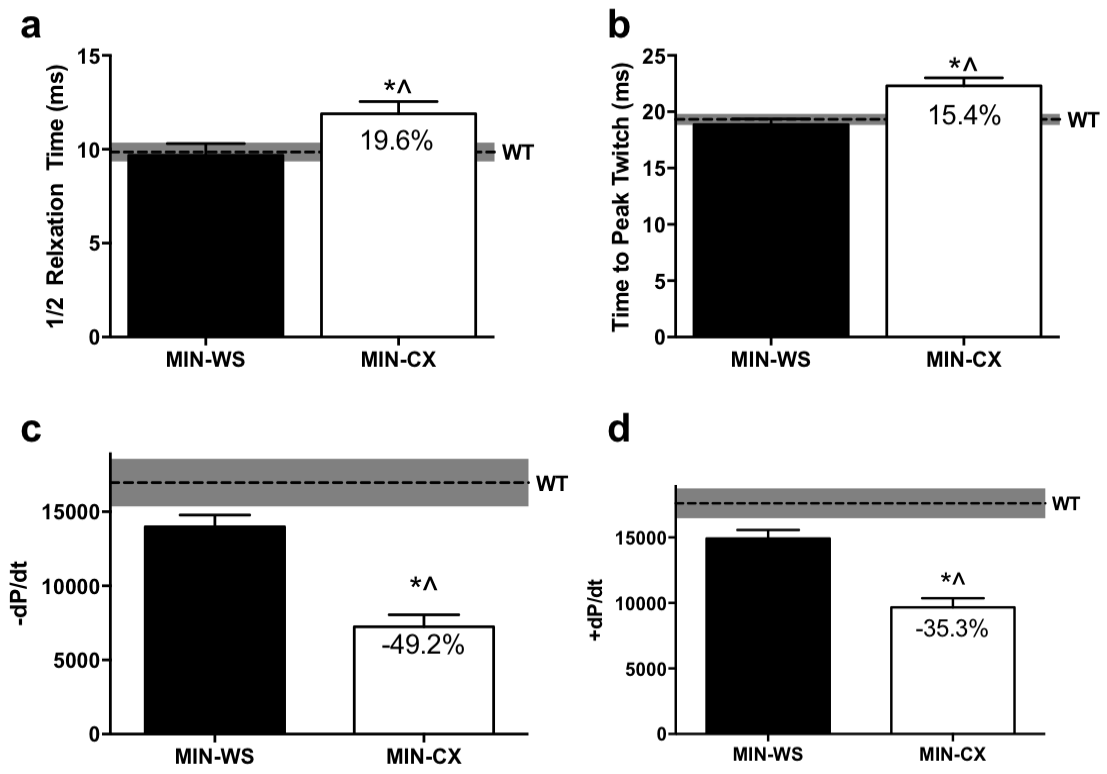

Figure 2.5 The effect of cachexia on the muscle force rates. (A) ½ Relaxation Time (RT) of TA muscle twitch at L_o in MIN-WS and MIN-CX. (B) Time to peak twitch (TPT) of TA muscle twitch at L_o in MIN-WS and MIN-CX. (C) Rate of relaxation (-dP/dt) of the TA muscle at 200 Hz. (D) Rate of rise (+dP/dt) of the TA muscle at 200 Hz. *Significant from MIN-WS. ^Significant from WT. Significance was set at $p<0.05$.

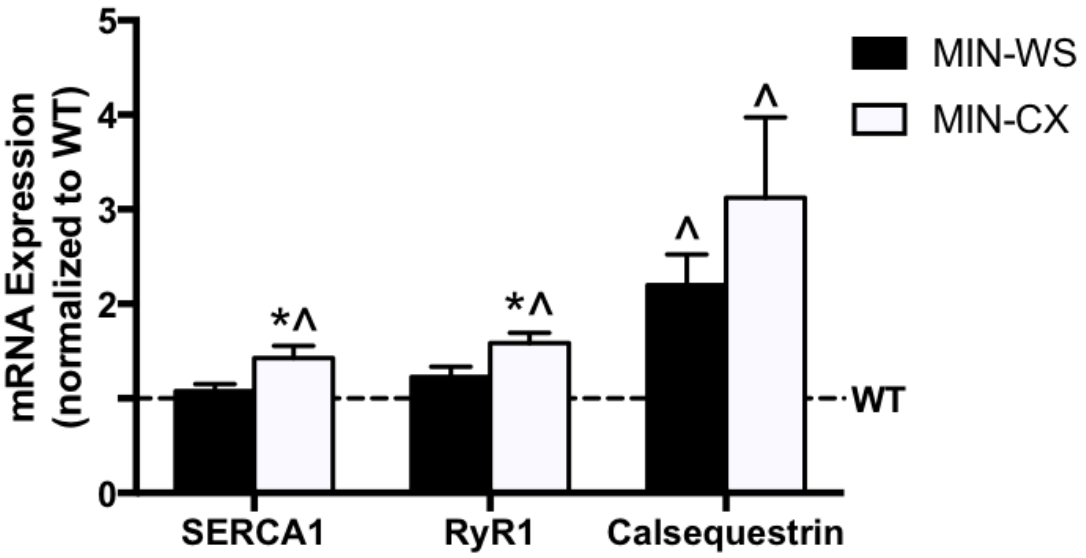

Figure 2.6 The effect of cachexia on calcium handling gene expression. mRNA expression of Sarco(endo)plasmic reticulum calcium ATPase 1 (SERCA1), Ryanodine Receptor 1 (RyR1), and Calciquestrin in the TA from MIN-WS and MIN-CX normalized to WT. *Significant from MIN-WS. ^Significant from WT. Significance was set at $p<0.05$.

CHAPTER 3

THE ROLE OF MUSCLE GP130 SIGNALING IN SKELETAL MUSCLE FATIGUE DURING THE PROGRESSION OF CACHEXIA

3.1 – Abstract

Interleukin-6 (IL-6) signaling through the muscle gp130 receptor regulates skeletal muscle mass and metabolism in physiological and pathological conditions. Elevated circulating IL-6 and associative muscle gp130 signaling have been linked to exercised-induced fatty-acid oxidation and glucose metabolism as well as cancer-induced metabolic dysfunction. Mitochondrial function has emerged as an intriguing regulator of inflammation induced skeletal muscle metabolic dysfunction. We have previously shown that elevated levels of circulating IL-6 decreased skeletal muscle mitochondrial protein expression in tumor-free mice and muscle gp130 signaling can regulate basal mitochondrial dynamics. Therefore, we investigated if chronically elevated systemic IL-6 was sufficient to disrupt skeletal muscle force, fatigue, and oxidative metabolism directly through muscle skeletal muscle gp130 signaling. Additionally, we investigated if loss of the muscle gp130 receptor could attenuate cancer-induced weakness and fatigue in a preclinical model of cancer cachexia. First, an IL-6 overexpression plasmid was electroporated into the quadriceps of male wildtype (WT) and skeletal muscle gp130 knockout (KO) mice. Next, *Apc*$^{Min/+}$ (MIN) mice were crossed with KO mice to obtain a MIN KO. The functional properties of the tibialis anterior (TA) were assessed *in situ*. IL-6 had no effect on body weight, muscle mass, force, or fiber-type in WT and KO mice.

Submaximal contraction-induced muscle fatigability was increased by IL-6 in WT but had no effect in the KO. IL-6 reduced TA respiration and COX activity associated with accelerated submaximal contraction-induced fatigue. MIN mice had reduced mitochondrial respiration which was rescued in the MIN KO. MIN mice had reduced muscle force and increased muscle fatigability; however, there was no effect of gp130 loss on muscle weakness or fatigue in the MIN. These results demonstrate that elevated IL-6 increased submaximal muscle fatigability and disrupted muscle oxidative metabolism through muscle gp130 signaling independent of body weight, skeletal muscle mass, or strength; however, the cancer environment does not appear to induce weakness and fatigue solely through the muscle gp130 receptor.

3.2 – Introduction

While cachexia is prevalent in patients with a variety of cancer types, cancer patients, independent of weight loss, suffer from functional limitations that negatively impact quality of life and survival (Montazeri 2009). Perceived fatigue and disrupted metabolic homeostasis occur with many chronic diseases and contribute to reduced life quality and poor prognosis (Sin and Man 2003; Deans and Wigmore 2005; Kuller et al. 2008; Vidt 2006). The difficulty in determining if the fatigue has central, peripheral, or musculoskeletal origins has served as a significant barrier to understanding fatigue's etiology. Fatigue remains the most frequently reported symptom in cancer patients (al-Majid and McCarthy 2001a; Chang et al. 2000; Kilgour RD 2010; Laird et al. 2011; Monga et al. 1997; Stewart, Skipworth, and Fearon 2006). Skeletal muscle fatigability, or the ability to sustain force over time, relies on several physiological phenomena, most notably,

adequate ATP production by mitochondrial respiration and glycolytic pathways and the accumulation of their metabolic biproducts (Holloszy and Booth 1976; Fitts and Holloszy 1977; Munkvik, Lunde, and Sejersted 2009; Thompson et al. 1992; Fitts 1994; Rutherford, Manning, and Newton 2016).

Independent of neural control, skeletal muscle force capacity primarily relies on muscle cross-sectional area (CSA, sarcomeres in parallel) and relative presence of non-contractile tissue (Close 1972). While there is significant overlap between the regulation of skeletal muscle force production and fatigability, they can be modulated independent of one another. For example, skeletal muscle mitochondrial dysfunction and increased fatigability have been demonstrated to occur independent of changes to muscle size and strength in tumor-bearing mice suggesting that cancer-induced muscle weakness and fatigue have distinct etiologies (VanderVeen et al. 2018; Brown et al. 2017). Classically, the contractile properties and fiber-type distribution has been associated with the muscle's fatigue properties; however, changes in mitochondrial respiration may regulate muscle function independent of changes in myosin heavy chain expression (Fitts 1994; Allen, Lamb, and Westerblad 2008; Westerblad and Allen 2003). The heterogeneity of skeletal muscle allows for differential recruitment patterns and functional properties of each fiber type (Westerblad and Allen 2003; Fitts and Holloszy 1977; Fitts 1994; Allen, Lamb, and Westerblad 2008; Altenburg et al. 2007; Close 1964; Close 1972). Higher percentages of type I or type IIa myosin ATPase isoform within a muscle has a slower, more oxidative, fatigue resistant phenotype, while higher percentage of type IIb/x myosin ATPase isoform results in a fast, more glycolytic, higher force production, fatigable phenotype (Fitts 1994; Westerblad and Allen 2003). While type I muscle fibers are susceptible to disuse atrophy

(Thomason and Booth 1990; Iqbal et al. 2013; Coyle et al. 1985), chronic inflammatory diseases such as cancer-induced muscle wasting have been associated with preferential atrophy of type II muscle fibers (Carson, Hardee, and VanderVeen 2016; Wang and Pessin 2013). The tibialis anterior (TA), which has primarily type II muscle fibers, has been shown to have increased muscle fatigability and reduced muscle force in tumor-bearing mice (VanderVeen et al. 2018; Murphy et al. 2012).

While tumor necrosis factor α (TNF-α) has been eloquently shown to disrupt skeletal muscle contractile function *in vivo* and *ex vivo* (Reid and Moylan 2011; Gilliam et al. 2011; Hardin et al. 2008; Reid, Lannergren, and Westerblad 2002; Li et al. 2000; Puppa, Gao, et al. 2014), the capacity for other inflammatory cytokines to disrupt skeletal muscle function has not been well described. The pleiotropic inflammatory cytokine interleukin-6 (IL-6) has been shown to be both pro- and anti-inflammatory and regulates several immune functions as well as whole-body metabolism during both physiological and pathological conditions (Carson and Baltgalvis 2010; Bonetto et al. 2011; Hardee, Counts, et al. 2018; Gao et al. 2017; Puppa, Gao, et al. 2014). IL-6 promotes intracellular signaling through binding to its receptor (IL-6r) which allows for its β subunit (glycoprotein 130; gp130) to homodimerize and activate downstream intracellular signaling (Garbers, Aparicio-Siegmund, and Rose-John 2015; Schwantner et al. 2004; Rose-John 2018). The anti-inflammatory nature of IL-6 contributes to the acute phase response and skeletal muscle's exercise adaptations, though chronically elevated IL-6 accelerates inflammation and contributes to several disease comorbidities including skeletal muscle wasting (Garbers, Aparicio-Siegmund, and Rose-John 2015; Carson and Baltgalvis 2010; Spate and Schulze 2004). While our understanding of IL-6 in exercise and disease has improved, whether the

detrimental effects of chronically elevated circulating IL-6 directly affect skeletal muscle through gp130-dependent mechanisms is currently unknown. We have previously shown that the TA is susceptible to IL-6 induced muscle wasting (Hardee, Fix, et al. 2018); whether IL-6 alone can disrupt the TA skeletal muscle function has not been determined.

The *Apc*$^{Min/+}$ (MIN) mouse is a preclinical model of Familial Adenomatous Polyposis in which there is a heterozygous nonsense mutation of the *adenomatous polyposis coli (apc)* gene. When the other copy of the *apc* gene is lost, they develop numerous intestinal polyps, or multiple intestinal neoplasia (Min). These mice initiate the devolvement of polyps around 4 weeks of age and continue until roughly 12 weeks of age at which the polyps increase in size rather than number. We have previously demonstrated that MIN mice initiate weight loss at roughly 16 weeks of age that progresses until 20-26 weeks of age. The progressive loss of muscle mass can be accelerated by systemic over expression of IL-6 and IL-6 null MIN mice did not lose body weight or muscle mass. While systemic IL-6's role in MIN-induced cachexia has been described, whether the tumor-burden in MIN mice initiates muscle wasting through direct muscle gp130 signaling or indirect mechanisms has not been established.

Systemic IL-6 overexpression can accelerate muscle mass loss in tumor-bearing mice, but the effects of IL-6 on skeletal muscle mass and function in tumor-free mice remains inconclusive (White et al. 2012; White, Baltgalvis, et al. 2011; Puppa et al. 2012). Mitochondrial function has emerged as an intriguing regulator of inflammation-induced skeletal muscle metabolic dysfunction (Boland, Chourasia, and Macleod 2013; Brown et al. 2017; Hardee et al. 2016; Carson, Hardee, and VanderVeen 2016). We have previously shown that 2 weeks of elevated circulating IL-6 decreased skeletal muscle mitochondrial

protein expression and loss of muscle gp130 signaling increased mitochondrial fission and reduced mitochondrial fusion in basal conditions (Fix et al. 2018; Puppa et al. 2012; Puppa, Gao, et al. 2014). Additionally, skeletal muscle fatigability has been demonstrated to occur synergistically with elevated muscle IL-6 transcription and increased plasma IL-6 levels immediately following exercise; however, a causal role for IL-6 to accelerate skeletal muscle fatigue has not been investigated. Furthermore, we have previously shown that gp130 expression is greater in the TA compared to the soleus and gastrocnemius suggesting greater IL-6 sensitivity in faster muscles (Puppa, Gao, et al. 2014). Interestingly, cancer-induced skeletal muscle weakness was associated with increased skeletal muscle STAT3 and SOCS3, two primary downstream targets of IL-6 (VanderVeen et al. 2018). The purpose of the current study was to determine if chronically elevated systemic IL-6 for two weeks was sufficient to disrupt skeletal muscle force, fatigue, and oxidative metabolism of the TA. Additionally, we examined if the muscle gp130 receptor mediates the effects of the systemic tumor burden on skeletal muscle. We hypothesized that chronically elevated circulating IL-6 can disrupt muscle oxidative metabolism and induce muscle weakness and fatigue through the activation of muscle gp130 signaling, and loss of the muscle gp130 receptor will mitigate the IL-6 and cachectic environments effects on skeletal muscle function.

3.3 – Methods

Animals

Male C57BL/6 mice were originally purchased from Jackson Laboratories and were bred at the University of South Carolina's Animal Resources Facility. Male mice on

a C57BL/6 background were bred with gp130$^{fl/fl}$ mice as previously described (Fix et al. 2018; Puppa, Gao, et al. 2014; Hardee, Fix, et al. 2018). Gp130$^{fl/fl}$ male mice were bred with Cre-expressing mice driven by myosin light chain (MLC), resulting in a skeletal muscle floxed gp130 heterozygote cre knockout mouse with a skeletal muscle specific deletion of gp130 (KO). An additional cohort was examined to investigate the role of muscle gp130 signaling in cancer-induced weakness and fatigue in tumor-bearing mice. gp130fl/fl mice were crossed with inducible Cre-expressing mice driven by human alpha skeletal actin (HSAcre/+) to develop an inducible gp130 KO mouse (iKO). Simultaneously, gp130 fl/fl mice were crossed with ApcMin/+ to produce a gp130 fl/fl ApcMin/+ (MIN). The resulting gp130 iKO and MIN were crossed to obtain an iKO-MIN mouse. Offspring were genotyped by using tail snips. All animals were group housed (<5 per cage) and kept on a 12:12-h light-dark cycle. All animals were fasted 5 hours prior to tissue collection. Mice were anesthetized with a ketamine-xylazine-acepromazine cocktail, and hindlimb muscles and select organs were carefully dissected and snap frozen in liquid nitrogen and stored at -80ºC until further analysis. All animal experiments were approved by the University of South Carolina's Institutional Animal Care and Use Committee.

IL-6 Overexpression

In vivo intramuscular electroporation of an IL-6 plasmid was performed to increase circulating IL-6 levels in mice as previously described (Hardee, Fix, et al. 2018; Hardee, Counts, et al. 2018; White et al. 2012). All mice were subjected to *in vivo* electroporation of the quadriceps muscle. Briefly, mice were electroporated with 50µg of the IL-6 plasmid driven by the CMV promoter, or empty control vector, into the quadriceps muscle. To accomplish this, mice were anaesthetized with a 2% mixture of isoflurane and oxygen (1

l/min), the leg was shaved, and a small incision was made over the quadriceps muscle. Fat was dissected away from the muscle, and the plasmid was injected in a 50-µl volume of phosphate-buffered saline (PBS). A series of eight 50-ms, 100-V pulses were used to promote uptake of the plasmid into myofibers, and then the incision was closed with a wound clip. Both vector control and IL-6 groups received the appropriate plasmid starting at 11 wk of age, and a second electroporation on the opposite leg was performed at 12 wk of age to maintain systemically elevated plasma IL-6 levels. The tibialis anterior (TA) and extensor digitorum longus (EDL) muscles used in the study were not subjected to electroporation. Mice were euthanized 2 weeks after the initial plasmid electroporation. A dose of 50 µg has been shown to increase circulating IL-6 levels similar to what's been observed with tumor-bearing mice (Hardee, Counts, et al. 2018; Puppa et al. 2012; White et al. 2012; Baltgalvis et al. 2008). Additionally, two weeks of elevated IL-6 was sufficient to accelerate cachexia in tumor-bearing mice and disrupt muscle metabolism in tumor-free mice (Puppa et al. 2012).

Plasma IL-6

Plasma IL-6 was quantified as previously published (Hardee, Fix, et al. 2018). Briefly, blood samples were centrifuged at 10,000 g for 10 min at 4°C. Plasma was collected and stored at -80°C until analysis. A commercially available IL-6 enzyme-linked immunosorbent assay kit was obtained from BD Biosciences (San Diego, CA). Briefly, a Costar clear 96-well plate (Corning, NY) was coated with IL-6 capture antibody and allowed to incubate overnight. The plate was then blocked with assay diluent buffer and IL-6 standards and plasma samples were added to the plate. The wells were then incubated with streptavidinhorseradish peroxidase reagent. After several washes, 3,3,5,5-

tetramethylbenzidine substrate was added, and the reaction was developed for 20 min. The reaction was stopped with sulfuric acid, and absorbance was measured. Samples that fell below the curve not reported; however, mice were given a Plasma IL-6 value of 7.8 pg/mL (low detection limit) for statistical analysis. All of the mice given the IL-6 plasmid fell within the detection limit.

Analysis of Muscle Function

In both experiments, mice were anesthetized with 2% isoflurane inhalation and anesthesia was maintained at 1.5 % isoflurane throughout the duration of the procedure (~1 hour). Functional analysis of the TA muscle *in situ*, which maintains the host nerve and blood supply, has been previously described (VanderVeen et al. 2018). After a 5-minute rest following a force-frequency response protocol, the TA was subjected to an intermittent fatigue protocol consisting of 0.5 second submaximal stimulation (50Hz) every second for 5 minutes for a total of 300 submaximal contractions. Immediately after the submaximal contractions, the TA was subjected to a maximal stimulation (200Hz) to elicit a maximal contraction. Fatigue was measure by the % reduction in maximal force following the 5-minute contraction protocol (Allen, Lamb, and Westerblad 2008; Fitts 1994). Disrupted fatigue properties were assessed as change in force throughout the force-time tracing (Crilly et al. 2016).

Immunohistochemistry for myosin heavy chain IIA, IIX, and IIB

Immunohistochemistry for myosin heavy chain (MHC) type IIa, IIx, and IIb was performed as previously described (Goodman et al. 2012). Transverse muscle sections (8μm) of the TA were blocked in 10% IgG Fab (Jackson Immunology) in PBS (5% BSA + 5% Triton X100) for 1 h at room temperature and then incubated overnight at 4°C with

primary antibodies [mouse IgG1 monoclonal anti-type IIa MHC (clone SC-71; 1:100) and mouse IgM monoclonal anti-type IIb MHC (clone BF-F3, 1:10). All MHC antibodies were obtained from the Developmental Studies Hybridoma Bank (University of Iowa, Iowa City, IA). Secondary antibodies (biotinylated anti-mouse IgG FITC, IgM AMCA; Thermo Fischer) were incubated with the sections for 1 hour at RT. Slides were air dried and covered in glycerol mounting medium containing DABCO and coverslipped. At least 8 random, non-overlapping digital images at 20X magnification were taken, and fibers stained positive or absent for MHC type IIa, IIx, and IIb were tabulated using imaging software (ImageJ; NIH). The analyses were performed by an investigator blinded to the treatment groups.

Cytochrome C Oxidase Activity

Cytochrome C Oxidase Activity was measured to determine changes in mitochondrial content across all groups. Due to tissue availability, the Extensor Digitorum Longus (EDL) muscle, a highly glycolytic muscle, was used. The whole EDL was homogenized in extraction buffer (0.1 M KH2P04/Na2HP04, 2 mM EDTA, pH 7.2) and cytochrome-c oxidase (COX) activity was determined by measuring the rate of oxidation of fully reduced cytochrome c at 550nm using Sigma Aldrich Kit (# CYTOCOX1)and spectrophotometer (Eppendorf) as previously described (VanderVeen et al. 2018).

Respiratory Control Ratio

Mitochondrial respiration was measured polarographically in a respiration chamber (Hansatech Instruments) maintained at 37°C as previously described (Kwon et al. 2015). A randomly selected cohort of 4 mice from each treatment group were used for analysis of mitochondrial function. A 7-10 mg piece of TA muscle was mechanically tweezed with

forceps under a dissecting microscope in ice-cold *buffer X* (60 mM K-MES, 35 mM KCl, 7.23 mM K2EGTA, 2.77 mM CaK2EGTA, 20 mM imidazole, 0.5 mM DTT, 20 mM taurine, 5.7 mM ATP, 15 mM phosphocreatine, and 6.56 mM MgCl2, pH 7.1). The fiber bundle was then incubated in 50uM saponin for 30 minutes and washed 3 times for 5 minutes in respiration buffer (105mM K-MES, 3mM KCl, 1mM EGTA, 10mM K2HPO4, 5mM MgCl2, 0.005mM Glutamate, 0.002mM Malate, 0.05% BSA, 20mM Creatine, pH 7.1). Fiber bundles were then placed into the oxygraph machine in 20mM creatine respiration buffer at 37 degrees and provided with 5mM of pyruvate and 2mM of malate. Two minutes following pyruvate and malate, 0.25mM of ADP was injected into the chamber to induce STATE 3 respiration for a duration of 5 minutes. 10ug/mL of Oligomycin was then injected to induce steady STATE 4 respiration for a duration of 10 minutes. Respiratory Control Ratio (RCR) was calculated by dividing STATE 3 by STATE 4 respirations.

Polyp counts.

At sacrifice, the intestines were excised, and intestinal sections were flushed with PBS, opened longitudinally, and flattened with a cotton swab. All sections were fixed in 10% buffered formalin (Fisher) for 24h. Formalin-fixed intestinal sections from all animals were rinsed in deionized water, briefly stained in 0.1% methylene blue, and counted by the same investigator who was blinded to the treatments. Polyps were counted under a dissecting microscope, using tweezers to pick through the intestinal villi and identify polyps. Polyps were categorized as <1mm, 1-2 mm, and >2mm for each segment (1-5) throughout the intestine.

Western blot analysis

Western blot analysis was performed as previously described (Fix et al. 2018). Briefly, the proximal portion of the TA muscle was homogenized, and protein concentration was determined using the Bradford standard curve method. Homogenates were fractionated on SDS-polyacrylamide gels and transferred to PVDF membrane. After the membranes were blocked, antibodies Total OXPHOS Cocktail (Abcam, Cambridge, United Kingdom), were incubated at dilutions of 1:5000 overnight at 4°C in 1% TBST milk. Anti-rabbit IgG-conjugated secondary antibodies (Cell Signaling Technology) were incubated with the membranes at 1:5000 dilutions for 1h in 1% TBST milk. Enhanced chemiluminescence developed by autoradiography was used to visualize the antibody–antigen interactions. Blots were analyzed by measuring the integrated optical density (IOD) of each band with ImageJ software (NIH, Bethesda, MD, USA).

Statistical analysis

Values are presented as means plus / minus standard error of the mean (SEM). A Bartlett's test was used to determine significantly different standard deviations ($p<0.05$). First, to understand the effects of IL-6, a pre-planned t-test was performed between WT and WT + IL-6. Second, to understand if IL-6 directly affects skeletal muscle, a Two-Way ANOVA was performed. If an interaction was observed a Tukey's multiple comparisons test was performed. A Pearson's correlation was run to determine a relationship between several properties of skeletal muscle function and key markers of muscle metabolic health. Significance was set at $p<0.05$.

3.4 – Results

The effect of IL-6 body weight and muscle mass

Circulating IL-6 was elevated at one- and two-weeks following electroporation in WT mice (Table 3.1). KO mice had higher levels of circulating IL-6 at both time points when compared to WT+IL-6 (WT+IL-6 range 15.6-371.0 pg/mL; KO+IL-6 range 99.1pg/mL, high-204.5pg/mL) and vector controls (Below the detection limit, 7.8 pg/mL). These levels were comparable to levels of tumor-bearing mice however lower than LPS (Copeland et al. 2005). While there was no effect on body weight or muscle weight, there was a main effect of IL-6 to reduce tibia length (Table 3.1). There was a main effect of KO to increase hindlimb mass by 3% (Table 3.1). There was no effect of IL-6 or KO on muscle weight when correcting for reduced tibia length. There was a main effect of IL-6 to increase spleen weight.

The effect of IL-6 on muscle oxidative metabolism

Mitochondrial function was assessed in a cohort of mice for each treatment group (n=4 per group). There was an interaction for WT+IL-6 to have a reduced respiratory control ratio (RCR) in the TA compared to all groups (Figure 3.1C). Reduced mitochondrial coupling in WT+IL-6 resulted from a reduction in STATE 3 respiration compared to all groups (Figure 3.1A), while no differences in STATE 4 respiration existed between groups (Figure 3.1B). Similarly, there was an interaction for WT+IL-6 to have reduced COX activity of the EDL (n=8 for each group) compared to all groups (Figure 3.2A). Protein analysis of mitochondrial complexes I-V demonstrated IL-6 reduced complex I, II, and IV expression in the TA of WT mice (Figure 3.2C). Interestingly, circulating levels of IL-6 demonstrated a strong trend to be negatively associated with COX

activity (R= -0.81, p=0.05) in WT+IL-6, but IL-6 was not associated with COX activity (R= -0.09, p=0.83) in KO+IL-6 mice.

The effect of IL-6 on skeletal muscle force production and cross-sectional area

There was no observed effect of IL-6 on muscle force production across all (10-200 Hz) frequencies during a force-frequency protocol in WT mice (Figure 3.3A). Furthermore, there was no effect of IL-6 or KO on maximal tetanic force (P_o; Table 3.2). Subsequent analysis of specific tension ($_sP_o$) showed no effect of IL-6 on force production across all (10-200 Hz) frequencies (Figure 3.3C). Specific tetanic force was reduced by muscle gp130 loss (Table 3.2). There was a main effect of KO to reduce $_sP_o$ by 8.7% regardless of IL-6 treatment (Table 3.2). Muscle twitch characteristics were not affected by IL-6 (Table 3.2); however, there was a main effect of KO to have 1/2 relaxation time reduced by 13.4% and time to peak twitch reduced by 5.6%. Additionally, there was a main effect of KO to have rate of contraction (change in force/change in time; +dP/dt) increased by 10.9% (Table 3.2). Fiber type frequency (i.e. type IIa, IIb or IIx) was not affected by IL-6 or muscle gp130 loss (Table 3.3).

The effect of IL-6 on skeletal muscle fatigability

There were no observed differences in maximal tetanic force following 5 minutes of submaximal contraction-induced fatigue; however, a preplanned t-test showed WT+IL-6 had reduced maximal tetanic force (mN) by 7% following 5 minutes of the submaximal contraction-induced fatigue compared to WT (Figure 3.4C). There was an interaction for WT+IL-6 to have reduced relative force by 18.5% and 18.0% following 90 seconds of a submaximal contraction-induced fatigue protocol compared to WT and KO+IL-6, respectively (Figure 3.4D).

The effect of gp130 loss on cachexia indices in tumor bearing mice

Our lab has previously shown that deletion of the muscle gp130 receptor in LLC tumor bearing mice was able to spare muscle mass without affecting tumor-burden (Puppa, Gao, et al. 2014). Deletion of the muscle gp130 receptor (Figure 3.5F) had no effect on plasma IL-6 levels in the MIN (Figure 3.5A). Additionally, there was no effect of KO on polyp number and size in the MIN (Figure 3.5B, C). There was no difference in body weight between all groups; however, there was a 2.4% difference in body weight loss between MIN Flox and Flox controls (Table 3.4). There was no difference in hindlimb mass between all groups (Table 3.4), but epididymal fat was reduced 77% in MIN Flox and 73% in MIN KO compared to Flox controls (Table 3.4).

The effect of gp130 loss on skeletal muscle function in tumor bearing mice

MIN mice have been demonstrated to exhibit skeletal muscle weakness, increased fatigability and disrupted twitch and contraction rates (VanderVeen et al. 2018). There was no difference in twitch 1/2 RT or TPT across all groups; however, rate of contraction (+dP/dt) was reduced 16% in MIN Flox and 13% in MIN KO compared to Flox controls (Table 3.5). Rate of relaxation (-dP/dt) was reduced 34% in MIN Flox and 29% in MIN KO compared to Flox controls (Table 3.5). As expected, MIN Flox mice had reduced maximal force by 21% (Figure 3.6B) compared to healthy Flox mice (Figure 3.6B). MIN KO was not different from MIN Flox but was reduced 17% compared to healthy Flox mice (Figure 3.6B). There was a trend ($p=0.10$) for specific force to be reduced by 11% in the MIN Flox compared to healthy Flox. There was no difference in specific force between MIN KO and all groups (Figure 3.6D). There was a 48%, 53%, and 64% reduction in maximal force following 300 submaximal contractions in Flox, MIN flox, and MIN KO,

respectively (Figure 3.7B). Comparatively, maximal force following fatigue is reduced by 29% and 44% in MIN flox and MIN KO, respectively, compared to Flox controls (Figure 3.7B). There was a 65%, 70%, and 76% reduction in maximal force following both 300 submaximal contractions and 300 maximal contractions in Flox, MIN flox, and MIN KO, respectively (Figure 3.7C). Comparatively, maximal force following fatigue is reduced by 30% and 41% in MIN flox and MIN KO, respectively, compared to Flox controls (Figure 3.7C).

The effect of gp130 loss on skeletal muscle mitochondria content, function, and quality control in tumor bearing mice

A key contributor to muscle fatigability and muscle mass maintenance with chronic disease is mitochondrial content, function, and quality control. There was no difference across all groups in muscle protein p/t AMPK, a key muscle energy stress sensor (Figure 3.8A). There was a 29% and 44% increase in muscle protein BNIP3 expression compared to Flox controls; however, there was no difference in Parkin or p62 expression (Figure 3.8B). There was a 24% reduction in PGC1α protein expression in MIN Flox compared to healthy Flox controls (Figure 3.8C). There was no difference in between MIN KO PGC1α protein expression and all groups. There was a 23% and 22% increase in DRP1 protein expression in MIN Flox and MIN KO, respectively, compared to Flox controls (Figure 3.8C). There was no difference in FIS1 protein expression between MIN Flox and all groups; however, FIS1 was reduced 24% in MIN KO compared to Flox controls (Figure 3.8C). There was no difference in MNF1 protein expression between MIN Flox and all groups; however, MFN1 protein expression was increased 18% in MIN KO compared to MIN Flox (Figure 3.8C). There was a 73% reduction in COXIV protein expression

compared to Flox controls (Figure 3.8E). COXIV protein expression was increased 2.6 fold in MIN KO compared to MIN Flox and was not significantly different from healthy Flox controls (Figure 3.8E). Surprisingly, cytochrome c protein expression was increased 46% and 32% in MIN Flox and MIN KO, respectively, compared to healthy Flox mice (Figure 3.8E). Lastly, there was a 40% reduction in RCR compared to Flox controls (Figure 3.8F). RCR was increased 69% increase in MIN KO compared to MIN Flox and was not significantly different from healthy Flox controls (Figure 3.8F).

3.5 – Discussion

IL-6 has an established role in exercise- and disease-induced changes to systemic and skeletal muscle metabolism (Wolf, Rose-John, and Garbers 2014; Lightfoot and Cooper 2016; Febbraio et al. 2004; Febbraio and Pedersen 2002). Although two weeks of IL-6 has been shown to accelerate cachexia in tumor-bearing mice and disrupt muscle metabolism in tumor-free mice (White et al. 2012), whether IL-6 disrupts mitochondrial function and muscle fatigability has not been measured. The current study investigated if chronically elevated systemic IL-6 was sufficient to disrupt skeletal muscle force, fatigue, and oxidative metabolism directly through muscle skeletal muscle gp130 signaling. Our results demonstrate that 2 weeks of elevated circulating IL-6 accelerated submaximal contraction-induced skeletal muscle fatigue of the TA muscle. Conversely, IL-6 was unable to induced submaximal fatigue in gp130 KO mice suggesting that IL-6 induced fatigue occurred through direct skeletal muscle gp130 activation. Additionally, our results demonstrated that 2 weeks of elevated IL-6 was sufficient to disrupt skeletal muscle oxidative metabolism and decrease mitochondrial content through gp130-dependent

signaling, mirroring the submaximal fatigue findings. While IL-6 was able to accelerate fatigue, the cancer environment does not appear to work through muscle gp130 signaling to induce weakness and fatigue, however cancer-induced muscle mitochondrial dysfunction was muscle gp130 receptor dependent.

While chronic inflammation is a nonspecific immune response, cytokines are inflammatory mediators that have been implicated in the progression of several diseases and associated comorbidities (Lightfoot and Cooper 2016; Deans and Wigmore 2005; Fearon, Glass, and Guttridge 2012; Zhou et al. 2016). In addition to tumor growth and development, elevated circulating IL-6 has been linked to disrupted protein turnover associated with cancer-induced muscle wasting (Cron, Allen, and Febbraio 2016; Carson and Baltgalvis 2010; Narsale and Carson 2014). IL-6 has been shown to regulate skeletal muscle metabolism through the activation of GLUT4 translocation and accelerated lipolysis (Cron, Allen, and Febbraio 2016). We have previously reported that IL-6 can reduce mitochondrial content in both tumor-free and tumor-bearing mice (Puppa et al. 2012). The current study extends these findings to suggest that elevated circulating IL-6 accelerates submaximal contraction-induced skeletal muscle fatigue. A potential mechanism for IL-6 regulation of fatigue is through the disruption of skeletal muscle metabolic homeostasis. Chronic activation of muscle AMPK and suppressed mitochondrial biogenesis can occur during cancer-induced muscle wasting (White et al. 2012; White et al. 2013). Here we report that elevated circulating IL-6 is sufficient to reduce muscle RCR, which is a strong indicator of mitochondrial function (Pettersen et al. 2017). Additionally, we found that IL-6 reduced COX activity suggesting a reduction in mitochondrial content. A recent study reported that weight stable and cachectic (>5% body weight loss) cancer

patients with elevated IL-6, had reduced nuclear factor erythroid 2-related factor 2 (Nrf2) expression associated with reduced antioxidant production (Brzeszczynska et al. 2016). Furthermore, Crilly et al. found that loss of Nrf2 alone was sufficient to reduce gastrocnemius force production during a submaximal contraction-induced fatigue protocol (Crilly et al. 2016).

Signaling through the skeletal muscle gp130 receptor has been an active area of investigation in disease-induced muscle wasting (Mihara M 2012; Miller et al. 2016; Puppa, Gao, et al. 2014). In this regard, constitutively activated STAT3, a direct downstream gp130 target, can inhibit myotube growth *in vitro* and induce muscle mass loss *in vivo* (Bonetto A 2012). In addition, increased STAT3 signaling can regulate mitochondrial respiration by disrupting the electron transport chain and increasing reactive oxygen species production (Carson, Hardee, and VanderVeen 2016; Wegrzyn et al. 2009). This is important because we recently found that skeletal muscle gp130 signaling can regulate protein expression related to basal mitochondria dynamics without affecting skeletal muscle fatigability (Fix et al. 2018). We extended these findings to demonstrate that the IL-6 disruption of submaximal contraction-induced skeletal muscle fatigue and oxidative metabolism are regulated through muscle gp130 signaling. Additionally, we show that loss of the muscle gp130 receptor was not able to suppress muscle STAT3 signaling or rescue skeletal muscle mass. Determining what other factors are contributing to increased muscle STAT3 activation and whether chronically elevated IL-6 directly effects skeletal muscle mitochondrial function via modulating STAT3 signaling is an intriguing area of future investigation.

IL-6 can also regulate the muscle macro- and microenvironment. IL-6 directly regulates fibroblast proliferation, liver glucose metabolism, lipolysis, and immune cell function (Narsale and Carson 2014; Lightfoot and Cooper 2016; Choi et al. 1994; Sundararaj et al. 2009; Cron, Allen, and Febbraio 2016; Febbraio et al. 2004; Pedersen et al. 2003). While the IL-6r is predominately expressed in hepatocytes, megakaryocytes, and leukocytes, the signal transducing gp130 β-subunit is detectable in every cell type (Wolf, Rose-John, and Garbers 2014). Interestingly, we report that the tumor-induced changes to submaximal and maximal contraction-induced skeletal muscle fatigability occur independent of muscle gp130 signaling. There is an established liver-skeletal muscle metabolic cross-talk involving lactate recycling and glucose availability which can alter muscle fatigue properties indirectly (Rui 2014). Similar studies examining systemic IL-6 overexpression showed IL-6 induced hepatic insulin resistance while having no effect on skeletal muscle insulin sensitivity (Glund and Krook 2008).

The results of the current study found that 2 weeks of systemic IL-6 overexpression had no effect on muscle mass or body weight, though regardless of treatment, gp130 loss resulted in increased muscle mass. IL-6 can regulate basal muscle protein synthesis and suppress the acute induction of protein synthesis by eccentric contraction (Hardee, Counts, et al. 2018; Gao et al. 2017); however, we observed no changes in muscle strength or contraction rates with IL-6 overexpression. Interestingly skeletal muscle lacking gp130 showed reduced specific tension, 1/2 RT, and TPT with no apparent effect on muscle fatigability which is similar to TNF-α overexpression (Reid, Lannergren, and Westerblad 2002). IL-6 also increased submaximal contraction-induced fatigue, which was not dependent on fiber type distribution or mass changes. Our results found that muscle

fatigability, force, and mass can be regulated independently, which points to muscle weakness and fatigue with chronic disease having distinct etiologies.

In summary, we report that chronically elevated IL-6 increased skeletal muscle fatigability and disrupted oxidative metabolism independent of fiber-type and mass changes. IL-6 accelerated submaximal fatigue and reduced oxidative metabolism through muscle gp130 signaling. While the effect of TNF-α on skeletal muscle function has been extensively characterized, to the best of our knowledge this is the first study investigating if IL-6 is sufficient to regulate skeletal muscle fatigue and muscle oxidative metabolism. Future studies are warranted to establish the mechanisms regulating IL-6 induced maximal contraction-induced fatigability and disrupted mitochondrial quality control which contribute to submaximal contraction-induced fatigue.

Table 3.1. Characteristic data of male gp130 KO and WT with elevated IL-6

	WT		KO	
	Control	IL-6	Control	IL-6
n	14	15	12	11
Body Weights (g)				
Pre	23.3 ± 1.5	23.4 ± 1.9	24.7 ± 2.0	24.0 ± 1.7
Mid	24.0 ± 1.5	23.4 ± 1.4	24.9 ± 2.0	24.1 ± 1.3
Post	24.9 ± 2.0	24.0 ± 2.1	25.1 ± 1.3	24.3 ± 1.7
Plasma IL-6 (pg/mL)				
Pre	-	-	-	-
Mid	-	63 ± 52*	-	98 ± 55&
Post	-	75 ± 43*	-	141 ± 31&
Tissues at Sacrifice				
Hindlimb (mg)	207 ± 14	200 ± 14	214 ± 11@	206 ± 14@
Hindlimb/Tibia (mg/mm)	12.2 ± 0.7	12.0 ± 0.7	12.7 ± 0.6	12.3 ± 0.8
Tibia Length (mm)	17.0 ± 0.3	16.8 ± 0.2#	16.8 ± 0.2	16.7 ± 0.2#
Epididymal Fat (mg)	362 ± 139	313 ± 96	308 ± 52	290 ± 85
Spleen (mg)	71 ± 12	122 ± 26#	93 ± 68	199 ± 92#

Values are means ± SD. Male C57BL/6 (WT) mice. Male skeletal muscle specific gp130 knockout (KO) mice. Age in weeks (wks). Body weight in grams (g). Plasma interleukin-6 (IL-6) in picograms/milliliters (pg/mL). All vector controls and pre-IL-6 levels fell below the detection limit and therefore weren't reported. Combined weight of the soleus, plantaris, gastrocnemius, and tibialis anterior (hindlimb) in milligrams (mg). Tibia length in millimeters (mm). Epididymal fat pad weight in milligrams. Spleen weight in milligrams. Significance set at $p<0.05$ (Two-Way ANOVA). #Significant main effect of IL-6. @ Significant main effect of KO. & Significantly different from all groups. * WT-IL-6 significant interaction from all groups. & KO-IL-6 significant interaction from all groups.

Table 3.2. The effect of elevated IL-6 on skeletal muscle's contractile properties

	WT		KO	
	Control	IL-6	Control	IL-6
TA Weight (mg)	48.4 ± 3.1	46.0 ± 3.4	49.8 ± 3.2@	48.8 ± 3.6@
Twitch Properties				
1/2 RT (ms)	8.7 ± 1.6	9.0 ± 1.5	7.7 ± 1.2@	7.8 ± 1.7@
TPT (ms)	15.7 ± 1.4	16.2 ± 1.4	14.8 ± 0.8@	15.1 ± 1.1@
Force Production				
P_o (mN)	1,655 ± 155	1,585 ± 136	1,628 ± 152	1,563 ± 100
${}_sP_o$ (kN/m^2)	302 ± 25	300 ± 22	276 ± 24@	273 ± 14@
Contraction Rates				
+ dP/dt (mN/s)	23,233 ± 1675	22,222 ± 3421	25,652 ± 2824@	24,709 ± 2020@
- dP/dt (mN/s)	20,221 ± 3222	18,664 ± 3253	19,069 ± 3437	20,045 ± 1740

Values are means ± SD. Male C57BL/6 (WT n=14, WT+IL-6 n=15) mice. Male skeletal muscle specific gp130 knockout (KO n=12, KO+IL-6 n=11) mice. Tibialis anterior (TA) weight in milligrams (mg). 1/2 Relaxation time (RT) in milliseconds. Time to peak twitch (TPT) in milliseconds. Maximal tetanic force (P_o) in millinewtons. Specific tetanic force (${}_sP_o$) in kilonewtons/meter^2. Rate of contraction at 200 Hz (+dP/dt). Rate of Relaxation at 200 Hz (-dP/dt). Significance set at $p<0.05$ (Two-Way ANOVA). @ Significant main effect of KO.

Table 3.3. The effect of elevated IL-6 on muscle fiber-type distribution

	WT		KO	
	Control	IL-6	Control	IL-6
Type IIa	10.9 ± 4.7	11.2 ± 6.8	9.5 ± 6.5	6.8 ± 3.1
Type IIb	38.4 ± 7.1	40.6 ± 4.3	38.9 ± 7.7	35.4 ± 9.2
Type IIx	50.7 ± 8.5	48.2 ± 5.4	51.8 ± 13.4	58.0 ± 11.3

Values are % means ± SD. C57BL/6 (WT). Skeletal muscle specific gp130 knockout (KO). n=5 for each group

Table 3.4. Animal characteristics of male skeletal muscle specific gp130 KO ApcMin/+ mice

	Flox	MIN Flox	MIN KO
n	7	7	9
Age (wks)	17.4 ± 0.6	17.0 ± 0.3	17.7 ± 0.2
Peak BW (g)	26.0 ± 0.9	25.2 ± 0.8	26.0 ± 0.7
Sac BW (g)	26.0 ± 0.9	23.5 ± 1.0	24.9 ± 1.0
BW Loss (%)	0.0 ± 0.0	6.7 ± 2.4*	4.2 ± 1.9
Hindlimb (mg)	294 ± 12	261 ± 8	277 ± 14
Epi Fat (mg)	326 ± 41	108 ± 30*	119 ± 31*
Spleen (mg)	72 ± 5	398 ± 25*	364 ± 40*
Testes (mg)	197 ± 4	135 ± 17*	174 ± 13
Sem Ves (mg)	195 ± 18	76 ± 17*	104 ± 18*
Tibia Length (mm)	17.6 ± 0.1	17.7 ± 0.1	17.8 ± 0.2

Values are means ± SE. Age given in weeks (wks). Body weights given in grams (g). % loss determined from peak weight to weight prior to sacrifice. All tissue weights expressed in milligrams (mg). Seminal vesicles (Sem Ves). gp130 floxed controls (Flox). *Apc*$^{Min/+}$ mice (MIN). gp130 floxed HSA Cre/+ *Apc*$^{Min/+}$ (MIN KO). *Significantly different from Flox. $p<0.05$ (One-way ANOVA).

Table 3.5. The role of the muscle gp130 receptor in cancer-induced skeletal muscle contractile dysfunction

	Flox	MIN Flox	MIN KO
Twitch Properties			
1/2 RT (ms)	8.3 ± 0.8	8.7 ± 1.0	9.0 ± 0.8
TPT (ms)	15.3 ± 0.5	15.4 ± 0.7	15.7 ± 0.3
Contraction Rates			
+ dP/dt (mN/s)	27506 ± 1477	23070 ± 1979*	24017 ± 1440*
- dP/dt (mN/s)	18644 ± 1610	12220 ± 1222*	13324 ± 1319*

Values are means ± SE. Twitch properties 1/2 Relaxation time (RT) and time to peak twitch (TPT) given in milliseconds (ms). The rate of maximal contraction (+dP/dT) measured from 200Hz given as the ratio of change in force over the change in time. The rate of maximal relaxation (-dP/dT) measured from 200Hz given as the ratio of change in force over the change in time. gp130 floxed controls (Flox). *Apc*$^{Min/+}$ mice (MIN). gp130 floxed HSA Cre/+ *Apc*$^{Min/+}$ (MIN KO). *Significantly different from Flox. $p<0.05$ (One-way ANOVA).

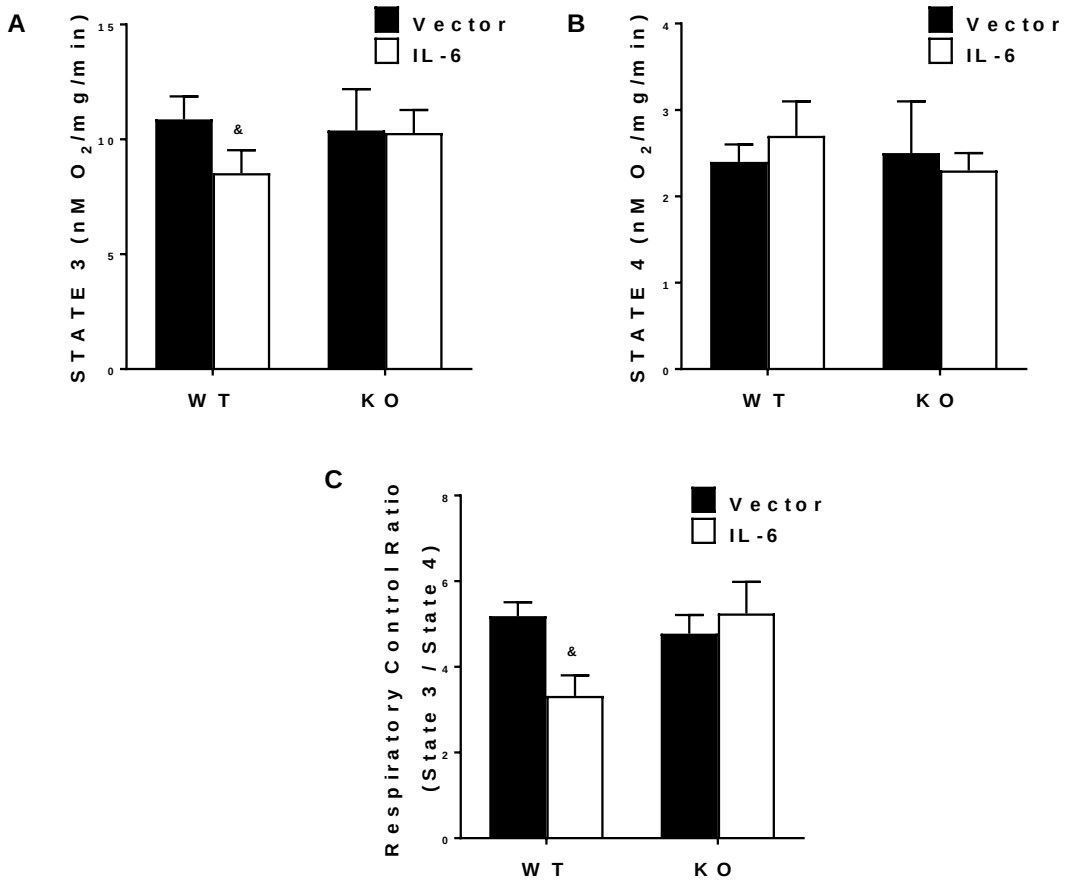

Figure 3.1. The effect of IL-6 on skeletal muscle mitochondrial function. Tibialis anterior (TA) respiratory control ratio (n=4 per group). Values are means plus / minus standard deviation (SD). A) 0.25mM of ADP was injected into the chamber to induce STATE 3 respiration for a duration of 5 minutes. B) 10ug/mL of Oligomycin was injected to induce steady STATE 4 respiration for a duration of 10 minutes. C) Respiratory Control Ratio (RCR) was calculated by dividing STATE 3 by STATE 4 respirations. & Significantly different from all groups. Significance was set at $p<0.05$. Two-Way ANOVA.

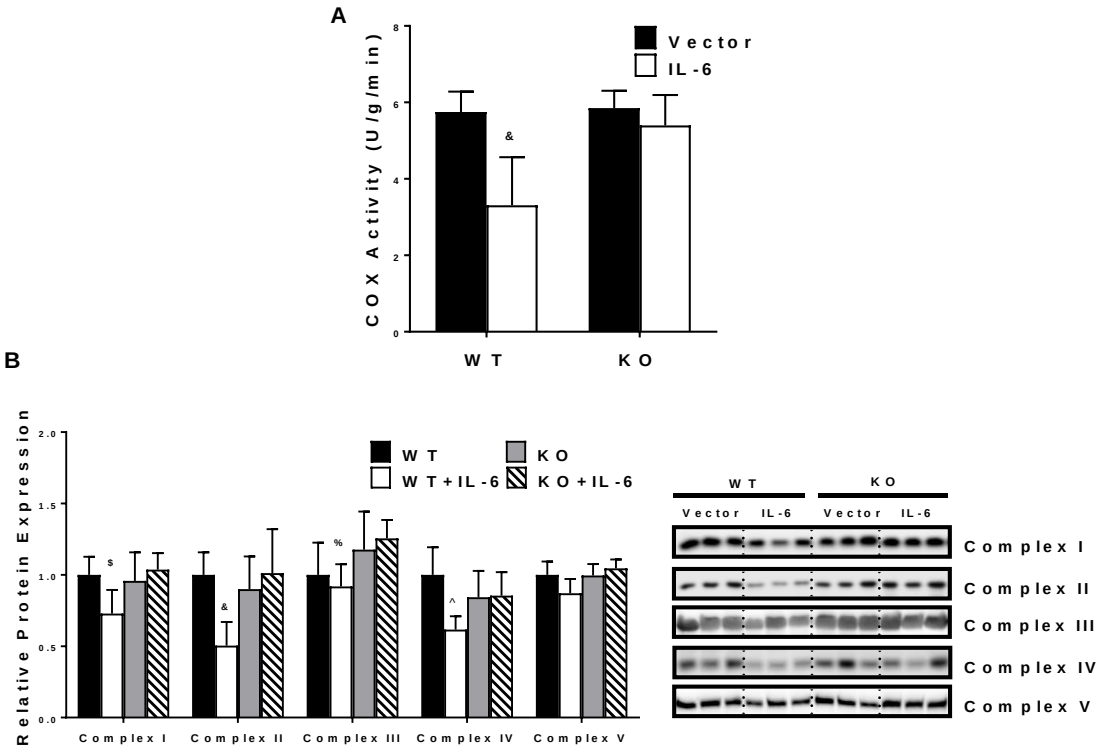

Figure 3.2. The effect of IL-6 on muscle mitochondrial content. A) Extensor digitorum longus (EDL) COX activity (WT n=14, WT+IL-6 n=15, KO n=12, KO+IL-6 n=11). B) Relative mitochondrial protein expression of Complexes 1-5 in the TA (n=6 per group). Representative western blot images are shown to the right of the graph. Values are means plus / minus standard error (SEM). C57BL/6 (WT). Skeletal muscle gp130 knockout (KO). Interleukin-6 (IL-6). $Significantly different from WT and KO + IL-6. &Significantly different from all groups. %Significantly different from KO + IL-6. ^Significantly different from WT. Significance was set at $p<0.05$. Two-Way ANOVA.

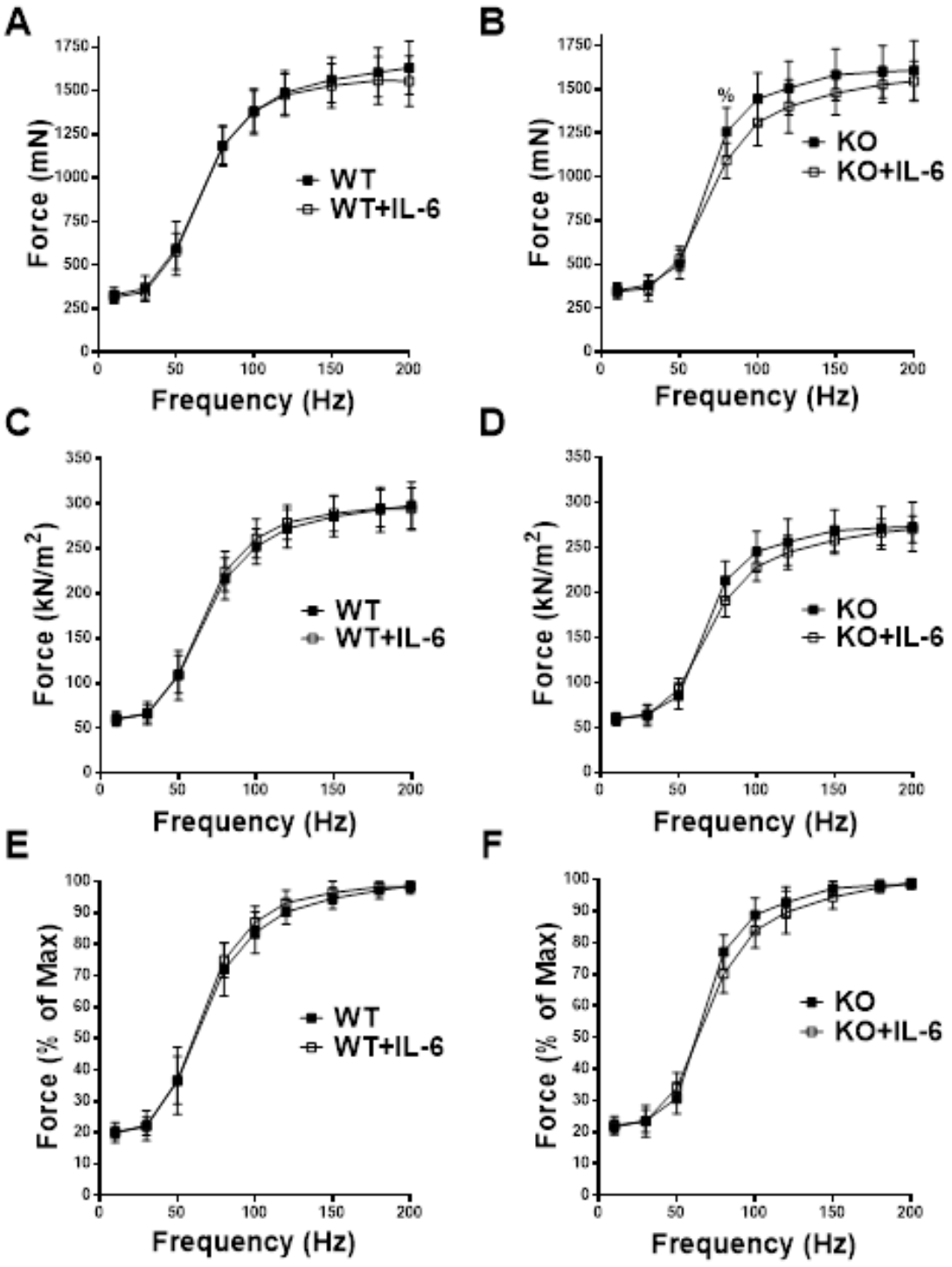

Figure 3.3. The effect of IL-6 on skeletal muscle force production. A) Absolute force-frequency curve of the TA in WT and WT+IL-6 in millinewtons (mN). B) Absolute force-frequency curve of the TA in KO and KO+IL-6 in mN. C) Specific force-frequency curve of the TA in WT and WT+IL-6 in kilonewtons/meters^2 (kN/m^2). D) Specific force-frequency curve of the TA in KO and KO+IL-6 in kN/m^2. E) Relative force-frequency

curve of the TA in WT and WT+IL-6 (% of maximal force). B) Relative force-frequency curve of the TA in KO and KO+IL-6 (% of maximal force). WT n=14, WT+IL-6 n=15, KO n=12, KO+IL-6 n=11. Values are means plus / minus standard error (SEM). C57BL/6 (WT). Skeletal muscle gp130 knockout (KO). Interleukin-6 (IL-6). %Significantly different from KO + IL-6. Significance was set at $p<0.05$. Pre-planned t-test.

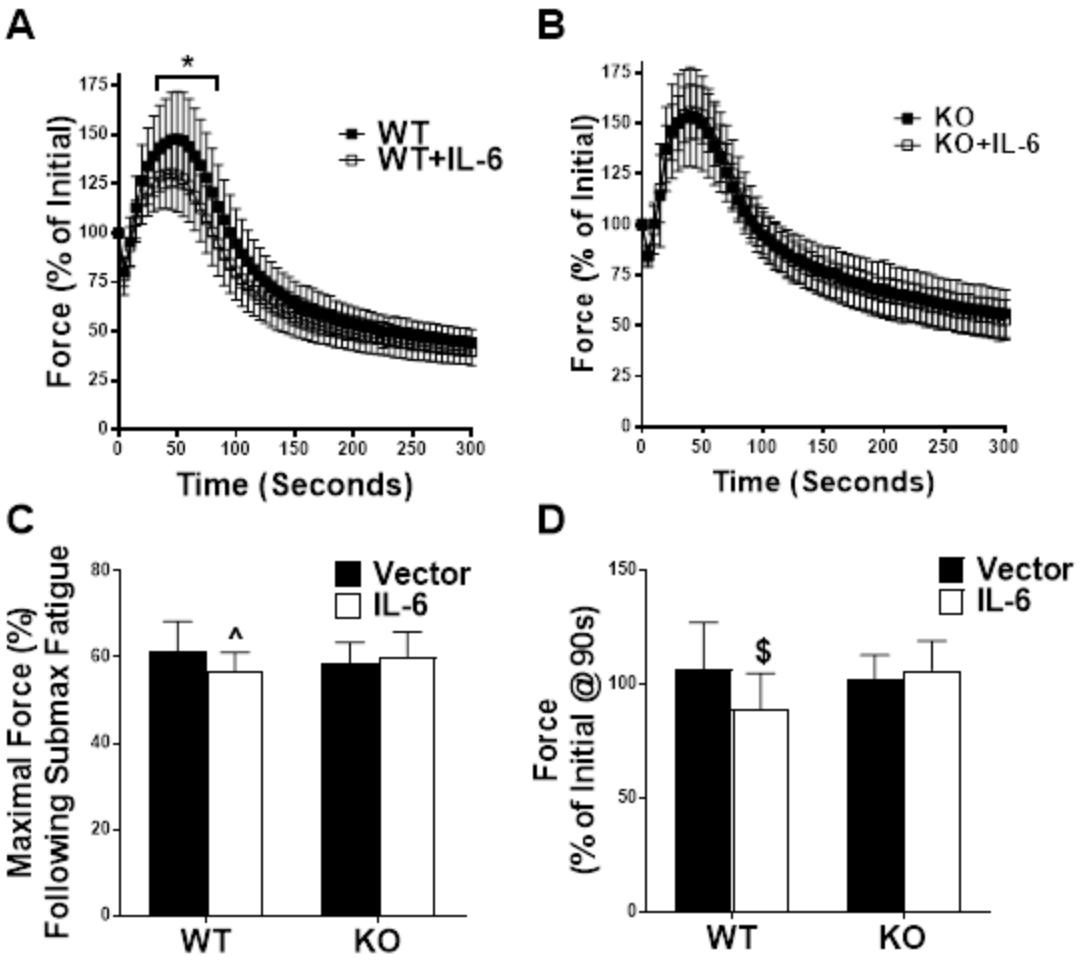

Figure 3.4. The effect of IL-6 on submaximal contraction-induced skeletal muscle fatigability. TA muscle's fatigability during a 5-minute submaximal (50 Hz) fatigue test. A) Relative (% of Initial) force-time tracing of the TA muscle's fatigability during a 5-minute submaximal (50 Hz) fatigue test from WT and WT + IL-6 mice. B) Relative (% of Initial) force-time tracing of the TA muscle's fatigability during a 5-minute submaximal (50 Hz) fatigue test from KO and KO + IL-6 mice. C) Relative (% of maximal tetanic force) force after the 5-minute submaximal contraction-induced fatigue test in all mice. D) Relative (% of Initial) force after 90 seconds of a submaximal (50 Hz) fatigue test in all mice. WT n=14, WT+IL-6 n=15, KO n=12, KO+IL-6 n=11. Values are means plus / minus standard error (SEM). C57BL/6 (WT). Skeletal muscle specific gp130 knockout (KO). $Significantly different from WT and KO+IL-6. Significance was set at $p<0.05$.

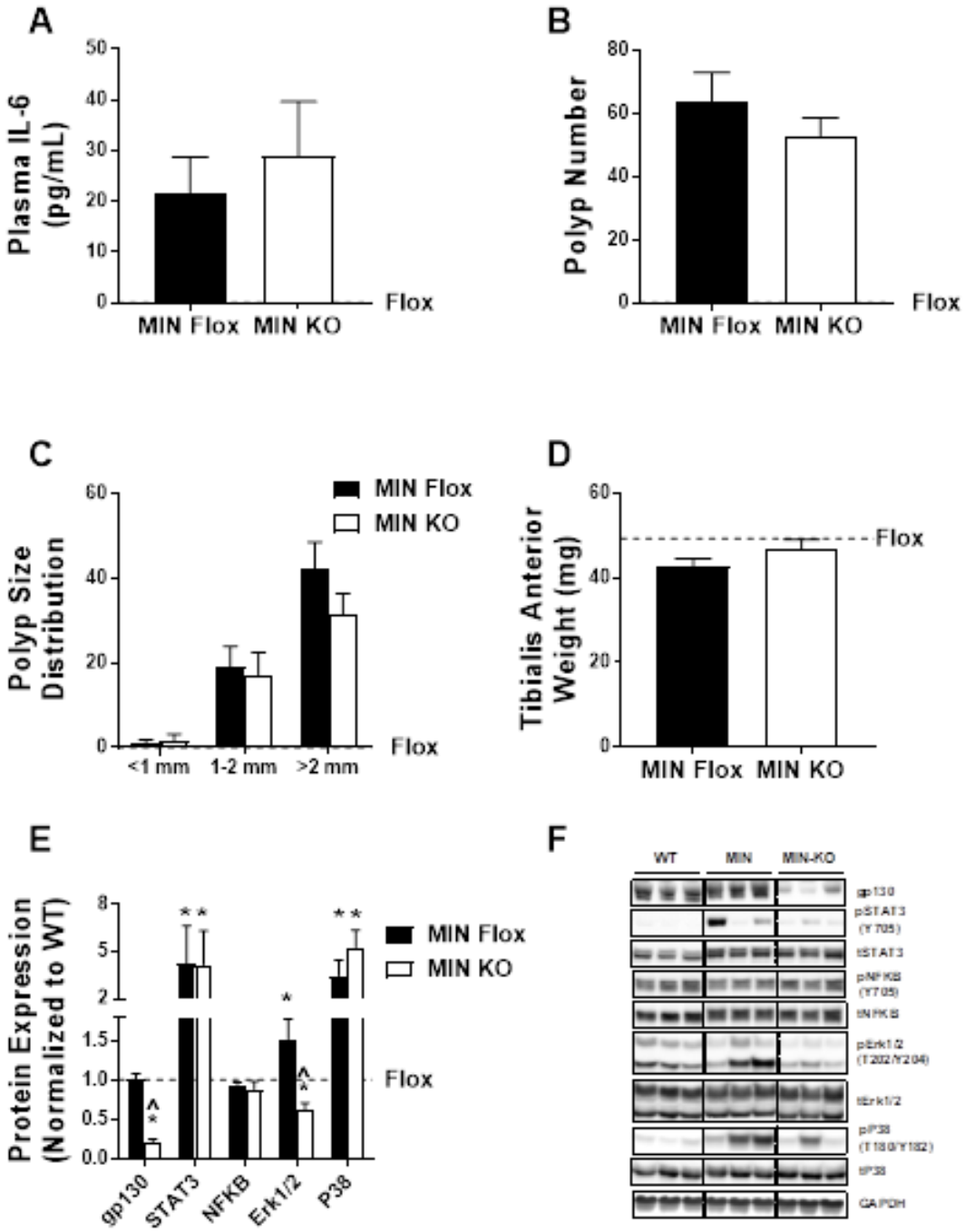

Figure 3.5 Indices of cachexia in gp130 KO MIN mice. A) Plasma levels of IL-6 in picograms per milliliter (pg/mL). B) Number of intestinal polyps in all MIN mice. C) Intestinal polyp size distribution in all MIN mice. D) Tibialis Anterior (TA) weight in milligrams (mg). E) The ratio of phosphorylated to total protein expression of key inflammatory signaling proteins gp130, STAT, P65, Erk 1/2, and P38 in the TA from MIN Flox and MIN KO normalized to Flox. F) Representative western blot images of phosphorylated (p) and total (t) protein expression of inflammatory proteins in the TA.

Values are means ± SE. gp130 floxed controls (Flox). *Apc*$^{Min/+}$ mice (MIN). gp130 floxed HSA Cre/+ *Apc*$^{Min/+}$ (MIN KO). *Significantly different from Flox. ^Significant from MIN Flox. $p<0.05$ (One-way ANOVA).

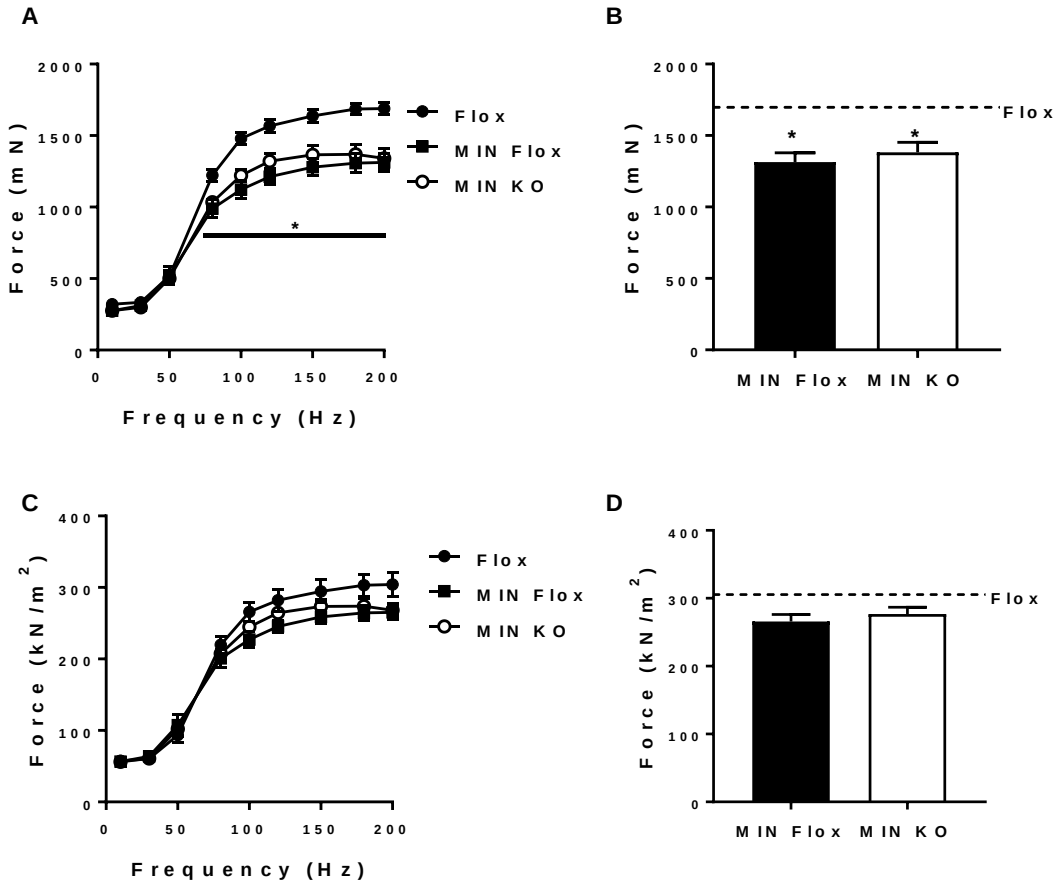

Figure 3.6. The role of the muscle gp130 receptor on cancer-induced muscle weakness. A) Absolute force-frequency curve of the TA from all groups in millinewtons (mN). B) Absolute force-frequency curve of the TA of all groups in mN. C) Specific force-frequency curve of the TA of all groups in kilonewtons/meters^2 (kN/m^2). D) Specific force-frequency curve of the TA from all groups in kN/m^2. Values are means ± SE. gp130 floxed controls (Flox). *Apc*$^{Min/+}$ mice (MIN). gp130 floxed HSA Cre/+ *Apc*$^{Min/+}$ (MIN KO). *Significantly different from Flox. $p<0.05$ (One-way ANOVA).

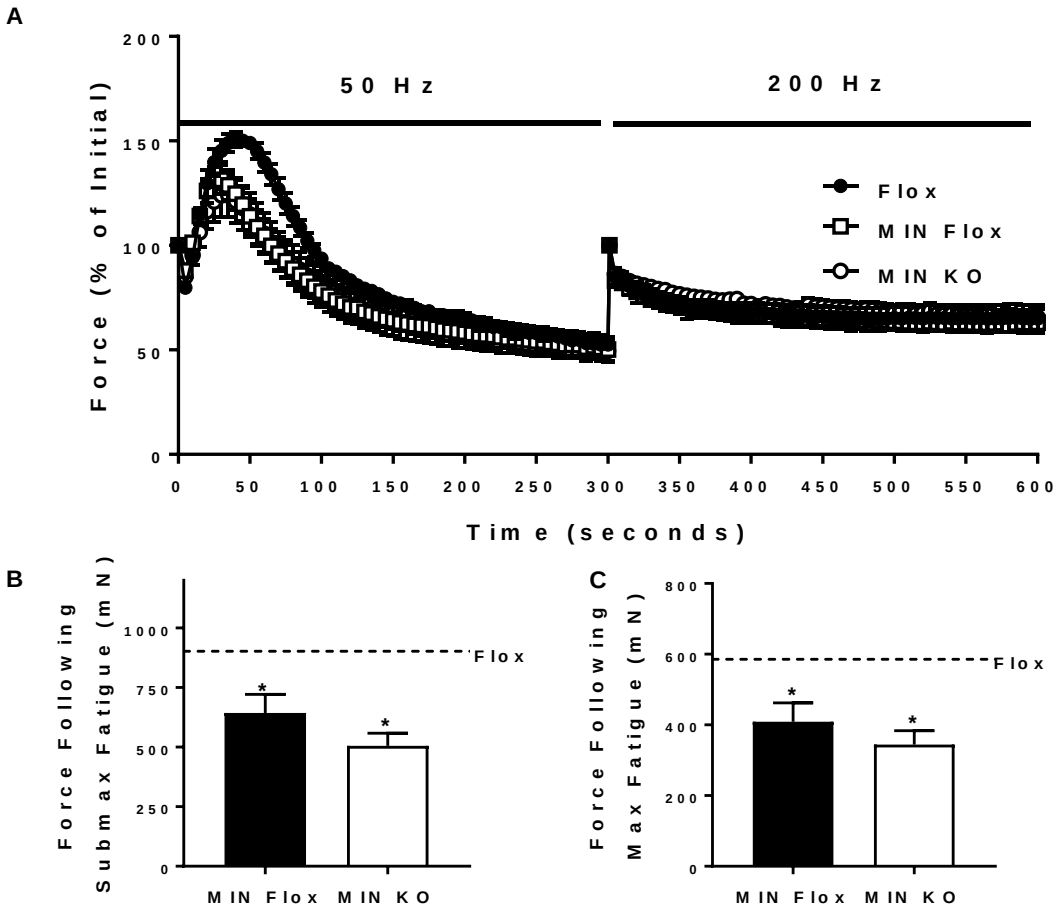

Figure 3.7. The role of the muscle gp130 receptor on cancer-induced muscle fatigability. TA muscle's fatigability during a 5-minute submaximal (50 Hz) and 5-minute maximal (200hz) fatigue test. A) Relative (% of Initial) force-time tracing of the TA muscle's fatigability during a 5-minute submaximal (50 Hz) and 5-minute maximal (200hz) fatigue test from all groups. B) Maximal tetanic force following the 5-minute submaximal contraction-induced fatigue test in all mice. C) Maximal tetanic force following both the 5-minute submaximal and 5-minute maximal contraction-induced fatigue test in all mice. Values are means ± SE. gp130 floxed controls (Flox). *Apc*$^{Min/+}$ mice (MIN). gp130 floxed HSA Cre/+ *Apc*$^{Min/+}$ (MIN KO). *Significantly different from Flox. $p<0.05$ (One-way ANOVA).

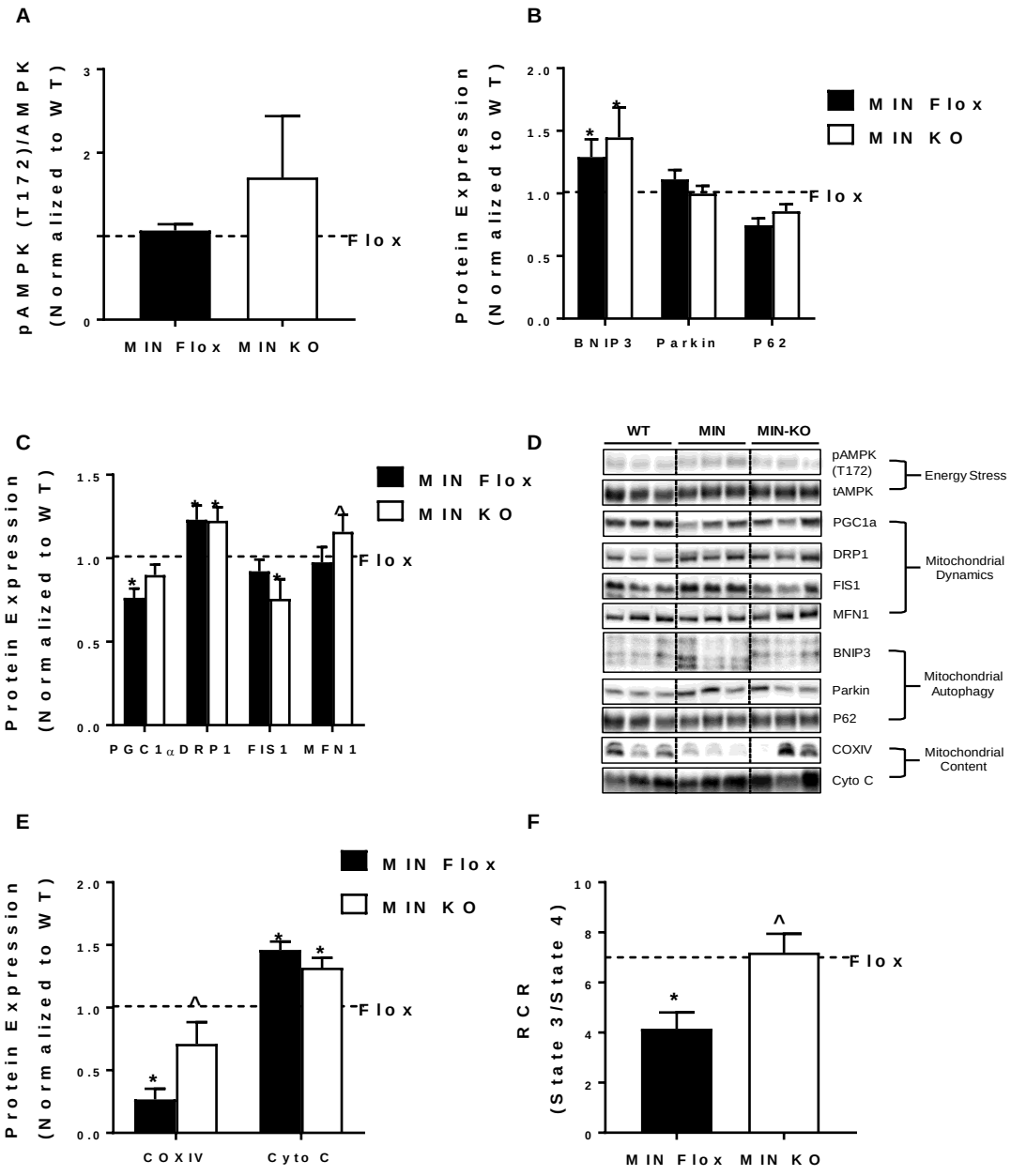

Figure 3.8. The effect of muscle gp130 loss on mitochondrial content, function, and quality control in MIN mice. A) The ratio of phosphorylated to total protein expression of key energy stress sensor AMPK in the TA from MIN Flox and MIN KO normalized to Flox. B) The total protein expression of mitophagy markers BNIP3, Parkin, and p62 in the TA from MIN Flox and MIN KO normalized to Flox. C) The total protein expression of mitochondrial quality control markers PGC1α, DRP1, FIS1, and MFN1 in the TA from MIN Flox and MIN KO normalized to Flox. D) Representative western blot images of protein expression of all mitochondria related proteins. E) The total protein expression of mitochondrial content markers COXIV and Cyto C in the TA from MIN Flox and MIN KO normalized to Flox. F) Respiratory Control Ratio (RCR) was calculated by dividing

STATE 3 by STATE 4 respirations. Values are means ± SE. gp130 floxed controls (Flox). *Apc*$^{Min/+}$ mice (MIN). gp130 floxed HSA Cre/+ *Apc*$^{Min/+}$ (MIN KO). *Significantly different from Flox. ^Significant from MIN Flox. $p<0.05$ (One-way ANOVA).

CHAPTER 4

THE ROLE OF MUSCLE USE ON SKELETAL MUSCLE FATIGUE DURING CACHEXIA PROGRESSION

4.1 – Abstract

Weakness and fatigue are among the most commonly reported complaints of cancer patients. Whether inactivity and muscle disuse are causal or consequence of muscle wasting with cancer, termed cachexia, remains largely unknown. Additionally, significant gaps remain in our understanding of the role of physical activity in the regulation of skeletal muscle function during cachexia progression. The purpose of the current study was to determine the role of physical activity in the development of weakness and fatigue during cachexia progression. Thirteen-week-old ApcMin/+ (MIN) and C57BL/6 (B6) mice were either given free wheel access (WA) or a locked wheel (C) for 5 weeks. WA had no effect on tumor burden (MIN-C 91 ± 8 polyps, MIN-WA 91 ± 4 polyps) or plasma IL-6 (MIN-C 30 ± 10 pg/mL, MIN-WA 33 ± 8 pg/mL). MINs had reduced muscle force 17% ($p=0.0004$) and increased muscle fatigability 18% ($p=0.015$) compared to B6; however, fatigue recovery was increased 17% ($p<0.05$) with WA regardless of genotype. There was a direct relationship between reduced cage activity and both time to fatigue ($R=0.66$, $p=0.04$) and *in situ* skeletal muscle fatigability ($R=0.73$, $p=0.02$), which was not present in the MIN-WA. There was a main effect of WA to increased mitochondrial complex I, II, and V by 31% ($p=0.001$), 96% ($p<0.0001$), and 17% ($p=0.0001$), respectively, regardless of genotype. These results demonstrate that increased activity improved overall functional

capacity, skeletal muscle fatigue recovery, and mitochondrial content in tumor-bearing mice without affecting tumor-burden or systemic IL-6.

4.2 – Introduction

Overall weakness and fatigue are among the most commonly reported consequences of cancer contributing to lower life quality and poor treatment outcomes (Chang et al. 2000; Greene et al. 1994; Stone et al. 1999; Vigano et al. 2000; von Haehling and Anker 2014). Patients with low performance scores and reduced physical activity have suffer from functional dependence and reduced survival (Barber, Ross, and Fearon 1999; Fearon KC 2006; O'Gorman, McMillan, and McArdle 1999; Vigano et al. 2000). Cancer-related fatigue (CRF) has been defined as subjective tiredness that is disproportional to activity which does not ease with rest (Rutherford, Manning, and Newton 2016; Stone et al. 1999; Winningham et al. 1994; Berger et al. 2015). While CRF's definition is inherently central, proposed mechanisms include several proinflammatory cytokines and the loss of skeletal muscle mass which are hallmarks of cancer-cachexia (Rutherford, Manning, and Newton 2016; Berger et al. 2015; Saligan et al. 2015). Cachexia is the progressive loss of skeletal muscle mass secondary to chronic disease and is prevalent in 20-80% of cancer patients depending on the cancer type (von Haehling and Anker 2014; Evans et al. 2008). While our understanding of cachexia progression has improved, identifying whether fatigue and inactivity contribute to or are consequence of muscle mass loss with cancer requires significant attention.

Whether CRF has central or peripheral (musculoskeletal) origins have served as a significant barrier to understanding fatigue's etiology (Rutherford, Manning, and Newton

2016; Davis 1995). Skeletal muscle fatigue has been classically defined as either the inability to maintain a given force output over time (Fitts 1994) or the decrease in maximal strength following strenuous or sustained activity which returns after a period of rest (Allen, Lamb, and Westerblad 2008). Classically, skeletal muscle's fatigue properties have been characterized but the contractile properties and relative fiber-type distribution (Close 1972). Skeletal muscle fatigability relies on several physiological phenomena, most notably, adequate ATP production by the mitochondria through oxidative metabolism (Fitts 1994; Thompson, Balog, and Fitts 1992). Skeletal muscle mitochondria content and function is maintained by the regulation of mitochondrial biogenesis, fusion, fission, and autophagy (mitophagy), together termed mitochondrial quality control (QC) (Romanello and Sandri 2015). The production of new mitochondria through PGC-1α mediated mitochondrial biogenesis is stimulated by post-translational modification of the key energy sensor 5' Adenosine monophosphate (AMP)-activated kinase (AMPK) (Reznick and Shulman 2006; Puigserver and Spiegelman 2003; Bergeron et al. 2001). AMPK phosphorylation is upregulated during energy stress/deprivation concomitant with increased reactive oxygen species (ROS) and increased mitochondrial fission proteins, DRP-1 and FIS-1, and mitochondrial fusion proteins, MFN-1,2 (Romanello et al. 2010; Carling 2017). After the removal of damaged or old mitochondria from the mitochondrial network through fission, mitophagic proteins PINK, Parkin-1, and LC3 recycle the organelles constituents for reuse. Disrupted mitochondrial content, QC, and oxidative capacity has been identified in cachectic muscle and are intriguing therapeutic targets (Julienne CM 2012; Brown et al. 2017; Carson, Hardee, and VanderVeen 2016). Mitochondrial QC is sensitive to skeletal muscle use (Yan, Lira, and Greene 2012; Hood

et al. 2018; Hood et al. 2011); however, the ability for increased activity to attenuate cancer-induced fatigue and mitochondrial dysregulation requires further investigation.

Reduced volitional activity and disputed mitochondrial QC has been identified prior to significant wasting in both cancer patients and pre-clinical cachexia models (Baltgalvis et al. 2010; Berger et al. 2015). The ApcMin/+ (MIN) is an established pre-clinical model of cancer-cachexia characterized by the development of intestinal polyps and a slow progressive wasting phenotype (Baltgalvis et al. 2008). MIN mice have a nonsense germline mutation in the *Adenomatous polyposis coli* (*Apc*) gene which predisposes mice to multiple intestinal neoplasia (min) resulting in the development of intestinal polyps (Moser, Pitot, and Dove 1990). MIN mice begin developing polyps at 4 weeks of age and polyp number continues to increase until 12-14 weeks at which size progressively increases (Puppa et al. 2011). Reduced voluntary wheel activity and reduced oxidative metabolism is present ~14-15 weeks of age while body weight is typically initiated at 16 weeks (Baltgalvis et al. 2010). We have previously shown the validity for exercise to attenuate muscle mass loss in the MIN, but these findings were associated with reduced tumor-burden or reduced systemic inflammation (Mehl et al. 2005; Puppa et al. 2012). Whether increasing volitional activity can attenuate body weight and muscle mass loss after full tumor-development has not been investigated.

Both increased volitional activity and regimented endurance exercise training has been positively associated with improved quality of life and survival in cancer patients regardless of cachexia diagnosis (Alves et al. 2015; Barbaric et al. 2010; Brown et al. 2012; al-Majid and McCarthy 2001a). While changes in physical activity has systemic effects that benefit overall health, skeletal muscle is highly sensitive to activity changes (Holloszy

2004; Holloszy and Booth 1976; Powers, Kavazis, and DeRuisseau 2005; Zhang, Chen, and Fan 2007). Identifying whether fatigue and disuse are causal or consequence of muscle wasting with cancer has eluded investigators likely due to the complexity of the syndrome. Moreover, several proposed therapeutics have failed in clinical trials due to their inability to improve muscle function independent of mass (Ramage and Skipworth 2018). The purpose of the current study was to determine if increased volitional activity could attenuate the development of weakness and fatigue during cachexia progression in tumor-bearing mice. We hypothesized that first there would be a direct relationship between cage activity and muscle fatigue in the MIN mouse, and second that MIN mice given free access to a wheel will have improved fatigue resistance associated with improved mitochondrial content and function. To test this hypothesis, B6 and MIN mice were given either free access to wheels or a locked wheel for 5 weeks. In order to control for exercise's effects on tumor development, wheel access will be initiated between 13-14 weeks, when MIN tumor-number plateaus (Puppa et al. 2011).

4.3 – Methods

Animals

Male C57BL/6 (B6) and *Apc*$^{Min/+}$ (MIN) mice were originally purchased from Jackson Laboratories and were bred at the University of South Carolina's Animal Resources Facility. All animals were group housed and kept on a 12:12-h light-dark cycle. Body weights were measured weekly, and animals were monitored for signs of distress. Animals were given food and water *ad libitum* throughout the duration of the study. All animals were fasted 5 hours prior to tissue collection. Mice were anesthetized with a

ketamine-xylazine-acepromazine cocktail, and hindlimb muscles and select organs were carefully dissected and snap frozen in liquid nitrogen and stored at -80ºC until further analysis. All animal experiments were approved by the University of South Carolina's Institutional Animal Care and Use Committee.

Voluntary Wheel Running

Voluntary wheel running was used as a marker of volitional physical activity and was performed as previously described (Baltgalvis 2010). At 13 weeks of age, B6 and MIN mice were individually housed in cages with 9.5-in.-diameter stainless steel wheels (MiniMitter, Bend, OR). B6 and MIN mice were randomized into 2 additional groups with either a fixed wheel (B6-C and MIN-C) or a free wheel access (B6-WA and MIN-WA). Wheel activity was monitored daily from 13 to 18 weeks of age. Bicycle computers (Specialized, Morgan Hill, CA) with magnetic sensors measured average speed, distance, time, and maximum speed, and the data were recorded daily.

Analysis of Muscle Function

At ~19 weeks of age, mice were anesthetized with 2% isoflurane inhalation and kept anesthetized at 1.5 % isoflurane for ~1hr throughout the duration of the procedure (~1 hour). Muscle function analysis of the TA *in situ*, which maintains the host nerve and blood supply, has been previously described (Murphy et al. 2012). Briefly, the distal tendon of the left TA was isolated and tied to a force transducer (Aurora Scientific, Ontario, Canada) using 5-0 silk sutures. The mouse was place on the apparatus maintained at 37ºC throughout the entirety of the procedure. The sciatic nerve was exposed proximal to the knee and maintained using warmed mineral oil. The sciatic nerve was then subjected to a single stimulus to determine L_o. Once L_o was obtained, a force-frequency curve was

generated, and maximal tetanic force was determined. Specific tension was determined using TA muscle CSA calculated by muscle mass/(L_f x 1.06), where L_f represents fiber length determined by multiplying L_o by 0.6, the predetermined TA muscle length to fiber length ratio, and 1.06 represents the skeletal muscle density. After a 5-minute rest the TA was subjected to an intermittent fatigue protocol consisting of 0.5 second submaximal stimulation (50Hz) every second for 5 minutes. Immediately, after submaximal fatigue the TA was subjected to an intermittent fatigue protocol consisting of 0.5 second maximal stimulation (200Hz) every second for 5 minutes. The fatiguing properties of skeletal muscle were determining be measuring the relative change in force (% of initial contraction) throughout the duration of the fatiguing contraction. Absolute muscle fatigue was measured as the reduction in maximal force following either the submaximal or maximal fatiguing contraction. After the completion of the fatigue protocol the muscle was rested for 5 minutes at L_o and then maximally stimulated (200hz) to determine fatigue recovery.

Polyp counts

At sacrifice, the intestines were excised, and intestinal sections were flushed with PBS, opened longitudinally, and flattened with a cotton swab. All sections were fixed in 10% buffered formalin (Fisher) for 24h. Formalin-fixed intestinal sections from all animals were rinsed in deionized water, briefly stained in 0.1% methylene blue, and counted by the same investigator who was blinded to the treatments. Polyps were counted under a dissecting microscope, using tweezers to pick through the intestinal villi and identify polyps. Polyps were categorized as <1mm, 1-2 mm, and >2mm for each segment (1-5) throughout the intestine.

Western blot analysis

Western blot analysis was performed as previously described (Fix et al. 2018). Protein concentration of the isolated mitochondrial fraction was determined using the Bradford standard curve method. Homogenates were fractionated on SDS-polyacrylamide gels and transferred to PVDF membrane. After the membranes were blocked, antibodies against the Total OXPHOS Cocktail (Abcam, Cambridge, United Kingdom) were incubated at dilutions of 1:5000 overnight at 4°C in 1% TBST milk. Anti-rabbit IgG-conjugated secondary antibodies (Cell Signaling Technology) were incubated with the membranes at 1:5000 dilutions for 1 h in 1% TBST milk. Enhanced chemiluminescence developed by autoradiography was used to visualize the antibody–antigen interactions. Blots were analyzed by measuring the integrated optical density (IOD) of each band with ImageJ software (NIH, Bethesda, MD, USA).

Cytochrome C Oxidase Activity

TA muscle samples were homogenized in extraction buffer (0.1 M KH2P04/Na2HP04, 2 mM EDTA, pH 7.2). Cytochrome-c oxidase (COX) activity was determined by measuring the rate of oxidation of fully reduced cytochrome c at 550nm using (CYTOCOX1) Sigma Aldrich Kit and spectrophotometer (Eppendorf) (Iqbal and Hood 2015).

Respiratory Control Ratio

Mitochondrial respiration was measured polarographically in a respiration chamber (Hansatech Instruments) maintained at 37°C as previously described (Kwon et al. 2015). A 7-10 mg piece of proximal TA muscle was mechanically tweezed with forceps under a dissecting microscope in ice-cold *buffer X* (60 mM K-MES, 35 mM KCl, 7.23 mM

K2EGTA, 2.77 mM CaK2EGTA, 20 mM imidazole, 0.5 mM DTT, 20 mM taurine, 5.7 mM ATP, 15 mM phosphocreatine, and 6.56 mM MgCl2, pH 7.1). The fiber bundle was then incubated in 50uM saponin for 30 minutes and washed 3 times for 5 minutes in respiration buffer (105mM K-MES, 3mM KCl, 1mM EGTA, 10mM K2HPO4, 5mM MgCl2, 0.005mM Glutamate, 0.002mM Malate, 0.05% BSA, 20mM Creatine, pH 7.1). Fiber bundles were then placed into the oxygraph machine in 20mM creatine respiration buffer at 37 degrees and provided with 5mM of pyruvate and 2mM of malate. Two minutes following pyruvate and malate, 0.25mM of ADP was injected into the chamber to induce STATE 3 respiration for a duration of 5 minutes. 10ug/mL of Oligomycin was then injected to induce steady state 4 respiration for a duration of 10 minutes. Respiratory Control Ratio (RCR) was calculated by dividing state 3 by state 4 respirations.

Skeletal Muscle Enriched Mitochondrial Fraction

Mitochondrial isolation from the right quadriceps muscle was performed following a previously described protocol (Boutagy et al. 2015). Briefly, freshly dissected quadriceps muscles were minced and digested for 30 min in isolation buffer 1 (2 M Tris·HCl, 1 M KCl, and 0.5 M EDTA/Tris) containing 0.05% trypsin solution. The digested solution was spun at 200 g for 3 min, and the pellet was resuspended and homogenized using a Teflon pestle. The homogenate was spun at 700 g for 10 min and the supernatant was collected and spun at 8,000 g for another 10 min. The supernatant was discarded, and the pellet was resuspended in 5 ml of isolation buffer 1 and spun again at 8,000 g for 10 min. The resulting pellet was gently resuspended in 50 mL of isolation buffer 2 (0.1 M EGTA/Tris and 1 M Tris·HCl) and contained the isolated mitochondrial suspension. The Bradford method was

used to determine total mitochondria protein concentration in the purified mitochondrial fraction.

Statistical analysis

Values are presented as means ± standard error of the mean (SEM). Student t-tests were performed to determine differences between genotypes. A two-way ANOVA was used to determine differences in muscle function and oxidative metabolism markers in between B6-C, B6-WA, MIN-C, and MIN-WA. Post hoc analyses were performed with student Newman-Keuls methods. A Bartlett's test was used to determine significantly different standard deviations ($p<0.05$). If a significant difference was observed between group standard deviations, a non-parametric Kruskal-Wallis one-way ANOVA was used. A Pearson correlation was used to determine correlations between inflammatory genes and proteins with muscle function properties in MIN mice. Significance was set at $p<0.05$.

4.4 – Results

Animal Characteristics

After 13 weeks of age, both MIN and B6 mice were given either access to a free or fixed wheel. There was a trend for a significant main effect of MIN to have reduced body weight at the start of wheel access at 13 weeks of age (23.6 ± 0.2, 23.0 ± 0.3; $p=0.068$). There was no difference in wheel activity between MIN and B6 mice at the first 4 weeks, but there was a 50% reduction in wheel running time throughout the 5th week in MIN mice (Figure 4.1B). A two-way ANOVA repeated measures showed an effect of time for body weight to increase between 12-18 weeks of age in B6-C, B6-WA, and MIN-WA; however, there was no increase in body weight over time in the MIN-C (Figure 4.1B). There was a

significant main effect of MIN to have 4% body weight loss from peak body weight (Table 4.1). While this cannot be characterized as cachexia (>5% BW loss), there was 3 MIN-C and 2 MIN-WA mice with >5% BW loss, 4 MIN-C and 4 MIN-WA mice between 0% and 5% BW loss, and 3 MIN-C and 4 MIN-WA with 0% BW loss. Additionally, there were significant main effects of MIN to have increased spleen weight, reduced hindlimb mass, and reduced testes mass which have been extensively characterized with cachexia and cancer progression (Table 4.3). Tumor number in the MIN mouse plateaus at 12 weeks of age (Puppa et al. 2011). There was no observed difference in tumor size or number in MIN-C or MIN-WA after 5 weeks of wheel access (Figure 4.1D, E). Additionally, there was no observed difference in plasma IL-6, a key regulator of cachexia development in the MIN mouse (Figure 4.1F) (Baltgalvis et al. 2008).

Body composition

There were no observed differences in body weight, bone mineral content, bone density, lean mass, fat mass, and body fat % across all groups at 12-13 weeks of age (Table 4.1). Additionally, there was no difference in daily food intake across all groups at the start of the study (Table 4.1). There was a significant main effect of MIN to have reduced bone mineral density and bone mineral content at 18 weeks of age (Table 4.1). There was a significant main effect of MIN to have reduced lean mass at 18 weeks of age, but there were no observed differences in overall fat mass of body fat percentage (Table 4.1). There was a significant main effect of MIN in absolute daily food intake, however this effect is lost when corrected for body weight (Table 4.1). When measuring the differences within individual mice over the duration of the study there was a significant main effect of MIN to reduce lean mass, however there was a main effect of Wheel to increase lean mass in

both genotypes (Table 4.1). Additionally, there was a significant main effect of MIN to reduced BMD and a significant main effect of Wheel to increase bone mineral density (Table 4.1). Lastly, there was a significant main effect of Wheel to increase food intake, but this effect was lost when corrected for body weight (Table 4.1).

Whole body function

There were no observed differences in cage activity, grip strength, run to fatigue, or latency to fall across all groups at 12-13 weeks of age (Table 4.2). There was a significant main effect of MIN to have reduced cage activity regardless of wheel access (Table 4.2). There was an interaction for MIN-C mice to have reduced relative grip strength compared to B6-C and B6-WA by 11% and 9%, respectively (Table 4.2). There was a significant main effect of MIN to have reduced time to fatigue, regardless of wheel access; however, there was also a significant main effect of wheel to increase time to fatigue regardless of genotype (Table 4.2). There were no observed differences in latency to fall across all groups.

Skeletal Muscle Twitch Properties

Skeletal muscle function has been classically characterized by the muscle's twitch properties, force production capabilities, and intrinsic fatigability (Close 1972). Similar to what has been previously reported in the MIN mouse (VanderVeen et al. 2018), there was a significant main effect of MIN to have increase ½ RT and TPT indicating a slower contractile phenotype (Table 4.4). There was no effect of wheel in either genotype. There was a significant main effect of MIN to have a reduced rate of relaxation (-dx/dt) from peak tetanic force; however, rate of peak contraction was not changed (Table 4.4).

Additionally, there was no effect of wheel on rate of relaxation or contraction in both genotypes (Table 4.4).

Skeletal Muscle Force Production

There was a significant main effect of MIN to have reduced absolute force production (mN) starting between 80-200 hz during a force frequency protocol (Figure 4.2). This is recapitulated in a significant main effect of MIN to have reduced absolute tetanic force (P_o, Figure 4.2B). There were no observed differences across all groups in specific force between 10-180hz of the force frequency protocol; however, there was a significant interaction for B6-WA to have increased specific force at 200 Hz compared to MIN-WA and MIN-C (Figure 4.2C). There was a significant main effect of MIN to have reduced maximal specific force ($_sP_o$); however, there was also a significant main effect of wheel to increase $_sP_o$ regardless of genotype (Figure 4.2D). Analysis of the relative force (% of P_o) during the force frequency curve showed as significant interaction for MIN-C to have increased relative force compared to B6-C and B6-WA at 50 and 80Hz (Figure 4.2E, F).

Skeletal Muscle Fatigability

To measure the effects of activity and tumor-burden on submaximal and maximal contraction induced TA fatigability, the sciatic nerve was stimulated 1 contraction/second for 5 minutes at 50Hz followed by 1 contraction/second for 5 minutes at 200Hz. The relative (% of initial) force-time tracing throughout both contraction periods is shown in figure 4.3. There was a significant main effect of MIN to have reduced maximal force following 5 minutes of repeated submaximal contractions (Figure 4.3B). There was a trend ($p=0.09$) for wheel access to have increased maximal force following the submaximal

contractions (Figure 4.3B). Since maximal force was reduced prior to the fatiguing protocol, force was corrected for P_o and there was a significant main effect of MIN to have reduced relative maximal force (% of P_o) following the 5 minutes of repeated submaximal contractions. There was a significant main effect of MIN to have reduced maximal and relative force following the additional 5-minute maximal contraction-induced fatigue protocol (Figure 4.3 C). Following for the submaximal and maximal contractions, the muscle was allowed to rest at L_o for 5 minutes and maximally stimulated (200Hz) to asses fatigue recovery. There was a significant main effect of MIN to have reduced maximal force following a fatigue recovery; however, there was a significant main effect of wheel to have increased maximal force following fatigue recovery (Figure 4.3D). Again, correcting for differences in P_o, there was a significant main effect of MIN to have reduced fatigue recovery and a significant main effect of wheel to have increased fatigue recovery regardless of genotype.

Skeletal Muscle Mitochondrial Content and Respiration

A key contributor to skeletal muscle fatigability and ATP production is the mitochondrial content and function. We have previously reported reduction in mitochondrial content of the TA and EDL with cachexia progression (VanderVeen et al. 2018; White et al. 2012). There was a significant main effect of MIN to reduce complex IV and II expression in isolated mitochondria (Figure 4.4C, D). There were significant main effects of wheel to have increased complex I, II, and V (Figure 4.4A, D, E). There was a significant interaction from WT-WA to have increased complex III compared to all groups (Figure 4.4B). Additionally, there was a significant main effect of wheel to increase cytochrome c protein expression regardless of genotype (Figure 4.4F). To assess muscle

mitochondrial function, a 7-10 mg piece of the proximal TA was teased and complex I mediated respiration was measured in permeabilized fibers. There were no observed differences in State 3 (Figure 4.5A). There was a significant main effect of MIN to increase state 4 which resulted in a significant main effect of MIN to have reduced respiratory control ratio (RCR, state 3/state 4; Figure 4.5B, C).

4.5 – Discussion

The current study sought to further elucidate the role of reduced physical activity in increased skeletal muscle fatigue during the early stages of cachexia progression in tumor bearing mice. While reduced physical activity has an established role in muscle mass maintenance, whether increasing volitional activity prior to significant wasting can attenuate the increase in skeletal muscle fatigue during cancer remained largely speculative. The current study showed that regardless of tumor presence, increased physical activity through volitional wheel running could improve skeletal muscle fatigue resistance. Additionally, we showed that wheel running improved mitochondrial quality control and content in both healthy and sick mice. While our results show no improvements in body weight or hindlimb muscle mass, increased volitional activity may provide a protective effect against cancer induced muscle mitochondrial disruptions and fatigue.

The loss of volitional activity has previously been considered a side effect of muscle mass loss (Evans et al. 2008), though several studies show changes in activity levels and increased sedentary behavior prior to, or without, significant weight loss (Baltgalvis et al. 2010; al-Majid and McCarthy 2001a; Barbaric et al. 2010). Our lab has previously shown that if initiated at 4 weeks of age, voluntary wheel running is reduced in prior to weight

loss in male MIN mice (Baltgalvis et al. 2010). The current study extends these results by showing a reduction in daily cage activity without significant weight loss. Interestingly, treadmill training exercise and free wheel access initiated at 4 weeks in the MIN showed that only treadmill training reduced total polyp number; however, both exercises reduced spleen weight and plasma IL-6 in male MINs (Mehl et al. 2005). To account for this potential confounder, the current study initiated wheel access at ~13 weeks of age, after tumor development in the MIN plateaus, and showed no effect of wheel on tumor burden or plasma IL-6. While MIN-C mice did not increase in body weight from 12-18 weeks, free wheel access was able to increase body weight over time which was directly related to an increase in lean body mass. While the beneficial effects of exercise on tumor metastasis, development, and growth has been studied extensively (Ashcraft et al. 2016), our results demonstrate that wheel access was able to improve lean body mass and body weight without changing tumor number or size. Low levels of physical activity have been strongly linked to the incidence of colon, breast, kidney, and digestive cancers (Barbaric et al. 2010); however, our results and others suggest that maintaining physical activity levels following diagnosis is important in attenuating cancer-related fatigue and cachexia (Knols et al. 2005; Schmitz et al. 2005; Finne et al. 2018; Speck et al. 2010). Additionally, further work is needed to determine if wheel access improved gut barrier dysfunction which develops concurrently with inflammation and tumor-burden in the MIN mouse (Puppa et al. 2011).

Regimented exercise and increased daily physical activity are commonly prescribed to cancer patients aimed at improving physical function and quality of life (Brown et al. 2012; Speck et al. 2010; Stricker et al. 2004), however our understanding of

physical activity's ability to improve muscle functional capacity during cachexia progression is still developing. Furthermore, our understanding of the progression of central and musculoskeletal fatigue during cancer remains extremely limited. While a cause-effect relationship between central and peripheral fatigue is generally accepted, their mechanistic link and causal sequence with aging and chronic disease is not well understood (Gandevia 2001). The current study demonstrates that wheel access was unable to improve central drive, demonstrated by no difference in cage activity between locked and free wheel access MIN mice; however, wheel access improved running time during a treadmill fatigue test as well as improved relative grip strength. Increased physical activity has been shown to improve physical functioning and improve both physiological and psychological outcomes contributing to improved life quality in cancer survivors (Finne et al. 2018; Schmitz et al. 2005; Mishra et al. 2012; Juvet et al. 2017). While our results are limited regarding central fatigue, our results suggest that wheel access improved several aspects of physical function without necessarily improving volitional activity. One potential hypothesis for why wheel access was unable to increase activity is the lack of improved systemic inflammation and tumor-burden. Chronic inflammation negatively impacts central fatigue since several inflammatory cytokines, namely TNF-α, IL-6, and IFNγ, have been shown to cross the blood brain barrier and disrupt the hypothalamic-pituitary-adrenal (HPA) axis (LaVoy, Fagundes, and Dantzer 2016). Whether activity altered neural inflammation of tumor-bearing mice was not determined, however this question serves as an intriguing inquiry for further research.

The regulation of skeletal muscle function during cachexia progression has only just begun to be unearthed. Several reports of disrupted skeletal muscle function have been

reported (Gorselink et al. 2006; Murphy et al. 2012; Roberts, Ahn, et al. 2013; Roberts, Frye, et al. 2013; VanderVeen et al. 2018; Jaweed et al. 1983); however, these studies were limited in mechanistic insight and provide contentious findings likely due to the muscle measured, tumor model used, and endpoint degree of weight loss. Additionally, a disconnect between muscle mass and function has been suggested to contribute to unsuccessful treatment outcomes which aimed to improve mass without accounting for functional changes in preclinical settings (Ramage and Skipworth 2018). Skeletal muscle function analysis has been relegated to the simple assessments of skeletal muscle strength without appropriately testing skeletal muscle fatigability. Improved muscle strength without improved muscle fatigue resistance has limited translation to cancer patients suffering from CRF which affect a large majority of cancer patients (Berger et al. 2015). To the best of our knowledge, this is the first study to report both reduced muscle force and increased submaximal contraction-induced skeletal muscle fatigue in pre-cachectic tumor-bearing mice. Furthermore, we provide evidence to suggest a direct relationship between inactivity and fatigue which can be mitigated by wheel activity. While increased activity was unable to attenuate muscle mass or strength losses, we have previously shown that repeated eccentric muscle contractions, a model of resistance exercise, could attenuate the loss of muscle CSA in the male MIN mouse (Hardee et al. 2016). Together, increased activity and resistance exercise should improve overall functional quality of cancer patients through attenuating the deleterious tumor effects on muscle mass, strength, and fatigability.

Emerging evidence suggests that metabolic dysfunction is a key regulator of the loss of muscle mass and function with cancer (Carson, Hardee, and VanderVeen 2016). Disrupted oxidative metabolism and mitochondrial dysfunction have been demonstrated in

both pre-cachectic and cachectic muscle which may directly disrupt the functional quality of skeletal muscle (Brown et al. 2017; VanderVeen, Fix, and Carson 2017). Our lab has previously shown that voluntary wheel running is reduced prior to weight loss in male MIN mice associated with anemia and decreased muscle citrate synthase (CS) activity (Baltgalvis et al. 2010). Regimented treadmill exercise and wheel access initiated at 4 weeks of age increased CS activity compared to sedentary controls; however, treadmill training reduced total polyp number and both exercise types reduced spleen weight and plasma IL-6 (Mehl et al. 2005). The current study demonstrated that MIN mice had a reduction in cage activity and voluntary wheel running without significant body weight loss. While TA muscle respiration was reduced in MINs regardless of treatment, wheel access was able to improve mitochondrial content in both healthy and tumor-bearing mice. Treadmill exercise training has been shown to be protective against IL-6-induced cachexia in the MIN mouse associated with improved triglyceride and glucose metabolism (Puppa et al. 2012). While mitochondria are especially susceptible to inflammation-induced wasting (VanderVeen, Fix, and Carson 2017; White et al. 2012), exercise has been shown to mitigate chronic inflammation, improve mitochondria quality control, and increase mitochondrial content (Mathur and Pedersen 2008; Yan, Lira, and Greene 2012).

The loss of functional independence and the burden of CRF plagues most cancer patients and contributes substantially to reduced life quality and survival. Identifying the musculoskeletal alteration that occur with disease progression will improve our understanding of these functional deficits and improve the efficacy of future therapeutics. The current study identified deficits in skeletal muscle mass, strength, and fatigue resistance before significant body weight loss occurred. Additionally, these changes

occurred concomitant with reduced volitional activity and disrupted mitochondrial function and quality control. We provide further evidence to suggest that increased activity improved fatigue resistance and mitochondrial content without changing the systemic inflammation or tumor burden. While muscle mass loss was not attenuated, increasing activity in addition to regimented resistance exercise may improve the functional quality of cancer patients in order to improve life quality and survival.

Table 4.1. Mouse body composition pre- and post-wheel access

	B6		MIN	
	Control	Wheel Access	Control	Wheel Access
n	10	9	10	10
Body Weight (g)				
12wk	23.6±0.3	23.8 ± 0.2	23.3±0.5*	22.6±0.4*
18wk	25.5±0.5$^{\$}$	25.4 ± 0.2$^{\$}$	23.6±0.5*	24.4±0.7*$^{\$}$
12 – 18 wks	1.96±0.20	1.58 ± 0.19	0.41±0.71	1.84±0.52
Lean Mass (g)				
12wk	17.9±0.3	17.9 ± 0.1	17.9±0.4	17.6±0.3
18wk	19.3±0.3$^{\$}$	19.5 ± 0.1$^{\$}$	18.0±0.4*	19.1±0.5*$^{\$}$
12 – 18 wks	1.43±0.08	1.56 ± 0.11^	0.12±0.41*	1.47±0.47*^
Fat Mass (g)				
12wk	2.7±0.1	2.6 ± 0.1	2.5±0.1	2.4±0.1
18wk	2.8±0.1	2.5 ± 0.1	2.5±0.2	2.5±0.1
12 – 18 wks	0.14±0.14	-0.18 ± 0.11	0.02±0.25	0.15±0.13

Values are means ± SEM. All measurements taken at 12 and 18 weeks (wk). Body weights (BW) given in grams. Lean mass from DEXA given in grams. Fat mass from DEXA given in grams. Change was calculated by the difference between 12 and 18 weeks. Two-way ANOVA. *Main effect of genotype. ^Main effect of treatment. $Paired t-test, effect of time. Significance was set a $p<0.05$

Table 4.2. Behavioral and functional characteristics pre- and post-wheel access

	B6		MIN	
	Control	Wheel Access	Control	Wheel Access
n	10	9	10	10
Behavioral				
Food Intake (g)				
12wk	3.7±0.1	3.7±0.1	3.8±0.2	3.7±0.1
18wk	4.0±0.1$^{\$}$	4.3±0.2$^{\$}$	3.7±0.2*	3.9±0.1*
12 – 18 wks	0.3±0.1	0.5±0.2^	-0.2±0.3*	0.2±0.1*^
Cage Activity (counts)				
12wk	19453±1319	19622±1381	21999±2747	23433±2765
18wk	26389±2003	29827±2622	12633±3437*	14056±1965*
12 – 18 wks	6936±2678$^{\$}$	10204±2579$^{\$}$	-9366±2922$^{\$}$*	-9376±3017$^{\$}$*
Functional				
Grip Strength (kN/g)				
12wk	10.6±0.1	10.3±0.3	10.8±0.3	10.3±0.2
18wk	11.3±0.4	11.3±0.1	10.0±0.2*	10.7±0.2*
12 – 18 wks	0.7±0.4	0.9±0.3$^{\$}$^	-0.8 ± 0.4*	0.4±0.3*^
Fall Latency (s)				
12wk	61.5±4.6	62.1±5.9	61.3±4.4	56.4±8.4
18wk	76.7±5.7	68.1±5.2	69.0±9.7	72.2±3.4
12 – 18 wks	15.2±5.1$^{\$}$	6.1±6.2$^{\$}$	7.8±9.6$^{\$}$	15.8±7.2$^{\$}$
Time to Fatigue (min)				
12wk	77.9±4.1	79.7±6.0	78.8±6.7	74.2±6.1
18wk	86.6±3.6	150.3±11.7^	40.8±6.9*	99.9±15.2*^
12 – 18 wks	8.7±4.1	70.7±13.7$^{\$}$^	-38±7.3$^{\$}$	25.7±15.2*^

Values are means ± SEM. All measurements taken at 12 and 18 weeks (wk). Average food intake measured over 3 days in grams. Average daily cage activity measured over 3 days in beams crossed. Relative grip strength given in kN force /grams of body weight. Time on the rotorod (fall latency) given in seconds. Time to fatigue during a graded exercise treadmill test given in minutes. Change was calculated by the difference between 12 and 18 weeks. Two-way ANOVA. *Main effect of genotype. ^Main effect of treatment. $Paired t-test, effect of time. Significance was set a $p<0.05$

Table 4.3. The effect of wheel access on the characteristic data of MIN and B6 mice

	B6		MIN	
	Control	Wheel Access	Control	Wheel Access
n	10	9	10	10
Age (wks)	19.6±0.2	19.8 ± 0.1	19.2±0.4	19.4 ± 0.2
Peak BW (g)	25.7±0.4	25.7 ± 0.3	24.7±0.3*	25.0 ± 0.4*
End BW (g)	25.5±0.5$^{\$}$	25.3 ± 0.2	23.5±0.6*$^{\$}$	24.4 ± 0.6*
BW Loss (%)	1.0±0.3	1.4 ± 0.7	4.7±2.0*	2.8 ± 1.4*
Tibia Length (mm)	17.0±0.0	17.1 ± 0.0	16.8±0.1*	16.9 ± 0.1*
Hindlimb (mg)	310±6	319 ± 4	266±14*	283 ± 12*
Hindlimb/Tibia Length	18.2±0.4	18.6 ± 0.2	15.8±0.8*	16.8 ± 0.7*
Epi Fat (mg)	255±19	192 ± 16	138±32*	134 ± 20*
Spleen (mg)	71±3	68 ± 5	313±34*	279 ± 21*
Testes (mg)	193±4	200 ± 3	179±9*	183 ± 7*
Sem Ves (mg)	305±8	261 ± 8	152±23*	201 ± 28*

Values are means ± SEM. Body weights (BW) given in grams (g). Percent body weight loss is determined from peak body weight to weight prior to sacrifice. Tissue weights given in milligrams (mg). Tibia length given in millimeters (mm). C57BL/6 (B6). *Apc*$^{Min/+}$ (MIN). Two-way ANOVA. *Main effect of genotype. $Paired t-test, effect of time. Significance was set a $p<0.05$

Table 4.4. The effect of wheel access on skeletal muscle's contractile properties in the MIN and B6

	B6		MIN	
	Control	Wheel Access	Control	Wheel Access
n	10	9	10	10
TA Weight (mg)	49.0±0.8	48.4±0.8	42.0±1.9*	44.6±1.9*
L_o (mm)	14.2±0.1	14.3±0.2	13.9±0.2	14.3±0.1
1/2 RT (ms)	7.3±0.2	7.5±0.1	9.4±0.8*	10.3±1.2*
TPT (ms)	15.1±0.2	14.8±0.2	16.2±0.4*	17.6±1.3*
+ dP/dt (mN/s)	24024±873	23197±970	20619±1993	20992±1691
- dP/dt (mN/s)	17549±1287	19700±977	12538±1313*	13090±1664*

Values are means ± SEM. Tibialis Anterior (TA) weight given in milligrams (mg). Optimal length (Lo) in millimeters (mm), 1/2 relaxation time (RT), and time to peak twitch (TPT) determined from isolated twitch contraction. The rate of maximal contraction (+dP/dT) and Relaxation (-dP/dT) obtained from 200hz maximal tetanic force contraction. C57BL/6 (B6). *Apc*$^{Min/+}$ (MIN). Two-way ANOVA. *Main effect of genotype. Significance was set a $p<0.05$

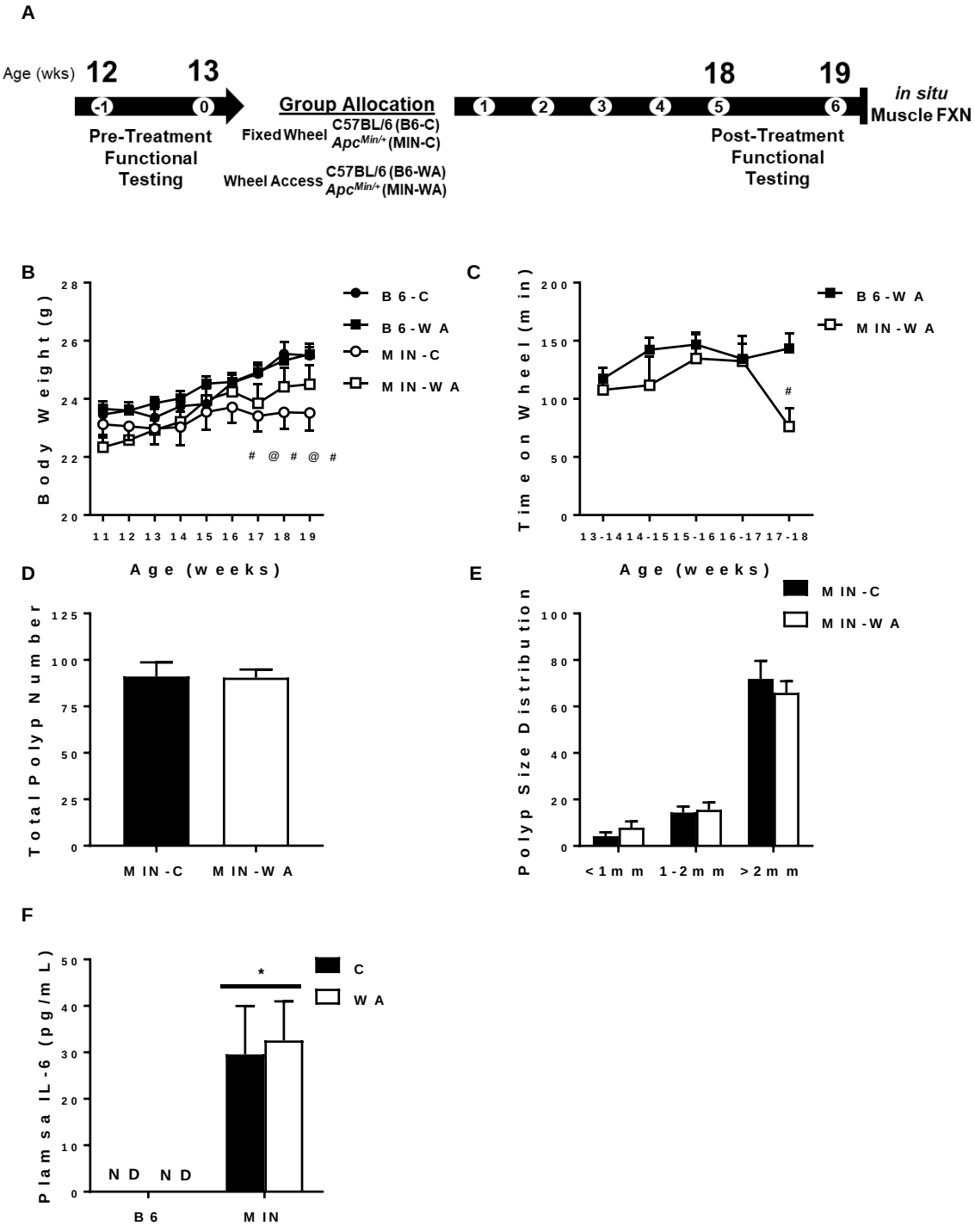

Figure 4.1 The effect of free wheel access on body weight, polyp size, and plasma IL-6. A) Experimental design. Pre-treatment measurements were performed at 12 weeks (wks) of age. Mice were then singled house with either a fixed or free wheel for 5 weeks. Post-treatment measurements were performed at 18 wks of age. Several properties of skeletal

muscle function were assessed at ~19 wks of age is all mice. B) Body weight in grams (g) over the duration of the study. C) Time spent on the wheel for mice given free wheel access. D) Number of intestinal polyps in all MIN mice. E) Intestinal polyp size distribution in all MIN mice. F) Plasma levels of IL-6 in picograms per milliliter (pg/mL) in all mice. Plasma IL-6 was not detectable (ND) in all B6 mice. C57BL/6 (B6). *Apc*$^{Min/+}$ (MIN). Fixed wheel control (C). Free wheel access (WA). Two-way ANOVA. *Main effect of genotype. #Significant difference between MIN-C and B6-WA. @Significant difference between MIN-C and B6-C. Significance was set a $p<0.05$

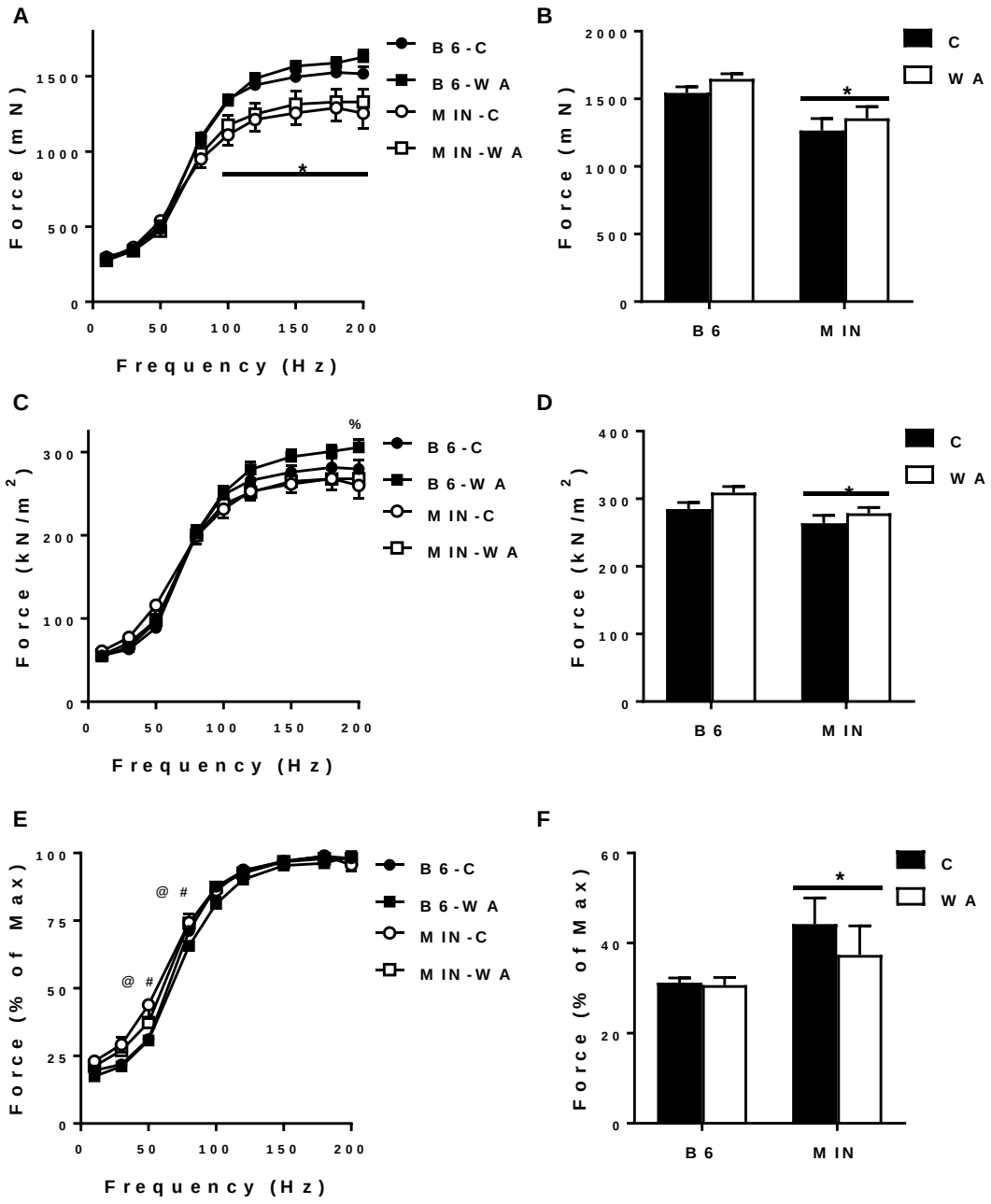

Figure 4.2 The effect of free wheel access on skeletal muscle force production in the male MIN. A) Absolute force-frequency curve of the TA from all groups in millinewtons (mN). B) Maximal tetanic force force-frequency curve of the TA of all groups in mN. C) Specific force-frequency curve of the TA of all groups in kilonewtons/meters^2 (kN/m^2). D) Maximal specific force of the TA from all groups in kN/m^2. E) Relative (% of maximal tetanic force) force-frequency curve of the TA of all groups. D) Relative (% of maximal tetanic force) force at 50Hz of the TA of all groups. Values are means ± SE. C57BL/6 (B6). *Apc*$^{Min/+}$ (MIN). Fixed wheel control (C). Free wheel access (WA). Two-way ANOVA. *Main effect

of genotype. #Significant difference between MIN-C and B6-WA. @Significant difference between MIN-C and B6-C. Significance was set a $p<0.05$

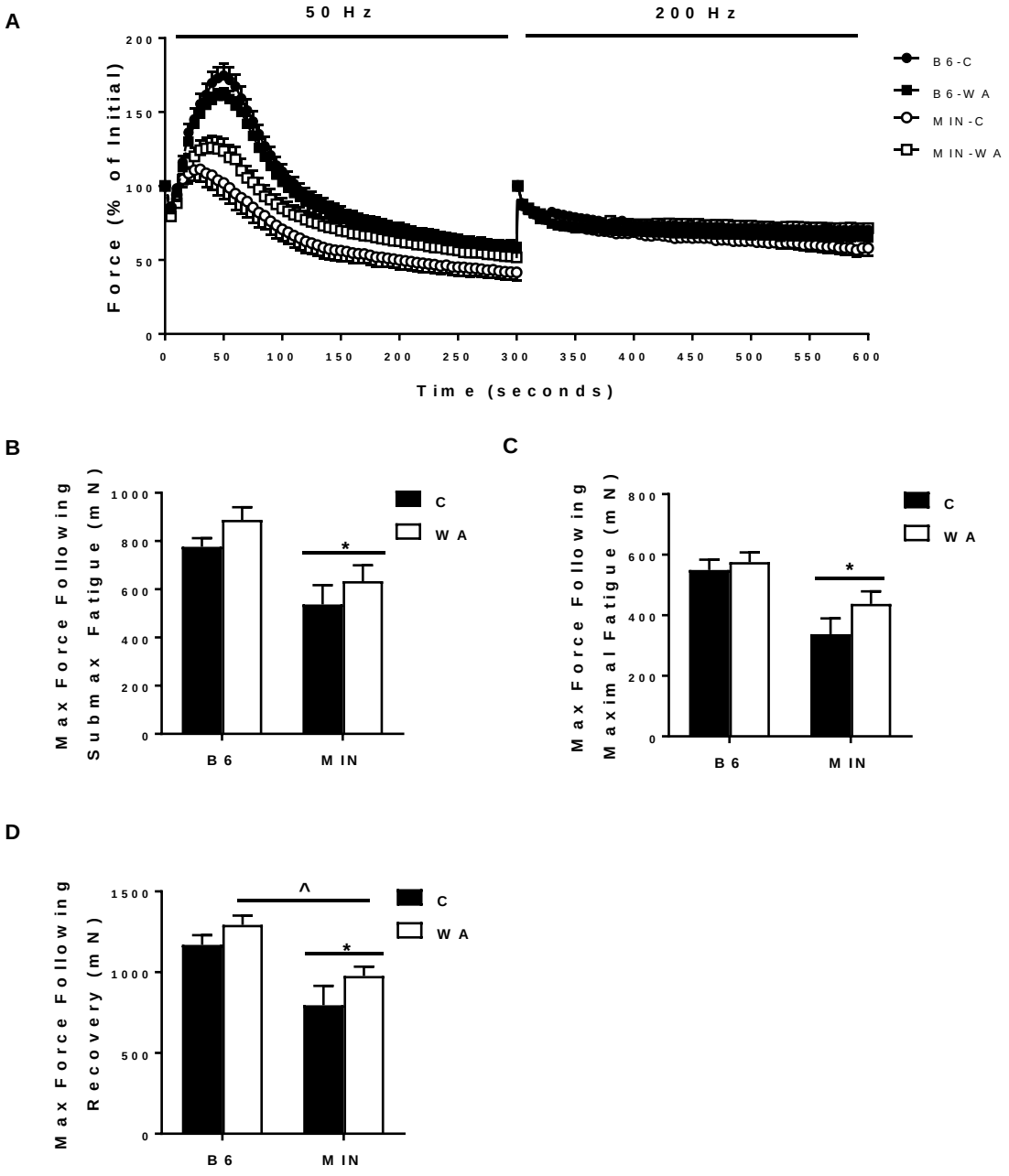

Figure 4.3 The effect of free wheel access on skeletal muscle fatigability in the male MIN. TA muscle's fatigability during a 5-minute submaximal (50 Hz) and 5-minute maximal (200hz) fatigue test. A) Relative (% of Initial) force-time tracing of the TA muscle's fatigability during a 5-minute submaximal (50 Hz) and 5-minute maximal (200hz) fatigue test from all groups. B) Maximal tetanic force in millinewtons (mN) following the 5-minute submaximal contraction-induced fatigue test in all mice. C) Maximal tetanic force in mN following both the 5-minute submaximal and 5-minute maximal contraction-induced

fatigue test in all mice. D) Maximal tetanic force in mN following a 5-minute rest after the completion of the entire contraction-induced fatigue test in all mice. Values are means ± SE. C57BL/6 (B6). *Apc*$^{Min/+}$ (MIN). Fixed wheel control (C). Free wheel access (WA). Two-way ANOVA. *Main effect of genotype. ^Main effect of treatment. Significance was set a $p<0.05$

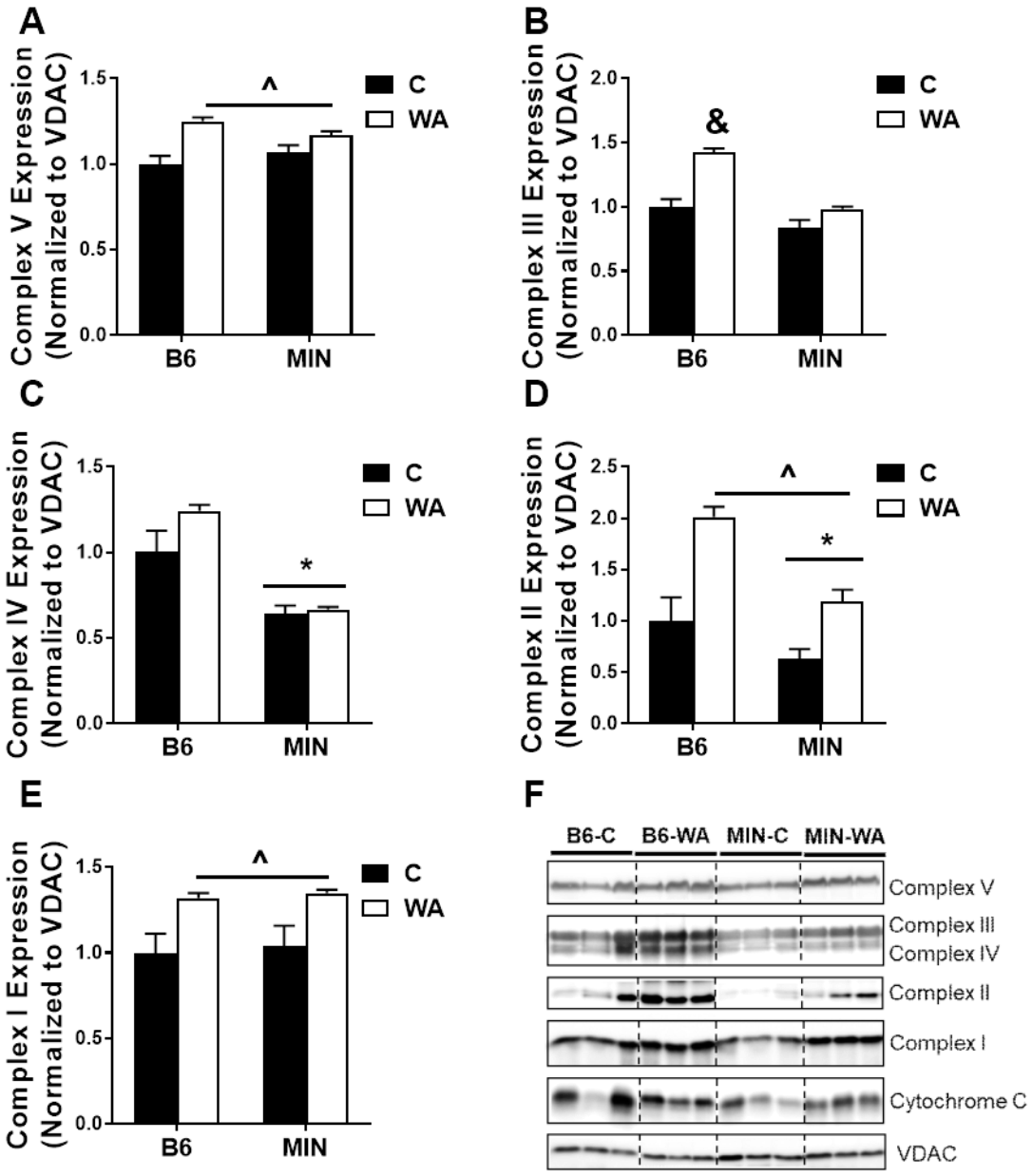

Figure 4.4 The effect of wheel access on skeletal muscle mitochondrial content in isolated skeletal muscle mitochondria in the male MIN. A) The total protein expression of mitochondrial complex V (A), III (B), IV (C), II (D), and I (E) relative to B6-C in isolated skeletal muscle mitochondria normalized to the loading control, VDAC. F) Representative western blot images of protein expression of all mitochondrial complexes. Values are means ± SE. C57BL/6 (B6). *Apc*$^{Min/+}$ (MIN). Fixed wheel control (C). Free wheel access (WA). Two-way ANOVA. *Main effect of genotype. ^Main effect of treatment. & Significantly different to all groups. Significance was set a $p<0.05$

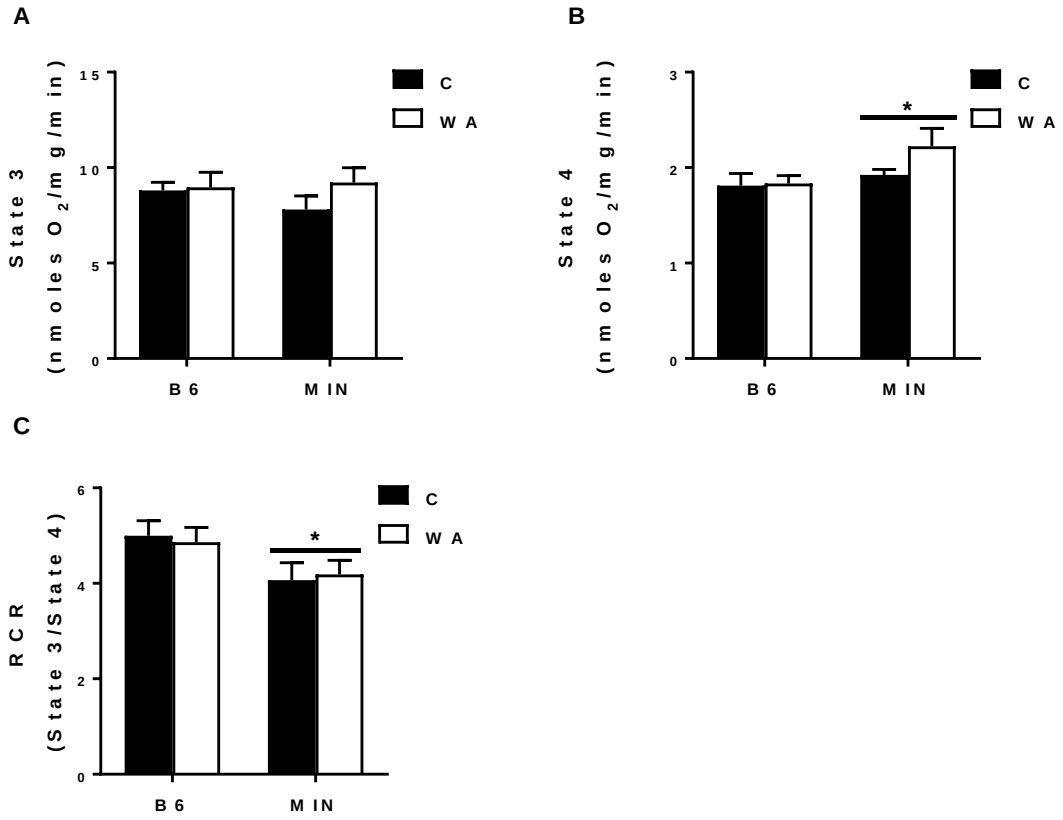

Figure 4.5 The effect of wheel access on skeletal muscle mitochondrial function in the male MIN. Tibialis anterior (TA) respiratory control ratio. A) 0.25mM of ADP was injected into the chamber to induce STATE 3 respiration for a duration of 5 minutes. B) 10ug/mL of Oligomycin was injected to induce steady STATE 4 respiration for a duration of 10 minutes. C) Respiratory Control Ratio (RCR) was calculated by dividing STATE 3 by STATE 4 respirations. Values are means ± SE. C57BL/6 (B6). *Apc*$^{Min/+}$ (MIN). Fixed wheel control (C). Free wheel access (WA). Two-way ANOVA. *Main effect of genotype. ^Main effect of treatment. & Significantly different to all groups. Significance was set a $p<0.05$

CHAPTER 5

OVERALL DISCUSSION

The overall purpose of this dissertation was to determine the development of skeletal muscle fatigue in tumor-bearing mice and identify the regulation of skeletal muscle fatigue by activity and/or muscle gp130 signaling. We hypothesized that cancer-induced skeletal muscle fatigue develops independent of significant weight loss in association with decreased muscle use and activated muscle gp130 signaling which disrupts muscle oxidative metabolism. We then sought to determine if increased muscle use through increased volitional activity could delay the induction of fatigue in tumor-bearing mice. Key findings from this dissertation's experiments demonstrated that (1) cachectic skeletal muscle displayed disrupted contractile properties and force production associated with increased muscle gp130 signaling, however, disrupted skeletal muscle fatigability develops without significant wasting in MIN mice, (2) IL-6 directly disrupted skeletal muscle fatigability and mitochondrial function through muscle gp130 signaling, though the loss of the gp130 receptor in MIN mice did not rescue skeletal muscle function, and (3) reduced activity is associated with skeletal muscle and whole body fatigue in MIN mice which can be improved with wheel access.

5.1 – Skeletal muscle dysfunction during cachexia progression

Cancer patients suffering from progressive body weight loss and low skeletal muscle mass have reduced functional independence and life quality contributing to reduced

chemotherapy tolerance and a poorer prognosis (Vigano et al. 2000; Evans et al. 2008; Moses et al. 2004; Fearon KC 2006; Argiles 2014; Amano et al. 2017; al-Majid and McCarthy 2001a; O'Gorman, McMillan, and McArdle 1999). Whether these functional deficits are causal or consequence of muscle mass loss with cancer patients remains unknown. Additionally, the neural, circulatory, or musculoskeletal contributions to these deficits are only beginning to be unearthed (Christensen et al. 2014; Gorselink et al. 2006; Murphy et al. 2012; Roberts, Frye, et al. 2013; Jaweed et al. 1983). While cachectic skeletal muscle force and fatigability have been studied, our understanding of the progression of these deficits and mechanistic explanations remain limited (al-Majid and McCarthy 2001a; Baltgalvis 2010; Christensen et al. 2014; Murphy et al. 2012; Roberts, Frye, et al. 2013; White, Baltgalvis, et al. 2011; White et al. 2012). Results from the current project demonstrate skeletal muscle weakness and contractile dysfunction occurs concomitant with body weight and muscle mass loss, while increased skeletal muscle fatigability develops prior to the initiation of cachexia.

Skeletal Muscle Contractile Properties

Skeletal muscle contractile dysfunction has been demonstrated across several chronic diseases (Sin and Man 2003; Deans and Wigmore 2005; Kuller et al. 2008; Vidt 2006). Whether contraction rates are disrupted during cachexia development has not been firmly established. The twitch properties of the TA from LLC and C-26 tumor-bearing mice were not different from healthy controls (Murphy et al. 2011; Murphy et al. 2012). There was a reduction in twitch force (Gorselink et al. 2006) and slower twitch properties (Roberts, Frye, et al. 2013) in the EDL of C-26 mice. The current studies demonstrated that twitch properties of the TA from MIN mice were slowed with severe cachexia.

Additionally, twitch properties were not affected by IL-6, but the loss of the muscle gp130 receptor increased the twitch contraction rates. While increased contraction rates are associated with reduced skeletal muscle activity, the slowing of cachectic muscle occurs concomitant with reduced activity which was not improved with wheel access. Skeletal muscle's contractile properties rely on the coordination of neural excitation, sarcomeric structure, calcium handling, and myosin isoform expression (Close 1972; Schiaffino and Reggiani 1996; Khodabukus and Baar 2015). Classically, twitch relaxation is dependent on the rate of calcium reuptake by the Sarcoplasmic Reticulum Calcium ATPase (SERCA) after stimulation (Close 1972; Berchtold, Brinkmeier, and Muntener 2000). Previous reports have shown increased expression of SERCA1 and SERCA2 contributing to aberrant calcium handling, mitochondrial dysfunction, EC uncoupling, and fatigue (Debold 2016; Fontes-Oliveira et al. 2013; Carson, Hardee, and VanderVeen 2016). It is generally accepted that preferential atrophy of type II occurs during cachexia, particularly at the early stages of wasting. Interestingly, we have previously demonstrated a loss of fiber-types (IIB , IIX, and IIA) in the TA of cachectic MIN mice, which coincided with the percent of myofibers with high succinate dehydrogenase enzyme activity (Hardee et al. 2016).

Skeletal Muscle Force

Reduced specific tension has been reported during LLC-induced cachexia (Roberts, Frye, et al. 2013), while others have reported a mass dependent loss of muscle force with C-26-induced wasting (Murphy et al. 2012; Gorselink et al. 2006). The results from the current study demonstrated that 20-week old weight stable male MINs had no disruption to absolute or specific skeletal muscle force while severely cachectic MINs had a loss of skeletal muscle force that was disproportionate to muscle mass loss. Interestingly, muscle

weakness was observed prior to weight loss in MIN mice with a high polyp count suggesting that muscle weakness was dependent on tumor-burden which contributes significantly to cachexia severity (Baltgalvis et al. 2008). While tumor-burden is strongly related to plasma IL-6, elevated levels of IL-6 were not able to induce muscle mass loss or weakness in tumor-free mice. Furthermore, loss of the muscle IL-6 receptor β-subunit (gp130) was not able to prevent muscle mass loss or muscle weakness in the MIN. Our lab has previously shown that IL-6 null MIN mice had spared body and muscle weight loss associated with reduced tumor-burden (Baltgalvis et al. 2008), and administration of an IL-6 antibody to MINs spared muscle mass without affecting tumor-burden (White, Baynes, et al. 2011). Together, these results suggest an interaction between circulating IL-6 and the tumor-environment to promote skeletal muscle mass loss and may also contribute muscle weakness independent of muscle gp130 signaling. Tumor-derived IL-6, IL-6 trans-signaling, and other members of the IL-6 family of cytokines have been shown to play an important role in muscle mass maintenance with cancer (Pettersen et al. 2017; Kandarian et al. 2018); however, their role in cancer-induced muscle weakness has not been investigated.

Skeletal muscle fatigue

Along with lean mass and strength, cancer-related fatigue is a strong predictor of survival in cancer patients (Vigano et al. 2000; Christensen et al. 2014). The results of the current study support a direct role for skeletal muscle in cancer fatigue development before the onset of cachexia. Accelerated skeletal muscle fatigue has been reported in cancer patients and preclinical models alike (Stone et al. 1999; Roberts, Frye, et al. 2013); however, several reports show do not see a difference in fatigability between tumor-burden

and healthy controls (Murphy et al. 2012; Gorselink et al. 2006). Our results demonstrate that fatigue develops without significant weight loss and suggests that muscular fatigue develops prior to wasting and contributes to muscle mass loss. Interestingly, while TNFα administration alone was sufficient to cause weakness and contractile dysfunction, TNFα had no effect on skeletal muscle fatigability (Hardin et al. 2008). High levels of IL-6 were able to accelerate muscle fatigue in tumor-free mice, but loss of the IL-6 gp130 receptor in tumor bearing mice was not sufficient to attenuate cancer-induced muscle fatigue. While muscle gp130 loss was unable to prevent cancer-induced fatigue, there is a strong relationship between activity and muscle fatigue with cachexia progression, which was attenuated by increased activity. These results suggest that activity and chronic inflammation can directly cause fatigue, however, may only partially contribute to cancer-induced fatigues' etiology. It is important to note, however, that in addition to the abundance of mitochondrial derived ATP, skeletal muscle fatigability can be affected by nutrient availability, blood supply, pH, and myosin heavy chain isoform expression, which were examined in this dissertation. Future inquiry into the regulation and contribution of these processes to cancer-induced fatigue are warranted.

5.2 – Skeletal muscle oxidative metabolism during cachexia progression

Disrupted metabolic homeostasis in skeletal muscle has been demonstrated across several chronic diseases (Sin and Man 2003; Deans and Wigmore 2005; Kuller et al. 2008; Vidt 2006). Recently, muscle mitochondrial dysfunction and increased fatigability has been shown to occur independent of changes to muscle size and strength (VanderVeen et al. 2018; Brown et al. 2017). Additionally, there is a loss of muscle functional quality that

is disproportionate to muscle mass demonstrating that muscle weakness and fatigue have distinct etiologies (Ramage and Skipworth 2018). IL-6 signaling through muscle gp130 regulates skeletal muscle mass and metabolic homeostasis during both physiological and pathological conditions (Carson and Baltgalvis 2010; Bonetto et al. 2011; Hardee, Counts, et al. 2018; Gao et al. 2017; Puppa, Gao, et al. 2014). Furthermore, the mitochondria have emerged as an intriguing target for inflammation induced skeletal muscle metabolic dysfunction (Boland, Chourasia, and Macleod 2013; Brown et al. 2017; Hardee et al. 2016; Carson, Hardee, and VanderVeen 2016). We have previously shown that IL-6 decreases mitochondrial protein expression in tumor-free mice and exercise can prevent the IL-6-induced loss of muscle mass in tumor bearing mice (Puppa et al. 2012). The results from the current study extend these findings to show that IL-6/gp130 signaling plays a direct role in muscle mitochondrial function and increase volitional activity can improve muscle mitochondrial content and fatigability in the tumor bearing mice.

Skeletal muscle mitochondrial content

Cachectic skeletal muscle has disrupted metabolic homeostasis thought to contribute to aberrant muscle mass maintenance and increased muscle-specific fatigue. We have previously found disrupted mitochondrial quality control (decreased content and biogenesis, disrupted dynamics, etc.) in MIN muscle (White et al. 2012; Carson, Hardee, and VanderVeen 2016), which coincides with decreased physical activity and reduced muscle mass (Baltgalvis 2010). Decrements in mitochondrial biogenesis and mitochondrial content have been strongly associated with increased fatigue in skeletal muscle (Lin et al. 2002; Brown et al. 2017). The results from the current study further extend this work by showing decreased COX activity in cachectic MIN muscle. Additionally, there was a

reduction in several muscle mitochondrial complexes in mitochondrial isolated from pre-cachectic mouse muscle. We also demonstrated that tumor-bearing mice, independent of weight loss, experienced increased fatigue measured by whole body exercise and *in situ* muscle function, which was not related to elevated circulating IL-6, activated muscle inflammatory signaling, or COX activity. Interestingly, gpo130 loss was able to partially rescue the loss of muscle PGC1α and COXIV protein expression, while increasing MFN1 and decreased FIS1 protein expression. Increasing physical activity in pre-cachectic MINs was able to increase protein expression of isolated mitochondrial complexes concomitant with increase run to fatigue time and improved muscle fatigue resistance.

Skeletal muscle mitochondrial function

Cancer-induced skeletal muscle mitochondrial dysfunction is currently an active area of investigation (Carson, Hardee, and VanderVeen 2016). While more work is needed, the activation of either nuclear factor κ B (NF-κB), STAT3, or mothers against decapentaplegic homolog 3 (Smad3) signaling have been associated with cancer-induced muscle mitochondria dysfunction in tumor bearing mice (VanderVeen, Fix, and Carson 2017). LLC-tumor cell induced cachexia demonstrated decreased muscle ATP synthesis rates and decreased electron transport chain efficiency with associative increases in TNF-α (Constantinou et al. 2011; McLean, Moylan, and Andrade 2014). Furthermore, blockade of NF-κB improved diaphragm mitochondrial respiration in mice bearing P07 lung derived tumors (Fermoselle et al. 2013). While our understanding of STAT3's role in skeletal muscle mitochondrial function is in its infancy, the current study demonstrated that IL-6 can disrupt mitochondrial respiration and through direct activation of muscle gp130 signaling (Wegrzyn et al. 2009). Additionally, MIN mice lacking the muscle gp130

receptor had increased muscle mitochondrial respiration when compare to floxed MINs; however, gp130 loss did not improve fatigability in the MIN. Lastly, increased wheel activity was able to improve muscle fatigability without improving muscle mitochondrial respiration.

5.3 – Summary

The purpose of this dissertation was to investigate the regulation of skeletal muscle fatigue in tumor-bearing mice. The loss of skeletal muscle's mass and functional quality are thought to develop primarily through disruptions to muscle metabolic homeostasis; however, what causes these disruptions still remain an active area of investigation (Tisdale 2009). While accelerated muscle protein catabolism and suppressed anabolism has been a primary target for cancer-cachexia therapeutics, several therapeutics have failed to improve skeletal muscle function and patient quality of life (al-Majid and McCarthy 2001a; Christensen et al. 2014; Aversa, Costelli, and Muscaritoli 2017; Biolo, Cederholm, and Muscaritoli 2014; Dobs et al. 2013; Ramage and Skipworth 2018). Recent evidence suggests an important role for disrupted oxidative metabolism in cancer-induced wasting, specifically, accelerated mitochondrial fission and autophagy in concert with reduced mitochondrial biogenesis and fusion contributing to mitochondrial dysfunction. While mitochondrial dysfunction contributes to muscle mass loss, results from the current study suggest that inflammation-induced mitochondrial dysfunction disrupts skeletal muscle fatigability independent of mass. Additionally, disruptions to muscle oxidative metabolism early in cachexia progression may contribute to accelerated muscle fatigability observed in weight stable and pre-cachectic MIN mice. Lastly, while regimented exercise has

established beneficial effects on tumor progression, global metabolism, and muscle function, the current study is the first to suggest that increased volitional activity improves muscle fatigability and mitochondrial content without affecting tumor-burden or plasma IL-6. The current study was limited to investigations of a preclinical model of colorectal cancer and cannot necessarily be extrapolated to all cancer types. Additionally, there are several factors that contribute to overall and skeletal muscle fatigability that were not measure and warrant future investigations. Together the results from the current study, however, suggest that cancer-induced skeletal muscle fatigue is distinct from IL-6-induced skeletal muscle fatigue and skeletal muscle fatigability occurs independent of body weight loss which can be improved with increased volitional activity.

REFERENCES

Abbas, Abul K., Andrew H. Lichtman, and Shiv Pillai. 2015. *Cellular and molecular immunology* (Elsevier Saunders: Philadelphia, PA).

Acharyya, S., and D. C. Guttridge. 2007. 'Cancer cachexia signaling pathways continue to emerge yet much still points to the proteasome', *Clin Cancer Res*, 13: 1356-61.

Adams, V., N. Mangner, A. Gasch, C. Krohne, S. Gielen, S. Hirner, H. J. Thierse, C. C. Witt, A. Linke, G. Schuler, and S. Labeit. 2008. 'Induction of MuRF1 is essential for TNF-alpha-induced loss of muscle function in mice', *J Mol Biol*, 384: 48-59.

Aihara, H., N. Kumar, and C. C. Thompson. 2014. 'Diagnosis, surveillance, and treatment strategies for familial adenomatous polyposis: rationale and update', *Eur J Gastroenterol Hepatol*, 26: 255-62.

al-Majid, S., and D. O. McCarthy. 2001a. 'Cancer-induced fatigue and skeletal muscle wasting: the role of exercise', *Biol Res Nurs*, 2: 186-97.

———. 2001b. 'Resistance exercise training attenuates wasting of the extensor digitorum longus muscle in mice bearing the colon-26 adenocarcinoma', *Biol Res Nurs*, 2: 155-66.

Allen, D. G., G. D. Lamb, and H. Westerblad. 2008. 'Skeletal muscle fatigue: cellular mechanisms', *Physiol Rev*, 88: 287-332.

Allen, D. L., B. C. Harrison, A. Maass, M. L. Bell, W. C. Byrnes, and L. A. Leinwand. 2001. 'Cardiac and skeletal muscle adaptations to voluntary wheel running in the mouse', *J Appl Physiol (1985)*, 90: 1900-8.

Altenburg, T. M., H. Degens, W. van Mechelen, A. J. Sargeant, and A. de Haan. 2007. 'Recruitment of single muscle fibers during submaximal cycling exercise', *J Appl Physiol (1985)*, 103: 1752-6.

Alves, C. R., T. F. da Cunha, N. A. da Paixao, and P. C. Brum. 2015. 'Aerobic exercise training as therapy for cardiac and cancer cachexia', *Life Sci*, 125: 9-14.

Amano, K., I. Maeda, T. Morita, M. Baba, T. Miura, T. Hama, I. Mori, N. Nakajima, T. Nishi, H. Sakurai, S. Shimoyama, T. Shinjo, H. Shirayama, T. Yamada, S. Ono, T. Ozawa, R. Yamamoto, N. Yamamoto, H. Shishido, and H. Kinoshita. 2017. 'C-reactive protein, symptoms and activity of daily living in patients with advanced cancer receiving palliative care', *Journal of cachexia, sarcopenia and muscle*, 8: 457-65.

Arany, Z., N. Lebrasseur, C. Morris, E. Smith, W. Yang, Y. Ma, S. Chin, and B. M. Spiegelman. 2007. 'The transcriptional coactivator PGC-1beta drives the formation of oxidative type IIX fibers in skeletal muscle', *Cell metabolism*, 5: 35-46.

Argiles, J. M., S. Busquets, A. Felipe, and F. J. Lopez-Soriano. 2005. 'Molecular mechanisms involved in muscle wasting in cancer and ageing: cachexia versus sarcopenia', *Int J Biochem Cell Biol*, 37: 1084-104.

Argiles, J. M., S. Busquets, and F. J. Lopez-Soriano. 2005. 'The pivotal role of cytokines in muscle wasting during cancer', *Int J Biochem Cell Biol*, 37: 2036-46.

Argiles, J. M., S. Busquets, M. Toledo, and F. J. Lopez-Soriano. 2009. 'The role of cytokines in cancer cachexia', *Curr Opin Support Palliat Care*, 3: 263-8.

Argiles, J.M.; Busquets, S; Lopez-Soriano, FJ; Costelli, P; Penna, F. 2012. 'Are there any benefits of exercise training in cancer cachexia?', *J Cachexia Saropenia Muscle*, 3: 73-6.

Argiles, J.M.; Busquets, S; Stemmler, B; Lopez-Soriano, F.J. 2014. 'Cancer cachexia: Understanding the molecular basis', *Nature Reviews*, 14: 754-62.

Arthur, S. T., J. M. Noone, B. A. Van Doren, D. Roy, and C. M. Blanchette. 2014. 'One-year prevalence, comorbidities and cost of cachexia-related inpatient admissions in the USA', *Drugs Context*, 3: 212265.

Ashcraft, K. A., R. M. Peace, A. S. Betof, M. W. Dewhirst, and L. W. Jones. 2016. 'Efficacy and Mechanisms of Aerobic Exercise on Cancer Initiation, Progression, and Metastasis: A Critical Systematic Review of In Vivo Preclinical Data', *Cancer Res*, 76: 4032-50.

Au, E. D., A. P. Desai, L. G. Koniaris, and T. A. Zimmers. 2016. 'The MEK-Inhibitor Selumetinib Attenuates Tumor Growth and Reduces IL-6 Expression but Does Not Protect against Muscle Wasting in Lewis Lung Cancer Cachexia', *Front Physiol*, 7: 682.

Aversa, Z., P. Costelli, and M. Muscaritoli. 2017. 'Cancer-induced muscle wasting: latest findings in prevention and treatment', *Ther Adv Med Oncol*, 9: 369-82.

Aversa, Z., F. Pin, S. Lucia, F. Penna, R. Verzaro, M. Fazi, G. Colasante, A. Tirone, F. Rossi Fanelli, C. Ramaccini, P. Costelli, and M. Muscaritoli. 2016. 'Autophagy is induced in the skeletal muscle of cachectic cancer patients', *Sci Rep*, 6: 30340.

Baar, Keith. 2004. 'Involvement of PPARg co-activator-1, nuclear respiratory factors 1 and 2, and PPARa in the adaptive response to endurance exercise', *Proceedings of the Nutrition Society*: 269-73.

Baltgalvis, K. A., F. G. Berger, M. M. Pena, J. M. Davis, S. J. Muga, and J. A. Carson. 2008. 'Interleukin-6 and cachexia in ApcMin/+ mice', *Am J Physiol Regul Integr Comp Physiol*, 294: R393-401.

Baltgalvis, K. A., F. G. Berger, M. M. Pena, J. M. Davis, J. P. White, and J. A. Carson. 2009. 'Muscle wasting and interleukin-6-induced atrogin-I expression in the cachectic Apc (Min/+) mouse', *Pflugers Arch*, 457: 989-1001.

Baltgalvis, K. A., F. G. Berger, M. M. Pena, J. Mark Davis, J. P. White, and J. A. Carson. 2010. 'Activity level, apoptosis, and development of cachexia in Apc(Min/+) mice', *J Appl Physiol (1985)*, 109: 1155-61.

Baltgalvis, K.A.; Berger, F.G.; Pena, M.M.; Davis, J.M.; White, J.P.; Carson, J.A. 2010. 'Activity level, apoptosis, and development of cachexia in Apc min/+ mice', *Journal of Applied Physiology*, 109: 1155-61.

Bannister, R. A. 2016. 'Bridging the myoplasmic gap II: more recent advances in skeletal muscle excitation-contraction coupling', *J Exp Biol*, 219: 175-82.

Barbaric, M., E. Brooks, L. Moore, and O. Cheifetz. 2010. 'Effects of physical activity on cancer survival: a systematic review', *Physiother Can*, 62: 25-34.

Barber, M. D., J. A. Ross, and K. C. Fearon. 1999. 'Changes in nutritional, functional, and inflammatory markers in advanced pancreatic cancer', *Nutr Cancer*, 35: 106-10.

Barreiro, E., A. S. Comtois, S. Mohammed, L. C. Lands, and S. N. Hussain. 2002. 'Role of heme oxygenases in sepsis-induced diaphragmatic contractile dysfunction and oxidative stress', *Am J Physiol Lung Cell Mol Physiol*, 283: L476-84.

Barreiro, E., and J. Gea. 2015. 'Respiratory and Limb Muscle Dysfunction in COPD', *COPD*, 12: 413-26.

Barreto, R., D. L. Waning, H. Gao, Y. Liu, T. A. Zimmers, and A. Bonetto. 2016. 'Chemotherapy-related cachexia is associated with mitochondrial depletion and the activation of ERK1/2 and p38 MAPKs', *Oncotarget*, 7: 43442-60.

Belizario, J. E., C. C. Fontes-Oliveira, J. P. Borges, J. A. Kashiabara, and E. Vannier. 2016. 'Skeletal muscle wasting and renewal: a pivotal role of myokine IL-6', *SpringerPlus*, 5: 619.

Berchtold, M. W., H. Brinkmeier, and M. Muntener. 2000. 'Calcium ion in skeletal muscle: its crucial role for muscle function, plasticity, and disease', *Physiol Rev*, 80: 1215-65.

Berger, A. M., K. Mooney, A. Alvarez-Perez, W. S. Breitbart, K. M. Carpenter, D. Cella, C. Cleeland, E. Dotan, M. A. Eisenberger, C. P. Escalante, P. B. Jacobsen, C. Jankowski, T. LeBlanc, J. A. Ligibel, E. T. Loggers, B. Mandrell, B. A. Murphy, O. Palesh, W. F. Pirl, S. C. Plaxe, M. B. Riba, H. S. Rugo, C. Salvador, L. I. Wagner, N. D. Wagner-Johnston, F. J. Zachariah, M. A. Bergman, C. Smith, and network National comprehensive cancer. 2015. 'Cancer-Related Fatigue, Version 2.2015', *J Natl Compr Canc Netw*, 13: 1012-39.

Bergeron, R., J. M. Ren, K. S. Cadman, I. K. Moore, P. Perret, M. Pypaert, L. H. Young, C. F. Semenkovich, and G. I. Shulman. 2001. 'Chronic activation of AMP kinase

results in NRF-1 activation and mitochondrial biogenesis', *Am J Physiol Endocrinol Metab*, 281: E1340-6.

Biolo, G., T. Cederholm, and M. Muscaritoli. 2014. 'Muscle contractile and metabolic dysfunction is a common feature of sarcopenia of aging and chronic diseases: from sarcopenic obesity to cachexia', *Clin Nutr*, 33: 737-48.

Bodine, S. C., R. R. Roy, E. Eldred, and V. R. Edgerton. 1987. 'Maximal force as a function of anatomical features of motor units in the cat tibialis anterior', *J Neurophysiol*, 57: 1730-45.

Boland, M. L., A. H. Chourasia, and K. F. Macleod. 2013. 'Mitochondrial dysfunction in cancer', *Front Oncol*, 3: 292.

Bonetto A, Aydogdu T, Jin X, Zhang Z, Zhan R, Puzis L, Koniaris LG, Zimmers TA. 2012. 'JAK/STAT3 pathway inhibition blocks skeletal muscle wasting downstream of IL-6 and in experimental cancer cachexia', *American Journal of Physiology Endocrinology and Metabolism*, 303: E410-21.

Bonetto, A., D. C. Andersson, and D. L. Waning. 2015. 'Assessment of muscle mass and strength in mice', *Bonekey Rep*, 4: 732.

Bonetto, A., T. Aydogdu, N. Kunzevitzky, D. C. Guttridge, S. Khuri, L. G. Koniaris, and T. A. Zimmers. 2011. 'STAT3 activation in skeletal muscle links muscle wasting and the acute phase response in cancer cachexia', *PLoS One*, 6: e22538.

Booth, F. W., and M. V. Chakravarthy. 2006. 'Physical activity and dietary intervention for chronic diseases: a quick fix after all?', *J Appl Physiol (1985)*, 100: 1439-40.

Booth, F. W., C. K. Roberts, and M. J. Laye. 2012. 'Lack of exercise is a major cause of chronic diseases', *Compr Physiol*, 2: 1143-211.

Bordi, M., F. Nazio, and S. Campello. 2017. 'The Close Interconnection between Mitochondrial Dynamics and Mitophagy in Cancer', *Front Oncol*, 7: 81.

Bossola, M., M. Muscaritoli, P. Costelli, G. Grieco, G. Bonelli, F. Pacelli, F. Rossi Fanelli, G. B. Doglietto, and F. M. Baccino. 2003. 'Increased muscle proteasome activity correlates with disease severity in gastric cancer patients', *Ann Surg*, 237: 384-9.

Boutagy, N. E., E. Pyne, G. W. Rogers, M. Ali, M. W. Hulver, and M. I. Frisard. 2015. 'Isolation of Mitochondria from Minimal Quantities of Mouse Skeletal Muscle for High Throughput Microplate Respiratory Measurements', *Journal of visualized experiments : JoVE*.

Brooks, S. V., and J. A. Faulkner. 1988. 'Contractile properties of skeletal muscles from young, adult and aged mice', *The Journal of physiology*, 404: 71-82.

Brown, J. C., K. Winters-Stone, A. Lee, and K. H. Schmitz. 2012. 'Cancer, physical activity, and exercise', *Compr Physiol*, 2: 2775-809.

Brown, J. L., M. E. Rosa-Caldwell, D. E. Lee, T. A. Blackwell, L. A. Brown, R. A. Perry, W. S. Haynie, J. P. Hardee, J. A. Carson, M. P. Wiggs, T. A. Washington, and N. P. Greene. 2017. 'Mitochondrial degeneration precedes the development of muscle atrophy in progression of cancer cachexia in tumour-bearing mice', *Journal of cachexia, sarcopenia and muscle*.

Bruera, E. 1997. 'ABC of palliative care. Anorexia, cachexia, and nutrition', *BMJ*, 315: 1219-22.

Brzeszczynska, J., N. Johns, A. Schilb, S. Degen, M. Degen, R. Langen, A. Schols, D. J. Glass, R. Roubenoff, C. A. Greig, C. Jacobi, KCh Fearon, and J. A. Ross. 2016.

'Loss of oxidative defense and potential blockade of satellite cell maturation in the skeletal muscle of patients with cancer but not in the healthy elderly', *Aging (Albany NY)*, 8: 1690-702.

Burkholder, T. J., B. Fingado, S. Baron, and R. L. Lieber. 1994. 'Relationship between muscle fiber types and sizes and muscle architectural properties in the mouse hindlimb', *J Morphol*, 221: 177-90.

Busquets, S., B. Alvarez, M. van Royen, N. Carbo, F. J. Lopez-Soriano, and J. M. Argiles. 2000. 'Lack of effect of the cytokine suppressive agent FR167653 on tumour growth and cachexia in rats bearing the Yoshida AH-130 ascites hepatoma', *Cancer Lett*, 157: 99-103.

Cannon TY, Guttridge D, Dahlman J, George JR, Lai V, Shores C, Buzkova P, Couch ME. 2007. 'The effect of altered toll-like receptor 4 signaling on cancer cachexia', *Arch Otolaryngol Head Neck Surg*, 133: 1263-9.

Carling, D. 2017. 'AMPK signalling in health and disease', *Curr Opin Cell Biol*, 45: 31-37.

Carson, J. A., and K. A. Baltgalvis. 2010. 'Interleukin 6 as a key regulator of muscle mass during cachexia', *Exerc Sport Sci Rev*, 38: 168-76.

Carson, J. A., J. P. Hardee, and B. N. VanderVeen. 2016. 'The emerging role of skeletal muscle oxidative metabolism as a biological target and cellular regulator of cancer-induced muscle wasting', *Semin Cell Dev Biol*, 54: 53-67.

Chang, V. T., S. S. Hwang, M. Feuerman, and B. S. Kasimis. 2000. 'Symptom and quality of life survey of medical oncology patients at a veterans affairs medical center: a role for symptom assessment', *Cancer*, 88: 1175-83.

Cheema, B., C. A. Gaul, K. Lane, and M. A. Fiatarone Singh. 2008. 'Progressive resistance training in breast cancer: a systematic review of clinical trials', *Breast Cancer Res Treat*, 109: 9-26.

Chen, J. L., T. D. Colgan, K. L. Walton, P. Gregorevic, and C. A. Harrison. 2016. 'The TGF-beta Signalling Network in Muscle Development, Adaptation and Disease', *Adv Exp Med Biol*, 900: 97-131.

Choi, I., H. S. Kang, Y. Yang, and K. H. Pyun. 1994. 'IL-6 induces hepatic inflammation and collagen synthesis in vivo', *Clin Exp Immunol*, 95: 530-5.

Choi, S. J., and J. J. Widrick. 2009. 'Combined effects of fatigue and eccentric damage on muscle power', *J Appl Physiol (1985)*, 107: 1156-64.

Christensen, J. F., L. W. Jones, J. L. Andersen, G. Daugaard, M. Rorth, and P. Hojman. 2014. 'Muscle dysfunction in cancer patients', *Ann Oncol*, 25: 947-58.

Close, R. 1964. 'Dynamic Properties of Fast and Slow Skeletal Muscles of the Rat during Development', *The Journal of physiology*, 173: 74-95.

Close, R. I. 1972. 'Dynamic properties of mammalian skeletal muscles', *Physiol Rev*, 52: 129-97.

Comtois, A. S., E. Barreiro, P. L. Huang, A. Marette, M. Perrault, and S. N. Hussain. 2001. 'Lipopolysaccharide-induced diaphragmatic contractile dysfunction and sarcolemmal injury in mice lacking the neuronal nitric oxide synthase', *Am J Respir Crit Care Med*, 163: 977-82.

Constantinou, C., C. C. Fontes de Oliveira, D. Mintzopoulos, S. Busquets, J. He, M. Kesarwani, M. Mindrinos, L. G. Rahme, J. M. Argiles, and A. A. Tzika. 2011. 'Nuclear magnetic resonance in conjunction with functional genomics suggests

mitochondrial dysfunction in a murine model of cancer cachexia', *Int J Mol Med*, 27: 15-24.

Cooke, R. 2007. 'Modulation of the actomyosin interaction during fatigue of skeletal muscle', *Muscle Nerve*, 36: 756-77.

Copeland, S., H. S. Warren, S. F. Lowry, S. E. Calvano, D. Remick, Inflammation, and Investigators the Host Response to Injury. 2005. 'Acute inflammatory response to endotoxin in mice and humans', *Clin Diagn Lab Immunol*, 12: 60-7.

Cornwell, E. W., A. Mirbod, C. L. Wu, S. C. Kandarian, and R. W. Jackman. 2014. 'C26 cancer-induced muscle wasting is IKKbeta-dependent and NF-kappaB-independent', *PLoS One*, 9: e87776.

Cosper, P. F., and L. A. Leinwand. 2011. 'Cancer causes cardiac atrophy and autophagy in a sexually dimorphic manner', *Cancer Research*, 71: 1710-20.

Coyle, E. F., W. H. Martin, 3rd, S. A. Bloomfield, O. H. Lowry, and J. O. Holloszy. 1985. 'Effects of detraining on responses to submaximal exercise', *J Appl Physiol (1985)*, 59: 853-9.

Crilly, M. J., L. D. Tryon, A. T. Erlich, and D. A. Hood. 2016. 'The role of Nrf2 in skeletal muscle contractile and mitochondrial function', *J Appl Physiol (1985)*, 121: 730-40.

Cron, L., T. Allen, and M. A. Febbraio. 2016. 'The role of gp130 receptor cytokines in the regulation of metabolic homeostasis', *J Exp Biol*, 219: 259-65.

Dahele, M., and K. C. Fearon. 2004. 'Research methodology: cancer cachexia syndrome', *Palliat Med*, 18: 409-17.

Dahele, M., R. J. Skipworth, L. Wall, A. Voss, T. Preston, and K. C. Fearon. 2007. 'Objective physical activity and self-reported quality of life in patients receiving palliative chemotherapy', *J Pain Symptom Manage*, 33: 676-85.

Davis, J. M. 1995. 'Central and peripheral factors in fatigue', *J Sports Sci*, 13 Spec No: S49-53.

De Paepe, B., and J. L. De Bleecker. 2013. 'Cytokines and chemokines as regulators of skeletal muscle inflammation: presenting the case of Duchenne muscular dystrophy', *Mediators Inflamm*, 2013: 540370.

Deans, C., and S. J. Wigmore. 2005. 'Systemic inflammation, cachexia and prognosis in patients with cancer', *Curr Opin Clin Nutr Metab Care*, 8: 265-9.

Deboer, M. D. 2009. 'Animal models of anorexia and cachexia', *Expert Opin Drug Discov*, 4: 1145-55.

Debold, E. P. 2016. 'Decreased Myofilament Calcium Sensitivity Plays a Significant Role in Muscle Fatigue', *Exerc Sport Sci Rev*, 44: 144-9.

Dellorusso, C., R. W. Crawford, J. S. Chamberlain, and S. V. Brooks. 2001. 'Tibialis anterior muscles in mdx mice are highly susceptible to contraction-induced injury', *J Muscle Res Cell Motil*, 22: 467-75.

Deng, P., and C. M. Haynes. 2017. 'Mitochondrial dysfunction in cancer: Potential roles of ATF5 and the mitochondrial UPR', *Semin Cancer Biol*.

Devine, R. D., S. Bicer, P. J. Reiser, M. Velten, and L. E. Wold. 2015. 'Metalloproteinase expression is altered in cardiac and skeletal muscle in cancer cachexia', *Am J Physiol Heart Circ Physiol*, 309: H685-91.

Ding, H., G. Zhang, K. W. Sin, Z. Liu, R. K. Lin, M. Li, and Y. P. Li. 2016. 'Activin A induces skeletal muscle catabolism via p38beta mitogen-activated protein kinase', *Journal of cachexia, sarcopenia and muscle*.

Dobs, A. S., R. V. Boccia, C. C. Croot, N. Y. Gabrail, J. T. Dalton, M. L. Hancock, M. A. Johnston, and M. S. Steiner. 2013. 'Effects of enobosarm on muscle wasting and physical function in patients with cancer: a double-blind, randomised controlled phase 2 trial', *Lancet Oncol*, 14: 335-45.

Drake, J. C., R. J. Wilson, and Z. Yan. 2016. 'Molecular mechanisms for mitochondrial adaptation to exercise training in skeletal muscle', *FASEB J*, 30: 13-22.

Drake, J. C., and Z. Yan. 2017. 'Mitophagy in maintaining skeletal muscle mitochondrial proteostasis and metabolic health with ageing', *The Journal of physiology*, 595: 6391-99.

Ekman, L., I. Karlberg, S. Edstrom, L. Lindmark, T. Schersten, and K. Lundholm. 1982. 'Metabolic alterations in liver, skeletal muscle, and fat tissue in response to different tumor burdens in growing sarcoma-bearing rats', *J Surg Res*, 33: 23-31.

Evans, W. J., J. E. Morley, J. Argiles, C. Bales, V. Baracos, D. Guttridge, A. Jatoi, K. Kalantar-Zadeh, H. Lochs, G. Mantovani, D. Marks, W. E. Mitch, M. Muscaritoli, A. Najand, P. Ponikowski, F. Rossi Fanelli, M. Schambelan, A. Schols, M. Schuster, D. Thomas, R. Wolfe, and S. D. Anker. 2008. 'Cachexia: a new definition', *Clin Nutr*, 27: 793-9.

Farkas J, von Haehling S, Kalantar-Zadeh K, Morley JE, Anker SD, Lainscak M. 2013. 'Cachexia as a major public health problem: Frequent, costly, and deadly', *J Cachexia Saropenia Muscle*, 4: 173-8.

Fearon, K. C. 2008. 'Cancer cachexia: developing multimodal therapy for a multidimensional problem', *Eur J Cancer*, 44: 1124-32.

Fearon, K. C., D. J. Glass, and D. C. Guttridge. 2012. 'Cancer cachexia: mediators, signaling, and metabolic pathways', *Cell metabolism*, 16: 153-66.

Fearon KC, Voss AC, Hustead DS. 2006. 'Definition of cancer cachexia: effect of weight loss, reduced food intake, and systemic inflammation on functional status and prognosis', *American Journal of Clinical Nutrition*, 83: 1345-50.

Febbraio, M. A., N. Hiscock, M. Sacchetti, C. P. Fischer, and B. K. Pedersen. 2004. 'Interleukin-6 is a novel factor mediating glucose homeostasis during skeletal muscle contraction', *Diabetes*, 53: 1643-8.

Febbraio, M. A., and B. K. Pedersen. 2002. 'Muscle-derived interleukin-6: mechanisms for activation and possible biological roles', *FASEB J*, 16: 1335-47.

Fermoselle, C., E. Garcia-Arumi, E. Puig-Vilanova, A. L. Andreu, A. J. Urtreger, E. D. de Kier Joffe, A. Tejedor, L. Puente-Maestu, and E. Barreiro. 2013. 'Mitochondrial dysfunction and therapeutic approaches in respiratory and limb muscles of cancer cachectic mice', *Experimental physiology*, 98: 1349-65.

Ferriolli, E., R. J. Skipworth, P. Hendry, A. Scott, J. Stensteth, M. Dahele, L. Wall, C. Greig, M. Fallon, F. Strasser, T. Preston, and K. C. Fearon. 2012. 'Physical activity monitoring: a responsive and meaningful patient-centered outcome for surgery, chemotherapy, or radiotherapy?', *J Pain Symptom Manage*, 43: 1025-35.

Finne, E., M. Glausch, A. K. Exner, O. Sauzet, F. Stolzel, and N. Seidel. 2018. 'Behavior change techniques for increasing physical activity in cancer survivors: a

systematic review and meta-analysis of randomized controlled trials', *Cancer Manag Res*, 10: 5125-43.

Fischer, C. P. 2006. 'Interleukin-6 in acute exercise and training: what is the biological relevance?', *Exerc Immunol Rev*, 12: 6-33.

Fitts, R. H. 1994. 'Cellular mechanisms of muscle fatigue', *Physiol Rev*, 74: 49-94.

Fitts, R. H., and J. O. Holloszy. 1977. 'Contractile properties of rat soleus muscle: effects of training and fatique', *Am J Physiol*, 233: C86-91.

———. 1978. 'Effects of fatigue and recovery on contractile properties of frog muscle', *J Appl Physiol Respir Environ Exerc Physiol*, 45: 899-902.

Fitts, R. H., J. P. Troup, F. A. Witzmann, and J. O. Holloszy. 1984. 'The effect of ageing and exercise on skeletal muscle function', *Mech Ageing Dev*, 27: 161-72.

Fitts, R. H., W. W. Winder, M. H. Brooke, K. K. Kaiser, and J. O. Holloszy. 1980. 'Contractile, biochemical, and histochemical properties of thyrotoxic rat soleus muscle', *Am J Physiol*, 238: C14-20.

Fix, D. K., J. P. Hardee, S. Gao, B. N. VanderVeen, K. T. Velazquez, and J. A. Carson. 2018. 'The Role of gp130 in Basal and Exercise Trained Skeletal Muscle Mitochondrial Quality Control', *J Appl Physiol (1985)*.

Flint, T. R., T. Janowitz, C. M. Connell, E. W. Roberts, A. E. Denton, A. P. Coll, D. I. Jodrell, and D. T. Fearon. 2016. 'Tumor-Induced IL-6 Reprograms Host Metabolism to Suppress Anti-tumor Immunity', *Cell metabolism*, 24: 672-84.

Fontes-Oliveira, C. C., S. Busquets, M. Toledo, F. Penna, M. Paz Aylwin, S. Sirisi, A. P. Silva, M. Orpi, A. Garcia, A. Sette, M. Ines Genovese, M. Olivan, F. J. Lopez-Soriano, and J. M. Argiles. 2013. 'Mitochondrial and sarcoplasmic reticulum

abnormalities in cancer cachexia: altered energetic efficiency?', *Biochim Biophys Acta*, 1830: 2770-8.

Fortunati, N., R. Manti, N. Birocco, M. Pugliese, E. Brignardello, L. Ciuffreda, M. G. Catalano, M. Aragno, and G. Boccuzzi. 2007. 'Pro-inflammatory cytokines and oxidative stress/antioxidant parameters characterize the bio-humoral profile of early cachexia in lung cancer patients', *Oncol Rep*, 18: 1521-7.

Franceschi, C., M. Bonafe, S. Valensin, F. Olivieri, M. De Luca, E. Ottaviani, and G. De Benedictis. 2000. 'Inflamm-aging. An evolutionary perspective on immunosenescence', *Ann N Y Acad Sci*, 908: 244-54.

Franceschi, C., and J. Campisi. 2014. 'Chronic inflammation (inflammaging) and its potential contribution to age-associated diseases', *J Gerontol A Biol Sci Med Sci*, 69 Suppl 1: S4-9.

Franzini-Armstrong, C., and A. O. Jorgensen. 1994. 'Structure and development of E-C coupling units in skeletal muscle', *Annu Rev Physiol*, 56: 509-34.

Friden, J., and R. L. Lieber. 1992. 'Structural and mechanical basis of exercise-induced muscle injury', *Medicine and science in sports and exercise*, 24: 521-30.

Fritzen, A. M., C. Frosig, J. Jeppesen, T. E. Jensen, A. M. Lundsgaard, A. K. Serup, P. Schjerling, C. G. Proud, E. A. Richter, and B. Kiens. 2016. 'Role of AMPK in regulation of LC3 lipidation as a marker of autophagy in skeletal muscle', *Cell Signal*, 28: 663-74.

Fujita, J., T. Tsujinaka, M. Yano, C. Ebisui, H. Saito, A. Katsume, K. Akamatsu, Y. Ohsugi, H. Shiozaki, and M. Monden. 1996. 'Anti-interleukin-6 receptor antibody prevents muscle atrophy in colon-26 adenocarcinoma-bearing mice with

modulation of lysosomal and ATP-ubiquitin-dependent proteolytic pathways', *Int J Cancer*, 68: 637-43.

Gandevia, S. C. 2001. 'Spinal and supraspinal factors in human muscle fatigue', *Physiol Rev*, 81: 1725-89.

Gao, S., and J. A. Carson. 2016. 'Lewis lung carcinoma regulation of mechanical stretch-induced protein synthesis in cultured myotubes', *Am J Physiol Cell Physiol*, 310: C66-79.

Gao, S., J. L. Durstine, H. J. Koh, W. E. Carver, N. Frizzell, and J. A. Carson. 2017. 'Acute myotube protein synthesis regulation by IL-6-related cytokines', *Am J Physiol Cell Physiol*, 313: C487-C500.

Garbers, C., S. Aparicio-Siegmund, and S. Rose-John. 2015. 'The IL-6/gp130/STAT3 signaling axis: recent advances towards specific inhibition', *Curr Opin Immunol*, 34: 75-82.

Garnier, A., D. Fortin, J. Zoll, B. N'Guessan, B. Mettauer, E. Lampert, V. Veksler, and R. Ventura-Clapier. 2005. 'Coordinated changes in mitochondrial function and biogenesis in healthy and diseased human skeletal muscle', *FASEB J*, 19: 43-52.

Gilliam, L. A., J. S. Moylan, L. F. Ferreira, and M. B. Reid. 2011. 'TNF/TNFR1 signaling mediates doxorubicin-induced diaphragm weakness', *Am J Physiol Lung Cell Mol Physiol*, 300: L225-31.

Glass, D. J. 2005. 'Skeletal muscle hypertrophy and atrophy signaling pathways', *Int J Biochem Cell Biol*, 37: 1974-84.

Glund, S., and A. Krook. 2008. 'Role of interleukin-6 signalling in glucose and lipid metabolism', *Acta Physiol (Oxf)*, 192: 37-48.

Gonzalez-Freire, M., R. de Cabo, S. A. Studenski, and L. Ferrucci. 2014. 'The Neuromuscular Junction: Aging at the Crossroad between Nerves and Muscle', *Front Aging Neurosci*, 6: 208.

Goodman, C. A., J. A. Kotecki, B. L. Jacobs, and T. A. Hornberger. 2012. 'Muscle fiber type-dependent differences in the regulation of protein synthesis', *PLoS One*, 7: e37890.

Gorselink, M., S. F. Vaessen, L. G. van der Flier, I. Leenders, D. Kegler, E. Caldenhoven, E. van der Beek, and A. van Helvoort. 2006. 'Mass-dependent decline of skeletal muscle function in cancer cachexia', *Muscle Nerve*, 33: 691-3.

Grande, A. J., V. Silva, R. Riera, A. Medeiros, S. G. Vitoriano, M. S. Peccin, and M. Maddocks. 2014. 'Exercise for cancer cachexia in adults', *Cochrane Database Syst Rev*: CD010804.

Gratas-Delamarche, A., F. Derbre, S. Vincent, and J. Cillard. 2014. 'Physical inactivity, insulin resistance, and the oxidative-inflammatory loop', *Free Radic Res*, 48: 93-108.

Greene, D., L. M. Nail, V. K. Fieler, D. Dudgeon, and L. S. Jones. 1994. 'A comparison of patient-reported side effects among three chemotherapy regimens for breast cancer', *Cancer Pract*, 2: 57-62.

Guttridge, D. C., M. W. Mayo, L. V. Madrid, C. Y. Wang, and A. S. Baldwin, Jr. 2000. 'NF-kappaB-induced loss of MyoD messenger RNA: possible role in muscle decay and cachexia', *Science*, 289: 2363-6.

Hagberg, J. M., D. Goldring, G. W. Heath, A. A. Ehsani, A. Hernandez, and J. O. Holloszy. 1984. 'Effect of exercise training on plasma catecholamines and

haemodynamics of adolescent hypertensives during rest, submaximal exercise and orthostatic stress', *Clin Physiol*, 4: 117-24.

Hagberg, J. M., R. C. Hickson, A. A. Ehsani, and J. O. Holloszy. 1980. 'Faster adjustment to and recovery from submaximal exercise in the trained state', *J Appl Physiol Respir Environ Exerc Physiol*, 48: 218-24.

Hardee, J. P., B. R. Counts, S. Gao, B. N. VanderVeen, D. K. Fix, H. J. Koh, and J. A. Carson. 2018. 'Inflammatory signalling regulates eccentric contraction-induced protein synthesis in cachectic skeletal muscle', *Journal of cachexia, sarcopenia and muscle*, 9: 369-83.

Hardee, J. P., D. K. Fix, X. Wang, E. C. Goldsmith, H. J. Koh, and J. A. Carson. 2018. 'Systemic IL-6 regulation of eccentric contraction-induced muscle protein synthesis', *Am J Physiol Cell Physiol*.

Hardee, J. P., J. E. Mangum, S. Gao, S. Sato, K. L. Hetzler, M. J. Puppa, D. K. Fix, and J. A. Carson. 2016. 'Eccentric contraction-induced myofiber growth in tumor-bearing mice', *J Appl Physiol (1985)*, 120: 29-37.

Hardin, B. J., K. S. Campbell, J. D. Smith, S. Arbogast, J. Smith, J. S. Moylan, and M. B. Reid. 2008. 'TNF-alpha acts via TNFR1 and muscle-derived oxidants to depress myofibrillar force in murine skeletal muscle', *J Appl Physiol (1985)*, 104: 694-9.

Hargreaves, M. 2000. 'Skeletal muscle metabolism during exercise in humans', *Clin Exp Pharmacol Physiol*, 27: 225-8.

Hetzler, K. L., J. P. Hardee, M. J. Puppa, A. A. Narsale, S. Sato, J. M. Davis, and J. A. Carson. 2015. 'Sex differences in the relationship of IL-6 signaling to cancer cachexia progression', *Biochim Biophys Acta*, 1852: 816-25.

Holloszy, J. O. 2004. 'Adaptations of skeletal muscle mitochondria to endurance exercise: a personal perspective', *Exerc Sport Sci Rev*, 32: 41-3.

Holloszy, J. O., and F. W. Booth. 1976. 'Biochemical adaptations to endurance exercise in muscle', *Annu Rev Physiol*, 38: 273-91.

Holloszy, J. O., and E. F. Coyle. 1984. 'Adaptations of skeletal muscle to endurance exercise and their metabolic consequences', *J Appl Physiol Respir Environ Exerc Physiol*, 56: 831-8.

Holloszy, O. 1982. 'Enzymatic adaptations of skeletal muscle to endurance exercise', *Curr Probl Clin Biochem*, 11: 118-21.

Hood, D. A. 2001. 'Invited Review: contractile activity-induced mitochondrial biogenesis in skeletal muscle', *J Appl Physiol (1985)*, 90: 1137-57.

Hood, D. A., J. M. Memme, A. N. Oliveira, and M. Triolo. 2018. 'Maintenance of Skeletal Muscle Mitochondria in Health, Exercise, and Aging', *Annu Rev Physiol*.

Hood, D. A., G. Uguccioni, A. Vainshtein, and D. D'Souza. 2011. 'Mechanisms of exercise-induced mitochondrial biogenesis in skeletal muscle: implications for health and disease', *Compr Physiol*, 1: 1119-34.

Hughes, D. C., M. A. Wallace, and K. Baar. 2015. 'Effects of aging, exercise, and disease on force transfer in skeletal muscle', *Am J Physiol Endocrinol Metab*, 309: E1-E10.

Hurley, B. F., J. M. Hagberg, W. K. Allen, D. R. Seals, J. C. Young, R. W. Cuddihee, and J. O. Holloszy. 1984. 'Effect of training on blood lactate levels during submaximal exercise', *J Appl Physiol Respir Environ Exerc Physiol*, 56: 1260-4.

Hussain, S. N. 1998. 'Respiratory muscle dysfunction in sepsis', *Mol Cell Biochem*, 179: 125-34.

Hussain, S. N., and M. Sandri. 2013. 'Role of autophagy in COPD skeletal muscle dysfunction', *J Appl Physiol (1985)*, 114: 1273-81.

Iqbal, S., and D. A. Hood. 2015. 'The role of mitochondrial fusion and fission in skeletal muscle function and dysfunction', *Front Biosci (Landmark Ed)*, 20: 157-72.

Iqbal, S., O. Ostojic, K. Singh, A. M. Joseph, and D. A. Hood. 2013. 'Expression of mitochondrial fission and fusion regulatory proteins in skeletal muscle during chronic use and disuse', *Muscle Nerve*, 48: 963-70.

Jackman, R. W., J. Floro, R. Yoshimine, B. Zitin, M. Eiampikul, K. El-Jack, D. N. Seto, and S. C. Kandarian. 2017. 'Continuous Release of Tumor-Derived Factors Improves the Modeling of Cachexia in Muscle Cell Culture', *Front Physiol*, 8: 738.

Jaweed, M. M., G. J. Herbison, E. E. Miller, and J. F. Ditunno. 1983. 'Compensatory hypertrophy of the soleus in tumor-bearing rats', *J Neurol Sci*, 61: 171-9.

Jheng, H. F., P. J. Tsai, S. M. Guo, L. H. Kuo, C. S. Chang, I. J. Su, C. R. Chang, and Y. S. Tsai. 2012. 'Mitochondrial fission contributes to mitochondrial dysfunction and insulin resistance in skeletal muscle', *Mol Cell Biol*, 32: 309-19.

Jokl, E. J., and G. Blanco. 2016. 'Disrupted autophagy undermines skeletal muscle adaptation and integrity', *Mamm Genome*, 27: 525-37.

Joseph, A. M., H. Pilegaard, A. Litvintsev, L. Leick, and D. A. Hood. 2006. 'Control of gene expression and mitochondrial biogenesis in the muscular adaptation to endurance exercise', *Essays Biochem*, 42: 13-29.

Judge, S. M., C. L. Wu, A. W. Beharry, B. M. Roberts, L. F. Ferreira, S. C. Kandarian, and A. R. Judge. 2014. 'Genome-wide identification of FoxO-dependent gene networks in skeletal muscle during C26 cancer cachexia', *BMC Cancer*, 14: 997.

Julienne CM, Dumas JF, Goupille C, Pinault M, Berri C, Collin A, Tesseraud S, Couet C, Servais S. 2012. 'Cancer cachexia is associated with a decrease in skeletal muscle mitochondrial oxidative capacities wirh alteration of ATP production efficiency', *J Cachex Sarco Musc*, 3: 265-75.

Juvet, L. K., I. Thune, I. K. O. Elvsaas, E. A. Fors, S. Lundgren, G. Bertheussen, G. Leivseth, and L. M. Oldervoll. 2017. 'The effect of exercise on fatigue and physical functioning in breast cancer patients during and after treatment and at 6 months follow-up: A meta-analysis', *Breast*, 33: 166-77.

Kandarian, S. C., R. L. Nosacka, A. E. Delitto, A. R. Judge, S. M. Judge, J. D. Ganey, J. D. Moreira, and R. W. Jackman. 2018. 'Tumour-derived leukaemia inhibitory factor is a major driver of cancer cachexia and morbidity in C26 tumour-bearing mice', *Journal of cachexia, sarcopenia and muscle*.

Kandarian, S. C., and J. H. Williams. 1993. 'Contractile properties of skinned fibers from hypertrophied skeletal muscle', *Medicine and science in sports and exercise*, 25: 999-1004.

Khal, J., A. V. Hine, K. C. Fearon, C. H. Dejong, and M. J. Tisdale. 2005. 'Increased expression of proteasome subunits in skeletal muscle of cancer patients with weight loss', *Int J Biochem Cell Biol*, 37: 2196-206.

Khodabukus, A., and K. Baar. 2015. 'Contractile and metabolic properties of engineered skeletal muscle derived from slow and fast phenotype mouse muscle', *J Cell Physiol*, 230: 1750-7.

Khodabukus, A., L. M. Baehr, S. C. Bodine, and K. Baar. 2015. 'Role of contraction duration in inducing fast-to-slow contractile and metabolic protein and functional changes in engineered muscle', *J Cell Physiol*, 230: 2489-97.

Kilgour RD, Vigano A, Trutschnigg B, Hornby L, Lucar E, Bacon SL, Morais JA. 2010. 'Cancer-related fatigue: the impact of skeleatl muscle mass and strength in patients with advanced cancer', *J Cachexia Saropenia Muscle*, 1: 177-85.

Kim, S. H., J. H. Koh, K. Higashida, S. R. Jung, J. O. Holloszy, and D. H. Han. 2015. 'PGC-1alpha mediates a rapid, exercise-induced downregulation of glycogenolysis in rat skeletal muscle', *The Journal of physiology*, 593: 635-43.

Kimura, N., T. Kumamoto, Y. Kawamura, T. Himeno, K. I. Nakamura, H. Ueyama, and R. Arakawa. 2007. 'Expression of autophagy-associated genes in skeletal muscle: an experimental model of chloroquine-induced myopathy', *Pathobiology*, 74: 169-76.

Klasing, K. C., and B. J. Johnstone. 1991. 'Monokines in growth and development', *Poult Sci*, 70: 1781-9.

Knols, R., N. K. Aaronson, D. Uebelhart, J. Fransen, and G. Aufdemkampe. 2005. 'Physical exercise in cancer patients during and after medical treatment: a systematic review of randomized and controlled clinical trials', *J Clin Oncol*, 23: 3830-42.

Kritchevsky, S. B., T. C. Wilcosky, D. L. Morris, K. N. Truong, and H. A. Tyroler. 1991. 'Changes in plasma lipid and lipoprotein cholesterol and weight prior to the diagnosis of cancer', *Cancer Res*, 51: 3198-203.

Kuller, L. H., R. Tracy, W. Belloso, S. De Wit, F. Drummond, H. C. Lane, B. Ledergerber, J. Lundgren, J. Neuhaus, D. Nixon, N. I. Paton, J. D. Neaton, and Insight Smart Study Group. 2008. 'Inflammatory and coagulation biomarkers and mortality in patients with HIV infection', *PLoS Med*, 5: e203.

Kumar, A., S. Bhatnagar, and P. K. Paul. 2012. 'TWEAK and TRAF6 regulate skeletal muscle atrophy', *Curr Opin Clin Nutr Metab Care*, 15: 233-9.

Kummitha, C. M., S. C. Kalhan, G. M. Saidel, and N. Lai. 2014. 'Relating tissue/organ energy expenditure to metabolic fluxes in mouse and human: experimental data integrated with mathematical modeling', *Physiol Rep*, 2.

Kwon, O. S., A. J. Smuder, M. P. Wiggs, S. E. Hall, K. J. Sollanek, A. B. Morton, E. E. Talbert, H. Z. Toklu, N. Tumer, and S. K. Powers. 2015. 'AT1 receptor blocker losartan protects against mechanical ventilation-induced diaphragmatic dysfunction', *J Appl Physiol (1985)*, 119: 1033-41.

Laird, B. J., A. C. Scott, L. A. Colvin, A. L. McKeon, G. D. Murray, K. C. Fearon, and M. T. Fallon. 2011. 'Pain, depression, and fatigue as a symptom cluster in advanced cancer', *J Pain Symptom Manage*, 42: 1-11.

LaVoy, E. C., C. P. Fagundes, and R. Dantzer. 2016. 'Exercise, inflammation, and fatigue in cancer survivors', *Exerc Immunol Rev*, 22: 82-93.

Lee, J. Y., M. Kapur, M. Li, M. C. Choi, S. Choi, H. J. Kim, I. Kim, E. Lee, J. P. Taylor, and T. P. Yao. 2014. 'MFN1 deacetylation activates adaptive mitochondrial fusion

and protects metabolically challenged mitochondria', *Journal of cell science*, 127: 4954-63.

Li, X., M. R. Moody, D. Engel, S. Walker, F. J. Clubb, Jr., N. Sivasubramanian, D. L. Mann, and M. B. Reid. 2000. 'Cardiac-specific overexpression of tumor necrosis factor-alpha causes oxidative stress and contractile dysfunction in mouse diaphragm', *Circulation*, 102: 1690-6.

Lightfoot, A. P., and R. G. Cooper. 2016. 'The role of myokines in muscle health and disease', *Curr Opin Rheumatol*, 28: 661-6.

Lin, J., H. Wu, P. T. Tarr, C. Y. Zhang, Z. Wu, O. Boss, L. F. Michael, P. Puigserver, E. Isotani, E. N. Olson, B. B. Lowell, R. Bassel-Duby, and B. M. Spiegelman. 2002. 'Transcriptional co-activator PGC-1 alpha drives the formation of slow-twitch muscle fibres', *Nature*, 418: 797-801.

Lin, M. C., S. Ebihara, Q. El Dwairi, S. N. Hussain, L. Yang, S. B. Gottfried, A. Comtois, and B. J. Petrof. 1998. 'Diaphragm sarcolemmal injury is induced by sepsis and alleviated by nitric oxide synthase inhibition', *Am J Respir Crit Care Med*, 158: 1656-63.

Lira, F. S., M. Antunes Bde, M. Seelaender, and J. C. Rosa Neto. 2015. 'The therapeutic potential of exercise to treat cachexia', *Curr Opin Support Palliat Care*, 9: 317-24.

Lira, V. A., C. R. Benton, Z. Yan, and A. Bonen. 2010. 'PGC-1alpha regulation by exercise training and its influences on muscle function and insulin sensitivity', *Am J Physiol Endocrinol Metab*, 299: E145-61.

Lira, V. A., M. Okutsu, M. Zhang, N. P. Greene, R. C. Laker, D. S. Breen, K. L. Hoehn, and Z. Yan. 2013. 'Autophagy is required for exercise training-induced skeletal

muscle adaptation and improvement of physical performance', *Faseb Journal*, 27: 4184-93.

Lonbro, S., U. Dalgas, H. Primdahl, J. Johansen, J. L. Nielsen, P. Aagaard, A. P. Hermann, J. Overgaard, and K. Overgaard. 2013. 'Progressive resistance training rebuilds lean body mass in head and neck cancer patients after radiotherapy--results from the randomized DAHANCA 25B trial', *Radiother Oncol*, 108: 314-9.

Loumaye, A., M. de Barsy, M. Nachit, P. Lause, L. Frateur, A. van Maanen, P. Trefois, D. Gruson, and J. P. Thissen. 2015. 'Role of Activin A and myostatin in human cancer cachexia', *J Clin Endocrinol metab*, 100: 2030-8.

Luo, Y., J. Yoneda, H. Ohmori, T. Sasaki, K. Shimbo, S. Eto, Y. Kato, H. Miyano, T. Kobayashi, T. Sasahira, Y. Chihara, and H. Kuniyasu. 2014. 'Cancer Usurps Skeletal Muscle as an Energy Repository', *Cancer Research*, 74: 330-40.

MacLennan, D. H., M. Asahi, and A. R. Tupling. 2003. 'The regulation of SERCA-type pumps by phospholamban and sarcolipin', *Ann N Y Acad Sci*, 986: 472-80.

Mathur, N., and B. K. Pedersen. 2008. 'Exercise as a mean to control low-grade systemic inflammation', *Mediators Inflamm*, 2008: 109502.

Mayers, J. R., C. Wu, C. B. Clish, P. Kraft, M. E. Torrence, B. P. Fiske, C. Yuan, Y. Bao, M. K. Townsend, S. S. Tworoger, S. M. Davidson, T. Papagiannakopoulos, A. Yang, T. L. Dayton, S. Ogino, M. J. Stampfer, E. L. Giovannucci, Z. R. Qian, D. A. Rubinson, J. Ma, H. D. Sesso, J. M. Gaziano, B. B. Cochrane, S. Liu, J. Wactawski-Wende, J. E. Manson, M. N. Pollak, A. C. Kimmelman, A. Souza, K. Pierce, T. J. Wang, R. E. Gerszten, C. S. Fuchs, M. G. Vander Heiden, and B. M.

Wolpin. 2014. 'Elevation of circulating branched-chain amino acids is an early event in human pancreatic adenocarcinoma development', *Nat Med*, 20: 1193-8.

McClellan, J. L., J. M. Davis, J. L. Steiner, S. D. Day, S. E. Steck, M. D. Carmichael, and E. A. Murphy. 2012. 'Intestinal inflammatory cytokine response in relation to tumorigenesis in the Apc(Min/+) mouse', *Cytokine*, 57: 113-9.

McClung, J. M., A. R. Judge, S. K. Powers, and Z. Yan. 2010. 'p38 MAPK links oxidative stress to autophagy-related gene expression in cachectic muscle wasting', *Am J Physiol Cell Physiol*, 298: C542-9.

McLean, J. B., J. S. Moylan, and F. H. Andrade. 2014. 'Mitochondria dysfunction in lung cancer-induced muscle wasting in C2C12 myotubes', *Front Physiol*, 5: 503.

McNeely, M. L., M. B. Parliament, H. Seikaly, N. Jha, D. J. Magee, M. J. Haykowsky, and K. S. Courneya. 2015. 'Sustainability of outcomes after a randomized crossover trial of resistance exercise for shoulder dysfunction in survivors of head and neck cancer', *Physiother Can*, 67: 85-93.

Mehan, R. S., B. J. Greybeck, K. Emmons, W. C. Byrnes, and D. L. Allen. 2011. 'Matrix metalloproteinase-9 deficiency results in decreased fiber cross-sectional area and alters fiber type distribution in mouse hindlimb skeletal muscle', *Cells Tissues Organs*, 194: 510-20.

Mehl, K. A., J. M. Davis, J. M. Clements, F. G. Berger, M. M. Pena, and J. A. Carson. 2005. 'Decreased intestinal polyp multiplicity is related to exercise mode and gender in ApcMin/+ mice', *J Appl Physiol (1985)*, 98: 2219-25.

Mehl KA, Davis JM, Berger FG, Carson JA. 2005. 'Myofiber degeneration/regeneration is induced in the cachectis Apc min/+ mouse', *Journal of Applied Physiology*, 99: 2379-87.

Mihara M, Hashizume M, Yoshida H, Suzuki M, Shiina M. 2012. 'IL-6/IL-6 receptor system and its role in physiological and pathlogical conditions', *Clinical Science*, 122: 143-59.

Miller, A., L. McLeod, S. Alhayyani, A. Szczepny, D. N. Watkins, W. Chen, P. Enriori, W. Ferlin, S. Ruwanpura, and B. J. Jenkins. 2016. 'Blockade of the IL-6 trans-signalling/STAT3 axis suppresses cachexia in Kras-induced lung adenocarcinoma', *Oncogene*.

Mishra, S. I., R. W. Scherer, P. M. Geigle, D. R. Berlanstein, O. Topaloglu, C. C. Gotay, and C. Snyder. 2012. 'Exercise interventions on health-related quality of life for cancer survivors', *Cochrane Database Syst Rev*: CD007566.

Monga, U., M. Jaweed, A. J. Kerrigan, L. Lawhon, J. Johnson, C. Vallbona, and T. N. Monga. 1997. 'Neuromuscular fatigue in prostate cancer patients undergoing radiation therapy', *Arch Phys Med Rehabil*, 78: 961-6.

Monitto, C. L., D. Berkowitz, K. M. Lee, S. Pin, D. Li, M. Breslow, B. O'Malley, and M. Schiller. 2001. 'Differential gene expression in a murine model of cancer cachexia', *Am J Physiol Endocrinol Metab*, 281: E289-97.

Montazeri, A. 2009. 'Quality of life data as prognostic indicators of survival in cancer patients: an overview of the literature from 1982 to 2008', *Health Qual Life Outcomes*, 7: 102.

Mori, M., K. Yamaguchi, S. Honda, K. Nagasaki, M. Ueda, O. Abe, and K. Abe. 1991. 'Cancer cachexia syndrome developed in nude mice bearing melanoma cells producing leukemia-inhibitory factor', *Cancer Res*, 51: 6656-9.

Moser, A. R., H. C. Pitot, and W. F. Dove. 1990. 'A dominant mutation that predisposes to multiple intestinal neoplasia in the mouse', *Science*, 247: 322-4.

Moses, A. W., C. Slater, T. Preston, M. D. Barber, and K. C. Fearon. 2004. 'Reduced total energy expenditure and physical activity in cachectic patients with pancreatic cancer can be modulated by an energy and protein dense oral supplement enriched with n-3 fatty acids', *British journal of cancer*, 90: 996-1002.

Mueller, T. C., J. Bachmann, O. Prokopchuk, H. Friess, and M. E. Martignoni. 2016. 'Molecular pathways leading to loss of skeletal muscle mass in cancer cachexia--can findings from animal models be translated to humans?', *BMC Cancer*, 16: 75.

Munkvik, M., P. K. Lunde, and O. M. Sejersted. 2009. 'Causes of fatigue in slow-twitch rat skeletal muscle during dynamic activity', *Am J Physiol Regul Integr Comp Physiol*, 297: R900-10.

Munoz-Canoves, P., C. Scheele, B. K. Pedersen, and A. L. Serrano. 2013. 'Interleukin-6 myokine signaling in skeletal muscle: a double-edged sword?', *FEBS J*, 280: 4131-48.

Murphy, K. T., A. Chee, B. G. Gleeson, T. Naim, K. Swiderski, R. Koopman, and G. S. Lynch. 2011. 'Antibody-directed myostatin inhibition enhances muscle mass and function in tumor-bearing mice', *Am J Physiol Regul Integr Comp Physiol*, 301: R716-26.

Murphy, K. T., A. Chee, J. Trieu, T. Naim, and G. S. Lynch. 2012. 'Importance of functional and metabolic impairments in the characterization of the C-26 murine model of cancer cachexia', *Dis Model Mech*, 5: 533-45.

Murphy, K. T., and T. Clausen. 2007. 'The importance of limitations in aerobic metabolism, glycolysis, and membrane excitability for the development of high-frequency fatigue in isolated rat soleus muscle', *Am J Physiol Regul Integr Comp Physiol*, 292: R2001-11.

Muscaritoli, M., S. D. Anker, J. Argiles, Z. Aversa, J. M. Bauer, G. Biolo, Y. Boirie, I. Bosaeus, T. Cederholm, P. Costelli, K. C. Fearon, A. Laviano, M. Maggio, F. Rossi Fanelli, S. M. Schneider, A. Schols, and C. C. Sieber. 2010. 'Consensus definition of sarcopenia, cachexia and pre-cachexia: joint document elaborated by Special Interest Groups (SIG) "cachexia-anorexia in chronic wasting diseases" and "nutrition in geriatrics"', *Clin Nutr*, 29: 154-9.

Narsale, A. A., and J. A. Carson. 2014. 'Role of interleukin-6 in cachexia: therapeutic implications', *Curr Opin Support Palliat Care*, 8: 321-7.

Narsale, A. A., M. J. Puppa, J. P. Hardee, B. N. VanderVeen, R. T. Enos, E. A. Murphy, and J. A. Carson. 2016. 'Short-term pyrrolidine dithiocarbamate administration attenuates cachexia-induced alterations to muscle and liver in ApcMin/+ mice', *Oncotarget*.

Norden, D. M., S. Bicer, Y. Clark, R. Jing, C. J. Henry, L. E. Wold, P. J. Reiser, J. P. Godbout, and D. O. McCarthy. 2015. 'Tumor growth increases neuroinflammation, fatigue and depressive-like behavior prior to alterations in muscle function', *Brain Behav Immun*, 43: 76-85.

O'Gorman, P., D. C. McMillan, and C. S. McArdle. 1999. 'Longitudinal study of weight, appetite, performance status, and inflammation in advanced gastrointestinal cancer', *Nutr Cancer*, 35: 127-9.

Onesti, J. K., and D. C. Guttridge. 2014. 'Inflammation based regulation of cancer cachexia', *Biomed Res Int*, 2014: 168407.

Op den Kamp, C. M., R. C. Langen, R. Minnaard, M. C. Kelders, F. J. Snepvangers, M. K. Hesselink, A. C. Dingemans, and A. M. Schols. 2012. 'Pre-cachexia in patients with stages I-III non-small cell lung cancer: systemic inflammation and functional impairment without activation of skeletal muscle ubiquitin proteasome system', *Lung Cancer*, 76: 112-7.

Padrao, A. I., P. Oliveira, R. Vitorino, B. Colaco, M. J. Pires, M. Marquez, E. Castellanos, M. J. Neuparth, C. Teixeira, C. Costa, D. Moreira-Goncalves, S. Cabral, J. A. Duarte, L. L. Santos, F. Amado, and R. Ferreira. 2013. 'Bladder cancer-induced skeletal muscle wasting: disclosing the role of mitochondria plasticity', *Int J Biochem Cell Biol*, 45: 1399-409.

Pal, M., M. A. Febbraio, and M. Whitham. 2014. 'From cytokine to myokine: the emerging role of interleukin-6 in metabolic regulation', *Immunol Cell Biol*, 92: 331-9.

Patel, H. J., and B. M. Patel. 2017. 'TNF-alpha and cancer cachexia: Molecular insights and clinical implications', *Life Sci*, 170: 56-63.

Peddle-McIntyre, C. J., G. Bell, D. Fenton, L. McCargar, and K. S. Courneya. 2012. 'Feasibility and preliminary efficacy of progressive resistance exercise training in lung cancer survivors', *Lung Cancer*, 75: 126-32.

Pedersen, B. K. 2012. 'Muscular Interleukin-6 and Its Role as an Energy Sensor', *Medicine and science in sports and exercise*, 44: 392-96.

Pedersen, B. K., and C. P. Fischer. 2007. 'Physiological roles of muscle-derived interleukin-6 in response to exercise', *Curr Opin Clin Nutr Metab Care*, 10: 265-71.

Pedersen, B. K., A. Steensberg, P. Keller, C. Keller, C. Fischer, N. Hiscock, G. van Hall, P. Plomgaard, and M. A. Febbraio. 2003. 'Muscle-derived interleukin-6: lipolytic, anti-inflammatory and immune regulatory effects', *Pflugers Arch*, 446: 9-16.

Pedersen, B. K., A. Steensberg, and P. Schjerling. 2001. 'Exercise and interleukin-6', *Curr Opin Hematol*, 8: 137-41.

Penna, F., S. Busquets, and J. M. Argiles. 2016. 'Experimental cancer cachexia: Evolving strategies for getting closer to the human scenario', *Semin Cell Dev Biol*, 54: 20-7.

Penna, F., S. Busquets, F. Pin, M. Toledo, F. M. Baccino, F. J. Lopez-Soriano, P. Costelli, and J. M. Argiles. 2011. 'Combined approach to counteract experimental cancer cachexia: eicosapentaenoic acid and training exercise', *Journal of cachexia, sarcopenia and muscle*, 2: 95-104.

Penna, F., D. Costamagna, A. Fanzani, G. Bonelli, F. M. Baccino, and P. Costelli. 2010. 'Muscle wasting and impaired myogenesis in tumor bearing mice are prevented by ERK inhibition', *PLoS One*, 5: e13604.

Penna, F., D. Costamagna, F. Pin, A. Camperi, A. Fanzani, E. M. Chiarpotto, G. Cavallini, G. Bonelli, F. M. Baccino, and P. Costelli. 2013. 'Autophagic degradation contributes to muscle wasting in cancer cachexia', *Am J Pathol*, 182: 1367-78.

Pettersen, K., S. Andersen, S. Degen, V. Tadini, J. Grosjean, S. Hatakeyama, A. N. Tesfahun, S. Moestue, J. Kim, U. Nonstad, P. R. Romundstad, F. Skorpen, S. Sorhaug, T. Amundsen, B. H. Gronberg, F. Strasser, N. Stephens, D. Hoem, A. Molven, S. Kaasa, K. Fearon, C. Jacobi, and G. Bjorkoy. 2017. 'Cancer cachexia associates with a systemic autophagy-inducing activity mimicked by cancer cell-derived IL-6 trans-signaling', *Sci Rep*, 7: 2046.

Picca, A., A. M. S. Lezza, C. Leeuwenburgh, V. Pesce, R. Calvani, F. Landi, R. Bernabei, and E. Marzetti. 2017. 'Fueling Inflamm-Aging through Mitochondrial Dysfunction: Mechanisms and Molecular Targets', *Int J Mol Sci*, 18.

Pieske, B., M. Sutterlin, S. Schmidt-Schweda, K. Minami, M. Meyer, M. Olschewski, C. Holubarsch, H. Just, and G. Hasenfuss. 1996. 'Diminished post-rest potentiation of contractile force in human dilated cardiomyopathy. Functional evidence for alterations in intracellular Ca2+ handling', *J Clin Invest*, 98: 764-76.

Pigna, E., E. Berardi, P. Aulino, E. Rizzuto, S. Zampieri, U. Carraro, H. Kern, S. Merigliano, M. Gruppo, M. Mericskay, Z. Li, M. Rocchi, R. Barone, F. Macaluso, V. Di Felice, S. Adamo, D. Coletti, and V. Moresi. 2016. 'Aerobic Exercise and Pharmacological Treatments Counteract Cachexia by Modulating Autophagy in Colon Cancer', *Sci Rep*, 6: 26991.

Pin, F., S. Busquets, M. Toledo, A. Camperi, F. J. Lopez-Soriano, P. Costelli, J. M. Argiles, and F. Penna. 2015. 'Combination of exercise training and erythropoietin prevents cancer-induced muscle alterations', *Oncotarget*, 6: 43202-15.

Powers, S. K., A. N. Kavazis, and K. C. DeRuisseau. 2005. 'Mechanisms of disuse muscle atrophy: role of oxidative stress', *Am J Physiol Regul Integr Comp Physiol*, 288: R337-44.

Prasai, K. 2017. 'Regulation of mitochondrial structure and function by protein import: A current review', *Pathophysiology*.

Puigserver, P., J. Rhee, J. D. Lin, Z. D. Wu, J. C. Yoon, C. Y. Zhang, S. Krauss, V. K. Mootha, B. B. Lowell, and B. M. Spiegelman. 2001. 'Cytokine stimulation of energy expenditure through p38 MAP kinase activation of PPAR gamma coactivator-1', *Molecular Cell*, 8: 971-82.

Puigserver, P., and B. M. Spiegelman. 2003. 'Peroxisome proliferator-activated receptor-gamma coactivator 1 alpha (PGC-1 alpha): transcriptional coactivator and metabolic regulator', *Endocr Rev*, 24: 78-90.

Puppa, M. J., S. Gao, A. A. Narsale, and J. A. Carson. 2014. 'Skeletal muscle glycoprotein 130's role in Lewis lung carcinoma-induced cachexia', *FASEB J*, 28: 998-1009.

Puppa, M. J., E. A. Murphy, R. Fayad, G. A. Hand, and J. A. Carson. 2014. 'Cachectic skeletal muscle response to a novel bout of low-frequency stimulation', *J Appl Physiol (1985)*, 116: 1078-87.

Puppa, M. J., J. P. White, S. Sato, M. Cairns, J. W. Baynes, and J. A. Carson. 2011. 'Gut barrier dysfunction in the Apc(Min/+) mouse model of colon cancer cachexia', *Biochim Biophys Acta*, 1812: 1601-6.

Puppa, M. J., J. P. White, K. T. Velazquez, K. A. Baltgalvis, S. Sato, J. W. Baynes, and J. A. Carson. 2012. 'The effect of exercise on IL-6-induced cachexia in the Apc (Min/+) mouse', *Journal of cachexia, sarcopenia and muscle*, 3: 117-37.

Puppa, M.J.; Gao, S; Narsale, A.A.; Carson, J.A. 2014. 'Skeleatl muscle glycoprotein 130's role in Lewis lung carcinoma-induced cachexia', *FASEB journal : official publication of the Federation of American Societies for Experimental Biology*, 28: 998-1009.

Ramage, M. I., and R. J. E. Skipworth. 2018. 'The relationship between muscle mass and function in cancer cachexia: smoke and mirrors?', *Curr Opin Support Palliat Care*.

Ravasco, P., I. Monteiro-Grillo, and M. Camilo. 2007. 'How relevant are cytokines in colorectal cancer wasting?', *Cancer J*, 13: 392-8.

Reid, M. B., J. Lannergren, and H. Westerblad. 2002. 'Respiratory and limb muscle weakness induced by tumor necrosis factor-alpha: involvement of muscle myofilaments', *Am J Respir Crit Care Med*, 166: 479-84.

Reid, M. B., and Y. P. Li. 2001. 'Tumor necrosis factor-alpha and muscle wasting: a cellular perspective', *Respir Res*, 2: 269-72.

Reid, M. B., and J. S. Moylan. 2011. 'Beyond atrophy: redox mechanisms of muscle dysfunction in chronic inflammatory disease', *The Journal of physiology*, 589: 2171-9.

Reznick, R. M., and G. I. Shulman. 2006. 'The role of AMP-activated protein kinase in mitochondrial biogenesis', *The Journal of physiology*, 574: 33-9.

Roberts, B. M., B. Ahn, A. J. Smuder, M. Al-Rajhi, L. C. Gill, A. W. Beharry, S. K. Powers, D. D. Fuller, L. F. Ferreira, and A. R. Judge. 2013. 'Diaphragm and ventilatory dysfunction during cancer cachexia', *FASEB J*, 27: 2600-10.

Roberts, B. M., G. S. Frye, B. Ahn, L. F. Ferreira, and A. R. Judge. 2013. 'Cancer cachexia decreases specific force and accelerates fatigue in limb muscle', *Biochemical and biophysical research communications*, 435: 488-92.

Rodriguez, J., B. Vernus, I. Chelh, I. Cassar-Malek, J. C. Gabillard, A. Hadj Sassi, I. Seiliez, B. Picard, and A. Bonnieu. 2014. 'Myostatin and the skeletal muscle atrophy and hypertrophy signaling pathways', *Cell Mol Life Sci*, 71: 4361-71.

Romanello, V., E. Guadagnin, L. Gomes, I. Roder, C. Sandri, Y. Petersen, G. Milan, E. Masiero, P. Del Piccolo, M. Foretz, L. Scorrano, R. Rudolf, and M. Sandri. 2010. 'Mitochondrial fission and remodelling contributes to muscle atrophy', *EMBO J*, 29: 1774-85.

Romanello, V., and M. Sandri. 2013. 'Mitochondrial biogenesis and fragmentation as regulators of protein degradation in striated muscles', *J Mol Cell Cardiol*, 55: 64-72.

———. 2015. 'Mitochondrial Quality Control and Muscle Mass Maintenance', *Front Physiol*, 6: 422.

Rose-John, S. 2018. 'Interleukin-6 Family Cytokines', *Cold Spring Harb Perspect Biol*, 10.

Rudolf, R., M. R. Deschenes, and M. Sandri. 2016. 'Neuromuscular junction degeneration in muscle wasting', *Curr Opin Clin Nutr Metab Care*, 19: 177-81.

Rui, L. 2014. 'Energy metabolism in the liver', *Compr Physiol*, 4: 177-97.

Rutherford, G., P. Manning, and J. L. Newton. 2016. 'Understanding Muscle Dysfunction in Chronic Fatigue Syndrome', *J Aging Res*, 2016: 2497348.

Saitoh, M., J. Ishida, W. Doehner, S. von Haehling, M. S. Anker, A. J. S. Coats, S. D. Anker, and J. Springer. 2017. 'Sarcopenia, cachexia, and muscle performance in heart failure: Review update 2016', *Int J Cardiol*, 238: 5-11.

Saligan, L. N., K. Olson, K. Filler, D. Larkin, F. Cramp, S. Yennurajalingam, C. P. Escalante, A. del Giglio, K. M. Kober, J. Kamath, O. Palesh, K. Mustian, and Group Multinational Association of Supportive Care in Cancer Fatigue Study Group-Biomarker Working. 2015. 'The biology of cancer-related fatigue: a review of the literature', *Support Care Cancer*, 23: 2461-78.

Sanchez, A. M. 2016. 'Autophagy regulation in human skeletal muscle during exercise', *The Journal of physiology*, 594: 5053-4.

Sanchez, A. M., H. Bernardi, G. Py, and R. B. Candau. 2014. 'Autophagy is essential to support skeletal muscle plasticity in response to endurance exercise', *Am J Physiol Regul Integr Comp Physiol*, 307: R956-69.

Sanchez, A. M., A. Csibi, A. Raibon, K. Cornille, S. Gay, H. Bernardi, and R. Candau. 2012. 'AMPK promotes skeletal muscle autophagy through activation of forkhead FoxO3a and interaction with Ulk1', *J Cell Biochem*, 113: 695-710.

Sandow, A. 1965. 'Excitation-contraction coupling in skeletal muscle', *Pharmacol Rev*, 17: 265-320.

Sandri, M. 2008. 'Signaling in muscle atrophy and hypertrophy', *Physiology (Bethesda)*, 23: 160-70.

———. 2010. 'Autophagy in skeletal muscle', *FEBS Lett*, 584: 1411-6.

Schiaffino, S., and C. Reggiani. 1996. 'Molecular diversity of myofibrillar proteins: gene regulation and functional significance', *Physiol Rev*, 76: 371-423.

Schmitz, K. H., J. Holtzman, K. S. Courneya, L. C. Masse, S. Duval, and R. Kane. 2005. 'Controlled physical activity trials in cancer survivors: a systematic review and meta-analysis', *Cancer epidemiology, biomarkers & prevention : a publication of the American Association for Cancer Research, cosponsored by the American Society of Preventive Oncology*, 14: 1588-95.

Schneider, M. F., and W. K. Chandler. 1973. 'Voltage dependent charge movement of skeletal muscle: a possible step in excitation-contraction coupling', *Nature*, 242: 244-6.

Schwalm, C., C. Jamart, N. Benoit, D. Naslain, C. Premont, J. Prevet, R. Van Thienen, L. Deldicque, and M. Francaux. 2015. 'Activation of autophagy in human skeletal muscle is dependent on exercise intensity and AMPK activation', *FASEB J*, 29: 3515-26.

Schwantner, A., A. J. Dingley, S. Ozbek, S. Rose-John, and J. Grotzinger. 2004. 'Direct determination of the interleukin-6 binding epitope of the interleukin-6 receptor by NMR spectroscopy', *The Journal of biological chemistry*, 279: 571-6.

Segal, S. S., T. P. White, and J. A. Faulkner. 1986. 'Architecture, composition, and contractile properties of rat soleus muscle grafts', *Am J Physiol*, 250: C474-9.

Seto, D. N., S. C. Kandarian, and R. W. Jackman. 2015. 'A Key Role for Leukemia Inhibitory Factor in C26 Cancer Cachexia', *The Journal of biological chemistry*, 290: 19976-86.

Sheldon, A., F. W. Booth, and C. R. Kirby. 1993. 'cAMP levels in fast- and slow-twitch skeletal muscle after an acute bout of aerobic exercise', *Am J Physiol*, 264: C1500-4.

Siegel, I. M. 1989. 'Update on Duchenne muscular dystrophy', *Compr Ther*, 15: 45-52.

Sin, D. D., and S. F. Man. 2003. 'Why are patients with chronic obstructive pulmonary disease at increased risk of cardiovascular diseases? The potential role of systemic inflammation in chronic obstructive pulmonary disease', *Circulation*, 107: 1514-9.

Smith, I. J., G. L. Godinez, B. K. Singh, K. M. McCaughey, R. R. Alcantara, T. Gururaja, M. S. Ho, H. N. Nguyen, A. M. Friera, K. A. White, J. R. McLaughlin, D. Hansen, J. M. Romero, K. A. Baltgalvis, M. D. Claypool, W. Li, W. Lang, G. C. Yam, M. S. Gelman, R. Ding, S. L. Yung, D. P. Creger, Y. Chen, R. Singh, A. J. Smuder, M. P. Wiggs, O. S. Kwon, K. J. Sollanek, S. K. Powers, E. S. Masuda, V. C. Taylor, D. G. Payan, T. Kinoshita, and T. M. Kinsella. 2014. 'Inhibition of Janus kinase signaling during controlled mechanical ventilation prevents ventilation-induced diaphragm dysfunction', *FASEB J*, 28: 2790-803.

Spate, U., and P. C. Schulze. 2004. 'Proinflammatory cytokines and skeletal muscle', *Curr Opin Clin Nutr Metab Care*, 7: 265-9.

Speck, R. M., K. S. Courneya, L. C. Masse, S. Duval, and K. H. Schmitz. 2010. 'An update of controlled physical activity trials in cancer survivors: a systematic review and meta-analysis', *J Cancer Surviv*, 4: 87-100.

Spinale, F. G. 2007. 'Myocardial matrix remodeling and the matrix metalloproteinases: influence on cardiac form and function', *Physiol Rev*, 87: 1285-342.

Stene, G. B., J. L. Helbostad, T. Amundsen, S. Sorhaug, H. Hjelde, S. Kaasa, and B. H. Gronberg. 2015. 'Changes in skeletal muscle mass during palliative chemotherapy in patients with advanced lung cancer', *Acta Oncol*, 54: 340-8.

Stewart, G. D., R. J. Skipworth, and K. C. Fearon. 2006. 'Cancer cachexia and fatigue', *Clin Med (Lond)*, 6: 140-3.

Stone, P., J. Hardy, K. Broadley, A. J. Tookman, A. Kurowska, and R. A'Hern. 1999. 'Fatigue in advanced cancer: a prospective controlled cross-sectional study', *British journal of cancer*, 79: 1479-86.

Stricker, C. T., D. Drake, K. A. Hoyer, and V. Mock. 2004. 'Evidence-based practice for fatigue management in adults with cancer: exercise as an intervention', *Oncol Nurs Forum*, 31: 963-76.

Sundararaj, K. P., D. J. Samuvel, Y. Li, J. J. Sanders, M. F. Lopes-Virella, and Y. Huang. 2009. 'Interleukin-6 released from fibroblasts is essential for up-regulation of matrix metalloproteinase-1 expression by U937 macrophages in coculture: cross-talking between fibroblasts and U937 macrophages exposed to high glucose', *The Journal of biological chemistry*, 284: 13714-24.

Sweeney, H. L., and D. W. Hammers. 2018. 'Muscle Contraction', *Cold Spring Harb Perspect Biol*, 10.

Talbert, E. E., G. A. Metzger, W. A. He, and D. C. Guttridge. 2014. 'Modeling human cancer cachexia in colon 26 tumor-bearing adult mice', *Journal of cachexia, sarcopenia and muscle*, 5: 321-8.

Talbert, E. E., J. Yang, T. A. Mace, M. R. Farren, A. B. Farris, G. S. Young, O. Elnaggar, Z. Che, C. D. Timmers, P. Rajasekera, J. M. Maskarinec, M. Bloomston, T.

Bekaii-Saab, D. C. Guttridge, and G. B. Lesinski. 2017. 'Dual Inhibition of MEK and PI3K/Akt Rescues Cancer Cachexia through both Tumor-Extrinsic and -Intrinsic Activities', *Mol Cancer Ther*, 16: 344-56.

Tessitore, L., P. Costelli, G. Bonetti, and F. M. Baccino. 1993. 'Cancer cachexia, malnutrition, and tissue protein turnover in experimental animals', *Arch Biochem Biophys*, 306: 52-8.

Thomason, D. B., and F. W. Booth. 1990. 'Atrophy of the soleus muscle by hindlimb unweighting', *J Appl Physiol (1985)*, 68: 1-12.

Thompson, L. V., E. M. Balog, and R. H. Fitts. 1992. 'Muscle fatigue in frog semitendinosus: role of intracellular pH', *Am J Physiol*, 262: C1507-12.

Thompson, L. V., E. M. Balog, D. A. Riley, and R. H. Fitts. 1992. 'Muscle fatigue in frog semitendinosus: alterations in contractile function', *Am J Physiol*, 262: C1500-6.

Thyfault, J. P., and F. W. Booth. 2011. 'Lack of regular physical exercise or too much inactivity', *Curr Opin Clin Nutr Metab Care*, 14: 374-8.

Tisdale, M. J. 2002. 'Cachexia in cancer patients', *Nat Rev Cancer*, 2: 862-71.

———. 2009. 'Mechanisms of cancer cachexia', *Physiol Rev*, 89: 381-410.

Toth, M. J., P. A. Ades, M. D. Tischler, R. P. Tracy, and M. M. LeWinter. 2006. 'Immune activation is associated with reduced skeletal muscle mass and physical function in chronic heart failure', *Int J Cardiol*, 109: 179-87.

Toth, M. J., D. M. Callahan, M. S. Miller, T. W. Tourville, S. B. Hackett, M. E. Couch, and K. Dittus. 2016. 'Skeletal muscle fiber size and fiber type distribution in human cancer: Effects of weight loss and relationship to physical function', *Clin Nutr*.

Vainshtein, A., P. Grumati, M. Sandri, and P. Bonaldo. 2014. 'Skeletal muscle, autophagy, and physical activity: the menage a trois of metabolic regulation in health and disease', *J Mol Med (Berl)*, 92: 127-37.

Vainshtein, A., L. D. Tryon, M. Pauly, and D. A. Hood. 2015. 'Role of PGC-1alpha during acute exercise-induced autophagy and mitophagy in skeletal muscle', *Am J Physiol Cell Physiol*, 308: C710-9.

van Hall, G., A. Steensberg, C. Fischer, C. Keller, K. Moller, P. Moseley, and B. K. Pedersen. 2008. 'Interleukin-6 markedly decreases skeletal muscle protein turnover and increases nonmuscle amino acid utilization in healthy individuals', *J Clin Endocrinol metab*, 93: 2851-8.

VanderVeen, B. N., D. K. Fix, and J. A. Carson. 2017. 'Disrupted Skeletal Muscle Mitochondrial Dynamics, Mitophagy, and Biogenesis during Cancer Cachexia: A Role for Inflammation', *Oxid Med Cell Longev*, 2017: 3292087.

VanderVeen, B. N., J. P. Hardee, D. K. Fix, and J. A. Carson. 2018. 'Skeletal muscle function during the progression of cancer cachexia in the male Apc(Min/+) mouse', *J Appl Physiol (1985)*, 124: 684-95.

Velazquez, K. T., R. T. Enos, A. A. Narsale, M. J. Puppa, J. M. Davis, E. A. Murphy, and J. A. Carson. 2014. 'Quercetin supplementation attenuates the progression of cancer cachexia in ApcMin/+ mice', *J Nutr*, 144: 868-75.

Vidt, D. G. 2006. 'Inflammation in renal disease', *Am J Cardiol*, 97: 20A-27A.

Vigano, A., M. Dorgan, J. Buckingham, E. Bruera, and M. E. Suarez-Almazor. 2000. 'Survival prediction in terminal cancer patients: a systematic review of the medical literature', *Palliat Med*, 14: 363-74.

von Haehling, S., and S. D. Anker. 2014. 'Prevalence, incidence and clinical impact of cachexia: facts and numbers-update 2014', *Journal of cachexia, sarcopenia and muscle*, 5: 261-3.

Wang, Y., and J. E. Pessin. 2013. 'Mechanisms for fiber-type specificity of skeletal muscle atrophy', *Curr Opin Clin Nutr Metab Care*, 16: 243-50.

Washington TA, White JP, Davis JM, Wlson LB, Lowe LL, Sato S, Carson JA. 2011. 'Skeletal muscle mass recovery from atrophy in IL-6 knockout mice', *Acta Physiologica*, 202: 657-69.

Wegrzyn, J., R. Potla, Y. J. Chwae, N. B. Sepuri, Q. Zhang, T. Koeck, M. Derecka, K. Szczepanek, M. Szelag, A. Gornicka, A. Moh, S. Moghaddas, Q. Chen, S. Bobbili, J. Cichy, J. Dulak, D. P. Baker, A. Wolfman, D. Stuehr, M. O. Hassan, X. Y. Fu, N. Avadhani, J. I. Drake, P. Fawcett, E. J. Lesnefsky, and A. C. Larner. 2009. 'Function of mitochondrial Stat3 in cellular respiration', *Science*, 323: 793-7.

Westerblad, H., and D. G. Allen. 2003. 'Cellular mechanisms of skeletal muscle fatigue', *Adv Exp Med Biol*, 538: 563-70; discussion 71.

White, J. P., K. A. Baltgalvis, M. J. Puppa, S. Sato, J. W. Baynes, and J. A. Carson. 2011. 'Muscle oxidative capacity during IL-6-dependent cancer cachexia', *Am J Physiol Regul Integr Comp Physiol*, 300: R201-11.

White, J. P., J. W. Baynes, S. L. Welle, M. C. Kostek, L. E. Matesic, S. Sato, and J. A. Carson. 2011. 'The regulation of skeletal muscle protein turnover during the progression of cancer cachexia in the Apc(Min/+) mouse', *PLoS One*, 6: e24650.

White, J. P., M. J. Puppa, S. Gao, S. Sato, S. L. Welle, and J. A. Carson. 2013. 'Muscle mTORC1 suppression by IL-6 during cancer cachexia: a role for AMPK', *Am J Physiol Endocrinol Metab*, 304: E1042-52.

White, J. P., M. J. Puppa, S. Sato, S. Gao, R. L. Price, J. W. Baynes, M. C. Kostek, L. E. Matesic, and J. A. Carson. 2012. 'IL-6 regulation on skeletal muscle mitochondrial remodeling during cancer cachexia in the ApcMin/+ mouse', *Skelet Muscle*, 2: 14.

White JP, Puppa MJ, Narsale A, Carson JA. 2013. 'Characterization of the male Apc min/+ mouse as a hypogonadism model related to cancer cachexia', *Biology Open*, 2: 1346-53.

White JP, Reecy JM, Washington TA, Sato S, Davis JM, Wilson LB, Carson JA. 2009. 'Overload-induced skeletal muscle extracellular matrix emodelling and myofibre growth in mice lacking IL-6', *Acta Physiologica*, 197: 321-32.

Widrick, J. J., J. G. Romatowski, M. Karhanek, and R. H. Fitts. 1997. 'Contractile properties of rat, rhesus monkey, and human type I muscle fibers', *Am J Physiol*, 272: R34-42.

Widrick, J. J., J. G. Romatowski, K. M. Norenberg, S. T. Knuth, J. L. Bain, D. A. Riley, S. W. Trappe, T. A. Trappe, D. L. Costill, and R. H. Fitts. 2001. 'Functional properties of slow and fast gastrocnemius muscle fibers after a 17-day spaceflight', *J Appl Physiol (1985)*, 90: 2203-11.

Williams, A., X. Sun, J. E. Fischer, and P. O. Hasselgren. 1999. 'The expression of genes in the ubiquitin-proteasome proteolytic pathway is increased in skeletal muscle from patients with cancer', *Surgery*, 126: 744-9; discussion 49-50.

Winegrad, S. 1965. 'Role of intracellular calcium movements in excitation-contraction coupling in skeletal muscle', *Fed Proc*, 24: 1146-52.

Winningham, M. L., L. M. Nail, M. B. Burke, L. Brophy, B. Cimprich, L. S. Jones, S. Pickard-Holley, V. Rhodes, B. St Pierre, S. Beck, and et al. 1994. 'Fatigue and the cancer experience: the state of the knowledge', *Oncol Nurs Forum*, 21: 23-36.

Wolf, J., S. Rose-John, and C. Garbers. 2014. 'Interleukin-6 and its receptors: a highly regulated and dynamic system', *Cytokine*, 70: 11-20.

Wolfe, R. R. 2006. 'The underappreciated role of muscle in health and disease', *The American journal of clinical nutrition*, 84: 475-82.

Wright, D. C., D. H. Han, P. M. Garcia-Roves, P. C. Geiger, T. E. Jones, and J. O. Holloszy. 2007. 'Exercise-induced mitochondrial biogenesis begins before the increase in muscle PGC-1alpha expression', *The Journal of biological chemistry*, 282: 194-9.

Wu, S., F. Zhou, Z. Zhang, and D. Xing. 2011. 'Mitochondrial oxidative stress causes mitochondrial fragmentation via differential modulation of mitochondrial fission-fusion proteins', *FEBS J*, 278: 941-54.

Wu, Z., P. Puigserver, U. Andersson, C. Zhang, G. Adelmant, V. Mootha, A. Troy, S. Cinti, B. Lowell, R. C. Scarpulla, and B. M. Spiegelman. 1999. 'Mechanisms controlling mitochondrial biogenesis and respiration through the thermogenic coactivator PGC-1', *Cell*, 98: 115-24.

Yan, Z., V. A. Lira, and N. P. Greene. 2012. 'Exercise training-induced regulation of mitochondrial quality', *Exerc Sport Sci Rev*, 40: 159-64.

Youle, R. J., and A. M. van der Bliek. 2012. 'Mitochondrial fission, fusion, and stress', *Science*, 337: 1062-5.

Yu, X., R. H. Kennedy, and S. J. Liu. 2003. 'JAK2/STAT3, not ERK1/2, mediates interleukin-6-induced activation of inducible nitric-oxide synthase and decrease in contractility of adult ventricular myocytes', *The Journal of biological chemistry*, 278: 16304-9.

Yu, X. W., Q. Chen, R. H. Kennedy, and S. J. Liu. 2005. 'Inhibition of sarcoplasmic reticular function by chronic interleukin-6 exposure via iNOS in adult ventricular myocytes', *The Journal of physiology*, 566: 327-40.

Zhang, G., B. Jin, and Y. P. Li. 2011. 'C/EBPbeta mediates tumour-induced ubiquitin ligase atrogin1/MAFbx upregulation and muscle wasting', *EMBO J*, 30: 4323-35.

Zhang, P., X. Chen, and M. Fan. 2007. 'Signaling mechanisms involved in disuse muscle atrophy', *Med Hypotheses*, 69: 310-21.

Zhang, Q., S. K. Joshi, D. H. Lovett, B. Zhang, S. Bodine, H. T. Kim, and X. Liu. 2014. 'Matrix metalloproteinase-2 plays a critical role in overload induced skeletal muscle hypertrophy', *Muscles Ligaments Tendons J*, 4: 446-54.

Zhou, J., B. Liu, C. Liang, Y. Li, and Y. H. Song. 2016. 'Cytokine Signaling in Skeletal Muscle Wasting', *Trends Endocrinol Metab*, 27: 335-47.

Zimmers, T. A., M. L. Fishel, and A. Bonetto. 2016. 'STAT3 in the systemic inflammation of cancer cachexia', *Semin Cell Dev Biol*, 54: 28-41.

Zurlo, F., K. Larson, C. Bogardus, and E. Ravussin. 1990. 'Skeletal muscle metabolism is a major determinant of resting energy expenditure', *J Clin Invest*, 86: 1423-7.

APPENDIX A

DETAILED PROTOCOLS

Tissue Homogenization

1. Materials and Reagents

   a. Mueller Buffer

Mueller Buffer	Stock Solution	Desired Concentration	Volume of stock needed(ul)
HEPES	500mM	50mM	600
Triton-X100	100%	0.10%	6
EGTA (pH 8.0)	500mM	4mM	48
EDTA (pH 8.0)	500mM	10mM	120
Na4P2O7	100mM	15mM	900
β-glycerophosphate	2M	100mM	300
NaF	500mM	25mM	300
NaVO4	1M	5mM	50
dH2O	-	-	3585
Protease Inhibitor	-	-	60

   b. Mueller Diluent:

Mueller Diluent	Stock Solution	Desired Concentration	Volume of stock needed (ul)
Glycerol	100%	50%	1500
Na4P2O7	100mM	50mM	1500
EGTA (pH 8.0)	500mM	2.5mM	15
β-mercaptoethanol	500mM	1mM	6
Protease Inhibitor	-	-	30

2. Procedure

   a. Weigh out the samples to be used and place weighted portion into an Eppendorf tube labeled with the sample and M.

   b. Add 10ul/mg tissue of Mueller buffer to the homogenization tube and add

sample.

c. Homogenize in glass on glass tissue homogenizer keeping the sample in ice while homogenizing. (homogenize ~30s check sample repeat if needed)

d. Wash glass tissue homogenizer 3 times by dH2O between two samples.

e. Transfer tissue homogenate back to Eppendorf tube.

f. Spin samples at 13,000rpm for 10min at 4℃.

g. Transfer supernatant to clean Eppendorf tube labeled with sample and D, discard the pellet.

h. Add 5ul/mg tissue of Diluent buffer to the D tube and vortex.

i. Run protein assay (Bradford).

j. Dilute samples down to a working concentration in a new tube labeled with the sample and the working concentration. Keep both D tube and diluted samples in -80℃.

Protein Assay (Bradford)

1. Materials and Reagents
    a. Bradford Reagent (Bio-Rad, Catalog #: 5000006)
    b. Make a stock of 1mg/ml BSA in PBS, store aliquot in -20°C.
    c. Costar 96 well plate
2. Procedure
    a. In a clear flat bottom 96 well plate create a standard curve with the 1ug/ul BSA solution from 0-14ug in duplicate or triplicate

b. Dilute samples 1:5 in a new tube with water (5ul sample: 20ul dH20)

c. Add 5ul of the diluted samples to the wells of the plate being sure to run them in duplicate or triplicate

d. Make a 1:5 dilution of Bradford reagent. You will need enough for 300ul/well. Be sure to clean the glassware well before you use it with soap and water.

e. Add 300ul of diluted Bradford reagent to each well.

f. Let sit in dark drawer for 15 minutes

g. Read in plate reader at 595nm

h. Calculate protein concentration based on standard curve

i. Create curve being sure to subtract out the zero value from both curve and samples.

j. Calculate protein concentration using y=mx+b equation (sample = con*slope + intercept -> con=(sample-intercept)/slope)

SDS-PAGE/Western Blot

1. Materials and Reagents

   a. Acrylamide Solution (38.5% Acrylamide + 1% Bis-Acrylamide) 1.5M Tris-HCL, pH 8.8

   b. 1.0M Tris-HCL, pH 6.8

   c. 10% SDS

   d. 10% APS

   e. TEMED

f. 4×SDS Loading Buffer: 200 mM Tris-Cl (pH 6.8), 400 mM DTT, 8% SDS, 0.4% bromophenol blue, 40% glycerol

g. SDS Running Buffer: 25mM Tris, 200mM Glycine, 0.1% SDS Protein Ladder (Bio-Rad, Catalog #: 1610373)

h. Transfer Buffer: 25mM Tris, 200mM Glycine, 20% Methanol 1×TBST: 50 mM Tris-Cl, 150 mM NaCl, 0.1% Tween-20 5% milk (solved in 1×TBST)

i. ECL plus (Thermo Scientific, Catalog #: 1610373)

2. Procedure – SDS-PAGE

a. Make gel. Base the % off of what molecular weight the protein of interest is.

b. Prepare samples

c. Pipette desired amount of protein into Eppendorf tube

d. Add correct volume of 4 × SDS loading dye

e. Vortex and do a quick spin

f. Heat in heat block at 100°C or in boiling water for 5 minutes

g. Quick spin

h. Load 4ul of protein ladder to the 1st lane in the gel

i. Load all of sample on gel

j. Run gel at 200V for ~1h or until samples have run through the gel

3. Procedure – Transfer

a. Prepare 750ml of transfer buffer

b. Prepare membrane by placing in a small amount of methanol for 1 minute

c. Pour methanol into the transfer buffer and wash membranes with the transfer buffer

d. Set up the transfer with the black side of the holder facing down, sponge, blotting paper, gel, membrane (be sure there are absolutely no bubbles between the gel and the membrane), blotting paper, sponge, white/clear side.

e. Carefully close the sandwich and place in the transfer box black side to black side and clear side facing the red side of the transfer box.

f. Place ice pack in the box and pour remaining transfer buffer into the box.

g. Transfer either overnight at 70mA or for 200min at 200mA making sure to pack well with ice.

4. Procedure – Probing

a. Prepare 5% milk in 1×TBST solution

b. Remove membrane from transfer and place in ponceau solution for 3-5 minute

c. Rinse off excess ponceau with dH2O and place membrane in plastic sheet and scan into computer

d. Wash off ponceau with 1×TBST

e. Block the membrane for 1h in 5% TBST milk solution (made in step 13)

f. Incubate in primary antibody in milk solution

g. Wash membranes 3× with 1×TBST for 5 minutes each

h. Incubate in secondary antibody in milk solution for 1 hour

i. Wash membranes 3× with 1×TBST for 5 minutes each

j. Develop with ECL or ECL quantum.

RNA Isolation

1. Materials and Reagents
    a. RNase AWAY (Thermo Scientific, Catalog #: 10328011) Trizol Reagents (Thermo Scientific, Catalog #: 15596026) Chloroform
    b. Isopropanol Alcohol DEPC H2O
    c. 75% ethanol in DEPC H2O
2. Procedure
    a. Clean work area thoroughly with alcohol
    b. Label 3 sets of sterile RNAase free 1.5mL eppendorf tubes
    c. Remove cell culture medium, and wash cells once by ice-cold PBS
    d. Remove PBS, add Trizol reagent onto the cell (1ml Trizol for each well of 6-well plate).
    e. Scrape cell off from cell culture plate gently with rubber scraper, pipette cell suspended in
    f. Trizol up and down several times with 1ml pipette to brake cell thoroughly.
    g. Transfer cell homogenate to a sterile 1.5mL tube.
    h. Let samples sit at RT for ~5 minutes.
    i. Add 200ul of chloroform to each tube
    j. Shake tubes (DO NOT VORTEX) for 15-30s (should be the color of pepto bismal).
    k. Let samples sit at RT for 2-3min.

l. Spin samples at 12000rpm for 15 minutes at 4℃.

m. Clean gloves and pipette with RNAase AWAY.

n. Transfer clear supernatant to new tube carefully, Do NOT disturb the protein interface (white layer) or organic phase (red/pink colored).

o. Add 500ul of isopropanol and invert to mix.

p. Incubate for 20-30 minutes at RT.

q. Spin samples at 12000rpm for 10 minutes at 4℃, gel like pellet can be visualized at the bottom of tube.

r. Dump the supernatant being careful not to lose the pellet.

s. Add 1mL 75% EtOH in DEPC to RNA pellet invert to break loose.

t. Spin at 9500rpm for 5 min at 4℃.

u. Repeat steps 18-20 once.

v. Air dry tubes upside down in hood for 10-20 minutes (on towel of Kimwipes).

w. Add ~20-40ul of DEPC water to dissolve pellet, pipette to solve RNA (Keep track of the amount of DEPC added).

x. Read on spec (1-2ul RNA+800ul dH2O) in quartz cuvette/NANO DROP and record 260/280/and 230 measurements. (Good quality of RNA samples should have 260/280 ratio > 1.8 and 260/230 > 1.8. Do not use samples with 260/280 below 1.6)

y. Calculate and Record RNA concentration: RNA= (OD260*40*0.8)/ volume RNA added to cuvette.

z. Store RNA samples in -80°C.

cDNA Synthesis

1. Materials and Reagents:

    a. High-Capacity cDNA Reverse Transcription Kit (Applied Biosystems, Catalog #: 4368813)

    b. DEPC H2O

2. Procedure

    a. Prepare reverse transcriptase cocktail as follows and keep on ice.

Reagent	ul/sample
DEPC	4.2
10X RT buffer	2.0
dNTP mix	0.8
10Xrandom Primers	2.0
Reverse Transcriptase	1.0
Total	10.0

    b. In a cold block add 3ug of RNA in a 200ul PCR tube and volume to 10ul with DEPC water.

    c. Add 10ul of reverse transcriptase cocktail to each tube.

    d. Put in thermocycler on program as follows:

    e. 25℃ for 10 min

    f. 42℃ for 50 min

    g. 70℃ for 15 min

    h. 4℃ Hold

    i. Store all samples in -20℃.

RT-PCR

1. Materials and Reagents:

    a. iTaq™ Universal SYBR® Green Supermix (Bio-Rad, Catalog #: 1725121) ddH2O

    b. Dilute cDNA samples 1:10 and 1:100 (serial dilution) with ddH2O, keep samples on cold block.

    c. Fill out plate template, all samples are in duplicate.

    d. Prepare master mix solutions as follows, keep master mix on ice.

Reagent	ul/sample
Syber Green Mix	10.0
Forward Primer (20uM)	1.0
Reverse Primer (20uM)	1.0
Total	12.0

2. Procedure

    a. Load 8ul of cDNA to each well as per template.

    b. Load 12ul of master mix solution into each well, DO NOT introduce bubbles.

    c. Cover plate with plate cover sheet

    d. Spin plate in centrifuge in environmental genomics core

    e. Put plate onto Applied Biosystems 7300 Real-Time PCR System

    f. Add dissociation step and set volume to 20ul.

    g. Start analysis.

    h. Turn OFF machine when finished.

IL-6 Electroporations

1. Prepare plasmids. They are typically at a concentration of 2-3 ug/ul. Dilute to 1 ug/ul in sterile saline. Need 40 ug of plasmid per injection.
2. Start anesthesia with Isoflurane at 1-2%/1L O2. (Change percentage of isoflurane based on the level of consciousness of the mice.)
3. Add mice to the anesthesia box.
4. Place mouse under nose cone. Shave top of quad. Alcohol off skin and betadyne.
5. Sterilize Scissors with bead sterilizer and alcohol. Make a small vertical snip with scissors over quad.
6. Inject plasmid (50 ug at 1 ug/ul=50 ul) VERY SLOWLY in the middle of the quad using insulin syringe.
7. Electroporate with default setting. 100 mV; 50 ms; 8 pulses. Make sure electrodes are under the skin, next to the quad. Touch foot pedal once to start the electrical current.
8. Close the incision with a wound clip.
9. Return mouse to cage.
10. Remove wound clip in 7-10 days.

IL-6 ELISA

1. Materials and Reagents:
    a. Coating Buffer: 100mM Sodium Carbonate, pH 9.5.
    b. Assay Diluent: PBS with 10% FBS
    c. Wash Buffer: PBS with 0.05% Tween-20

d. TMB-ELISA Substrate Solution (Thermo Scientific, Catalog #: 34028) Stop Solution: 2N H2SO4

e. Mouse IL-6 ELISA Kit (BD Bioscience, Catalog #: 555240) IL-6 Standard (Reconstitute by dH2O to 1ng/ml)

f. Capture Antibody (Anti-Mouse IL-6 monoclonal antibody, 1:250)

g. Detection Antibody (Biotinylated Anti-Mouse IL-6 monoclonal antibody,1:500) Enzyme

h. Reagent (Streptavidin-horseradish peroxidase conjugate (SAv-HRP)1:250)

2. Procedure

a. Coat microwells with 100 µL per well of Capture Antibody diluted 1:250 in Coating Buffer.

b. Seal plate and incubate overnight at 4°C.

c. Aspirate wells and wash 3 times with ≥ 300 µL/well Wash Buffer. After last wash, invert plate and blot on absorbent paper to remove any residual buffer.

d. Block plates with ≥ 200 µL/well Assay Diluent. Incubate at RT for 1 hour.

e. Prepare the IL-6 standards.

f. Prepare a 1000 pg/mL standard from the stock standard. Vortex to mix.

g. Add 300 µL Assay Diluent to 6 tubes. Label as 500 pg/mL, 250 pg/mL, 125pg/mL, 62.5 pg/mL, 31.3 pg/mL, and 15.6 pg/mL.

h. Perform serial dilutions by adding 300 µL of each standard to the next tube and vortexing between each transfer. Assay Diluent serves as the zero standard (0 pg/mL).

i. Aspirate/wash as in step 2.

j. Pipette 100 µL of each standard, sample, and control into appropriate wells. Seal plate and incubate for 2 hours at RT.

k. Aspirate/ wash as in step 2, but with 5 total washes.

l. Add 100 µL of Working Detector (1:500 Detection Antibody + 1:250 SAv-HRP reagent, solved in Assay Diluent) to each well. Seal plate and incubate for 1 hour at RT.

m. Aspirate/ wash as in step 2, but with 7 total washes.

n. Add 100 µL of TMB-ELISA Substrate Solution to each well. Incubate plate (without plate sealer) for 30 minutes at room temperature in the dark.

o. Add 50 µL of Stop Solution to each well.

p. Read absorbance at 450 nm within 30 minutes of stopping reaction.

q. Calculate protein concentration based on standard curve

r. Create curve being sure to subtract out the zero value from both curve and samples.

s. Calculate protein concentration using y=mx+b equation (sample=con*slope+intercept -> con=(sample-intercept)/slope)

Skeletal muscle function – *in situ*

1. Materials and Reagents

    a. Aurora scientific force transducer

    b. Heat Therapy Pump (HTP-1500)

    c. Jari monopolar electrodes (25 mm)

    d. Isoflurane

e. Mineral oil

f. 5-0 silk suture

2. Procedure

a. Anesthetize mouse with 2% isoflurane

b. Shave the entire hindlimb and clean with alcohol

c. Make a 1 mm incision is made just above the anterior portion of the talocrural joint to expose the distal tendon of the TA

d. Tease the distal tendon of the TA away from surrounding tissue

e. Tie distal tendon tightly with a 5-0 silk suture and then cut tendon distal to knot

f. Make a 2 mm incision at the midpoint between the lateral aspect of the knee and hip to expose the lateral quadriceps

g. Carefully dissect the muscle to expose the sciatic nerve

h. Maintain exposed nerve in warmed mineral oil or warmed saline

i. Place the mouse on the aurora scientific force transducer *in situ* apparatus maintained at 37°C using heat therapy pump

j. Fix the mouse's knee to the base plate

k. Tie the other end of the suture (end that is not tied to the tendon) to the force transducer

l. Delicately place the electrode under the sciatic nerve so that contact is maintained throughout the duration of the protocol

m. Stimulate the sciatic nerve with a single stimulus to elicit a muscle twitch

n. Slightly lengthen between twitches (>30 seconds apart) the muscle to obtain

the optimal length (Lo)

o. Once Lo was obtained, stimulate the sciatic nerve at 10, 30, 50, 80, 100, 120, 150, 180, 200, 250, and 300hz (3 minute rest between contractions) to produce a force-frequency curve

p. Rest the muscle for 5-minutes

q. Stimulate the sciatic nerve for 0.5 second at 50Hz every second for 5 minutes for a total of 300 submaximal contractions

r. Immediately after the submaximal contractions, stimulate the sciatic nerve for 0.5 second at 200Hz every second for 5 minutes for a total of 300 additional contractions (600 total)

s. Rest the muscle for 5 minutes

t. Stimulate the sciatic nerve at 200 Hz to elicit a maximal contraction

Isolation of skeletal muscle mitochondria

1. Material and Reagents

   a. 3 single edge razor blades

   b. PFTE pestle

   c. 0.25% Trypsin

   d. Isolation buffer for Mitochondria 1 (IBM1)

IBM1	Stock Solution	Desired Concentration	Volume of stock needed
Sucrose	-	67mM	11.47g
Tris/HCl (pH 7.4)	2M	50mM	12.5mL
KCl	1M	50 mM	25mL
EDTA/Tris (pH 8.0)	0.5M	10mM	10mL
FA Free BSA	-	0.20%	1g

e. Isolation buffer for Mitochondria 1 (IBM1)

IBM2	Stock Solution	Desired Concentration	Volume of stock needed
D-Mannitol	-	200mM	10.9g
Sucrose	-	70mM	7.188g
EGTA/Tris	100mM	5mM	15mL
Tris/HCl (pH 7.4)	1M	10mM	3mL

2. Procedure

a. Excise a piece of muscle 75-100mg from mouse

b. Place in chilled small cell culture dish containing ~5mL IBM1

c. Mince tissue for 2 minutes with 3 single edge blades (45s each)

d. Transfer minced tissue to 15mL tube with 5mL IBM1/0.05 Trypsin

e. Incubate fore 30 minutes on ice

f. Spin tube at 200 x g for 3 minutes at 4ºC

g. Dispose of supernatant

h. Resuspend pellet in 3mL of ice cold IBM1 (cut tip)

i. Transfer to 45mL glass homogenizer tube

j. Rinse 15mL conical tube with 1.5mL of IBM1 (cut tip)

k. Transfer to the previously mentioned 45mL tube

l. Place homogenizer tube in a beaker with ice

m. Homogenize tissue with PFTE pestle (10, 2s passes @ 80 RPM)

n. Transfer to a new 15mL tube (cut tip)

o. Rinse glass homogenizer with 6.5 mL of IBM1

p. Transfer to the previously mentioned 15mL tube containing homogenate (cut tip)

q. Spin 15mL tube at 700 x g for 10 minutes at 4ºC

r. Pour supernatant into a new 15mL tube

s. Spin supernatant at 8,000 x g for 10 minutes at 4ºC

t. Dispose of supernatant

u. Resuspend in 0.5mL of IBM2 (cut tip)

v. Add 4.5mL of IBM2

w. Spin tube at 8,000 x g for 10 minutes at 4ºC

x. Dispose of supernatant

y. Resuspend pellet in 25uL of IBM2 (cut tip)

Respiration

1. Materials and Reagents

    a. Buffer X

        i. 60 mM K-MES, 35 mM KCl, 7.23 mM K2EGTA, 2.77 mM CaK2EGTA, 20 mM imidazole, 0.5 mM DTT, 20 mM taurine, 5.7 mM ATP, 15 mM phosphocreatine, and 6.56 mM MgCl2, pH 7.1

    b. 50uM Saponin

    c. Respiration buffer

        i. 05mM K-MES, 3mM KCl, 1mM EGTA, 10mM K2HPO4, 5mM MgCl2, 0.005mM Glutamate, 0.002mM Malate, 0.05% BSA, 20mM Creatine, pH 7.1

    d. 20mM Creatine in respiration buffer

    e. 5mM Pyruvate

f. 2mM Malate

g. 0.25mM ADP

h. Oligomycin

i. Buffer Z

    i.

j. Hansatech Oxygraph+

2. Procedure

a. Mechanically tweeze a 7-10 mg piece of muscle with forceps under a dissecting microscope in ice-cold *buffer X*.

b. Incubate the fiber bundle in 50uM saponin for 30 minutes

c. Wash 3 times for 5 minutes in respiration buffer

d. Place fiber bundles into the oxygraph machine in 20mM creatine respiration buffer at 37 degrees

e. Syringe 5mM of pyruvate and 2mM of malate into the chamber

f. Two minutes following pyruvate and malate, inject 0.25mM of ADP into the chamber to induce STATE 3 respiration

g. Wait 5 minutes

h. Inject 10ug/mL of Oligomycin to induce steady state 4 respiration

i. Wait 10 minutes

j. Respiratory Control Ratio (RCR) was calculated by dividing state 3 by state 4 respirations.

Cytochrome C Oxidase Activity

1. Materials and Reagents
    a. 20 mM KCN; MW= 65.12, 13.02 mg/10 ml dH_2O
    b. 100 mM KPO_4 Buffer (pH 7)
        1. 0.1 M KH_2PO_4 (pH 5)
        2. 0.1 M $K_2HPO_4.3H_2O$ (pH 8)
    c. 10 mM K-Phosphate Buffer
    d. Extraction Buffer (100 mM Na-K-Phosphate, 2 mM EDTA; pH 7.2)
        1. 500 ml 0.1 M $Na_2HPO_4. 2H_2O$;
            1. 8.9 g sodium phosphate with 0.372 g EDTA up to 500 ml
        2. 200 ml 0.1 M KH_2PO_4
            1. 2.7 g potassium phosphate with 0.149 g EDTA up to 200 ml.
        3. combine both solutions and pH to 7.2
    e. Test Solution (reduced cytochrome c, 2 mg/ml), for 10 ml (enough for 36 microplate wells);
        1. 20 mg of horse heart cytochrome c (Sigma, C-2506) in a scintillation vial
        2. add 1 ml of 10 mM KPO_4 buffer and dissolve cytochrome c
        3. make up a small volume of 10 mg/ml sodium dithionite-10 mM KPO_4 stock solution (make fresh each experiment and use within twenty minutes)

4. add 40 μl of the dithionite stock solution to the test solution and observe red-orange colour change
5. add 8 ml of ddH_2O
6. add 1 ml of 100 mM KPO_4 buffer.

2. Procedure

a. Place powdered muscle samples in liquid N_2.

b. Add 50 μl of extraction Buffer to 1.5 ml Eppendorf tubes in the aluminum block on ice. (One Eppendorf per sample).

c. Add 5-7.5 mg tissue to each tube, recording exact tissue mass. Mix by tapping.

d. Add the volume of Extraction Buffer required to obtain a 20-fold dilution.

e. Add a stir bar and mix for 15 min. Make up Test Solution during this time and wrap in foil.

f. Sonicate each tube 3 x 3 seconds, cleaning the probe between samples.

g. Pipette some of 20-fold sample extract into new Eppendorf tube and add volume of Extraction Buffer required to obtain an 80-fold dilution. (eg. 50 μl of 20-fold extract + 150 μl Ext. Buffer = 200 μl of 80-fold sample extract). Keep 80-fold sample extract tube on ice for duration of experiment

h. Add 270 μl of Test Solution into 4-8 wells of 96-well microplate and incubate at 30°C for 10 minutes to stabilize the temperature and absorbance.

i. Open KC4 plate reader program (on Triton). Select CONTROL icon, then

PRE-HEATING tab, enter 30°C and select ON. (Do not run assay until KC4 temperature has reached 30°C.)

j. Select WIZARD icon, then READING PARAMETERS icon.

1. Select Kinetic for Reading Type.
2. Select Absorbance for Reader and 550 nm for wavelength (drop-down menu).
3. Select Sweep for Read Mode.
4. Select 96 Well Plate (default) for Plate Type.
5. Enter first and last well to be read (eg. A1 and A4 if reading 4 samples simultaneously).
6. Select Yes and Pre-heating and enter 30 for Temperature Control.
7. For Shaking enter 0 for both intensity and duration (shaking is not necessary and it will delay the first reading).
8. Do not select either of the two options for Pre-reading.
9. Click on the KINETIC… rectangular tile to open the Kinetic window.
10. Enter run time (1 minute is recommended) and select MINIMUM for Interval time (under these conditions the minimum Interval time should be 3 seconds).
11. Select Allow Well Zoom During Read to see data in real time (optional).
12. Under Scales, checkmarks should appear for both Auto check

boxes. Do not select Individual Well Auto Scaling.

13. Press OK to return to Reading Parameters window. Press OK to return to Wizard window. Press OK. Do not save the protocols

k. Set the multipipette to 250 μl and secure 4-8 yellow tips on the white projections (make sure they are on tight and all at the same height).

l. In a second, clean 96 well plate, pipette samples into 4-8 empty wells (start with A1). Recommended volumes: 30 μl of 80-fold extract for Mixed Gastroc, 10 μl for Heart. Adjust volumes according to oxidative capacity of the tissue. (eg. 25 μl for Red Gastrocnemius and 35 μl for White Gastrocnemius).

m. Remove microplate with Test Solution in 4-8 wells from the incubator (as long as it has been incubating for 10 minutes). Place this plate beside the plate with the sample extracts in it.

n. On KC4 program, select the READ icon and press the START READING icon, then press the READ PLATE button. A box will appear that says, "Insert plate and start reading". Do not press OK yet, but move the mouse so that the cursor hovers over the OK button.

o. Using the multipipette (set to 250 μl) carefully draw up the Test Solution. Make sure the volume is equal in all the pipette tips, and that no significant air bubbles have entered any of the tips.

p. Pipette the Test Solution into the wells with the sample extracts (the second plate). As soon as all the Test Solution has been expelled from the tips (do not wait for the second push from the multipipette), place the plate

onto the tray of the plate reader and with the other hand on the mouse, press the OK button. (Speed at this point is paramount, as there is an unavoidable latency period between the time of pressing the OK button and the time of the first reading.)

q. If desired, add 5 μl KCN to one of the wells to measure any absorbance changes in the presence of the CYTOX inhibitor.

r. Once reading is complete, hold the CTRL key on the keyboard, and use the mouse to click once on each of the squares corresponding to a well that had sample in it. Once all the desired wells have been highlighted by a black square (up to a maximum of 8 wells), let go of the CTRL key and a large graph will appear with lines on it representing each sample.

s. To obtain the rate of change of absorbance over different time periods, select Options and enter the amount of time for which you would like a rate of change of absorbance to be calculated. The graph, along with one rate (at whichever time interval is selected) for each sample can be printed on a single sheet of paper, and the results can be saved.

t. The delta absorbance will appear in units of mOD/min and the number given will be negative. Convert this to OD/min by dividing by 1000 and omit the negative sign in the calculation. (eg. if Mean V: -394.8 mOD/mn, then use 0.395 OD/min)

APPENDIX B

PROPOSAL

2.1 – Specific Aims

Cachexia

The unintentional loss of body weight with chronic disease, termed cachexia, is associated with reduced life quality, poor treatment outcomes, and increased mortality (al-Majid and McCarthy 2001a; Arthur et al. 2014; Christensen et al. 2014; Evans et al. 2008; Deans and Wigmore 2005; Fearon KC 2006; Tisdale 2002; von Haehling and Anker 2014). Specifically, cancer-induced cachexia has been associated with nutrient resistance, anemia, hypogonadism, and chronic inflammation (Evans et al. 2008; Carson and Baltgalvis 2010; Deans and Wigmore 2005; Fearon KC 2006), all of which contribute to weakness, fatigue, and physical inactivity resulting in loss of functional independence and increased health care costs (Deans and Wigmore 2005; Evans et al. 2008; Christensen et al. 2014; Op den Kamp et al. 2012; Roberts, Frye, et al. 2013; Wolfe 2006; Winningham et al. 1994; O'Gorman, McMillan, and McArdle 1999; Montazeri 2009; Fearon KC 2006; Arthur et al. 2014). While our mechanistic understanding of cancer-induced muscle wasting has improved, further investigation is needed to understand the regulatory mechanisms of functional decrements that occur with cancer and cancer-induced cachexia.

Skeletal Muscle Fatigue

Functional outcomes can be affected by central, peripheral, and muscular alterations, and the difficulty delineating their individual roles has hindered our mechanistic understanding of the functional decrements the occur with aging and disease (Hughes, Wallace, and Baar 2015; Wolfe 2006; Norden et al. 2015). While several cancer-induced skeletal muscle functional decrements have been described, the regulation of skeletal muscle fatigue in cancer patients and preclinical models appears distinct from changes to mass and strength which may contribute to the initiation of cachexia (Winningham et al. 1994; Roberts, Frye, et al. 2013; Jaweed et al. 1983). We have previously shown that tumor-bearing mice had reduced cage activity and increased muscle fatigability independent of body weight loss (Roberts, Frye, et al. 2013; Baltgalvis 2010). Furthermore, recent evidence suggests that mitochondrial degeneration develops prior to significant weight loss demonstrating that fatigue and disrupted oxidative metabolism occur early in cachexia progression (Baltgalvis 2010; Brown et al. 2017). While increased muscle fatigability and disrupted oxidative metabolism has been reported with cachexia, significant gaps remain in our mechanistic understanding of the role of disrupted oxidative metabolism in muscle fatigue and when these dysfunctions occur during the progression of cachexia.

Skeletal Muscle gp130 Signaling

Chronic inflammation is a hallmark of cancer and cancer-induced wasting, and several inflammatory cytokines have been implicated as drivers of cachexia with chronic disease (Deans and Wigmore 2005). Specifically, the interleukin-6 (IL-6) family of

cytokines and associated muscle signaling through the membrane gp130 receptor plays a role in muscle mass regulation and oxidative metabolism during both physiological and pathological conditions (Carson and Baltgalvis 2010). Our lab has demonstrated that loss of IL-6 and/or muscle gp130 signaling attenuated muscle mass loss in tumor-bearing mice while high levels of IL-6 and muscle gp130 signaling are associated with reduced mitochondrial protein expression and disrupted mitochondrial quality control in tumor-bearing and tumor-free mice (Fix et al. 2018; Baltgalvis et al. 2008; Baltgalvis et al. 2009; Puppa, Gao, et al. 2014; Puppa et al. 2012). Additionally, increasing muscle use by treadmill exercise or repeated eccentric contractions attenuated the loss of muscle mass and succinate dehydrogenase activity with cachexia without affecting downstream muscle gp130 signaling targets STAT3 and Erk 1/2 (Hardee et al. 2016). While the role of IL-6 and associated gp130 signaling in skeletal muscle mass maintenance and metabolic homeostasis has received significant attention, their contribution to skeletal muscle fatigue during the progression of cachexia remains largely unknown.

Purpose and Hypothesis

Our long-term goal is to identify the regulatory mechanisms driving cancer-induced skeletal muscle dysfunction to better understand the cachectic condition and improve the life quality of cancer patients. The overall purpose of the current proposal is to determine the regulatory mechanisms of skeletal muscle fatigue in tumor-bearing mice. Our central hypothesis is that cancer-induced skeletal muscle fatigue develops prior to cachexia development in association with decreased muscle use and activated muscle gp130 signaling which disrupt muscle oxidative metabolism. Furthermore, increased muscle use

through increased volitional activity will delay the induction of fatigue in tumor-bearing mice. To test this hypothesis, we will first determine the onset of fatigue in tumor-bearing mice and determine its relationship to known cachexia indices including body weight loss, systemic inflammation, and muscle inflammatory signaling in tumor-bearing mice. Next, we will determine if modulating muscle gp130 signaling alone can regulate skeletal muscle fatigue and muscle oxidative metabolism in healthy tumor-bearing mice. Last, we will determine if increased muscle use can attenuate the cancer-induced skeletal muscle fatigue and improve muscle oxidative metabolism.

Specific Aims

Using preclinical models of cancer-cachexia, we plan to test our hypothesis using the following 3 specific aims:

> **Specific Aim 1: Examine the impact of cachexia progression on the development of skeletal muscle fatigue in tumor-bearing mice.**
>
> **Specific Aim 2: Determine the role of muscle gp130 signaling in skeletal muscle fatigue during the progression of cachexia.**
>
> **Specific Aim 3: Determine the effect of muscle use on skeletal muscle fatigue during cachexia progression.**

Our lab has previously shown that functional decrements occur prior to significant weight loss (Baltgalvis 2010). Significant gaps remain in our mechanistic understanding of cachexia-induced skeletal muscle dysfunction and whether these decrements are causal, or consequent, of weight loss is unknown. The results from this study will extend our current understanding of muscle fatigue with cancer and elucidate the mechanisms regulating skeletal muscle metabolism which directly impacts skeletal muscle function.

Specific Aim 1: Examine the impact of cachexia progression on the development of skeletal muscle fatigue in tumor-bearing mice.

Aim 1.1: Determine the fatigue properties of skeletal muscle in male tumor-bearing MIN mice.

Aim 1.2: Determine the relationship between systemic inflammatory markers, muscle gp130 signaling, body weight loss, and skeletal muscle function in weight stable and cachectic MIN mice.

Aim 1.3: Determine the relationship between skeletal muscle oxidative and glycolytic metabolism with skeletal muscle fatigue in MIN mice.

Specific Aim 2: Determine the role of muscle gp130 signaling in skeletal muscle fatigue during the progression of cachexia.

Aim 2.1: Determine if the IL-6 induction of fatigue is through direct activation of muscle gp130 signaling in tumor-free mice.

Aim 2.2: Determine the effect of elevated skeletal muscle gp130 signaling on skeletal muscle oxidative and glycolytic metabolism.

Aim 2.3: Determine the role of skeletal muscle gp130 signaling in cancer induced skeletal muscle fatigue in MIN mice.

Specific Aim 3. Determine the role of muscle use on skeletal muscle fatigue during cachexia progression.

Aim 3.1: Determine the relationship between volitional activity and skeletal muscle fatigue during the progression of cachexia.

Aim 3.2: Determine if 5 weeks of free access to a wheel can prevent the induction of skeletal muscle fatigue in MIN mice.

Aim 3.3: Determine if 5 weeks of free access to a wheel can prevent the loss of muscle oxidative metabolism in MIN mice.

2.2 – Preliminary Results

The culmination of several published and preliminary findings from our laboratory contribute to the premise for the proposed study. Cachexia-induced skeletal muscle mass loss is associated with reduced ability to perform basic daily tasks leading to a loss of functional independence (Vigano et al. 2000; Evans et al. 2008; Moses et al. 2004; Fearon KC 2006; Argiles 2014; Amano et al. 2017). More clinically relevant, cancer patients with decreased functional ability and increased fatigue, regardless of cachexia diagnosis, experience decreased quality of life and respond poorly to treatment (O'Gorman, McMillan, and McArdle 1999; al-Majid and McCarthy 2001a). Cachectic patients and preclinical cachexia models exhibit decreased volitional activity, whole body weakness, and fatigue (Baltgalvis 2010; Murphy et al. 2012; Roberts, Frye, et al. 2013; Toth et al. 2016; Puppa, Gao, et al. 2014). Recently, specific decrements to skeletal muscle's contractile quality have been identified in cachectic patients and tumor bearing mice (Christensen et al. 2014; Gorselink et al. 2006; Murphy et al. 2012; Roberts, Frye, et al. 2013; Jaweed et al. 1983). However, the drivers of these functional deficits in skeletal muscle have not been clearly defined (Op den Kamp et al. 2012; Christensen et al. 2014; Biolo, Cederholm, and Muscaritoli 2014). To this end, several proposed cancer cachexia therapeutics have failed in clinical trials due to their inability to improve overall patient function (Dobs et al. 2013; Aversa, Costelli, and Muscaritoli 2017; Biolo, Cederholm, and Muscaritoli 2014; Ramage and Skipworth 2018). This inability of proposed therapeutics to

improve muscle function illustrates our lack of understanding of the cachectic factors that induce these functional deficits.

Critical gaps in our knowledge of this regulation are likely related to the dearth of studies examining both muscle function and cachectic factors in the same cohort of tumor bearing mice. This lack of cohesive integration with these measurements has likely contributed to the plethora of unsuccessful cancer cachexia treatment paradigms (al-Majid and McCarthy 2001a; Baltgalvis 2010; Christensen et al. 2014; Murphy et al. 2012; Roberts, Frye, et al. 2013; White, Baltgalvis, et al. 2011; White et al. 2012; Ramage and Skipworth 2018). We have previously shown that MIN mice demonstrate decreased voluntary wheel running and cage activity prior to significant weight loss (Baltgalvis 2010). However, it is not known if this decreased volitional activity is associated with decrements in skeletal muscle function. Our preliminary data suggests that the loss of skeletal muscle force occurs in cachectic muscle (Figure 2.2 A, B) which cannot be explained by loss of muscle mass alone (Figure 2.2 C, D). Additionally, our preliminary examination of whole-body fatigue showed reduced time to exhaustion in weight stable MIN mice that is exacerbated by cachexia (Figure 2.3 A). Furthermore, skeletal muscle fatigue appears increased in MIN mice regardless of significant body weight loss (Figure 2.3 B).

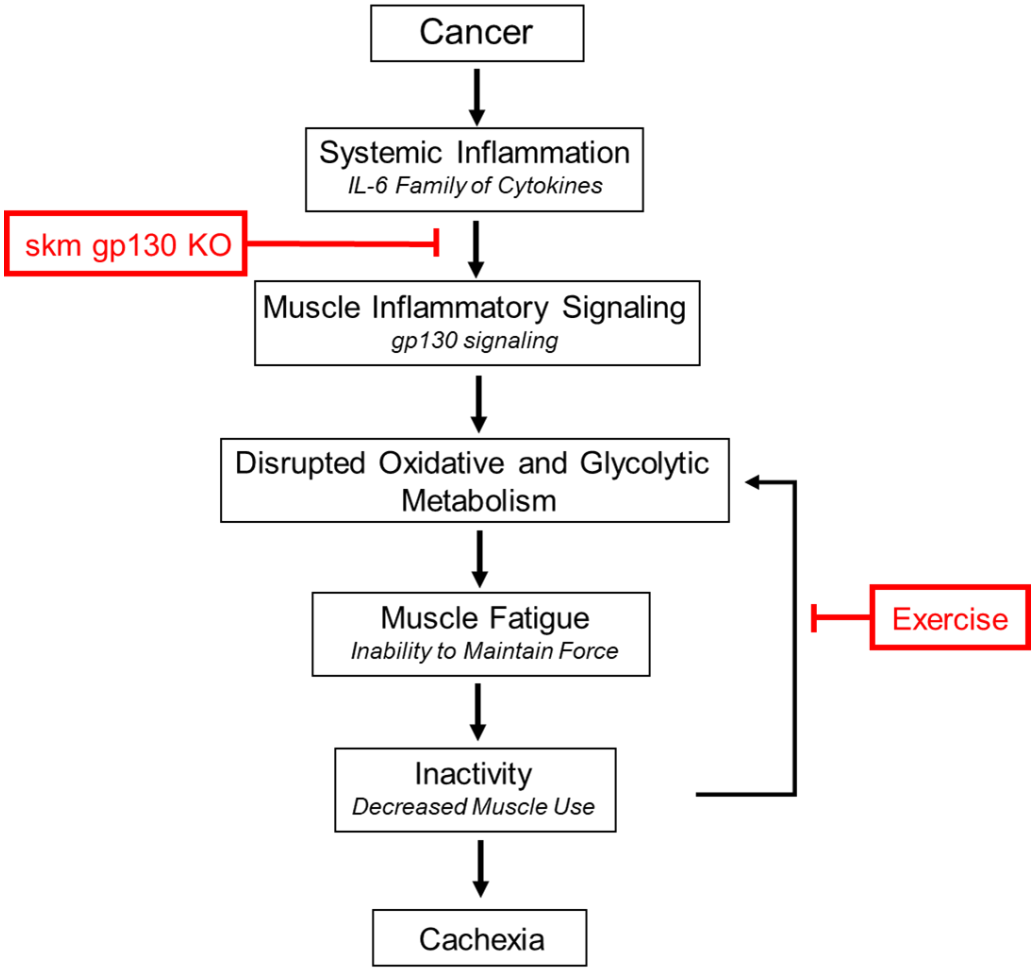

Figure B.1 Proposed working model of cancer induced fatigue. The overall purpose of the current study is to determine the regulatory mechanisms of skeletal muscle fatigue during cachexia progression. Our central hypothesis is that skeletal muscle fatigue develops early in cachexia progression in association with disrupted oxidative and glycolytic metabolism. Furthermore, we hypothesize that activated muscle gp130 signaling increases volitional fatigue through the regulation of muscle oxidative metabolism and increasing skeletal muscle use will suppress the induction of cancer-induced fatigue and delay cachexia progression. Specific aim 1 will examine the relationship between skeletal muscle function and known cachexia indices, including body weight loss, systemic inflammation, and muscle inflammatory signaling in tumor bearing mice. Specific aim 2 will directly examine the role of muscle gp130 signaling in skeletal muscle fatigue in tumor-free and tumor-bearing mice. Specific aim 3 will examine the effects of wheel access on the induction of fatigue during cachexia progression.

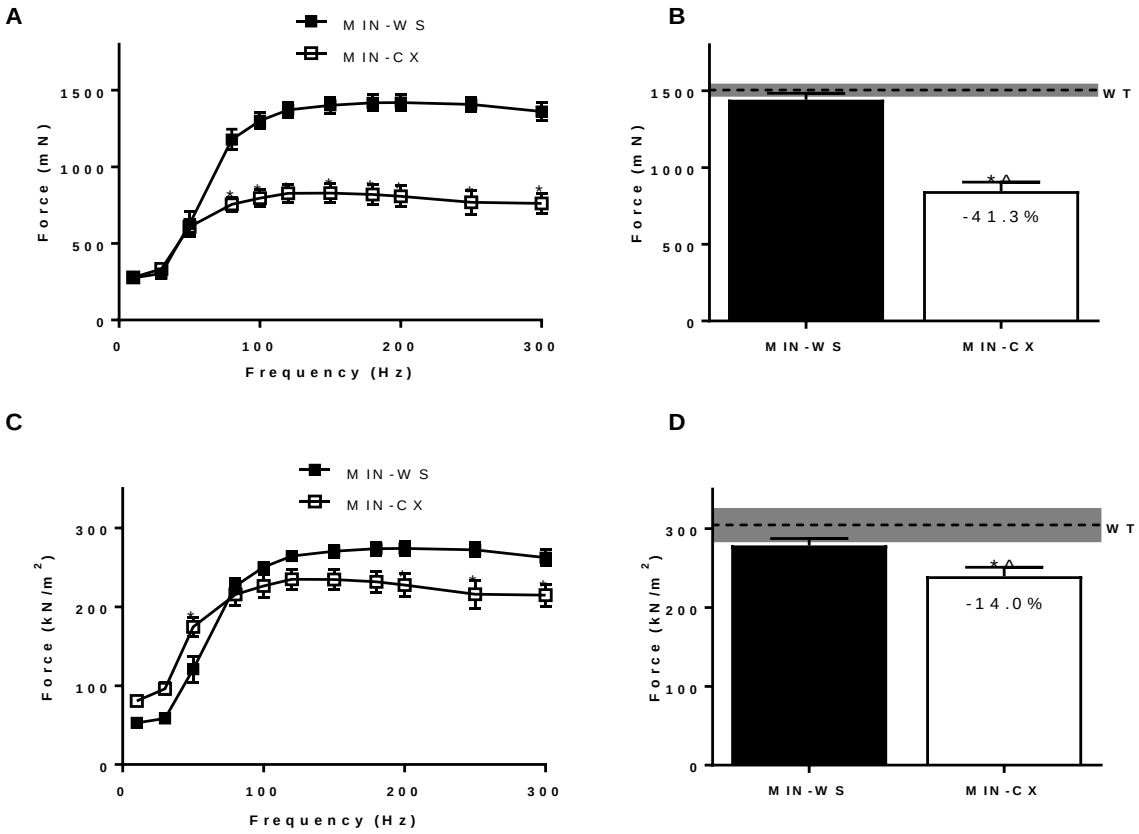

Figure B.2 The effect of cachexia on absolute and specific maximal tetanic force. (A) Force-frequency curve of the tibialis anterior (TA) absolute force measurements (millinewtons) in weight stable $Apc^{Min/+}$ mice (<5% body weight loss, MIN-WS) and cachectic $Apc^{Min/+}$ mice (>5% body weight loss, MIN-CX) compared to age-matched C57BL/6 (WT) mice. Muscle force analysis was assessed using *in situ* muscle function. (B) Absolute maximal tetanic force (P_o) of the TA in MIN-WS and MIN-CX. (C) Force-frequency curve of the tibialis anterior (TA) specific force measurements (Force in kilonewtons / calculated muscle CSA in m^2) in MIN-WS and MIN-CX. Muscle force analysis was assessed using *in situ* muscle function. (D) Specific maximal tetanic force ($_sP_o$) of the TA in MIN-WS and MIN-CX. Values are means ± SE *Significant from MIN-WS. ^Significant from MIN-WS. Significance was set at $p<0.05$. One-Way ANOVA.

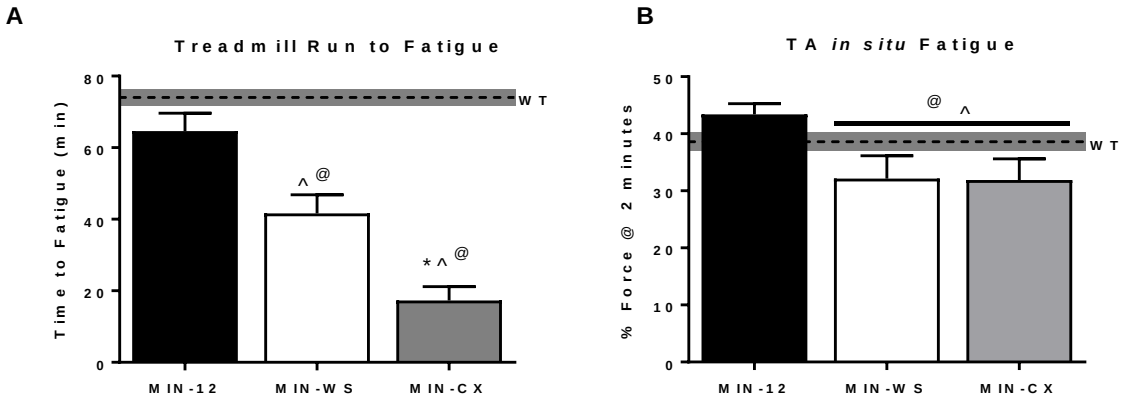

Figure B.3 The effect of tumor burden on whole body and muscle specific fatigue. (A) Treadmill time to fatigue in 12-week-old $Apc^{Min/+}$ mice (MIN-12), weight stable $Apc^{Min/+}$ mice (<5% body weight loss, MIN-WS), and cachectic $Apc^{Min/+}$ mice (>5% body weight loss, MIN-CX) compared to age-matched C57BL/6 (WT) mice. (B) In situ muscle fatigability shown as % of maximal tension after 2 minutes of an intermittent fatigue protocol. Values are means ± SE. *Significant from MIN-WS. ^Significant from WT. @Significant from MIN-12. Significance was set at $p<0.05$

Muscle gp130 Signaling and Skeletal Muscle Function

Skeletal muscle contractile dysfunction and disrupted metabolic homeostasis have been demonstrated across several chronic diseases (Sin and Man 2003; Deans and Wigmore 2005; Kuller et al. 2008; Vidt 2006). Recent evidence suggest that muscle mitochondrial dysfunction and increased fatigability can occur independent of changes to muscle size and strength suggesting that muscle weakness and fatigue have distinct etiologies (VanderVeen et al. 2018; Brown et al. 2017). Muscle fatigability, or the ability to sustain force over time, relies on several physiological phenomena, most notably, adequate ATP production by mitochondrial respiration and glycolytic pathways, while skeletal muscle force can be modulated by myofiber CSA (sarcomeres in parallel), percent non-contractile tissue (fibrosis), and MHC expression (fiber-type) (Holloszy and Booth 1976; Fitts and Holloszy 1977; Munkvik, Lunde, and Sejersted 2009; Thompson et al. 1992; Fitts 1994; Rutherford, Manning, and Newton 2016).

Chronic inflammation is a broadly defined term used to describe an unrelenting immune response; however, several inflammatory mediators, specifically cytokines, have been implicated in the progression of several diseases and disease comorbidities (Deans and Wigmore 2005; Onesti and Guttridge 2014). IL-6 signaling through the membrane gp130 receptor has been implicated as a regulator of skeletal muscle mass and metabolic homeostasis during both physiological and pathological conditions (Carson and Baltgalvis 2010; Bonetto et al. 2011; Hardee, Counts, et al. 2018; Gao et al. 2017; Puppa, Gao, et al. 2014). While IL-6 overexpression in tumor-bearing mice accelerated muscle mass loss, whether IL-6 alone can induce body weight or muscle mass loss in tumor-free mice remains inconclusive (White et al. 2012; White, Baltgalvis, et al. 2011; Puppa et al. 2012). Recently,

the mitochondria have emerged as an intriguing target for inflammation induced skeletal muscle metabolic dysfunction (Boland, Chourasia, and Macleod 2013; Brown et al. 2017; Hardee et al. 2016; Carson, Hardee, and VanderVeen 2016). We have previously shown that elevated levels of circulating IL-6 was sufficient to decrease mitochondrial protein expression in tumor-free mice (Puppa et al. 2012); however, whether this occurs directly through the muscle gp130 receptor to increase muscle fatigue was not been examined.

TNF-α alone has been eloquently shown to directly reduce skeletal muscle force and slow muscle contractile properties *in vivo* and *ex vivo* without any apparent effect on fatigue, further emphasizing that weakness and fatigue have distinct etiologies (Reid and Moylan 2011; Gilliam et al. 2011; Hardin et al. 2008; Reid, Lannergren, and Westerblad 2002; Li et al. 2000). We have previously shown that chronically elevated IL-6 reduced mitochondrial proteins in addition to the muscle gp130 receptor regulating mitochondrial quality control; however, the effect of IL-6 and muscle gp130 signaling on skeletal muscle force and fatigue remains largely unknown. Our preliminary results suggest that two weeks of IL-6 over-expression is sufficient to increase plasma IL-6 (Figure 2.4 B) and induce skeletal muscle gp130 signaling (Figure 2.4 C). While IL-6 over-expression had no effect on muscle force (Figure 2.5 A), IL-6 induced submaximal and maximal contraction-induced skeletal muscle fatigue (Figure 2.5 B, C).

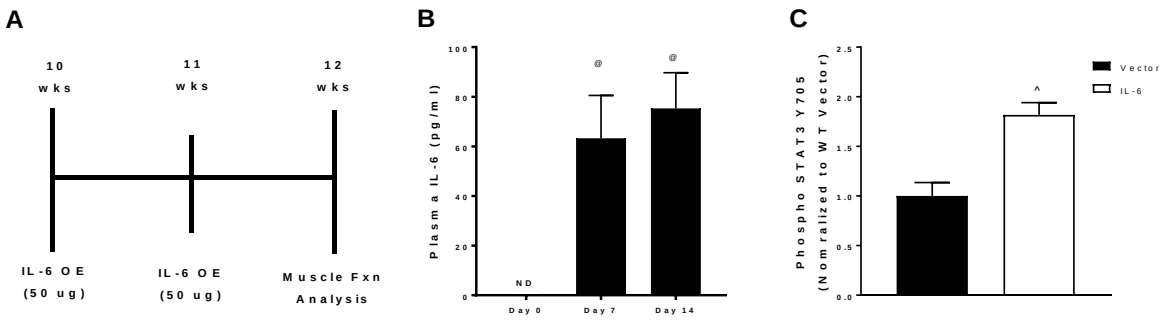

Figure B.4 IL-6 over-expression experimental design. (A) At 10 weeks of age, male C57BL/6 mice were subjected to 2 weeks of systemic IL-6 overexpression. Mice were injected with 50 ug of IL-6 plasmid into the Quad for muscle electroporation. After 1 week this process was repeated. Muscle function analysis was conducted after 2 full weeks of IL-6 overexpression. (B) Plasma levels of IL-6 throughout the duration of the study. (C) Summary data of relative expression of phosphorylated muscle STAT3 (Y705) in the TA following 2 weeks of IL-6 over-expression. Values are means ± SEM. @ Significantly different from Day 0. One-way ANOVA. ^Significantly different from Vector controls. Significance was set at $p<0.05$. Students t-test.

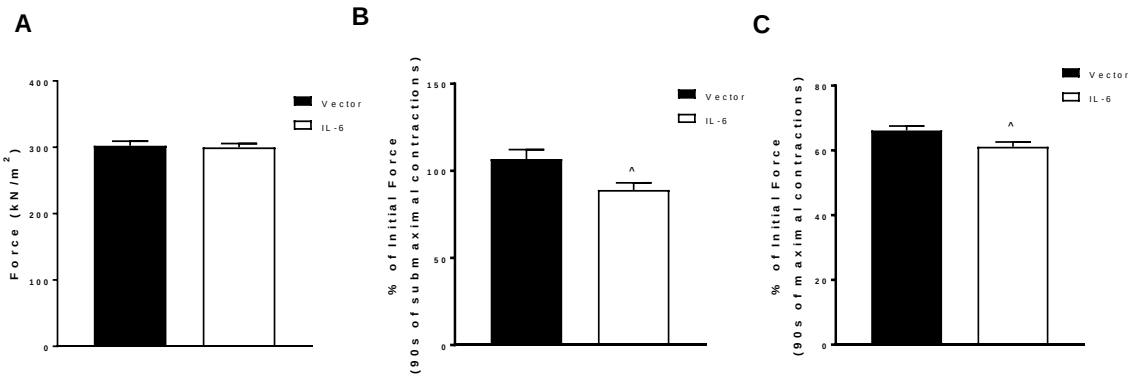

Figure B.5 The effect of IL-6 over-expression of skeletal muscle function. (A) Specific maximal tetanic force ($_sP_o$) of the tibialis anterior (TA) two weeks following the first electroporation in Vector and IL-6 mice. (B) *in situ* muscle fatigability shown as % of initial tension produced by the TA after 90 seconds of a submaximal fatigue protocol. (C) In situ muscle fatigability shown as % of maximal tension produced by the TA after 90 seconds of a maximal fatigue protocol. Values are means ± SEM. ^Significant from Vector controls. Significance was set at $p<0.05$. Students t-test.

2.3 – Experimental Design and Methods

Specific Aim 1. Examine the impact of cachexia progression on the development of skeletal muscle fatigue in tumor-bearing mice.

Premise

Cachexia-induced skeletal muscle mass loss is associated with reduced ability to perform basic daily tasks leading to a loss of functional independence and reduced life quality (Vigano et al. 2000; Evans et al. 2008; Moses et al. 2004; Fearon KC 2006; Argiles 2014; Amano et al. 2017). Additionally, regardless of significant body weight loss, cancer patients with reduced functional testing scores have worse chemotherapy tolerance and have reduced survival (O'Gorman, McMillan, and McArdle 1999; al-Majid and McCarthy 2001a). While overall functional capacity can be impacted by the nervous (both central and peripheral), circulatory, and musculoskeletal systems, specific decrements to skeletal muscle's contractile quality have been identified in cachectic patients and tumor bearing mice (Christensen et al. 2014; Gorselink et al. 2006; Murphy et al. 2012; Roberts, Frye, et al. 2013; Jaweed et al. 1983). The drivers of functional deficits in skeletal muscle during cachexia progression have not been clearly defined (Op den Kamp et al. 2012; Christensen et al. 2014; Biolo, Cederholm, and Muscaritoli 2014).

Aim 1.1 Experimental Design

The purpose of aim 1.1 was to determine the functional properties of skeletal muscle during the progression of cancer cachexia in MIN mice. We hypothesized that cachectic skeletal muscle would exhibit a decreased in force production and increased fatigability when compared to weight stable and healthy controls. To test this hypothesis,

male MIN mice were stratified by percent body weight (BW) loss ([End BW - Peak BW]/Peak BW) into weight stable (MIN-WS; <5% BW loss) or cachectic (MIN-CX; >5% BW loss). This delineation is a clinically relevant classification and has previously used to describe the progression of cachexia in the male MIN mouse (Fearon 2008; White, Baynes, et al. 2011). Age-matched male WT mice served as healthy non-tumor bearing controls. The TA was stimulated *in situ* and analyzed for several properties of muscle function.

Aim 1.1 Primary outcomes

Skeletal Muscle Contractile Properties:

The contractile properties on the TA were assessed using *in situ* skeletal muscle function analysis. The sciatic nerve was stimulated to elicit a single action potential which subsequently causes a single muscle twitch. Once the optimal length (L_o) of the muscle was determined by generating a twitch length-tension curve, the TPT and 1/2 RT was measured and recorded. The muscle was then stimulated with increased frequencies (10-300 hz) to generate a force-frequency curve. The relative increase in force (% of maximal tetanic force) was calculated. Lastly, the rate of muscle contraction and relaxation from maximal tension (+dP/dt and -dP/dt, respectively) was calculated from a 200 hz stimulation. Collectively, these outcomes have been classically used to describe the contractile properties of skeletal muscle.

Skeletal Muscle Force Production:

Skeletal muscle's force production capacity was measured in the TA using *in situ* skeletal muscle function analysis. Maximal tetanic force (P_o) was recorded as the greatest absolute force (millinewtons, mN) of the muscle at L_o generated during a force-frequency

curve. $_sP_o$ was assessed by dividing the P_o by the calculated muscle CSA. Muscle CSA was calculated by muscle mass/(L_f x 1.06), where L_f represents the fiber length determined by multiplying the L_o by 0.6, the predetermined TA muscle length to fiber length ratio, and 1.06 represents the skeletal muscle density (Brooks and Faulkner 1988).

Skeletal Muscle Fatigability:

Skeletal muscle's fatigue properties were measured in the TA using *in situ* skeletal muscle function analysis. The TA was rested for 5-minutes at L_o before being subjected to an intermittent fatigue protocol. The TA was subjected to a 4-minute intermittent fatigue protocol consisting of a 1 second long maximal contraction (250 hz) every 5 seconds (1 second on, 4 seconds rest) (Murphy et al. 2012). The force production of the TA was measured at each contraction. Fatigue was determined by the calculating the relative force production (% of the initial, time 0, contraction) of the TA throughout the duration of the fatigue protocol. A significantly lower relative force production was classified as an increase in muscle fatigability and/or accelerated fatigue.

Aim 1.1 Statistical analysis

Determining Statistical Significance:

Given the purpose and hypothesis of the study was to determine the effect of cachexia progression on muscle function, mice were separated into 3 groups for statistical analysis, WT, MIN-WS and MIN-CX. Initially, a Bartlett's test was performed to determine if there is a statistical difference in the groups standard deviations (SD). If there was no significant difference in groups SD a one-way ANOVA assuming Gaussian distribution was performed to appropriately test for significant differences in our primary

outcomes between the 3 groups. If a significant difference in group SD was observed, a Kruskal-Wallis test was performed to appropriately test for significant differences in our primary outcomes between the 3 groups. All statistical analysis was performed using GraphPad Prism 7. Values were presented as means plus / minus SEM (standard error of the mean). Significance will be set at $p<0.05$.

Power analysis:

A power analysis was performed to determine the sample size needed to observe statistical significance using a one-way ANOVA. Power (1-β) was set to 0.8 and error of probability (α) was set at 0.05. Based on previously published results and our preliminary data, to achieve significance for an estimated 15 ± 5 % difference between groups, a sample size of 9 is needed for each group.

Aim 1.2 Experimental Design

The purpose of aim 1.2 was to determine the relationship between systemic inflammatory markers, muscle gp130 signaling, body weight loss, and properties of skeletal muscle function in during the progression of cachexia in MIN mice. We hypothesized that there would be a negative linear relationship between several indices of cachexia and the properties of skeletal muscle function in MIN mice. To test this hypothesis, analysis of several properties of skeletal muscle function was conducted in male MIN mice with varying degrees of cachexia (0-25% Body Weight loss). Immediately following muscle function analysis and prior to sacrifice, each mouse's tissues were excised and snap frozen in liquid nitrogen. Protein and mRNA expression of muscle gp130 signaling was examined in the contralateral TA. Following data collection, the relationship

between several cachexia indices and the properties of skeletal muscle function correlations was examined.

Aim 1.2 Primary outcomes

Skeletal Muscle Contractile Properties: See aim 1.1

Skeletal Muscle Force Production: See aim 1.1

Skeletal Muscle Fatigability: See aim 1.1

Indices of Cachexia:

The progression of cachexia in the male MIN mouse has been well described. Body weight was measured weekly throughout the early and mid-stages of adulthood of the mice to determine the relative loss of body weight in individual mice. The muscle and tissue weights of each mouse was determined prior to sacrifice. Blood was collected immediately prior to sacrifice and Plasma IL-6 levels will be examined using an ELISA.

Skeletal Muscle Inflammatory Signaling:

Phosphorylated and total protein expression of direct (STAT3 (Y705) and ERK1/2 (T202/Y204)0 and indirect (NFκB (S536) and P38 (Y182)) downstream gp130 targets were measured in the proximal TA using Western blot techniques. The phosphorylated to total ratio of these proteins was used to determine the activation of each respective protein. Additionally, mRNA expression of gp130 signaling associated transcriptional targets, IL-6, SOCS3, TNFα were measured using RT-PCR.

Relationship Between Indices of Cachexia and Skeletal Muscle Function:

Pearson's correlations and stepwise linear regression models were performed analyzing the cachexia indices (BW, % BW Loss, muscle mass, plasma IL-6, and muscle

inflammatory signaling) as the independent variable and the properties of skeletal muscle function (1/2 RT, TPT, +dP/dt, -dP/dt, P_o, $_sP_o$, and fatigue) as the dependent variable.

Aim 1.2 Statistical analysis

Determining Statistical Significance:

See aim 1.1. A Pearson's correlation was used to determine correlations between inflammatory genes and proteins with muscle function properties in MIN mice. Stepwise linear regression models were used to identify predictors (cachexia indices) of the 8 measured outcomes related to skeletal muscle function. Significance was set at $p<0.05$.

Power analysis: See aim 1.1

Aim 1.3 Experimental Design

The purpose of aim 1.3 was to determine the relationship between skeletal muscle oxidative and glycolytic metabolism with skeletal muscle fatigue in MIN mice. We hypothesized that there would be a direct relationship between skeletal muscle fatigability and mitochondrial content, and mitochondrial and glycolytic gene expression. To test this hypothesis, analysis of several properties of skeletal muscle function was conducted in male MIN mice with varying degrees of cachexia (0-25% Body Weight loss). Immediately following muscle function analysis and prior to sacrifice, each mouse's tissues was excised and snap frozen in liquid nitrogen. mRNA expression of key mitochondrial and glycolytic targets in addition to EDL COX activity was determined from the contra-lateral TA to determine relationships to muscle function.

Aim 1.3 Primary outcomes

Skeletal Muscle Contractile Properties: See aim 1.1

Skeletal Muscle Force Production: See aim 1.1

Skeletal Muscle Fatigability: See aim 1.1

Skeletal Muscle Metabolic Gene Expression:

mRNA expression of mitochondrial content and quality control, PGC-1α, FIS1, MFN1 and 2, and COXIV, as well as key glycolytic metabolism genes, hexokinase and phosphofructokinase, were measured using RT-PCR.

Relationship Between Skeletal Muscle Metabolic Gene Expression and Skeletal Muscle Function:

Pearson's correlations and stepwise linear regression models were performed analyzing the mRNA expression of metabolism (PGC-1α, FIS1, MFN1 and 2, COXIV, hexokinase, and phosphofructokinase) as the independent variable and the properties of skeletal muscle function (1/2 RT, TPT, +dP/dt, -dP/dt, P_o, $_sP_o$, and fatigue) as the dependent variable.

Aim 1.3 Statistical analysis

Determining Statistical Significance: See aim 1.1

Power analysis: See aim 1.1

Relationship Between Muscle Metabolism and Skeletal Muscle Function: See aim 1.2

Specific Aim 1 Research Methods

Animals

Male WT and MIN mice were purchased from Jackson Laboratories and were bred at the University of South Carolina's Animal Resources Facility. All animals were group housed and kept on a 12:12-h light-dark cycle. Body weights were measured weekly, and animals were monitored for signs of distress. Animals were given food and water *ad libitum* throughout the duration of the study. All animals were fasted 5 hours prior to tissue collection. Mice were anesthetized with a ketamine-xylazine-acepromazine cocktail, and hindlimb muscles and select organs were carefully dissected and snap frozen in liquid nitrogen and stored at -80ºC until further analysis. The University of South Carolina's Institutional Animal Care and Use Committee approved all animal experiments.

Analysis of Muscle Function

At ~20 weeks of age, mice were anesthetized with 2% isoflurane inhalation and kept anesthetized at 1.5 % isoflurane throughout the duration of the procedure (~1 hour). Muscle function analysis of the TA *in situ*, which maintains the host nerve and blood supply, has been previously described (Murphy et al. 2012; Bonetto, Andersson, and Waning 2015; Dellorusso et al. 2001). Briefly, the distal tendon of the left TA was isolated and tied to a force transducer (Aurora Scientific, Ontario, Canada) using 5-0 silk sutures. The mouse was place on the apparatus maintained at 37°C throughout the entirety of the procedure (Bonetto, Andersson, and Waning 2015). The sciatic nerve was exposed proximal to the knee and maintained using warmed mineral oil. The sciatic nerve was then subjected to a single stimulus to determine L_o. Once L_o was obtained, a force-frequency

curve was generated, and maximal tetanic force was determined. After a 5-minute rest the TA was subjected to a 4-minute intermittent fatigue protocol consisting of 1 second maximal stimulation every 4 seconds (Murphy et al. 2012). Maximal tension was again measured 5 and 10 minutes after completion of the fatigue protocol. Specific tension was determined using TA muscle CSA calculated by muscle mass/(L_f x 1.06), where L_f represents fiber length determined by multiplying L_o by 0.6, the predetermined TA muscle length to fiber length ratio, and 1.06 represents the skeletal muscle density (Brooks and Faulkner 1988).

Western blot analysis

Western blot analysis was performed as described previously (Puppa, Gao, et al. 2014). Briefly, the right proximal TA was homogenized, and protein concentration was determined using the standard Bradford protein assay. Homogenates were fractionated on 7-10% SDS-polyacrylamide gels and transferred to a polyvinylidene difluoride membrane. Primary antibodies for phosphorylated (p) and total (t) P65, STAT3, P38, and Erk1/2 (Cell Signaling Technology) were incubated 1:1000 overnight at 4ºC in 5% TBST milk. Anti-rabbit IgG-conjugated secondary antibodies (cell signaling) were incubated 1:2000 for 1 hour at room temperature in 5% TBST milk. Enhanced Chemiluminescence was used to visualize antibody-antigen interaction and captured using the Syngene: G-Box. Blots were analyzed by determining the integrated optical density of each band using ImageJ (NIH software).

RNA isolation and RT-PCR

RNA isolation, cDNA synthesis, and RT-PCR were performed as previously described (Narsale et al. 2016) using reagents from Applied Biosystems (Foster City, CA, USA). Primers for GAPDH, IL-6, IL-1β, TNF-α, SOCS3, PGC1, FIS1, MFN 1 and 2, Hexokinase II, and Phophofructokinase will purchased from IDT (Coralville, Iowa, USA) and run using SYBR green PCR buffer (Narsale et al. 2016). Data were analyzed using the $2^{-\Delta\Delta CT}$ method.

Cytochrome C Oxidase Activity

EDL muscle samples will be homogenized in extraction buffer (0.1 M KH2P04/Na2HP04, 2 mM EDTA, pH 7.2). Cytochrome-c oxidase (COX) activity was determined by measuring the rate of oxidation of fully reduced cytochrome c at 550nm using (CYTOCOX1) Sigma Aldrich Kit and spectrophotometer (Eppendorf) (Iqbal and Hood 2015).

Statistical analysis

Values are presented as means ± standard error of the mean (SEM). Student t-tests were performed to determine differences between genotypes. A one-way ANOVA was used to determine differences in muscle function and inflammatory signaling when MIN mice were stratified by age or body weight loss. Post hoc analyses were performed with student Newman-Keuls methods. A Bartlett's test was used to determine significantly different standard deviations ($p<0.05$). If a significant difference was observed between group standard deviations, a non-parametric Kruskal-Wallis one-way ANOVA was used. A Pearson correlation was used to determine correlations between inflammatory genes and

proteins with muscle function properties in MIN mice. Stepwise linear regression models were used to identify predictors (cachexia indices) of the 8 measured outcomes related to skeletal muscle function. Significance was set at $p<0.05$.

Specific Aim 2. Determine the role of muscle gp130 signaling in skeletal muscle fatigue during the progression of cachexia.

Premise

Skeletal muscle contractile dysfunction and disrupted metabolic homeostasis have been demonstrated across several chronic diseases (Sin and Man 2003; Deans and Wigmore 2005; Kuller et al. 2008; Vidt 2006). Recent evidence suggests that muscle mitochondrial dysfunction and increased fatigability can occur independent of changes to muscle size and strength demonstrating that muscle weakness and fatigue have distinct etiologies (VanderVeen et al. 2018; Brown et al. 2017). IL-6 signaling through the membrane gp130 receptor has been implicated as a regulator of skeletal muscle mass and metabolic homeostasis during both physiological and pathological conditions (Carson and Baltgalvis 2010; Bonetto et al. 2011; Hardee, Counts, et al. 2018; Gao et al. 2017; Puppa, Gao, et al. 2014). Furthermore, the mitochondria have emerged as an intriguing target for inflammation induced skeletal muscle metabolic dysfunction (Boland, Chourasia, and Macleod 2013; Brown et al. 2017; Hardee et al. 2016; Carson, Hardee, and VanderVeen 2016). We have previously shown that elevated levels of circulating IL-6 was sufficient to decrease mitochondrial protein expression in tumor-free mice (Puppa et al. 2012); however, whether this occurs directly through the muscle gp130 receptor to increase muscle fatigue was not been examined. Furthermore, the muscle gp130 receptor has

recently been shown to play a role in skeletal muscle mitochondrial quality control; however, the effects of IL-6 and gp130 signaling on skeletal muscle fatigue has not been examined.

Both systemic inflammation and muscle inflammatory signaling have been extensively examined for their regulation of muscle wasting with cancer (Tisdale 2002; Evans et al. 2008; Carson and Baltgalvis 2010; VanderVeen, Fix, and Carson 2017; Argiles et al. 2009; Argiles 2014; Deans and Wigmore 2005; Sandri 2008; Onesti and Guttridge 2014). Chronic inflammation has been undoubtably linked to disrupted muscle protein turnover and oxidative metabolism, which are both integral to the pathology of muscle mass loss during cachexia progression (White, Baltgalvis, et al. 2011; Carson, Hardee, and VanderVeen 2016; Argiles et al. 2009; White, Baynes, et al. 2011; Deans and Wigmore 2005; Seto, Kandarian, and Jackman 2015; Cannon TY 2007; Onesti and Guttridge 2014; Fearon, Glass, and Guttridge 2012). Systemic overexpression of IL-6 in the MIN mouse is sufficient to accelerate the cachectic phenotype, while IL-6 null MIN mice had no significant muscle mass loss; however, global manipulation of IL-6 is shown to directly modulate tumor-burden (Baltgalvis et al. 2008). To this end, LLC tumor-bearing gp130 muscle specific knockout (KO) mice demonstrated an attenuation muscle mass loss compared to intact controls, associated with suppressed STAT3 and p38; however, whether gp130 loss improved skeletal muscle function remains unknown (Puppa, Gao, et al. 2014).

Aim 2.1 Experimental Design

The purpose of aim 2.1 was to determine if elevated skeletal muscle gp130 signaling is sufficient to induce skeletal muscle fatigue in tumor-free mice. We

hypothesized that elevating circulating levels of IL-6 would induce fatigue through the activation of skeletal muscle gp130 signaling. To test this hypothesis, male WT and skeletal muscle specific gp130 knockout (skm gp130 KO) mice were electroporated with an IL-6 plasmid to increased plasma IL-6. Control WT and skm gp130 KO mice were given an empty vector. After two weeks of elevated IL-6, several properties of skeletal muscle function were assessed *in situ*.

Aim 2.1 Primary outcomes

Skeletal Muscle Inflammatory Signaling: See aim 1.2

Skeletal Muscle Contractile Properties:

The contractile properties on the TA will be assessed using *in situ* skeletal muscle function analysis. The sciatic nerve was stimulated to elicit a single action potential which subsequently caused a single muscle twitch. Once L_o of the muscle was determined by generating a twitch length-tension curve, the TPT and 1/2 RT were measured and recorded. The muscle was then stimulated with increased frequencies (10-200 hz) to generate a force-frequency curve. The relative increase in force (% of maximal tetanic force) was calculated. Lastly, the rate of muscle rise and relaxation from maximal tension (+dP/dt and -dP/dt, respectively) was calculated from a 200 hz stimulation.

Skeletal Muscle Force Production:

Skeletal muscle's force production capacity was measured in the TA using *in situ* skeletal muscle function analysis. P_o was recorded as the greatest absolute force (millinewtons) of the muscle at L_o generated during a force-frequency curve. $_sP_o$ was assessed by dividing the P_o by muscle CSA. Muscle CSA was calculated by muscle

mass/(L_f x 1.06), where L_f represents the fiber length determined by multiplying the L_o by 0.6, the predetermined TA muscle length to fiber length ratio, and 1.06 represents the skeletal muscle density (Brooks and Faulkner 1988).

Skeletal Muscle Fatigability:

Skeletal muscle's fatigue properties were measured in the TA using *in situ* skeletal muscle function analysis. The TA was rested for 5-minutes at L_o before being subjected to an intermittent fatigue protocol. The TA was subjected to a 5-minute submaximal fatigue protocol consisting of a 0.5-second-long contraction (50 hz) every second. After completion of the submaximal fatigue protocol, the TA was subjected to an additional 5-minute maximal fatigue protocol consisting of a 0.5-second-long contraction (200 hz) every second. The force production of the TA was measured at each contraction. Fatigue was determined by the calculating the relative force production (% of the initial, time 0, contraction) of the TA throughout the duration of each fatigue protocol. The two protocols were analyzed separately. A significantly lower relative force production was classified as an increase in submaximal and/or maximal muscle fatigability.

Aim 2.1 Statistical analysis

Determining Statistical Significance:

Given the purpose and hypothesis of the study was to determine if elevated skeletal muscle gp130 signaling was sufficient to induce skeletal muscle fatigue in tumor-free mice, 4 groups of mice were used, WT Vector or IL-6, and skm gp130 KO Vector or IL-6. Initially, a Bartlett's test was performed to determine if there is a statistical difference in the groups SD. If there was no significant difference in groups SD a standard two-way

ANOVA was performed to appropriately test for significant differences between treatments and genotypes. If an interaction was observed, a Tukey's multiple comparison was performed to determine changes within a treatment and/or genotype. All statistical analysis was performed using GraphPad Prism 7. Values are presented as means plus / minus SEM (standard error of the mean). Significance will be set at $p<0.05$.

Power analysis:

A power analysis was performed to determine the sample size needed to observe statistical significance using a two-way ANOVA. Power (1-β) was set to 0.8 and error of probability (α) was set at 0.05. Based on previously published results and our preliminary data, to achieve significance difference between groups for an estimated effect size of 1.2, a sample size of 9 is needed for each group.

Aim 2.2 Experimental Design

The purpose of Aim 2.2 was to determine the effect of elevated skeletal muscle gp130 signaling on skeletal muscle oxidative and glycolytic metabolism. We hypothesized that elevating circulating levels of IL-6 would induce mitochondrial dysfunction through the activation of skeletal muscle gp130 signaling. To test this hypothesis, male WT and skm gp130 KO mice were electroporated with an IL-6 plasmid to increased plasma IL-6. Control WT and skm gp130 KO mice were given an empty vector. After two weeks of elevated L-6, the TA was analyzed for several indices of mitochondrial content, quality, and function.

Aim 2.2 Primary outcomes

Respiratory Control Ratio:

Mitochondrial respiration was measured polarographically in a respiration chamber (Hansatech Instruments) maintained at 37°C as previously described (Kwon et al. 2015). A randomly selected cohort of mice from each treatment group were used for analysis of mitochondrial function. A 7-10 mg piece of TA muscle was mechanically tweezed with forceps under a dissecting microscope in ice-cold *buffer X* (60 mM K-MES, 35 mM KCl, 7.23 mM K2EGTA, 2.77 mM CaK2EGTA, 20 mM imidazole, 0.5 mM DTT, 20 mM taurine, 5.7 mM ATP, 15 mM phosphocreatine, and 6.56 mM MgCl2, pH 7.1). The fiber bundle was then incubated in 50uM saponin for 30 minutes and washed 3 times for 5 minutes in respiration buffer (105mM K-MES, 3mM KCl, 1mM EGTA, 10mM K2HPO4, 5mM MgCl2, 0.005mM Glutamate, 0.002mM Malate, 0.05% BSA, 20mM Creatine, pH 7.1). Fiber bundles were then placed into the oxygraph machine in 20mM creatine respiration buffer at 37 degrees and provided with 5mM of pyruvate and 2mM of malate. Two minutes following pyruvate and malate, 0.25mM of ADP was injected into the chamber to induce STATE 3 respiration for a duration of 5 minutes. 10ug/mL of Oligomycin was then injected to induce steady state 4 respiration for a duration of 10 minutes. Respiratory Control Ratio (RCR) was calculated by dividing state 3 by state 4 respirations.

Mitochondrial Content and Quality Control:

The distal TA was sectioned to examine succinate dehydrogenase (SDH) enzyme activity histologically. Thresholds corresponding to high SDH enzyme activity will set manually and uniformly across all images, and myofibers will be classified as having high

or low SDH enzyme activities. All muscle regions were included in analysis, and the percentage of high SDH enzyme activity myofibers is expressed as the percentage per total number of myofibers.

See aim 1.3 for gene expression.

Aim 2.2 Statistical analysis

Determining Statistical Significance: See aim 2.1 and 1.3

Power analysis: See aim 2.1

Aim 2.3 Experimental Design

The purpose of aim 2.3 was to determine the role of skeletal muscle gp130 signaling in cancer induced skeletal muscle fatigue in MIN mice. We hypothesized that loss of muscle gp130 signaling would attenuate the skeletal muscle fatigue progression in MIN mice that have initiated cachexia. To test this hypothesis, skeletal muscle specific (HSA cre/+) gp130 inducible knock out (iKO) mice will be crossed with MIN mice to produce the MIN iKO. Floxed gp130 wildtype and MIN mice will serve as their respective controls. All groups will be administered tamoxifen for 5 days at 12 weeks of age. Following a 1-week washout period the mice will be tracked and monitored for 4 weeks. At ~17 weeks of age, the functional properties of skeletal muscle will be assessed *in situ*.

Aim 2.3 Primary outcomes

Skeletal Muscle Inflammatory Signaling: See aim 1.2

Skeletal Muscle Contractile Properties: See aim 1.1

Skeletal Muscle Force Production: See aim 1.1

Skeletal Muscle Fatigability: See aim 2.1

Respiratory Control Ratio: See aim 2.2

Mitochondrial Content and Quality Control: See aim 2.2

Aim 2.2 Statistical analysis

Determining Statistical Significance: See aim 2.1

Power analysis: See aim 2.1

Specific Aim 2 Research Methods

Animals

For experiments in aims 2.1 and 2.2, male mice on a C57BL/6 background were bred with gp130$^{fl/fl}$ mice provided by Dr. Colin Stewart's laboratory [Laboratory of Cancer and Developmental Biology, National Cancer Institute, U.S. National Institutes of Health (NIH), Frederick, MD, USA] in collaboration with Dr. Lothar Hennighausen (Laboratory of Genetics and Physiology, National Institute of Diabetes and Digestive and Kidney Diseases, NIH, Bethesda, MD, USA). gp130$^{fl/fl}$ male mice were bred with Cre-expressing mice driven by myosin light chain (MLC), from Dr. Steven Burden (New York University, New York, NY, USA). The resulting fl/fl cre/+ (KO) mice have a skeletal muscle deletion of gp130. Offspring were genotyped by using tail snips to obtain Cre recombinase (forward, 5′-AGCCCTGACCCTTTAGATTCCATTT-3′, and reverse, 5′-AAAACGCCTGGCGATCCCTGAAC-3′; and wild type 5′-GCGGGCTTCTTCACGTCTTTCTTT-3′) and floxed gp130 (forward, 5′-

ACGTCACAGAGCTGAGTGATGCAC-3′, and reverse, 5′-GGCTTTTCCTCTGGTTCTTG-3′).

For experiments in aims 2.3, gp130$^{fl/fl}$ mice were crossed with inducible Cre-expressing mice driven by human alpha skeletal actin (HSAcre/+) to develop an inducible gp130 KO mouse (iKO). Simultaneously, gp130$^{fl/fl}$ mice were crossed with MIN to produce a gp130 $^{fl/fl}$ MIN (gp130 $^{fl/fl}$ MIN). The resulting gp130 iKO and gp130$^{fl/fl}$ MIN were crossed to obtain an iKO-MIN mouse. Offspring were genotyped by using tail snips.

All animals were group housed and kept on a 12:12-h light-dark cycle. Body weights were measured weekly, and animals were monitored for signs of distress. Animals were given food and water *ad libitum* throughout the duration of the study. All animals were fasted 5 hours prior to tissue collection. Mice were anesthetized with a ketamine-xylazine-acepromazine cocktail, and hindlimb muscles and select organs were carefully dissected and snap frozen in liquid nitrogen and stored at -80ºC until further analysis. All animal experiments were approved by the University of South Carolina's Institutional Animal Care and Use Committee.

IL-6 Overexpression

in vivo intramuscular electroporation of an IL-6 plasmid was used to increase circulating IL-6 levels in mice as previously described. The quadriceps muscle was used as a vessel to produce IL-6 and secrete it into circulation and was not used for any analyses in the study. The TA muscle used in the study was not subjected to electroporation. Briefly, mice were injected with 50 μg of the IL-6 plasmid driven by the CMV promoter, or empty control vector, into the quadriceps muscle. Mice were anesthetized with a 2% mixture of

isoflurane and oxygen (2 l/min). The leg was shaved, and a small incision was made over the quadriceps muscle. Fat was dissected away from the muscle, and the plasmids were injected in a 50-µl volume of phosphate-buffered saline (PBS). A series of eight 50-ms, 100-V pulses was used to promote uptake of the plasmid into myofibers, and then the incision was closed with a wound clip. Both vector control and IL-6 groups received the appropriate plasmid starting at 10 weeks of age. Mice were euthanized after 2 weeks after IL-6 overexpression.

Analysis of Muscle Function

At ~12 weeks of age, mice were anesthetized with 2% isoflurane inhalation and kept anesthetized at 1.5 % isoflurane for ~1hr throughout the duration of the procedure (~1 hour). Muscle function analysis of the TA *in situ*, which maintains the host nerve and blood supply, has been previously described. Briefly, the distal tendon of the left TA was isolated and tied to a force transducer (Aurora Scientific, Ontario, Canada) using 5-0 silk sutures. The mouse was place on the apparatus maintained at 37ºC throughout the entirety of the procedure. The sciatic nerve was exposed proximal to the knee and maintained using warmed mineral oil. The sciatic nerve was then subjected to a single stimulus to determine the optimal length (L_o). Once L_o was obtained, a force-frequency curve was generated, and maximal tetanic force was determined. After a 5-minute rest the TA was subjected to an intermittent fatigue protocol consisting of 0.5 second submaximal stimulation (50Hz) every second for 5 minutes. After submaximal fatigue the TA was subjected to an intermittent fatigue protocol consisting of 0.5 second maximal stimulation (200Hz) every second for 5 minutes. Specific tension was determined using TA muscle CSA calculated by muscle mass/(L_f x 1.06), where L_f represents fiber length determined by multiplying L_o

by 0.6, the predetermined TA muscle length to fiber length ratio, and 1.06 represents the skeletal muscle density.

Immunohistochemistry for myosin heavy chain IIA, IIX, and IIB

Immunohistochemistry for myosin heavy chain (MHC) type IIa, IIx, and IIb was performed as previously described (Goodman et al. 2012). Transverse muscle sections (8μm) of the TA were blocked in 10% IgG Fab (Jackson Immunology) in PBS (5% BSA + 5% Triton X100) for 1 h at room temperature and then incubated overnight at 4°C with primary antibodies [mouse IgG1 monoclonal anti-type IIa MHC (clone SC-71; 1:100) and mouse IgM monoclonal anti-type IIb MHC (clone BF-F3, 1:10). All MHC antibodies were obtained from the Developmental Studies Hybridoma Bank (University of Iowa, Iowa City, IA). Secondary antibodies (biotinylated anti-mouse IgG FITC, IgM AMCA; Thermo Fischer) were incubated with the sections for 1 hour at RT. Slides were air dried and covered in glycerol mounting medium containing DABCO and coverslipped. At least 8 random, non-overlapping digital images at 20X magnification were taken, and fibers stained positive or absent for MHC type IIa, IIx, and IIb were tabulated using imaging software (ImageJ; NIH). The analyses were performed by an investigator blinded to the treatment groups.

Western blot analysis

Western blot analysis was performed as described previously. Briefly, the right proximal TA was homogenized, and protein concentration was determined using the standard Bradford protein assay. Homogenates were fractionated on 7-10% SDS-polyacrylamide gels and transferred to a polyvinylidene difluoride membrane. Primary antibodies for gp130 (Santa Cruz) and phosphorylated (p) and total (t) STAT3 (Cell

Signaling Technology) were incubated 1:1000 overnight at 4ºC in 5% TBST milk. Anti-rabbit IgG-conjugated secondary antibodies (cell signaling) were incubated 1:2000 for 1 hour at room temperature in 5% TBST milk. Enhanced Chemiluminescence was used to visualize antibody-antigen interaction and captured using the Syngene: G-Box. Blots were analyzed by determining the integrated optical density of each band using ImageJ (NIH software).

Cytochrome C Oxidase Activity

EDL muscle samples were homogenized in extraction buffer (0.1 M KH2P04/Na2HP04, 2 mM EDTA, pH 7.2). Cytochrome-c oxidase (COX) activity was determined by measuring the rate of oxidation of fully reduced cytochrome c at 550nm using (CYTOCOX1) Sigma Aldrich Kit and spectrophotometer (Eppendorf).

Respiratory Control Ratio

Mitochondrial respiration was measured polarographically in a respiration chamber (Hansatech Instruments) maintained at 37°C as previously described (Kwon et al. 2015). A randomly selected cohort of mice from each treatment group were used for analysis of mitochondrial function. A 7-10 mg piece of TA muscle was mechanically tweezed with forceps under a dissecting microscope in ice-cold *buffer X* (60 mM K-MES, 35 mM KCl, 7.23 mM K2EGTA, 2.77 mM CaK2EGTA, 20 mM imidazole, 0.5 mM DTT, 20 mM taurine, 5.7 mM ATP, 15 mM phosphocreatine, and 6.56 mM MgCl2, pH 7.1). The fiber bundle was then incubated in 50uM saponin for 30 minutes and washed 3 times for 5 minutes in respiration buffer (105mM K-MES, 3mM KCl, 1mM EGTA, 10mM K2HPO4, 5mM MgCl2, 0.005mM Glutamate, 0.002mM Malate, 0.05% BSA, 20mM Creatine, pH 7.1). Fiber bundles were then placed into the oxygraph machine in 20mM creatine

respiration buffer at 37 degrees and provided with 5mM of pyruvate and 2mM of malate. Two minutes following pyruvate and malate, 0.25mM of ADP was injected into the chamber to induce STATE 3 respiration for a duration of 5 minutes. 10ug/mL of Oligomycin was then injected to induce steady state 4 respiration for a duration of 10 minutes. Respiratory Control Ratio (RCR) was calculated by dividing state 3 by state 4 respirations.

Statistical analysis

Values are presented as means plus / minus standard error of the mean (SEM). A Bartlett's test was used to determine significantly different standard deviations ($p<0.05$). A Two-Way ANOVA was used to determine a difference between treatment and genotype. If a statistical interaction was observed, a Tukey's multiple comparison's test was performed to determine specific differences. Significance was set at $p<0.05$.

Specific Aim 3. Determine the role of muscle use on skeletal muscle fatigue during cachexia progression.

Premise

Cancer patients with decreased functional ability and increased fatigue, regardless of cachexia diagnosis, experience decreased quality of life and a poorer prognosis (O'Gorman, McMillan, and McArdle 1999; al-Majid and McCarthy 2001a). Fatigue is the most frequently reported symptom by cancer patients (al-Majid and McCarthy 2001a). Cancer patients and preclinical cachexia models exhibit decreased volitional activity and increased fatigue that precedes significant weight loss (Baltgalvis 2010; Murphy et al. 2012; Roberts, Frye, et al. 2013; Toth et al. 2016; Puppa, Gao, et al. 2014). We have

previously demonstrated that the MIN mouse continues normal growth and development up to 16 weeks of age where body weight begins to plateau. At 18 weeks of age there is evidence of significant body weight loss (~5-10%) that continues for 2-4 weeks (~20%). Interestingly, reductions in wheel activity, most notably max velocity, is reduced at 15 weeks of age and steadily declines until they are near completely sedentary at 18 weeks (Baltgalvis 2010). Additionally, we have reported that 8 weeks of endurance exercise training prevented IL-6 induced muscle wasting in MIN mice; however, these results were associated with significant reductions in tumor-burden. Lastly, we have reported that 2 weeks, 7 sessions, of repeated eccentric muscle contractions could attenuate muscle mass loss associated with improve SDH activity without affecting tumor burden in mice that initiated cachexia (~7% BW loss) (Hardee et al. 2016). Collectively, these results demonstrate that physical activity and skeletal muscle use can modulate cachexia progression; however, whether this modulation affects cancer-induced skeletal muscle dysfunction has not been established.

Aim 3.1 Experimental Design

The purpose of aim 3.1 was to determine the relationship between volitional activity and skeletal muscle fatigue during the progression of cachexia. We hypothesized that skeletal muscle fatigue occurs prior to significant body weight loss which would be directly related to reduced physical activity. To test this hypothesis, WT and MIN mice were monitored for daily cage activity at starting 12 weeks of age, when tumor-burden is set, and tracked for 5 weeks (Allen et al. 2001). MIN mice were further stratified into 2 groups

corresponding with high and low activity. At 17 weeks of age, the functional properties of skeletal muscle were assessed *in situ*.

Aim 3.1 Primary outcomes

Voluntary Cage Activity:

From 12-17 weeks of age, mice were single-housed and placed in activity monitor cages (Opto-M3 Activity Meter, Columbus Instruments). Activity was measured for 12 hours during the dark cycle (7PM–7AM) and 12 hours during the day cycle (7AM–7PM); the number of beams crossed in an X–Y plane was recorded for two consecutive nights. Food consumption was also recorded during this time while the mice were single-housed.

Skeletal Muscle Contractile Properties: See aim 1.1

Skeletal Muscle Force Production: See aim 1.1

Skeletal Muscle Fatigability: See aim 2.1

Indices of Cachexia: See aim 1.1

Relationship Between Indices of Cachexia and Skeletal Muscle Function:

Pearson's correlations and stepwise linear regression models were performed analyzing the cachexia indices (BW, BW Loss, muscle mass, plasma IL-6, and muscle inflammatory signaling) as well as physical activity levels as the independent variable and the properties of skeletal muscle function (1/2 RT, TPT, +dP/dt, -dP/dt, P_o, $_sP_o$, and fatigue) as the dependent variable.

Aim 3.1 Statistical analysis

Determining Statistical Significance:

Given the purpose of this study was to determine the relationship between volitional activity and skeletal muscle fatigue during the progression of cachexia, mice will be separated into 3 groups for statistical analysis, WT, MIN Low Activity (MIN-LA), and MIN High Activity (MIN-HA). Initially, a Bartlett's test was performed to determine if there was a statistical difference in the groups SD. If there was no significant difference in groups SD a one-way ANOVA assuming Gaussian distribution was performed to appropriately test for significant differences in our primary outcomes between the 3 groups. If a significant difference in group SD was observed, a Kruskal-Wallis test was performed to appropriately test for significant differences in our primary outcomes between the 3 groups. A Pearson's correlation was used to determine correlations between volitional activity and skeletal muscle function properties in MIN mice. All statistical analysis was performed using GraphPad Prism 7. Values are presented as means plus / minus SEM (standard error of the mean). Significance will be set at $p<0.05$.

Power analysis:

A power analysis was performed to determine the sample size needed to observe statistical significance using a one-way ANOVA. Power (1-β) was set to 0.8 and error of probability (α) was set at 0.05. Based on previously published results, to achieve significance for an estimated 15 ± 5 % difference between groups, a sample size of 9 is needed for each group.

Aim 3.2 Experimental Design

The purpose of aim 3.2 was to determine if 5 weeks of free access to a wheel prior to significant body weight loss can prevent the induction of skeletal muscle fatigue in MIN mice. We hypothesized that increased volitional activity would delay the onset of skeletal muscle fatigue in MIN mice. As previously described, reduced volitional activity presents as early as 3 weeks prior to significant body weight loss (Baltgalvis 2010). To test our hypothesis, WT and MIN mice were given free access to a wheel at 12 weeks of age and monitored until 17 weeks of age. After 5 weeks of free access to wheels, the functional properties of skeletal muscle will be assessed *in situ*.

Aim 3.2 Primary outcomes

Voluntary Wheel Activity: See aim 3.1

Skeletal Muscle Contractile Properties: See aim 1.1

Skeletal Muscle Force Production: See aim 1.1

Skeletal Muscle Fatigability: See aim 2.1

Indices of Cachexia: See aim 1.1

Relationship Between Indices of Cachexia and Skeletal Muscle Function:

Pearson's correlations and stepwise linear regression models were performed analyzing the cachexia indices (BW, % BW Loss, muscle mass, plasma IL-6, and muscle inflammatory signaling) as well as physical activity levels as the independent variable and the properties of skeletal muscle function (1/2 RT, TPT, +dP/dt, -dP/dt, P_o, $_sP_o$, and fatigue) as the dependent variable.

Aim 3.2 Statistical analysis

Determining Statistical Significance:

Given the purpose and hypothesis of the study was to determine if 5 weeks of free access to wheels prior to significant body weight loss can prevent the induction of skeletal muscle fatigue in MIN mice, mice were separated into 4 groups for statistical analysis, WT Control (WT-C), WT Wheel Access (WT-WA), MIN Control (MIN-C), MIN Wheel Access (MIN-WA). Initially, a Bartlett's test was performed to determine if there was a statistical difference in the groups SD. If there was no significant difference in groups SD a two-way ANOVA assuming Gaussian distribution was performed to appropriately test for significant differences in our primary outcomes between the 4 groups. If a significant difference in group SD was observed, a Kruskal-Wallis test was performed to appropriately test for significant differences in our primary outcomes between the 4 groups. A Pearson's correlation was used to determine correlations between volitional activity and skeletal muscle function properties in MIN mice. All statistical analysis was performed using GraphPad Prism 7. Values will be presented as means plus / minus SEM (standard error of the mean). Significance will be set at $p<0.05$.

Power analysis:

A power analysis was performed to determine the sample size needed to observe statistical significance using a two-way ANOVA. Power (1-β) was set to 0.8 and error of probability (α) was set at 0.05. Based on previously published results, to achieve significance for an estimated 15 ± 5 % difference between groups, a sample size of 9 is needed for each group.

Aim 3.3 Experimental Design

The purpose of aim 3.3 was to determine if 5 weeks of free access to a wheel prior to significant body weight loss would prevent the reduction in skeletal muscle oxidative metabolism in MIN mice. We hypothesized that increased volitional activity would delay the reduction in skeletal muscle oxidative metabolism in MIN mice. As previously described, reduced volitional activity presents as early as 3 weeks prior to significant body weight loss (Baltgalvis 2010). To test our hypothesis, WT and MIN mice were given free access to a wheel at 12 weeks of age and monitored until 17 weeks of age. At 17 weeks of age the oxidative capacity of skeletal muscle was assessed using respiratory control ratio.

Aim 3.3 Primary outcomes

Voluntary Wheel Activity: See aim 3.1

Skeletal Muscle Contractile Properties: See aim 1.1

Skeletal Muscle Force Production: See aim 1.1

Skeletal Muscle Fatigability: See aim 2.1

Respiratory Control Ratio: See aim 2.2

Relationship Between Skeletal Muscle Oxidative Metabolism and Skeletal Muscle Function: See aim 1.3

Aim 3.3 Statistical analysis

Determining Statistical Significance: See aim 3.2

Power analysis: See aim 3.2

Specific Aim 3 Research Methods

Animals

Male WT and MIN mice were purchased from Jackson Laboratories and were bred at the University of South Carolina's Animal Resources Facility. All animals were group housed and kept on a 12:12-h light-dark cycle. Body weights were measured weekly, and animals were monitored for signs of distress. Animals were given food and water *ad libitum* throughout the duration of the study. All animals were fasted 5 hours prior to tissue collection. Mice were anesthetized with a ketamine-xylazine-acepromazine cocktail, and hindlimb muscles and select organs were carefully dissected and snap frozen in liquid nitrogen and stored at -80ºC until further analysis. All animal experiments were approved by the University of South Carolina's Institutional Animal Care and Use Committee.

Voluntary Wheel Running

Voluntary wheel running was used as a marker of volitional physical activity and was performed as previously described (Baltgalvis 2010). At 12 wk of age, WT and MIN mice were housed individually in cages with 9.5-in.-diameter stainless steel activity wheels (MiniMitter, Bend, OR). Running activity was monitored daily from 12 to 17 weeks of age. Bicycle computers (Specialized, Morgan Hill, CA) with magnetic sensors measured average speed, distance, time, and maximum speed, and the data were recorded daily. Mice were separated into 4 groups for statistical analysis, WT-C, WT-WA, MIN-C, and MIN-WA.

Analysis of Muscle Function

At ~17 weeks of age, mice were anesthetized with 2% isoflurane inhalation and kept anesthetized at 1.5 % isoflurane for ~1hr throughout the duration of the procedure (~1 hour). Muscle function analysis of the TA *in situ*, which maintains the host nerve and blood supply, has been previously described. Briefly, the distal tendon of the left TA was isolated and tied to a force transducer (Aurora Scientific, Ontario, Canada) using 5-0 silk sutures. The mouse was place on the apparatus maintained at 37ºC throughout the entirety of the procedure. The sciatic nerve was exposed proximal to the knee and maintained using warmed mineral oil. The sciatic nerve was then subjected to a single stimulus to determine L_o. Once L_o was obtained, a force-frequency curve was generated, and maximal tetanic force was determined. After a 5-minute rest the TA was subjected to an intermittent fatigue protocol consisting of 0.5 second submaximal stimulation (50Hz) every second for 5 minutes. After submaximal fatigue the TA was subjected to an intermittent fatigue protocol consisting of 0.5 second maximal stimulation (200Hz) every second for 5 minutes. Specific tension was determined using TA muscle CSA calculated by muscle mass/(L_f x 1.06), where L_f represents fiber length determined by multiplying L_o by 0.6, the predetermined TA muscle length to fiber length ratio, and 1.06 represents the skeletal muscle density.

Western blot analysis

Western blot analysis was performed as described previously (Puppa, Gao, et al. 2014). Briefly, the right proximal TA was homogenized, and protein concentration was determined using the standard Bradford protein assay. Homogenates were fractionated on 7-10% SDS-polyacrylamide gels and transferred to a polyvinylidene difluoride membrane.

Primary antibodies for phosphorylated (p) and total (t) P65, STAT3, P38, and Erk1/2 (Cell Signaling Technology) were incubated 1:1000 overnight at 4ºC in 5% TBST milk. Anti-rabbit IgG-conjugated secondary antibodies (cell signaling) were incubated 1:2000 for 1 hour at room temperature in 5% TBST milk. Enhanced Chemiluminescence was used to visualize antibody-antigen interaction and captured using the Syngene: G-Box. Blots were analyzed by determining the integrated optical density of each band using ImageJ (NIH software).

RNA isolation and RT-PCR

RNA isolation, cDNA synthesis, and real-time PCR were performed as previously described (Narsale et al. 2016) using reagents from Applied Biosystems (Foster City, CA, USA). Primers for GAPDH, IL-6, IL-1β, TNF-α, SOCS3, PGC1, FIS1, MFN 1 and 2, Hexokinase II, and Phophofructokinase will purchased from IDT (Coralville, Iowa, USA) and run using SYBR green PCR buffer (Narsale et al. 2016). Data were analyzed using the $2^{-\Delta\Delta CT}$ method.

Cytochrome C Oxidase Activity

EDL muscle samples were homogenized in extraction buffer (0.1 M KH2P04/Na2HP04, 2 mM EDTA, pH 7.2). Cytochrome-c oxidase (COX) activity was determined by measuring the rate of oxidation of fully reduced cytochrome c at 550nm using (CYTOCOX1) Sigma Aldrich Kit and spectrophotometer (Eppendorf) (Iqbal and Hood 2015).

Respiratory Control Ratio

Mitochondrial respiration was measured polarographically in a respiration chamber (Hansatech Instruments) maintained at 37°C as previously described (Kwon et al. 2015). A randomly selected cohort of 4 mice from each treatment group were used for analysis of mitochondrial function. A 7-10 mg piece of TA muscle was mechanically tweezed with forceps under a dissecting microscope in ice-cold *buffer X* (60 mM K-MES, 35 mM KCl, 7.23 mM K2EGTA, 2.77 mM CaK2EGTA, 20 mM imidazole, 0.5 mM DTT, 20 mM taurine, 5.7 mM ATP, 15 mM phosphocreatine, and 6.56 mM MgCl2, pH 7.1). The fiber bundle was then incubated in 50uM saponin for 30 minutes and washed 3 times for 5 minutes in respiration buffer (105mM K-MES, 3mM KCl, 1mM EGTA, 10mM K2HPO4, 5mM MgCl2, 0.005mM Glutamate, 0.002mM Malate, 0.05% BSA, 20mM Creatine, pH 7.1). Fiber bundles were then placed into the oxygraph machine in 20mM creatine respiration buffer at 37 degrees and provided with 5mM of pyruvate and 2mM of malate. Two minutes following pyruvate and malate, 0.25mM of ADP was injected into the chamber to induce STATE 3 respiration for a duration of 5 minutes. 10ug/mL of Oligomycin was then injected to induce steady state 4 respiration for a duration of 10 minutes. RCR was calculated by dividing state 3 by state 4 respirations.

Statistical analysis

Values are presented as means ± standard error of the mean (SEM). Student t-tests were performed to determine differences between genotypes. A one-way ANOVA was used to determine differences in muscle function and inflammatory signaling when MIN mice were stratified by age or body weight loss. Post hoc analyses were performed with

student Newman-Keuls methods. A Bartlett's test was used to determine significantly different standard deviations ($p<0.05$). If a significant difference was observed between group standard deviations, a non-parametric Kruskal-Wallis one-way ANOVA was used. A Pearson correlation was used to determine correlations between inflammatory genes and proteins with muscle function properties in MIN mice. Stepwise linear regression models were used to identify predictors (cachexia indices and activity) of the 8 measured outcomes related to skeletal muscle function. Significance was set at $p<0.05$.

APPENDIX C

RAW DATA

Table C.1. Characteristic data of ~20-week-old male MIN and WT mice

	Peak Weight (g)	Final Weight (g)	% loss	Hindlimb mass (mg)	Testes (mg)	Epi Fat (mg)	Spleen (mg)	Tibia Length (mm)
WT	28.3	28.3	0%	219	213	480	65	16.8
	26.4	26.4	0%	205	196	401	52	16.9
	29	29	0%	217	205	467	71	16.7
	27.8	27.8	0%	224	198	335	80	16.8
	24.2	24.2	0%	177	165	329	67	16.55
	25.2	25.2	0%	188	169	358	60	16.85
	27.3	27.1	-1%	207	202	418	66	16.8
	24.5	24.5	0%	192	200	370	59	16.6
	27	27	0%	219	202	455	79	16.95
	27.2	27.2	0%	210	207	346	67	16.95
MIN-WS	25.9	25.3	-2%	189	190	190	594	16.9
	27.8	27.3	-2%	198	220	115	536	16.95
	25.6	25.1	-2%	194	202	214	400	16.9
	25.4	25.4	0%	211	196	267	113	17.0
	26.4	26.4	0%	184	181	167	420	16.8
	30.1	30.1	0%	223	180	274	119	16.9
	27.7	27.7	0%	207	192	257	504	17
MIN-CX	24.6	19.5	-21%	149	158	0	442	16.8
	23.3	18.4	-21%	104	58	0	406	16.9
	22.4	19.3	-14%	127	142	0	479	16.7
	26.5	22.1	-17%	163	158	0	521	17.05
	24.3	20.1	-17%	153	169	0	518	16.9
	24.5	20.5	-16%	120	109	0	316	16.9
	23.7	19	-20%	107	94	0	434	16.55
	23.5	19.4	-17%	129	105	0	490	16.85
	24.5	19.3	-21%	89	72	0	472	16.65

Table C.2 Indices of cachexia in MIN mice

	Plasma IL-6 (pg/ml)	TA Weight (mg)	p/t STAT3	p/t P65	p/t ERK 1/2	p/t P38
WT	ND	47	0.21	1.17	0.40	0.45
	ND	44	0.58	0.73	1.11	1.09
	ND	43	1.36	0.71	0.57	0.87
	ND	41	1.45	1.00	0.40	1.99
	ND	43	1.57	1.01	1.34	1.34
	ND	41	1.03	1.05	1.03	0.69
	ND	28	0.86	0.98	1.07	0.84
	ND	47	0.96	1.36	2.09	0.74
	ND	46	0.21	1.17	0.40	0.45
	ND	50	0.58	0.73	1.11	1.09
MIN-WS	42.99	38	0.50	0.66	0.76	0.26
	41.01	44	0.27	1.14	0.82	0.37
	18.09	42	0.36	0.91	0.90	1.09
	ND	43	1.79	0.97	0.52	1.11
	ND	37	1.60	1.60	0.35	1.97
	ND	47	0.24	0.97	1.08	1.12
	ND	47	0.65	1.13	0.87	0.71
MIN-CX	ND	31	0.78	1.32	0.72	0.68
	ND	20	13.96	1.89	2.72	1.94
	ND	27	16.93	1.38	3.18	1.89
	32.98	36	16.22	0.97	1.78	1.73
	31.15	33	7.47	1.79	0.34	1.43
	355.25	27	16.86	1.60	0.89	2.00
	936.36	25	18.81	2.56	0.79	2.35
	65.78	29	44.00	1.04	14.15	2.54
	50.99	21	7.59	1.69	2.02	2.59

Table C.3 Indices of cachexia in MIN mice

	IL-6 mRNA	SOCS3 mRNA	IL-1β mRNA	TNF-α mRNA	COX Activity
WT	0.89	0.74	0.63	0.82	5.38
	0.86	0.82	0.92	1.04	3.07
	1.01	0.57	0.82	1.17	4.05
	1.26	1.88	1.44	1.43	4.96
	0.50	1.68	1.73	1.09	4.53
	0.68	0.83	0.74	0.82	4.85
	1.01	1.00	1.17	0.91	5.83
	1.06	0.76	0.81	0.95	5.23
	1.73	0.73	0.74	0.79	3.99
	0.89	0.74	0.63	0.82	5.38
MIN-WS	1.45	2.14	0.87	0.95	4.37
	1.16	1.77	0.28	0.82	6.51
	0.84	1.43	0.35	0.77	5.18
	1.29	1.25	0.93	0.65	4.68
	0.69	1.46	0.89	0.76	1.46
	0.86	0.70	0.81	0.69	5.33
	1.75	0.45	1.02	1.06	3.69
MIN-CX	57.23	37.09	19.15	1.02	1.80
	2.44	16.31	2.23	0.76	2.31
	7.69	20.79	9.95	0.88	2.85
	1.33	7.58	2.65	1.15	1.77
	1.42	7.13	0.76	1.05	3.64
	1.83	11.58	1.57	0.94	3.53
	6.96	18.10	0.87	1.38	1.18
	0.89	5.63	3.43	1.39	1.27
	2.44	16.03	2.60	1.35	1.73

Table C.4 The effect of cachexia on whole body and muscle specific fatigue

	Time to Fatigue (minutes)
WT	67
	79
	75.5
	72
	81.75
MIN-12	77
	52.25
	75
	56
	63
MIN-WS	45.33
	47.75
	50.5
	43.17
	21.33
MIN-CX	13.33
	13.18
	17.33
	14.67
	8.25
	15
	39.5

Table C.5 The effect of cachexia on whole body and muscle specific fatigue

	Muscle Fatigue (Muscle force @ 90 seconds)
WT	31
	33
	32
	40
	38
	24
	31
	28
	41
	33
MIN-WS	32
	33
	19
	25
	46
	46
	24
MIN-CX	32
	40
	30
	25
	43
	34
	6
	38
	39

Table C.6 The effect of cachexia on whole body and muscle specific fatigue

	0	30	60	90	120	150	180	210	240
	1647	1368	927	591	503	488	423	391	340
	1390	850	650	561	464	407	362	311	271
	1343	1102	687	455	431	398	333	284	247
	1295	1022	776	561	513	490	471	443	421
WT	1420	1172	943	649	546	509	483	458	436
	1368	1141	649	415	331	286	250	228	202
	1711	1347	884	635	533	462	400	354	309
	1315	1045	626	441	364	323	311	282	271
	1506	1272	1021	705	617	584	575	569	546
	1682	1410	887	659	562	543	487	439	370
	1586	1281	1027	719	597	519	469	436	385
	1329	1090	720	532	445	403	369	334	303
MIN-	1372	1152	701	555	416	377	314	264	216
12	1381	1127	775	579	470	408	339	301	265
	1410	1105	961	710	562	495	451	420	400
	1431	1188	622	455	404	366	334	310	273
	1338	1098	660	446	357	302	249	210	174
	1443	1203	461	269	185	125	81	52	36
MIN-	1618	1147	650	405	308	265	215	192	159
WS	1336	1071	878	620	513	484	454	441	419
	1545	1274	870	708	626	519	454	408	368
	1522	1260	573	370	280	212	166	123	95
	738	577	316	235	194	163	156	156	141
	718	536	414	289	246	232	228	211	211
	909	766	362	277	224	200	163	164	146
	972	784	381	245	183	164	120	94	80
MIN-	1157	886	696	498	401	409	386	388	384
CX	772	604	393	262	221	202	190	187	185
	786	574	167	48	50	67	81	93	97
	849	676	438	322	264	229	201	183	172
	591	472	342	233	194	180	170	157	152

Table C.7 The effect of cachexia on maximal tetanic force

	10 hz	30 hz	50 hz	80 hz	100 hz	120 hz	150 hz	180 hz	200 hz	250 hz	300 hz
	268	271	447	1333	1477	1521	1579	1602	1620	1613	1607
	229	271	573	1131	1391	1459	1482	1555	1525	1567	1542
	215	246	553	1146	1262	1333	1324	1329	1349	1352	1312
	325	392	826	1132	1204	1262	1274	1258	1290	1284	1278
WT	342	402	903	1223	1366	1309	1382	1396	1394	1367	1350
	348	406	943	1186	1277	1275	1269	1339	1351	1308	1298
	310	391	820	1172	1404	1554	1619	1650	1652	1648	1599
	263	281	506	1264	1383	1426	1462	1499	1480	1489	1399
	271	295	493	1042	1387	1575	1586	1618	1648	1597	1544
	370	440	952	1388	1513	1589	1642	1638	1678	1677	1600
	331	362	854	1206	1248	1301	1355	1387	1365	1324	1102
	243	270	471	1224	1240	1278	1314	1319	1287	1281	1256
	305	349	657	1156	1319	1353	1343	1376	1388	1383	1362
MIN-	207	232	404	1059	1294	1488	1548	1572	1574	1589	1574
WS	187	201	384	869	1062	1174	1197	1199	1249	1307	1323
	305	294	647	1416	1470	1512	1542	1542	1530	1516	1507
	346	413	964	1322	1475	1494	1518	1539	1545	1459	1400
	224	215	388	558	572	669	644	680	756	696	701
	277	280	561	698	743	765	743	748	735	709	692
	267	290	629	855	899	926	945	942	920	896	868
	345	411	740	879	916	950	962	967	970	944	902
MIN-	280	363	768	980	1102	1157	1182	1188	1187	1166	1117
CX	306	395	583	656	669	698	705	610	474	323	436
	283	382	628	746	781	803	807	799	797	783	764
	294	421	708	854	891	899	895	860	850	835	816
	227	245	473	565	584	581	576	583	584	563	556

Table C.8 The effect of cachexia on specific tetanic force

	10 hz	30 hz	50 hz	80 hz	100 hz	120 hz	150 hz	180 hz	200 hz	250 hz	300 hz
	49	49	81	243	269	277	287	292	295	294	293
	42	50	106	209	257	270	274	288	282	290	285
	41	47	106	220	242	255	254	255	258	259	251
	65	79	166	227	242	254	256	253	259	258	257
WT	65	76	171	232	259	248	262	264	264	259	256
	73	85	197	247	266	266	265	279	282	273	271
	95	120	250	358	429	475	495	504	505	503	489
	48	51	92	230	252	260	266	273	269	271	255
	54	58	97	206	274	311	313	320	326	315	305
	65	77	167	244	266	279	288	288	295	295	281
	72	79	186	263	272	284	295	302	298	289	240
	44	49	85	220	223	230	237	237	232	231	226
	59	68	127	224	256	262	260	267	269	268	264
MIN-	39	44	77	201	245	282	293	298	298	301	298
WS	42	45	85	193	236	261	266	267	278	291	295
	53	52	113	248	258	265	270	270	268	266	264
	62	74	172	236	263	267	271	275	276	261	250
	55	53	95	137	140	164	158	167	186	171	172
	103	104	208	259	276	284	276	277	273	263	257
	82	89	192	261	274	282	288	287	281	273	265
	78	93	167	198	207	214	217	218	219	213	204
MIN-	53	69	145	185	209	219	224	225	225	221	211
CX	93	121	178	200	204	213	215	186	145	99	133
	90	121	199	236	247	254	256	253	253	248	242
	85	122	205	247	258	260	259	249	246	241	236
	87	94	181	216	224	223	221	224	224	216	213

Table C.9 The effect of cachexia on the muscle force rates

	½ RT	TPT	-dP/dt	+dP/dt
	8	17	17876	18391
	8.7	18	16673	19277
	8.8	20	15039	14413
	10.5	21	14096	12748
WT	10.2	21	16609	13051
	12.4	20	14418	11599
	12.1	21	16604	15797
	9.4	17	25174	15538
	7.2	18	23681	30195
	11.2	21	15830	14945
	11	20	15432	13868
	9.2	21	13900	12657
	11.5	18	15070	12414
MIN-	8.6	18	14224	17405
WS	7.6	17	13356	13896
	8.3	19	13920	16166
	11.6	20	18523	11488
	8.4	19	10274	5531
	12.4	19	7218	7411
	10.1	22	12578	8008
	11.7	24	11894	6855
MIN-	15.4	25	9786	12659
CX	12.4	24	10499	4652
	12.8	24	9552	7682
	12.6	23	9268	7655
	11.3	22	5915	4754

Table C.10 The effect of cachexia on calcium handling gene expression

	SERCA1	RyR1	Calsequestrin
WT	1.4	1.0	0.5
	1.2	1.4	1.0
	0.7	0.7	1.9
	0.9	0.9	1.0
	0.8	0.7	1.0
	1.1	0.9	0.8
	0.8	1.0	0.8
	0.8	0.8	1.0
	1.2	1.4	0.9
	0.8	1.1	0.7
MIN-WS	1.3	1.5	1.6
	1.0	1.1	2.3
	1.2	1.6	1.7
	0.8	1.2	1.9
	1.2	1.4	4.0
	1.2	1.0	1.9
	0.9	0.8	1.6
MIN-CX	1.4	1.7	2.2
	1.7	2.0	2.1
	1.5	1.7	4.5
	1.5	1.5	1.4
	0.9	1.1	1.8
	1.8	1.7	1.9
	1.0	1.4	7.6

Table C.11 Characteristic data of male gp130 KO and WT with elevated IL-6

Treatment	Group	Body Weight (g)			Plasma IL-6 (pg/mL)		
		Pre	Mid	Post	Pre	Mid	Sac
Vector	WT	22.3	22.8	23.2	0	0	0
		24.1	24.5	25.2	0	0	0
		22.8	23.6	23.1	0	0	0
		23.8	24.5	24.1	0	0	0
		22.5	24.3	26.1	0	0	0
		20.7	21.5	22.3	0	0	0
		21.9	22.7	23.5	0	0	0
		21.5	22.3	23.1	0	0	0
		22.8	23.6	24.4	0	0	0
		22.2	23.3	24.3	0	0	0
		25.5	26.3	27.1	0	0	0
		26.0	26.5	29.0	0	0	0
		26.0	26.5	27.9	0	0	0
		24.3	25.1	25.9	0	0	0
Vector	KO	23.0	22.8	23.1	0	0	0
		25.3	25.8	26.1	0	0	0
		22.5	23.2	23.8	0	0	0
		24.0	24.1	24.2	0	0	0
		24.8	24.9	25.0	0	0	0
		24.6	24.6	24.5	0	0	0
		24.7	24.9	25.0	0	0	0
		26.6	27.1	27.6	0	0	0
		28.1	27.7	27.2	0	0	0
		24.2	25.3	25.1	0	0	0
		24.0	24.5	25.0	0	0	0
		24.3	24.5	24.7	0	0	0

Table C.12 Characteristic data of male gp130 KO and WT with elevated IL-6

		Body Weight (g)			Plasma IL-6 (pg/mL)		
Treatment	**Group**	**Pre**	**Mid**	**Post**	**Pre**	**Mid**	**Sac**
		24.2	23.6	23.2	0	151.18	125.06
		21.7	21.9	20.2	0	142.28	166.75
		23.3	22.8	22.1	0	64.562	53.253
		24.4	24.6	23.5	0	121.26	90.264
		22.0	22.6	23.2	0	46.777	58.702
		21.0	21.8	22.6	0	26.975	53.95
		22.7	23.5	24.3	0	24.333	58.4
IL-6	WT	21.4	22.2	23.0	0	7.4286	15.6
		21.4	22.2	23.0	0	34.341	99.589
		23.1	23.9	24.7	0	13.778	31.69
		25.4	26.2	27.0	0	98.1	80.29
		27.4	28.2	29.0	0	16.1	94.395
		21.6	22.4	23.2	0	35.52	54.32
		23.7	24.5	25.3	0	31.025	79.775
		24.0	24.8	25.6	0	154.53	371.03
		21.8	22.2	22.9	0	49.525	134.78
		22.9	22.9	23.7	0	67.275	164.78
		24.8	25.0	26.1	0	65.775	154.53
		23.9	23.1	22.3	0	74.895	99.157
		25.7	25.5	25.3	0	87.643	117.1
IL-6	KO	24.0	23.8	23.6	0	218	123.83
		26.6	26.6	26.5	0	63.071	125.89
		22.5	23.1	23.6	0	158.58	204.53
		23.2	24.0	24.8	0	180.5	230.4
		25.2	26.0	26.8	0	65.2	110.5
		20.2	21.0	21.8	0	50.2	90.2

Table C.13 Characteristic data of male gp130 KO and WT with elevated IL-6

		Tissue Weights (mg)				
Treatment	**Group**	**Hindlimb**	**HL/TL**	**Tibia**	**Epi Fat**	**Spleen**
Vector	WT	210.5	12.31	17.10	293	86
		214.5	12.692	16.90	292	78
		189.5	11.28	16.80	292	56
		214.5	12.618	17.00	382	61
		215.5	12.639	17.05	278	72
		181	10.904	16.6	236	54
		187.5	11.194	16.75	349	57
		207	12.176	17.00	295	67
		200.5	12.115	16.55	215	58
		197.5	11.826	16.7	360	76
		224	13.099	17.1	385	80
		230	13.068	17.60	573	91
		206	11.873	17.35	742	69
		215.5	12.676	17.00	376	86
Vector	KO	216	13.051	16.55	228	61
		216	12.857	16.80	297	70
		202	12.169	16.60	377	54
		209	12.59	16.60	312	56
		221.5	13.145	16.85	363	57
		206.5	12.255	16.85	286	66
		217.5	12.946	16.80	292	63
		233	13.626	17.10	392	80
		234.5	13.754	17.05	346	76
		211	12.485	16.90	260	293
		202.5	12.126	16.70	301	150
		199.5	11.875	16.80	244	91

Table C.14 Characteristic data of male gp130 KO and WT with elevated IL-6

		Tissue Weights (mg)				
Treatment	**Group**	**Hindlimb**	**HL/TL**	**Tibia**	**Epi Fat**	**Spleen**
IL-6	WT	204.5	12.136	16.85	314	161
		170.5	10.333	16.50	212	141
		204	12.179	16.75	262	138
		211	12.522	16.85	331	147
		204.5	12.173	16.80	270	125
		191	11.541	16.55	200	94
		204.5	12.029	17	124	122
		194	11.652	16.65	362	73
		186.5	11.201	16.65	359	122
		196	11.737	16.7	385	98
		205	12.202	16.80	374	143
		222.5	13.012	17.10	497	130
		184	11.018	16.7	314	93
		211.5	12.703	16.65	257	92
		216.5	12.887	16.80	434	152
IL-6	KO	195.5	11.813	16.55	270	90
		193	11.592	16.65	202	108
		216	12.706	17.00	261	272
		204	11.965	17.05	238	136
		223	13.195	16.90	346	123
		211.5	12.627	16.75	272	258
		222.5	13.166	16.90	499	133
		193.5	11.518	16.80	299	178
		199.5	12.018	16.60	249	231
		224	13.453	16.65	352	390
		181.5	11.204	16.20	201	268

Table C.15. The effect of elevated IL-6 on skeletal muscle's contractile properties

Treatment	Group	TA	Lo	1/2 RT	TPT	Po	sPo	-dP/dt	+dP/dt
Vector	WT	47.0	14.0	8.6	16.6	1559	294	20337	21850
		48.0	14.0	7.1	13.6	1778	329	25300	22670
		44.5	13.0	7.4	13.9	1512	280	20153	22522
		48.0	13.5	6.2	14.1	1898	338	24396	22975
		51	14	12.4	18.8	1460	254	15050	23766
		45	13.5	10.5	16.4	1686	320	21167	20500
		45	14	9.7	16.6	1419	280	16013	22529
		51.0	14.0	9.1	14.1	1627	283	22014	21793
		51.0	14.0	9.9	16.1	1621	282	17041	22255
		44.5	14.0	8.4	16.7	1597	318	19629	23432
		51.5	14.3	9.7	17.0	1760	309	17286	25694
		55.5	14.3	7.4	14.8	1976	321	25851	26840
		47.5	14.0	7.3	14.9	1551	290	20304	22785
		47.5	14.5	7.8	16.1	1730	335	18556	25656
Vector	KO	49.5	13.0	8.2	15.3	1329	221	11712	24776
		51.0	14.0	10.2	16.6	1622	282	20657	22264
		46.5	13.0	7.7	15.1	1566	277	15652	25807
		48.5	13.5	7.2	15.2	1787	315	24113	26244
		52.0	13.0	8.6	15.0	1635	259	17430	27858
		49.0	13.0	6.6	15.1	1681	283	19803	27645
		51.0	13.5	6.2	13.9	1690	283	15843	28451
		54.5	14.0	8.7	14.7	1795	292	20971	24416
		56.5	14.5	6.2	14.3	1862	303	19393	31552
		46.5	13.0	8.3	14.4	1595	283	23645	20631
		46.0	13.0	6.5	13.5	1364	244	21883	24011
		46.5	12.5	8.2	15.0	1613	275	17730	24173

Table C.16. The effect of elevated IL-6 on skeletal muscle's contractile properties

Treatment	Group	TA	Lo	1/2 RT	TPT	Po	sPo	-dP/dt	+dP/dt
		47.0	13.5	7.8	15.9	1661	302	19721	20211
		37.0	13.0	8.6	14.9	1445	322	20769	18694
		41.5	13.0	8.0	13.8	1569	311	20710	23751
		47.5	13.0	6.6	14.7	1611	279	18146	24640
		46.0	13.3	7.9	14.5	1912	349	26393	26735
		46.5	14	12.1	15.6	1618	309	18534	20450
		46.5	14.5	10.2	17.9	1408	278	15292	16911
IL-6	WT	46.5	14.5	10.7	17.3	1555	307	13821	20412
		43	14	9.1	17	1329	274	15712	15551
		46	14	11.2	18.1	1487	287	15192	21968
		45.0	13.5	9.8	18.1	1710	325	18981	25705
		50.5	13.5	8.8	17.8	1644	279	14340	25411
		46.5	14.5	8.9	15.8	1568	310	20118	23066
		49.5	13.5	8.5	16.4	1707	295	20657	22279
		51	14	7.3	15	1558	271	21581	27546
		47.0	14.0	8.7	16.3	1495	282	18106	21183
		46.5	13.5	6.8	15.5	1494	275	19835	23759
		52.0	13.5	7.4	15.0	1650	271	23558	24921
		48.5	13.0	12.3	17.3	1513	257	17982	22403
		53.0	13.5	7.7	13.3	1676	270	21985	27387
IL-6	KO	47.5	13.3	7.6	14.9	1602	283	20548	26482
		53.0	13.0	6.8	15.0	1703	265	20870	25545
		50.5	14.0	9.2	15.5	1400	246	19648	24620
		46.0	14.0	6.4	14.2	1581	305	17360	26922
		52.0	13.5	6.3	15.0	1655	272	20893	26514
		40.5	12.5	6.2	13.8	1423	278	19711	22061

Table C.17. The effect of elevated IL-6 on muscle fiber-type distribution

Treatment	Group	Type IIa	Type IIx	Type IIb
		16.4	31.2	52.4
		8	47	45
Vector	WT	8.9	34.6	56.5
		15.4	45.1	39.4
		6	34	60
		9	35	55
		6	44	50
IL-6	WT	10	43	48
		8	44	48
		23	37	40
		16.7	45.1	38.4
		5.4	36.5	58.1
Vector	KO	9.6	46	44.4
		15	40	46
		1	27	72
		11	35	54
		9	50	41
IL-6	KO	4	28	69
		4	37	59
		6	27	67

Table C.18 Animal characteristics of male skeletal muscle specific gp130 KO ApcMin/+ mice

Geno	Age	Peak BW	BW	% BW Loss
Flox	18.4	24.2	24.2	0%
	15.3	24.6	24.6	0%
	17.0	30.2	30.2	0%
	16.4	24.8	24.8	0%
	16.4	24.4	24.4	0%
	19.3	27.9	27.9	0%
	19.0	26.2	26.2	0%
MIN Flox	17.4	27.3	27.3	0%
	16.0	25.6	25.1	2%
	17.3	21.1	20.1	5%
	16.4	23.9	22.4	6%
	17.4	27.5	25.6	7%
	18.4	25.6	23.6	8%
	16.0	25.6	20.6	20%
MIN KO	16.7	22.6	22.6	0%
	17.3	26.7	26.7	0%
	17.6	27.5	27.5	0%
	18.4	28.8	28.8	0%
	18.4	28.2	28.2	0%
	18.4	25.9	24.4	6%
	17.6	25.0	23.5	6%
	18.0	26.0	22.5	13%
	16.7	23.0	20.1	13%

Table C.19. Animal characteristics of male skeletal muscle specific gp130 KO ApcMin/+ mice

Geno	Hindlimb	Spleen	Testes	Sem Ves	Tibia
Flox	268	87	183	221	17.3
	298.5	61	208	220	17.45
	364	88	192	251	17.6
	284	54	201	120	17.7
	282.5	65	206	137	17.6
	283	79	189	202	17.4
	279.5	68	201	212	17.9
MIN Flox	296	374	167	163	17.65
	278	492	123	79	18.1
	232.5	301	121	40	17.3
	249.5	460	53	58	17.5
	263.5	425	170	102	17.95
	262	376	192	54	17.5
	245	358	119	33	17.7
MIN KO	255	369	215	141	17.45
	320.5	261	167	144	17.9
	314.5	341	185	153	17.5
	333	158	215	165	18.35
	312	378	220	142	18.5
	256	366	150	45	18.3
	245	462	144	37	17.8
	229.5	595	160	64	17.2
	230	345	106	43	17.55

Table C.20. The role of the muscle gp130 receptor in cancer-induced skeletal muscle contractile dysfunction

Geno	TA	Lo	1/2 RT	TPT	-dP/dt	+dP/dt
Flox	45.0	14.0	10.9	17.4	23365	26493
	53.0	13.5	8.0	15.1	17125	22257
	57.5	14.0	8.7	14.9	13010	31413
	48.0	14.0	8.5	14.9	21518	26694
	47.0	13.5	8.9	14.3	19058	24114
	45.0	14.0	9.8	16.2	20348	27972
	49.5	14.0	5.2	14.0	18201	30673
MIN Flox	48.5	14.0	5.5	14.4	18591	23197
	45.5	14.5	5.6	12.8	13591	24740
	39.0	13.5	7.5	17.0	11925	24505
	35.5	13.0	13.8	18.9	10076	12940
	44.5	14.0	10.7	14.6	6502	24146
	46.0	13.5	9.5	14.3	11079	23075
	40.5	13.0	10.4	16.2	12184	19127
MIN KO	43.0	14.5	8.2	15.0	19778	22511
	53.5	15.0	6.6	15.8	11439	27366
	53.5	14.5	13.5	16.2	9164	22607
	56.5	16.0	7.7	15.1	15707	29273
	52.0	15.5	7.5	15.3	15446	26247
	43.0	14.0	7.8	16.0	11265	18924
	42.0	14.0	8.6	16.3	9389	26257
	38.0	15.0	14.4	17.8	6727	16305
	39.5	14.0	7.2	14.1	18385	17604

Table C.21. The effect of IL-6 on muscle mitochondrial content

Treatment	Geno	COX Activity	Complex I	Complex II	Complex III	Complex IV	Complex V
Vector	WT	6.19	1.16	1.06	1.28	1.38	1.13
		6.85	1.14	1.22	1.17	0.83	1.05
		5.41	1.00	1.10	1.15	0.98	1.05
		5.28	0.97	0.85	0.87	0.98	0.91
		5.67	0.84	0.81	0.79	0.89	0.97
		5.26	0.90	0.96	0.74	0.95	0.89
		5.72	-	-	-	-	-
		5.61	-	-	-	-	-
		5.57	-	-	-	-	-
		5.53	-	-	-	-	-
Vector	KO	6.18	1.11	0.90	1.30	0.73	1.02
		5.78	1.06	0.88	1.13	0.90	1.08
		6.28	0.61	0.55	0.66	0.58	0.87
		6.43	0.86	0.96	1.26	0.91	0.94
		5.29	0.95	0.85	1.30	1.13	1.00
		5.38	1.15	1.27	1.40	0.81	1.06
		5.62	-	-	-	-	-
IL-6	WT	3.49	0.94	0.64	0.80	0.67	0.85
		1.44	0.76	0.70	1.15	0.68	1.04
		3.78	0.56	0.52	0.87	0.70	0.79
		2.48	0.77	0.43	0.99	0.60	0.89
		5.15	0.83	0.50	0.99	0.60	0.91
		3.53	0.51	0.23	0.72	0.45	0.76
		3.45	-	-	-	-	-
IL-6	KO	4.05	1.10	1.15	1.23	0.82	1.04
		6.17	1.03	1.00	1.11	0.85	0.95
		6.04	1.13	1.28	1.18	0.71	1.06
		5.69	1.15	1.29	1.44	1.15	1.10
		4.65	0.95	0.88	1.18	0.70	1.01
		6.04	0.85	0.48	1.38	0.89	1.12
		5.77	-	-	-	-	-
		4.75	-	-	-	-	-

Table C.22. The effect of IL-6 on skeletal muscle force production

Treatment	Geno	10	30	50	80	100	120	150	180	200
Vector	WT	342	373	595	1269	1393	1445	1513	1559	1538
		343	318	430	1290	1528	1629	1704	1703	1778
		240	268	446	983	1331	1417	1468	1488	1504
		352	340	487	1126	1460	1606	1688	1832	1893
		398	482	870	1255	1344	1413	1430	1460	1437
		323	385	737	1292	1415	1499	1623	1667	1684
		364	360	688	1093	1211	1247	1300	1366	1401
		285	346	557	1112	1307	1345	1524	1514	1595
		304	336	546	1100	1382	1477	1519	1539	1601
		327	328	588	1248	1430	1505	1576	1597	1584
		389	550	902	1400	1522	1640	1722	1760	1664
		349	358	541	1221	1554	1706	1787	1818	1912
		269	281	397	1143	1335	1415	1478	1507	1539
		324	384	557	1031	1134	1517	1563	1671	1718
Vector	KO	349	338	433	984	1119	1135	1319	1329	1267
		426	473	714	1332	1529	1602	1622	1618	1600
		324	329	477	1316	1450	1497	1528	1540	1559
		405	424	570	1238	1415	1567	1666	1725	1775
		361	506	565	1404	1617	1559	1539	1593	1602
		339	352	477	1362	1545	1602	1602	1653	1676
		318	333	428	1281	1514	1649	1690	1605	1630
		384	382	514	1334	1556	1661	1751	1795	1784
		388	411	511	1422	1564	1542	1817	1826	1862
		327	376	469	1233	1427	1495	1567	1586	1581
		280	339	410	1049	1218	1290	1337	1353	1356
		315	331	451	1120	1385	1485	1547	1579	1601

Table C.23. The effect of IL-6 on skeletal muscle force production

Treatment	Geno	10	30	50	80	100	120	150	180	200
		339	388	510	1287	1465	1542	1601	1640	1658
		255	283	450	1064	1223	1310	1393	1422	1445
		298	303	567	1329	1470	1509	1539	1551	1547
		268	288	438	1108	1390	1487	1537	1557	1496
		375	405	494	1365	1614	1721	1816	1868	1893
		321	350	525	1212	1414	1523	1584	1608	1618
		322	287	629	1056	1077	1304	1353	1383	1408
IL-6	WT	324	361	643	1191	1449	1551	1555	1484	1454
		305	363	561	1081	1253	1301	1329	1326	1284
		319	410	813	1216	1340	1416	1473	1487	1473
		397	432	758	1220	1348	1397	1447	1650	1647
		287	321	600	1311	1504	1548	1618	1644	1624
		307	338	536	1177	1356	1456	1528	1523	1549
		319	354	623	1166	1486	1628	1687	1707	1688
		313	325	533	1009	1333	1446	1487	1550	1558
		325	357	568	1052	1208	1352	1412	1441	1455
		360	370	571	1145	1309	1370	1435	1469	1494
		393	384	613	1005	1417	1481	1526	1603	1648
		370	552	644	1100	1299	1481	1498	1510	1465
		357	318	493	1134	1382	1588	1650	1622	1676
IL-6	KO	367	363	557	1166	1398	1468	1538	1576	1602
		360	321	536	1301	1563	1642	1603	1627	1685
		391	392	503	1061	1226	1278	1355	1369	1400
		294	299	487	1134	1299	1377	1496	1542	1554
		302	355	498	974	1259	1273	1546	1655	1649
		281	292	384	941	1049	1106	1203	1372	1372

Table C.24. The effect of IL-6 on skeletal muscle force production

Treatment	Geno	10	30	50	80	100	120	150	180	200
Vector	WT	65	70	112	240	263	273	286	294	290
		63	59	79	238	282	301	315	315	329
		44	50	83	182	246	262	272	275	278
		63	61	87	201	260	286	301	326	337
		69	84	151	218	234	246	249	254	250
		61	73	140	246	269	285	309	317	320
		72	71	136	215	239	246	256	269	276
		50	60	97	193	227	234	265	263	277
		53	58	95	191	240	257	264	268	278
		65	65	117	249	285	300	314	318	316
		68	96	158	245	267	287	302	309	292
		57	58	88	199	253	278	291	296	311
		50	52	74	213	249	264	276	281	287
		63	74	108	199	219	293	302	323	332
Vector	KO	58	56	72	164	186	189	220	221	211
		74	82	124	232	266	279	282	281	278
		57	58	84	233	257	265	271	273	276
		71	75	100	218	250	276	294	304	313
		57	80	89	222	256	247	244	252	254
		57	59	80	229	260	269	269	278	282
		53	56	72	215	254	277	283	269	273
		63	62	84	217	253	270	285	292	290
		63	67	83	231	254	251	295	297	303
		58	67	83	218	253	265	278	281	280
		50	61	73	188	218	231	239	242	243
		54	56	77	191	236	253	263	269	273

Table C.25. The effect of IL-6 on skeletal muscle force production

Treatment	Geno	10	30	50	80	100	120	150	180	200
		62	71	93	234	267	281	291	298	302
		57	63	100	237	272	292	310	317	322
		59	60	113	264	292	299	305	308	307
		46	50	76	192	241	258	267	270	259
		68	74	90	249	295	314	331	341	346
		61	67	100	231	270	291	302	307	309
		64	57	124	209	213	258	267	273	278
IL-6	WT	64	71	127	235	286	306	307	293	287
		63	75	116	223	259	268	274	273	265
		62	79	157	235	258	273	284	287	284
		75	82	144	232	256	265	275	314	313
		49	54	102	222	255	262	274	279	275
		61	67	106	233	268	288	302	301	306
		55	61	108	202	257	281	291	295	292
		54	56	93	176	232	251	259	270	271
		61	67	107	199	228	255	266	272	275
		66	68	105	211	241	252	264	270	275
		65	63	101	165	233	244	251	264	271
		63	94	109	187	221	252	254	256	249
		58	51	80	183	223	256	266	262	270
IL-6	KO	65	64	98	206	247	259	272	278	283
		56	50	83	202	243	255	249	253	262
		69	69	88	186	215	224	238	240	246
		57	58	94	219	251	266	288	297	300
		50	58	82	160	207	209	254	272	271
		55	57	75	184	205	216	235	268	268

Table C.26. The effect of IL-6 on submaximal contraction-induced skeletal muscle fatigability

Treatment	Geno	0	5	10	15	20	25	30	35	40	45	50
Vector	WT	500	350	382	491	571	631	672	706	726	728	722
		456	377	454	565	635	685	716	747	772	793	801
		388	292	332	425	503	544	580	603	624	638	644
		514	411	445	542	638	682	717	749	782	804	818
		795	718	797	847	873	882	886	887	892	895	894
		648	427	537	608	654	680	698	714	733	737	750
		569	460	550	608	649	681	700	709	713	709	699
		361	314	411	541	621	645	658	671	675	688	698
		573	458	573	635	671	691	709	734	736	749	761
		649	490	641	733	791	825	847	860	866	870	869
		478	377	455	576	645	685	702	711	705	712	710
		548	432	471	506	611	655	697	719	738	756	759
		374	302	334	420	518	575	608	640	661	673	671
		562	529	697	765	809	816	844	844	839	832	816
Vector	KO	361	301	410	201	517	536	540	540	529	504	479
		603	493	600	680	718	726	753	753	744	735	728
		408	352	414	552	636	676	687	694	691	686	670
		542	413	448	516	622	681	719	747	767	771	771
		348	322	366	418	513	574	607	630	646	647	639
		387	339	390	489	597	652	676	685	689	692	685
		447	392	491	643	711	745	761	764	762	758	742
		527	415	530	648	718	757	776	786	789	786	780
		472	428	535	667	736	777	788	789	794	763	731
		416	327	355	383	403	417	425	436	442	451	451
		388	340	395	509	581	620	637	651	658	661	656
		476	379	419	455	542	585	599	613	620	625	625

55	60	65	70	75	80	85	90	95	100	105	110	115	120	125
707	686	664	642	613	582	555	525	496	474	446	431	411	395	374
796	780	754	721	682	643	602	565	529	503	482	460	441	428	411
643	628	607	589	556	520	467	431	395	369	345	337	323	320	294
812	803	784	754	731	699	666	635	597	566	540	519	497	478	463
888	876	856	854	776	729	678	627	588	551	526	500	483	468	454
754	752	747	735	719	696	671	639	605	571	537	506	476	450	426
686	666	634	601	561	522	488	458	438	424	404	384	372	354	347
698	695	683	664	639	610	576	544	511	478	453	427	403	381	364
762	761	756	744	728	708	683	659	633	608	577	546	524	496	476
860	837	801	755	704	636	601	567	524	492	469	460	428	424	419
704	695	675	648	622	588	553	518	483	452	426	401	376	359	344
749	728	703	676	668	620	598	557	531	502	477	446	420	398	373
672	654	635	606	572	537	500	463	430	406	386	366	350	335	325
798	768	696	678	623	571	501	474	440	413	377	370	359	344	332
455	437	426	417	407	402	391	371	355	344	332	327	317	313	307
712	677	659	619	608	574	542	540	523	496	501	473	468	449	440
641	603	558	515	480	453	428	414	401	390	380	376	370	366	361
745	721	695	666	635	602	571	540	512	487	466	448	429	417	402
607	573	529	491	452	429	404	387	380	358	352	336	324	314	307
665	631	579	526	476	436	406	384	363	351	339	326	317	311	305
716	677	641	592	552	516	486	462	450	435	426	423	416	411	407
768	755	735	710	683	659	631	612	590	568	551	535	520	506	492
689	655	620	605	551	522	509	483	472	459	453	454	447	432	424
446	443	433	423	411	397	383	366	347	346	319	303	321	291	281
647	629	603	573	544	514	494	477	465	453	445	432	425	421	416
619	609	589	563	528	488	450	413	386	366	350	337	326	316	308

130	135	140	145	150	155	160	165	170	175	180	185	190	195	200
359	349	330	320	304	291	283	268	259	251	246	244	235	227	225
399	388	376	371	362	352	347	341	335	330	328	317	312	306	302
283	274	266	259	251	260	238	234	224	221	233	215	209	209	205
448	432	422	412	402	392	382	374	366	358	352	346	338	332	325
441	431	420	415	407	401	394	393	388	383	378	379	373	369	367
406	392	375	363	351	342	334	327	320	319	308	302	299	292	284
341	328	320	313	300	297	296	291	288	284	282	277	276	273	273
346	330	319	307	296	290	299	298	293	280	267	255	252	246	243
458	439	423	411	397	384	370	362	354	345	340	329	323	317	312
410	400	401	396	376	368	368	366	366	361	351	346	347	346	346
326	315	298	291	282	278	270	265	263	258	259	256	258	254	252
357	347	341	319	316	309	306	306	290	307	291	284	279	279	285
320	313	308	303	299	285	289	279	275	273	275	264	259	255	249
328	320	313	292	299	294	287	277	260	271	267	256	258	251	250
318	297	296	294	291	289	309	283	284	278	280	277	274	275	275
435	419	415	419	398	388	391	376	370	367	364	354	352	347	342
359	358	354	349	348	345	342	340	335	333	331	329	324	321	318
391	383	371	359	347	342	333	325	318	309	307	296	289	281	276
304	293	287	275	267	273	260	258	250	246	240	234	234	230	224
301	293	290	286	282	279	271	265	259	256	252	246	244	235	233
402	397	396	393	389	387	384	384	378	379	374	373	369	365	360
478	470	459	452	443	436	429	422	416	410	401	396	391	385	382
422	415	411	381	402	400	393	392	387	385	381	375	370	367	406
297	276	271	265	266	259	285	261	246	243	240	235	227	231	229
407	402	394	390	385	381	375	367	364	362	357	355	349	344	341
302	293	283	280	275	262	256	254	247	239	236	231	226	221	218

205	210	215	220	225	230	235	240	245	250	255	260	265	270	275
220	221	229	222	225	226	210	205	218	207	206	203	201	200	199
296	291	286	281	277	271	268	268	263	262	259	254	254	253	249
202	201	203	198	188	188	210	190	207	186	189	184	179	184	176
321	313	308	305	303	300	298	297	297	294	288	285	288	287	287
360	359	355	356	351	350	346	344	342	343	337	338	338	338	334
282	275	269	266	261	256	254	250	248	244	246	249	242	238	231
269	270	263	261	255	256	255	254	251	252	243	242	244	240	239
234	231	226	222	224	218	220	219	213	213	212	210	208	210	207
309	302	298	294	287	285	280	274	270	270	264	263	253	248	247
337	340	329	326	320	317	315	316	310	295	304	301	302	299	293
258	255	255	250	246	236	241	243	239	236	235	234	229	229	231
279	269	272	264	264	258	254	253	256	251	245	241	242	236	235
248	250	244	236	231	232	230	226	222	220	218	213	212	210	206
235	243	239	235	198	229	223	216	208	205	216	206	198	201	204
269	268	270	271	282	265	278	259	256	256	254	264	252	250	256
356	337	331	330	331	325	320	320	315	313	313	308	304	306	303
315	312	306	304	299	294	295	291	285	282	280	277	267	268	267
273	272	267	263	271	259	255	251	250	249	256	241	251	234	233
216	224	216	215	215	211	200	213	197	195	193	194	188	199	187
227	219	218	216	210	213	207	206	203	203	199	198	195	195	194
359	355	352	350	348	346	344	341	339	334	331	327	325	324	323
376	372	365	362	359	355	350	344	340	336	331	327	323	318	317
387	365	380	347	354	352	349	349	345	340	337	337	336	332	319
220	222	219	230	231	226	214	219	206	208	207	208	212	210	202
336	330	329	327	322	321	315	313	307	306	307	302	299	296	293
215	211	208	202	204	202	198	193	195	194	192	187	188	187	183

280	285	290	295	300
198	201	196	196	198
249	245	243	242	242
178	174	173	181	175
284	281	275	279	270
330	329	327	295	312
233	233	227	225	226
239	231	230	230	229
206	201	206	200	199
252	241	242	241	238
288	284	285	290	272
226	227	227	220	219
240	234	236	233	228
203	202	195	197	195
203	198	201	194	194
256	248	247	244	243
305	297	295	299	301
265	261	257	255	252
233	241	227	226	230
193	183	180	181	179
190	188	188	186	185
318	317	313	311	309
314	308	304	300	298
329	326	323	324	320
194	197	193	191	197
292	291	288	287	285
182	181	179	177	177

Table C.27 The effect of IL-6 on submaximal contraction-induced skeletal muscle fatigability

Treatment	Geno	0	5	10	15	20	25	30	35	40	45	50
		474	374	482	574	629	663	684	697	704	708	709
		370	266	294	365	427	461	480	490	497	502	507
		466	356	437	540	603	636	661	716	732	744	747
		412	361	393	429	506	573	610	634	652	656	654
		479	374	405	449	527	567	581	584	577	565	533
		747	563	671	734	771	794	808	818	823	825	820
		670	623	706	782	834	869	899	919	932	941	939
IL-6	WT	617	382	448	512	562	599	633	668	694	708	713
		547	375	484	537	562	573	570	570	569	566	568
		735	668	759	799	831	841	846	852	842	841	834
		714	668	773	834	861	874	877	875	869	867	862
		856	593	790	878	924	944	954	956	955	939	926
		486	347	490	575	619	641	652	657	662	661	658
		476	347	406	511	582	622	645	659	668	666	659
		277	235	269	293	324	348	372	393	389	392	377
		359	308	352	432	499	551	543	565	572	557	561
		435	391	532	635	676	695	698	701	691	671	628
		477	393	432	530	605	648	667	688	695	695	683
		424	349	390	516	563	596	627	644	659	670	669
		545	471	506	636	715	755	787	815	845	861	861
IL-6	KO	506	406	446	550	638	676	693	703	708	708	703
		493	384	413	453	554	603	638	652	651	652	649
		395	340	373	424	501	550	564	586	598	610	612
		456	406	531	679	747	780	795	800	795	765	720
		351	318	354	397	469	545	588	617	623	632	638
		414	329	370	449	559	619	645	668	681	684	700

55	60	65	70	75	80	85	90	95	100	105	110	115	120	125
702	689	672	642	614	578	541	507	481	459	437	419	404	388	377
505	501	496	486	474	456	433	410	384	366	345	327	317	304	293
741	717	655	615	582	538	503	478	451	433	411	400	386	368	355
641	619	587	550	509	477	447	424	402	383	368	355	342	330	320
509	486	454	429	408	392	377	360	347	333	313	297	288	272	267
806	787	756	717	670	622	581	551	519	495	472	456	439	432	422
929	894	835	751	672	603	553	519	488	460	444	426	414	402	394
705	689	663	633	602	568	535	506	482	466	446	431	418	404	396
565	562	553	544	530	514	493	471	446	427	402	382	359	341	320
816	779	722	655	603	547	504	467	437	419	396	382	368	357	343
857	845	834	812	787	752	724	677	637	599	573	534	507	485	470
907	880	831	777	729	668	596	550	527	496	469	445	435	421	405
654	646	632	615	594	570	536	506	469	439	412	394	378	363	357
646	623	607	583	557	537	523	497	484	466	449	438	425	409	397
366	359	340	319	298	276	256	241	229	219	209	199	192	187	184
557	548	530	521	499	466	442	406	383	361	337	322	305	293	284
584	516	462	443	415	400	386	373	363	351	344	338	333	327	323
668	642	617	587	561	532	511	491	493	460	446	433	420	410	400
652	641	612	577	544	501	476	458	426	409	381	371	353	342	329
854	835	798	755	703	653	603	565	533	506	486	467	454	443	433
685	665	628	595	556	522	490	466	441	418	403	386	371	359	350
646	634	618	592	563	535	509	476	453	426	404	382	366	353	341
614	602	601	590	578	559	539	509	494	472	449	432	407	394	387
669	620	577	541	511	488	469	451	441	429	416	409	402	396	390
626	608	580	548	508	477	443	423	396	384	365	354	343	330	324
682	662	639	610	579	539	506	481	457	436	426	420	405	403	391

130	135	140	145	150	155	160	165	170	175	180	185	190	195	200
368	360	350	344	338	334	324	320	314	312	306	303	297	294	292
287	276	267	259	253	243	237	230	226	218	213	208	205	201	197
345	332	331	317	309	303	298	287	282	280	275	270	265	262	256
309	303	296	287	280	273	268	261	254	246	242	238	232	228	222
255	244	238	234	226	224	219	216	215	212	210	205	204	201	199
409	399	395	387	376	369	362	360	353	353	350	347	346	344	337
384	380	374	369	370	369	373	360	356	360	356	356	349	351	353
387	376	366	361	354	348	344	336	333	326	319	315	313	312	311
306	291	279	265	253	245	235	227	219	211	206	197	196	189	185
334	320	314	312	304	303	295	294	293	292	289	279	283	279	274
442	423	411	404	383	373	364	354	342	334	328	323	314	306	301
400	389	382	374	365	361	356	353	350	348	342	334	331	327	323
353	340	335	333	327	324	327	316	315	308	308	305	303	299	298
385	366	357	346	334	326	317	306	301	293	289	279	274	269	262
176	173	172	167	167	165	158	157	147	152	153	152	151	146	148
276	265	254	247	245	236	233	229	223	223	220	218	222	219	216
317	311	310	306	303	300	297	293	291	280	282	289	278	276	275
392	382	376	369	362	356	349	340	336	329	322	318	313	307	301
322	316	308	299	293	289	283	282	275	275	264	262	262	259	253
423	415	408	402	395	388	385	374	369	366	360	358	350	346	339
341	335	329	322	317	311	308	303	301	296	291	287	280	276	272
328	313	312	299	291	290	276	276	268	262	259	259	251	246	246
376	363	354	340	340	324	316	311	311	304	298	293	282	271	269
388	383	380	373	374	370	365	364	361	358	355	351	353	352	346
314	309	301	293	286	275	271	269	262	271	263	262	251	252	243
384	382	372	373	374	368	364	360	357	357	354	349	345	333	337

205	210	215	220	225	230	235	240	245	250
289	285	283	278	274	269	263	263	259	258
193	188	184	181	179	176	174	172	171	174
251	249	242	240	236	232	229	226	221	217
216	212	205	201	194	191	189	184	178	175
196	193	194	196	199	198	187	193	184	182
335	330	325	320	315	316	314	311	304	306
354	353	364	371	371	362	347	334	321	315
308	307	305	303	301	303	301	294	293	291
178	174	174	168	165	166	161	161	157	153
277	270	269	274	269	269	267	262	261	262
297	291	290	285	282	276	265	263	261	253
317	317	311	309	308	304	303	303	300	296
296	292	289	287	283	281	278	274	270	267
259	246	247	239	238	232	226	222	220	215
144	145	136	145	143	136	138	133	146	146
213	217	220	217	221	225	215	216	216	210
273	271	268	268	265	261	257	252	252	250
296	292	287	280	276	268	263	259	255	248
251	245	240	235	231	226	223	223	220	209
332	326	325	320	316	309	308	301	299	296
267	262	259	254	251	248	242	239	234	231
248	244	244	241	238	239	237	231	230	233
271	265	262	256	264	255	254	244	252	249
347	346	346	343	342	336	336	331	333	329
244	242	237	234	229	236	230	231	226	222
334	335	330	326	322	317	312	311	309	308

255	260	265	270	275	280	285	290	295	300
252	250	247	248	242	241	235	235	233	228
166	168	163	166	163	161	159	159	159	156
214	208	206	202	198	196	192	190	187	187
175	171	172	168	167	167	163	160	160	157
180	181	182	181	179	181	180	184	181	175
300	314	307	311	298	291	307	305	314	301
316	314	316	317	321	311	319	321	320	315
288	284	283	279	276	275	274	275	275	274
153	155	154	152	149	149	148	145	141	141
258	256	253	250	248	250	251	247	248	244
251	246	242	241	240	236	238	231	227	223
291	296	282	281	278	281	277	274	277	272
266	261	266	253	251	247	243	240	237	234
214	210	208	207	204	203	199	197	196	195
143	147	139	145	137	133	137	134	133	136
211	213	218	217	209	212	214	207	209	208
242	238	237	235	232	232	229	226	223	221
245	239	236	233	227	223	219	214	211	208
212	202	202	199	197	193	206	196	181	190
291	287	281	281	275	272	269	264	259	261
227	223	221	216	213	212	208	205	203	201
231	230	223	221	220	216	214	212	212	212
244	229	231	236	224	228	228	232	231	227
328	328	326	324	321	320	318	317	314	314
224	221	214	214	211	212	208	206	204	197
304	300	298	297	292	288	288	285	280	280

Table C.28. The effect of IL-6 on submaximal contraction-induced skeletal muscle fatigability

Treatment	Geno	Max Force following 30 contractions	Force @ 90s of submaximal contraction
Vector	WT	58%	34%
		62%	32%
		63%	28%
		64%	33%
		69%	43%
		66%	38%
		44%	32%
		68%	33%
		66%	41%
		62%	35%
		67%	29%
		63%	28%
		53%	30%
		55%	27%
Vector	KO	63%	28%
		59%	33%
		54%	26%
		57%	30%
		55%	24%
		58%	23%
		58%	27%
		65%	34%
		50%	26%
		63%	23%
		66%	35%
		54%	26%

Table C.29. The effect of IL-6 on submaximal contraction-induced skeletal muscle fatigability

Treatment	Geno	Max Force following 30 contractions	Force @ 90s of submaximal contraction
IL-6	WT	46	31%
		53	28%
		52	30%
		59	26%
		51	19%
		56	35%
		59	32%
		56	36%
		62	35%
		54	31%
		66	40%
		54	33%
		59	32%
		55	29%
		52	15%
IL-6	KO	70	27%
		52	25%
		57	30%
		57	30%
		65	34%
		58	29%
		62	28%
		64	36%
		53	29%
		58	26%
		66	34%

Table C.30. Indices of cachexia in gp130 KO MIN mice.

Geno	Plasma IL-6	Total Polyps	<1mm	1-2mm	>2mm	TA Weight
Flox	0	0	0	0	0	45
	0	0	0	0	0	53
	0	0	0	0	0	57.5
	0	0	0	0	0	47
	0	0	0	0	0	45
	0	0	0	0	0	48
	0	0	0	0	0	49.5
MIN Flox	7.3	48	0	25	22	48.5
	33.2	23	0	0	23	45.5
	0	78	0	13	62	39
	21.6	45	1	10	32	35.5
	23.0	80	0	20	60	44.5
	4.6	83	6	29	47	46
	64.9	88	0	37	50	40.5
MIN KO	3.6	59	14	30	12	43
	8.2	26	0	0	24	53.5
	25.2	42	0	12	28	53.5
	18.7	64	0	40	19	56.5
	10.0	39	0	2	35	52
	100.8	72	0	15	54	43
	10.0	39	0	0	37	42
	98.5	72	0	15	54	38
	21.3	64	0	40	19	39.5

Table C.31. Indices of cachexia in gp130 KO MIN mice

Geno	gp130	STAT3	NFKB	Erk1/2	P38
Flox	0.91	0.89	0.80	1.14	2.24
	1.34	1.45	1.60	0.48	0.23
	1.00	1.01	0.81	1.45	1.05
	0.78	0.87	0.84	1.08	0.45
	0.95	0.79	0.95	0.86	1.02
	1.02	1.03	0.83	1.44	1.03
	0.89	0.91	0.84	1.16	2.20
MIN Flox	1.02	1.49	0.91	0.60	1.77
	0.78	3.18	0.88	2.38	9.25
	0.99	0.62	1.03	0.73	2.89
	0.88	1.58	0.94	1.07	5.90
	1.33	1.87	1.06	1.70	3.58
	0.99	20.67	0.85	1.28	1.66
	1.18	4.07	1.00	2.56	2.05
MIN KO	0.24	0.61	1.13	0.38	6.94
	0.12	2.24	1.04	0.71	7.22
	0.41	0.84	1.14	0.37	1.24
	0.14	1.52	1.04	0.30	5.03
	0.16	0.68	0.78	0.74	1.19
	0.16	1.94	0.52	0.41	1.30
	0.21	1.75	0.47	0.59	1.81
	0.12	25.32	0.70	0.59	9.51
	0.06	0.46	0.58	0.62	7.36

Table C.32. The role of the muscle gp130 receptor on cancer-induced muscle weakness.

Geno	10	30	50	80	100	120	150	180	200
Flox	348	434	676	1259	1555	1750	1854	1898	1911
	273	265	406	1201	1520	1494	1520	1631	1589
	340	355	537	1262	1389	1503	1578	1616	1615
	285	340	417	1021	1281	1393	1548	1653	1636
	273	264	508	1311	1489	1566	1609	1602	1611
	346	358	653	1370	1533	1575	1604	1637	1690
	374	327	420	1138	1591	1695	1745	1765	1773
MIN Flox	240	250	412	1133	1362	1425	1499	1540	1536
	289	279	337	846	950	1192	1321	1415	1423
	264	287	452	1108	1223	1288	1357	1389	1397
	332	384	745	932	995	1035	1050	1035	1033
	267	269	363	718	930	1044	1106	1136	1145
	260	285	607	1142	1279	1341	1380	1390	1391
	276	425	743	1045	1113	1168	1245	1252	1260
MIN KO	239	271	365	942	1317	1470	1535	1544	1469
	240	257	391	1143	1317	1437	1486	1498	1450
	346	359	562	1282	1320	1369	1347	1355	1291
	228	237	465	1010	1371	1542	1600	1650	1619
	266	285	446	1007	1222	1370	1529	1574	1588
	288	373	646	1076	1162	1192	1184	1166	1145
	318	317	565	1031	1198	1290	1331	1332	1326
	293	328	674	858	946	989	1016	1017	1011
	271	270	394	962	1131	1222	1257	1188	1167

Table C.33. The role of the muscle gp130 receptor on cancer-induced muscle weakness

Geno	10	30	50	80	100	120	150	180	200
Flox	69	86	133	248	307	345	365	374	377
	44	43	65	194	245	241	245	263	256
	52	55	83	195	214	232	243	249	249
	53	63	77	189	237	257	286	305	302
	50	48	92	239	271	285	293	292	293
	68	71	129	270	302	310	316	323	333
	67	59	75	204	285	304	313	316	318
MIN Flox	44	46	75	207	249	261	274	282	281
	58	56	68	171	192	241	267	286	287
	58	63	99	243	268	282	298	305	306
	77	89	173	216	231	240	244	240	240
	53	54	72	143	185	208	221	226	228
	48	53	113	212	238	249	257	258	259
	56	86	151	212	226	238	253	255	256
MIN KO	51	58	78	201	281	314	328	330	314
	43	46	70	203	234	255	264	266	258
	59	62	96	220	227	235	231	233	222
	41	42	83	181	246	277	287	296	290
	50	54	84	190	231	259	289	297	300
	59	77	133	222	240	246	244	240	236
	67	67	119	218	253	272	281	281	280
	73	82	169	215	237	247	254	254	253
	61	61	88	216	254	274	282	267	262

Table C.34. The role of the muscle gp130 receptor on cancer-induced muscle fatigability

Geno	0	5	10	15	20	25	30	35	40	45	50
Flox	557	434	516	663	767	819	838	850	857	861	865
	433	311	412	501	552	583	598	611	622	626	634
	518	407	483	633	725	774	786	806	803	801	803
	356	304	338	359	376	416	457	485	499	503	498
	495	414	442	578	658	693	707	713	718	714	708
	359	300	341	380	427	476	509	536	568	588	601
	412	350	390	471	563	621	649	659	657	640	610
MIN Flox	285	241	267	287	304	325	348	363	374	378	380
	343	288	320	361	420	457	481	481	479	473	459
	408	361	415	506	612	647	647	625	596	558	526
	605	574	603	616	614	596	563	526	486	450	420
	300	281	319	377	406	419	418	409	395	376	353
	537	457	589	669	708	723	727	723	701	678	634
	545	449	570	648	683	681	656	613	564	519	486
MIN KO	284	208	225	241	252	262	269	278	285	290	292
	294	250	300	317	343	359	374	379	368	357	346
	239	197	221	246	264	277	288	306	300	286	273
	346	324	344	412	472	495	520	533	533	542	535
	316	279	310	357	428	486	515	517	506	496	510
	411	371	457	513	555	560	596	597	571	528	487
	445	418	559	671	691	668	614	558	515	480	452
	692	635	587	521	469	427	393	368	342	310	273
	332	227	238	250	257	262	267	272	272	275	282

55	60	65	70	75	80	85	90	95	100
856	845	822	795	766	726	687	647	613	586
630	618	599	576	537	509	474	445	419	390
794	751	719	664	615	573	549	503	479	463
483	465	443	417	397	377	361	345	334	323
685	664	636	598	565	531	503	483	465	448
609	595	589	564	538	503	465	438	411	387
560	525	498	464	446	438	421	402	393	384
383	380	379	370	359	348	334	321	309	296
438	419	393	380	362	350	335	328	316	315
499	479	463	446	436	423	411	401	389	381
398	379	364	345	328	310	291	276	256	241
331	307	287	273	257	244	235	223	214	207
591	553	517	483	468	443	427	416	404	389
459	465	416	399	386	371	356	345	334	322
292	292	289	280	278	270	262	255	247	238
339	336	333	325	323	317	310	305	297	295
262	259	256	252	253	257	252	248	242	237
516	486	472	457	433	421	411	398	393	399
490	466	453	425	408	389	371	357	352	339
448	415	387	363	343	322	301	284	263	258
424	401	382	369	353	344	335	328	321	316
243	211	191	170	154	138	132	125	118	113
271	271	263	252	237	227	219	215	208	202

105	110	115	120	125	130	135	140	145	150
559	538	523	510	500	491	483	475	466	461
369	354	340	328	315	305	297	292	291	282
447	427	422	409	401	405	397	398	376	360
317	306	301	295	287	282	276	269	264	260
436	423	416	405	394	392	384	377	377	366
361	345	328	322	313	299	288	287	269	268
352	370	361	354	345	333	330	320	313	309
282	271	262	255	248	245	240	236	232	231
311	301	300	296	314	290	287	285	284	280
372	366	359	352	346	339	336	330	327	321
226	211	198	187	175	165	157	149	141	135
201	192	189	184	180	176	173	167	164	164
385	377	368	361	356	348	349	345	343	337
312	304	296	288	282	276	271	267	258	258
230	223	220	216	212	207	203	195	199	194
290	282	279	275	266	264	261	257	251	251
234	232	227	223	220	212	209	213	215	210
391	374	372	364	357	350	344	334	326	323
329	331	308	286	281	281	280	275	272	270
243	229	215	205	182	187	179	172	166	161
313	306	304	299	295	289	288	284	282	279
107	105	104	102	101	100	100	100	99	99
196	191	187	186	182	179	177	173	172	169

155	160	165	170	175	180	185	190	195	200
456	448	443	438	434	429	425	419	416	411
281	274	266	262	261	252	245	240	236	234
365	368	360	363	357	340	337	339	341	328
253	247	244	242	238	237	237	235	234	229
362	351	352	352	344	339	338	336	329	329
263	254	246	247	242	238	234	229	228	227
301	291	292	267	282	272	279	272	267	274
229	227	225	228	224	221	220	219	220	216
277	276	272	271	269	266	264	261	261	257
319	316	311	309	308	303	303	299	297	294
128	123	117	114	113	109	106	106	104	102
159	156	153	150	147	145	144	141	139	139
335	332	334	329	329	325	324	321	319	320
254	251	249	243	245	242	239	238	240	235
188	192	190	189	184	185	177	174	170	171
243	245	237	235	232	229	221	222	221	223
205	206	199	190	189	191	181	186	181	176
318	316	307	304	294	301	297	289	289	286
263	292	256	259	246	243	232	244	245	240
156	151	149	145	140	139	135	134	131	131
276	275	272	269	269	266	263	263	260	259
97	97	95	97	95	94	94	94	96	93
170	165	163	163	160	157	160	157	156	156

205	210	215	220	225	230	235	240	245	250
405	401	397	392	386	384	380	376	370	368
232	223	222	226	216	212	209	207	211	203
338	324	324	324	322	311	312	301	306	299
229	227	224	224	219	218	217	215	214	214
327	322	323	318	314	312	305	311	303	298
225	226	212	223	213	209	210	204	204	212
263	260	259	240	259	246	230	245	233	244
211	210	213	210	209	205	207	201	201	199
252	251	251	248	244	241	239	238	235	229
290	289	287	285	285	279	278	278	277	273
101	101	101	100	102	103	103	104	102	101
137	136	134	136	127	131	131	132	129	131
315	316	312	310	311	308	308	306	303	303
236	232	230	231	229	228	227	225	225	220
171	170	167	165	165	165	160	163	161	159
219	217	217	213	217	215	211	208	207	207
180	172	180	170	170	169	166	165	162	163
284	284	275	272	261	266	266	258	257	259
230	230	214	216	208	210	215	206	200	205
129	128	128	125	126	126	124	125	117	123
258	257	256	253	254	250	250	249	249	246
94	92	91	91	90	91	91	90	90	89
154	154	153	152	151	149	149	146	147	147

255	260	265	270	275	280	285	290	295	300
365	362	358	354	351	348	345	341	337	335
200	197	202	195	189	194	188	181	184	185
297	308	289	295	291	284	271	267	264	270
208	208	206	206	203	203	203	200	199	197
298	294	291	291	284	287	280	280	273	274
202	202	211	197	195	199	200	190	186	187
242	237	235	224	217	222	216	220	216	218
197	195	195	193	192	191	188	188	186	186
230	229	227	223	222	222	214	218	216	214
273	270	268	266	265	264	263	261	258	256
102	101	99	102	102	102	99	99	97	97
128	129	128	127	127	130	121	130	126	126
303	301	294	294	294	295	292	291	289	276
222	217	218	213	214	213	210	214	213	208
159	156	155	153	153	151	154	150	149	149
202	202	203	200	198	192	197	193	195	236
162	159	160	156	155	156	156	155	153	149
253	245	246	244	246	246	240	239	243	236
188	201	198	194	198	195	189	188	186	186
123	123	123	121	120	119	118	120	119	119
245	244	244	245	242	242	238	238	238	154
89	89	86	85	84	83	83	82	80	178
146	142	144	142	141	138	140	141	139	136

301	305	310	315	320	325	330	335	340	345	350
1109	948	913	871	839	818	795	773	766	761	753
774	772	763	747	740	720	701	687	677	670	670
895	679	673	657	634	626	607	599	589	591	581
1002	834	813	787	766	753	742	730	721	714	712
981	830	826	800	768	752	729	715	698	687	677
869	780	762	747	716	698	686	665	657	640	637
739	590	587	560	504	526	516	524	502	494	486
949	838	787	742	705	677	658	648	642	637	629
849	726	710	685	669	649	640	633	625	623	619
639	551	542	533	531	523	515	507	508	499	494
250	181	180	177	174	173	169	171	162	158	154
664	524	508	488	468	454	405	428	421	413	406
600	488	489	481	476	466	468	464	461	482	449
452	396	396	390	379	372	367	358	351	344	338
749	667	637	609	589	573	563	558	543	544	545
629	555	553	548	541	543	538	537	533	528	529
406	365	364	359	362	356	352	353	351	348	348
610	547	542	535	517	516	517	510	505	476	467
624	502	497	482	492	482	479	452	467	455	449
275	221	219	217	216	212	208	205	200	196	193
458	393	395	392	387	386	384	383	382	377	378
146	107	106	100	100	97	97	95	93	90	88
566	540	522	496	480	478	468	463	456	449	445

355	360	365	370	375	380	385	390	395	400
752	750	743	742	740	734	737	732	730	726
662	660	658	656	652	649	647	647	650	648
567	568	560	562	557	548	549	551	548	544
707	702	704	701	694	696	696	695	692	697
674	670	663	662	657	655	656	654	655	652
634	625	615	611	613	614	611	610	603	604
442	482	459	474	460	456	453	425	443	429
628	629	623	622	622	626	625	622	621	618
609	614	608	608	605	608	605	603	604	601
494	483	481	479	477	472	467	469	471	456
151	149	150	142	140	137	135	135	132	131
404	398	381	393	389	387	390	385	383	385
449	447	441	435	435	428	429	410	420	430
331	329	324	324	323	321	322	318	318	314
533	533	537	535	533	529	533	528	520	520
525	520	525	521	519	518	514	512	512	510
346	342	343	343	340	338	336	336	335	332
482	471	475	489	472	476	476	474	459	449
449	435	421	436	434	432	458	501	376	420
189	187	184	182	177	178	178	175	173	174
373	373	369	369	368	367	364	364	361	362
86	84	81	80	80	77	76	74	71	70
446	442	437	442	434	433	434	433	435	434

405	410	415	420	425	430	435	440	445	450
729	729	724	722	721	727	722	720	718	716
651	649	648	649	651	644	645	650	643	650
544	539	536	533	533	528	524	529	524	529
691	692	691	688	686	689	689	689	684	683
652	652	648	648	642	644	640	640	639	639
603	610	608	602	597	603	598	594	589	589
451	427	432	412	391	416	395	397	400	397
615	615	615	613	613	610	609	610	609	603
597	600	598	596	595	594	595	592	591	591
459	462	457	457	458	455	458	451	452	443
129	129	129	126	127	126	124	124	123	123
382	382	383	382	380	381	379	379	382	381
398	411	407	406	419	414	405	396	389	394
315	316	314	310	311	310	306	307	310	310
507	516	516	515	513	513	509	508	501	502
509	510	511	506	506	506	505	502	499	505
332	328	329	329	327	326	321	325	322	319
448	450	446	447	455	433	428	434	433	431
407	423	398	399	359	384	405	508	502	487
158	172	173	171	171	170	171	169	169	173
363	359	359	361	359	359	358	356	359	357
68	69	69	68	67	65	61	62	58	59
431	428	429	430	434	426	429	427	422	424

455	460	465	470	475	480	485	490	495	500
712	708	706	708	704	704	702	702	705	705
645	640	644	640	643	643	643	644	647	656
522	521	521	510	519	522	507	518	517	515
683	681	679	680	678	678	678	678	678	678
637	638	638	633	636	635	636	635	636	632
590	577	586	585	581	580	581	567	569	580
391	392	388	378	393	376	382	379	380	374
606	604	606	604	600	605	602	599	589	581
591	589	588	587	586	585	583	583	583	583
448	447	447	446	446	445	440	441	437	441
122	122	124	123	124	122	122	122	125	123
381	383	383	383	383	350	382	381	378	377
400	396	392	389	389	395	384	387	388	376
309	310	304	310	307	305	306	305	303	302
499	499	497	497	495	494	485	493	489	485
501	499	497	496	497	493	495	492	492	492
321	319	319	319	317	319	316	318	318	313
419	421	422	418	419	427	425	411	408	402
463	496	489	472	445	459	459	461	440	437
174	158	172	173	171	171	170	171	169	169
359	357	357	357	356	357	356	352	357	358
59	56	53	54	53	56	53	54	52	52
420	418	416	421	416	418	419	420	416	415

505	510	515	520	525	530	535	540	545	550
706	707	704	703	700	698	697	696	697	698
661	669	672	676	677	675	677	683	678	683
513	506	505	504	508	507	509	500	505	501
678	678	678	678	678	678	678	678	678	678
629	633	634	634	633	633	636	630	631	629
566	564	571	562	566	565	560	561	562	562
378	382	381	379	376	374	368	373	372	373
576	572	571	571	572	578	576	578	582	578
583	582	579	580	578	580	578	578	577	576
443	437	436	437	435	432	435	432	431	431
123	123	123	125	124	124	124	127	126	128
378	378	379	377	378	377	380	377	379	379
379	383	375	374	381	372	367	372	372	366
302	302	301	299	300	298	298	294	297	297
488	489	479	484	485	484	483	483	482	478
494	493	492	492	493	495	491	489	492	491
316	315	315	313	314	313	310	312	309	310
412	415	414	404	399	388	389	395	386	396
459	434	408	422	502	433	443	440	429	424
173	174	158	172	173	171	171	170	171	169
353	351	350	351	352	349	347	353	344	345
51	51	54	51	49	49	49	48	46	46
414	416	419	414	416	414	412	414	406	406

555	560	565	570	575	580	585	590	595	600
697	696	696	695	694	695	690	690	693	690
679	683	680	682	683	687	694	689	689	689
503	500	497	503	501	500	507	499	496	501
678	678	678	678	678	678	678	678	678	678
626	628	628	631	632	631	635	637	631	631
561	553	550	552	555	553	564	556	554	556
367	375	370	372	368	367	368	366	368	370
575	576	573	570	572	566	569	566	567	568
577	577	575	576	574	576	575	571	569	573
429	433	427	428	430	425	427	429	426	421
129	129	131	130	132	132	132	135	135	137
380	379	378	379	380	379	374	377	376	378
366	342	357	359	361	315	357	358	368	369
291	295	289	293	293	294	289	293	292	294
478	479	479	478	477	478	475	479	473	475
489	489	482	482	487	483	483	483	483	480
310	311	311	312	314	312	312	313	309	311
391	381	389	395	375	386	387	393	382	388
440	417	471	373	403	415	388	384	407	435
169	173	174	158	172	173	171	171	170	171
347	344	342	343	343	340	339	342	342	338
44	45	44	44	45	44	45	48	43	42
416	415	403	399	400	405	396	406	403	395

Table C.35. The role of the muscle gp130 receptor on cancer-induced muscle fatigability

Geno	Force Following Submax Fatigue	Force Following Max Fatigue
Flox	1109	690
	774	689
	895	501
	1002	678
	981	631
	869	556
	739	370
MIN Flox	949	568
	849	573
	639	421
	250	137
	664	378
	600	369
	452	294
MIN KO	749	475
	629	480
	406	311
	610	388
	624	435
	275	171
	458	338
	146	42
	566	395

Table C.36. The effect of muscle gp130 loss on mitochondrial content, function, and quality control in MIN mice

Geno	APMK	BNIP3	Parkin	P62	PGC1	DRP1	FIS1	MFN1	COXIV	Cyto C
Flox	1.49	0.45	1.38	1.03	0.86	1.81	0.56	0.74	2.00	0.55
	1.25	1.26	1.02	1.46	1.27	0.86	1.65	0.75	1.02	0.99
	0.81	1.08	0.85	0.99	0.97	0.96	1.04	0.89	0.43	0.91
	0.72	0.99	0.89	0.83	0.91	0.62	1.03	1.31	0.73	1.18
	0.74	1.22	0.86	0.69	0.99	0.76	0.72	1.30	0.82	1.36
MIN Flox	0.79	1.74	1.29	0.86	0.85	1.30	0.80	1.24	0.11	1.54
	0.86	0.86	1.03	0.71	0.58	1.17	0.87	1.12	0.82	1.31
	1.09	1.72	1.13	0.79	0.92	0.95	1.38	1.11	0.10	1.67
	1.24	1.17	0.87	0.89	0.61	1.65	0.77	0.90	0.25	1.67
	1.38	1.44	0.93	0.70	0.88	0.96	0.85	0.72	0.12	1.45
	1.03	0.79	1.33	0.41	0.55	1.30	0.98	0.49	0.35	1.13
	1.09	0.92	1.42	0.74	0.84	1.09	0.82	1.08	0.24	1.35
MIN KO	1.48	1.07	1.29	0.76	0.85	1.30	0.63	1.14	0.09	1.50
	0.75	0.72	0.73	0.86	0.61	1.00	0.75	1.18	1.40	1.03
	0.84	1.30	0.90	0.88	1.20	1.60	0.60	1.46	1.00	1.67
	0.45	0.93	0.84	0.87	0.83	1.15	0.25	1.63	0.99	0.80
	0.45	1.23	0.88	0.85	0.93	1.32	0.48	1.62	1.51	1.18
	8.89	1.61	0.88	0.97	1.29	1.48	0.62	1.42	1.16	1.33
	1.35	1.20	0.97	0.91	0.78	1.25	0.61	1.06	1.05	1.41
	0.71	2.68	1.01	0.65	0.83	0.73	0.46	0.96	0.13	1.64
	2.10	1.15	0.92	0.77	0.78	1.54	1.09	0.84	0.28	1.41

Table C.37. The effect of muscle gp130 loss on mitochondrial content, function, and quality control in MIN mice

Geno	RCR
Flox	6.1929
	7.1706
	7.2879
	7.3543
MIN Flox	5.7639
	2.9933
	3.0492
	5.7062
	3.275
MIN KO	8.9278
	7.707
	5.3497
	6.7902

Table C.38. Mouse body composition and behavior pre- and post-wheel access

Treatment	geno	12 Wk Body Weight	12 Wk Food Intake	12 Wk Lean Mass	12 Wk Fat mass	12 Wk Fat %
Control	B6	23.8	3.33	18.2	2.1	10.4
		23.7	3.62	17.6	3.2	15.3
		25.0	3.56	18.6	3.0	13.9
		24.0	4.00	18.1	2.7	12.9
		23.5	3.62	18.3	2.5	11.9
		23.6	3.78	18.1	2.8	13.3
		24.1	3.72	19.0	2.6	12.2
		24	3.46	17.8	2.6	12.8
		22.8	3.8	17.2	2.6	13.2
		21.5	3.76	15.7	2.5	13.8
Wheel	B6	23.3	3.78	17.6	2.4	12.2
		23.5	3.86	18.0	2.8	13.7
		23.9	3.38	18.3	2.4	11.5
		24.8	3.98	17.9	2.7	12.9
		22.6	4.18	17.4	2.4	12.0
		23.9	3.30	18.1	2.4	11.7
		23.8	3.02	18.2	2.6	12.3
		24.5	3.74	17.5	3.5	16.6
		24.1	4.24	18.1	2.5	12.1

Treatment	geno	12 Wk Body Weight	12 Wk Food Intake	12 Wk Lean Mass	12 Wk Fat mass	12 Wk Fat %
Control	Min	22.7	3.00	18.1	2.3	11.3
		24.2	3.07	19.3	2.8	12.6
		21.7	3.73	18.6	2.2	10.6
		21.5	3.90	15.9	2.4	13.1
		24.0	3.83	17.9	2.5	12.2
		26.6	4.39	20.3	3.4	14.3
		23.2	3.63	17.1	2.5	12.7
		23.1	3.88	17.8	2.4	11.8
		23.4	3.77	17.3	2.7	13.4
		22.4	5.13	16.9	1.8	9.8
Wheel	Min	23.2	2.93	18.8	2.4	11.2
		20.7	3.73	16.5	2.4	12.6
		21.8	3.26	16.9	2.2	11.8
		23.5	3.74	18.3	2.5	12.0
		23.7	3.86	18.2	2.6	12.4
		23.9	4.06	19.0	2.3	10.7
		22.8	4.30	17.9	2.1	10.7
		23.5	4.25	18.1	2.4	11.7
		20.3	3.56	15.7	2.3	12.7
		22.4	3.38	16.9	2.7	13.7

Table C.39. Mouse body composition and behavior pre- and post-wheel access

Treatment	geno	18 Wk Body Weight	18 Wk Food Intake	18 Wk Lean Mass	18 Wk Fat Mass	18 Wk Fat %
Control	B6	25.5	3.88	19.2	3.1	14
		25.6	4.08	19	2.6	12.1
		27.8	4.24	20.4	3.4	14.3
		26.9	3.96	19.5	3.2	14.2
		26	3.20	19.6	2.9	13.1
		25.2	3.57	19.5	2.9	13
		26.0	4.35	20.2	2.5	11.1
		25.7	4.33	19.6	2.6	11.6
		24.6	4.17	18.6	2.5	12
		22.3	4.13	17.3	2.3	11.6
Wheel	B6	24.5	4.25	19.6	2.5	11.4
		25.1	4.42	19.4	2.0	9.3
		25.3	4.53	20.0	2.1	9.7
		26.2	4.65	19.5	2.4	11.1
		24.7	5.10	19.4	2	9.5
		24.9	4.90	19.2	2.4	10.9
		24.4	4.50	19.2	2.6	12.1
		25.3	4.19	19.3	2.1	10
		26.6	4.29	20.2	2.6	11.2

Treatment	geno	18 Wk Body Weight	18 Wk Food Intake	18 Wk Lean Mass	18 Wk Fat Mass	18 Wk Fat %
Control	Min	22.7	4.98	17	2.5	12.8
		23.9	3.80	19.5	1.8	8.6
		25.5	3.94	17.9	2.7	13.1
		23.5	3.40	17.9	2.9	13.9
		25.1	3.46	18.6	3.0	13.7
		22.7	3.75	19.5	1.8	8.3
		24.3	3.41	18.5	3.3	15.2
		25.1	3.37	18.5	3.0	13.8
		24.2	3.47	18.3	2.8	13.2
		19.9	3.10	14.7	1.4	8.7
Wheel	Min	21.5	3.20	16.7	1.9	10.3
		23.9	3.86	17.8	3.1	14.7
		25.8	3.04	19.1	2.8	12.7
		26.6	4.10	19.7	2.5	11.1
		26.0	4.07	20.2	3.0	12.9
		26.2	4.10	22.0	2.3	9.7
		24.5	3.63	20.0	2.5	11.2
		25.5	4.50	18.9	2.9	13.5
		20.4	4.27	16.5	2.0	10.7
		23.8	4.10	20.1	2.4	10.7

Table C.40. Functional characteristics pre- and post-wheel access

Treatment	geno	12 Wk Cage Activity	12 Wk Time to Fatigue	12 Wk Grip Strength	12 Wk G.S. / BW	12 Wk Rotorod
Control	B6	16028.1	72	2.54	0.1090	34.83
		16624.3	56	2.64	0.1103	83.07
		16201.1	95	2.61	0.1043	64.07
		18612.1	80	2.48	0.1035	72.97
		13415.3	68	2.49	0.1065	75.90
		26947.4	88	2.41	0.1010	54.37
		22177.9	72	2.67	0.1074	62.23
		23890.0	66	2.64	0.1075	54.93
		21790.3	90	2.47	0.1073	66.3
		18841.9	92	2.26	0.1054	45.9
Wheel	B6	23982.6	106	2.24	0.0962	79.27
		20668.1	70	2.62	0.1094	21.80
		24214.4	90	2.66	0.1104	67.67
		23861.9	77	2.63	0.1059	72.30
		21664.4	55	2.29	0.1014	67.67
		16205.1	52	2.52	0.1056	70.40
		13426.6	95	2.56	0.1062	72.50
		17209.4	82	2.65	0.1083	46.30
		15374.0	90	2.07	0.0869	60.60

Treatment	geno	12 Wk Cage Activity	12 Wk Time to Fatigue	12 Wk Grip Strength	12 Wk G.S. / BW	12 Wk Rotorod
Control	Min	15528.6	77	2.34	0.1011	55.87
		18880.6	65	2.15	0.0894	58.87
		18014.5	70	2.29	0.1058	62.43
		14179.6	92	2.25	0.1018	46.07
		21998.7	78.8	2.51	0.1084	61.28
		13558.8	50	3.01	0.1133	45.73
		22360.8	89	2.66	0.1176	81.67
		35885.6	122	2.65	0.1158	55.53
		38872.3	90	2.62	0.1118	88.33
		20707.3	54	2.66	0.1186	57.00
Wheel	Min	15001.1	75	2.46	0.1067	30.97
		37668.6	110	2.42	0.1167	61.97
		11359.3	78	2.08	0.0947	42.77
		21139.7	50	2.46	0.1051	58.83
		34789.3	92	2.35	0.0988	38.23
		26059.0	75	2.28	0.0962	33.93
		30596.9	85	2.23	0.0982	35.43
		16312.4	61	2.42	0.1030	57.37
		22995.6	45	2.16	0.1065	95.83
		18403.9	71	2.47	0.1090	108.4

Table C.41. Functional characteristics pre- and post-wheel access

Treatment	geno	18 Wk Cage Activity	18 Wk Time to Fatigue	18 Wk Grip Strength	18 Wk G.S. / BW	18 Wk Rotorod
Control	B6	22976.2	91	2.70	0.1037	60.2
		25272.5	88	2.66	0.1036	115.6
		19284.0	84	2.73	0.1002	73.3
		27680.8	82	2.88	0.1088	66.5
		31720.8	69	2.62	0.1026	81.0
		15151.7	90	2.85	0.1109	58.6
		24026.6	73	2.92	0.1131	69.7
		29384.4	86	3.14	0.1259	61.7
		32627.0	93	3.11	0.1278	87.0
		35762.0	110	3.01	0.1342	93.5
Wheel	B6	32350.8	180	2.82	0.1133	42.6
		18435.2	165	2.95	0.1193	52.1
		39396.2	180	2.91	0.1138	77.4
		27625.7	185	2.86	0.1112	78.1
		34113.0	142	2.71	0.1107	89.0
		22130.0	175	2.83	0.1115	77.9
		37567.3	61	2.74	0.1121	104.7
		41240.0	115	2.50	0.0989	55.5
		40416.7	175	2.73	0.1027	50.5

Treatment	geno	18 Wk Cage Activity	18 Wk Time to Fatigue	18 Wk Grip Strength	18 Wk G.S. / BW	18 Wk Rotorod
Control	Min	4292.6	19	2.46	0.1069	120.7
		2762.4	24	2.27	0.0935	53.8
		16894.0	49	2.63	0.1030	68.5
		24144.8	87	2.59	0.1073	89.3
		3561.4	46	2.52	0.1033	33.9
		3203.0	39	2.11	0.0930	44.7
		18602.3	47	2.38	0.0974	81.6
		28991.0	37	2.51	0.1035	82.4
		23562.0	53	2.55	0.1073	94.3
		316.3	7	1.54	0.0847	21.0
Wheel	Min	2241.2	17	2.17	0.1021	67.4
		21137.4	120	2.49	0.1072	68.9
		16875.3	72	2.67	0.1054	84.7
		12224.3	160	2.84	0.1117	61.1
		16121.3	162	2.49	0.0994	60.9
		12607.7	116	2.85	0.1105	70.2
		12463.3	90	2.92	0.1207	68.3
		19568.3	60	2.64	0.1033	67.6
		6349.7	61	2.20	0.1081	95.9
		20973.0	141	2.59	0.1051	76.8

Table C.42. The effect of wheel access on the characteristic data of MIN and B6 mice

Treatment	geno	Age	Peak Weight	current weight	Pre-Fast Sac BW	current loss
Control	B6	18.3	25.8	25.8	25.5	-1.2%
		19.4	25.9	25.7	25.6	-1.2%
		19.7	27.6	27.3	27.8	0.7%
		19.7	26.8	26.3	26.9	0.4%
		20.7	26.0	26.0	26.0	0.0%
		19.7	25.7	25.7	25.2	-1.9%
		19.0	26.0	25.7	26.0	0.0%
		20.1	26.2	25.7	25.7	-1.9%
		19.9	24.7	24.6	24.6	-0.4%
		19.9	22.9	22.3	22.3	-2.6%
Wheel	B6	20.3	25.4	25.2	24.5	-3.5%
		20.0	25.2	25.6	25.1	-0.4%
		20.0	26.5	25.6	25.3	-4.5%
		19.7	26.1	26.2	26.2	0.4%
		19.7	24.3	24.7	24.7	1.6%
		19.7	25.4	24.9	24.9	-2.0%
		19.7	24.5	24.8	24.8	1.2%
		19.7	25.9	25.6	25.6	-1.2%
		19.7	26.6	26.3	26.3	-1.1%

Treatment	geno	Age	Peak Weight	current weight	Pre-Fast Sac BW	current loss
Control	Min	18.7	24.3	22.7	22.5	-7.4%
		18.7	24.8	23.9	24.5	-1.2%
		18.7	25.5	25.5	25.1	-1.6%
		19.0	23.7	23.5	23.5	-0.8%
		18.6	25.1	25.1	24.5	-2.4%
		20.1	26.7	21.9	21.9	-18.0%
		20.3	24.8	24.3	25.4	2.4%
		20.3	25.1	25.1	25.2	0.4%
		18.9	24.4	24.2	24.2	-0.8%
		18.9	22.9	19.1	19.1	-16.6%
Wheel	Min	18.4	24.6	21.2	21.5	-12.6%
		18.4	24.0	24	23.9	-0.4%
		19.4	25.8	25	25.8	0.0%
		19.0	26.6	25.9	26.6	0.0%
		19.7	26.0	26.0	26.0	0.0%
		19.7	26.6	26.6	26.2	-1.5%
		19.7	24.5	24.2	24.5	0.0%
		19.7	25.5	25.5	25.5	0.0%
		20.0	21.9	20.4	20.4	-6.8%
		20.0	25.6	24.6	23.8	-7.0%

Table C.43. The effect of wheel access on the characteristic data of MIN and B6 mice

Treatment	Geno	Tibia	Hind limb	Hindlimb/Tibia	Epi Fat	Spleen	Testes	Sem Ves
Control	B6	17.05	298	17.5	264	74	185	280
		17.00	317	18.6	255	73	209	290
		17.00	353	20.8	360	80	209	331
		17.10	324	18.9	288	70	198	351
		16.80	303	18.0	309	78	187	329
		16.95	298	17.6	221	79	195	264
		17.1	316	18.5	294	73	188	298
		17.05	303	17.7	178	64	205	313
		16.95	311	18.3	187	66	183	307
		16.80	274	16.3	191	54	170	289
Wheel	B6	16.95	302	17.8	208	76	213	285
		17.00	314	18.4	178	59	193	250
		17.15	336	19.6	197	60	193	262
		17.20	319	18.5	183	55	197	282
		17.10	318	18.6	117	103	191	233
		17.20	313	18.2	125	63	195	220
		17.10	310	18.1	245	76	203	260
		17.05	322	18.9	224	56	208	266
		17.20	340	19.7	253	66	204	290

Treatment	Geno	Tibia	Hindlimb	Hindlimb/ Tibia	Epi Fat	Spleen	Testes	Sem Ves
Control	Min	16.90	242	14.3	57	353	181	124
		17.00	246	14.5	54	502	188	84
		16.60	285	17.1	220	210	190	222
		16.7	283	16.9	201	179	183	155
		16.90	300	17.8	171	372	202	196
		17.00	233	13.7	0	289	147	50
		16.75	304	18.1	288	177	200	220
		17.20	304	17.7	229	435	205	204
		16.90	298	17.6	156	315	191	225
		16.40	167	10.2	0	297	106	35
Wheel	Min	17.00	226	13.3	0	342	149	40
		16.80	274	16.3	173	265	185	280
		16.70	308	18.4	193	199	187	343
		17.25	316	18.3	138	189	190	210
		17.10	272	15.9	185	237	201	205
		17.10	313	18.3	154	351	211	239
		16.75	295	17.6	121	383	179	164
		17.00	313	18.4	168	253	203	249
		16.40	206	12.6	42	305	137	85
		16.70	309	18.5	164	269	191	191

Table C.44. The effect of wheel access on skeletal muscle's contractile properties in the MIN and B6

Geno	Treatment	TA	Lo	1/2 RT	TPT	-dP/dt	+dP/dt
B6	Control	49.5	14.5	8.2	14.3	17205.9	22550.5
		52.0	14.0	7.2	15.0	16525.8	21396.6
		53.5	14.5	8.0	16.6	11816.5	25134.6
		51.0	14.0	6.7	15.4	17804.7	28989.3
		48.5	14.0	7.6	14.9	25886.2	24339.4
		46.0	14.0	7.4	14.4	18734.1	18553.0
		48.0	14.5	7.2	15.5	23102.8	24273.7
		47.5	14.5	7.7	15.4	16915.1	27002.9
		49.5	14.0	6.3	14.6	14301.7	25054.3
		44.0	14.0	6.5	14.6	13195.4	22950.6
B6	Wheel	45.0	13.5	7.3	15.9	12637.8	20704.8
		48.0	14.5	8.1	14.7	17758.6	18858.6
		50.5	14.0	7.4	13.3	20159.1	23443.6
		50.5	15.0	7.7	14.8	21926.7	24893.4
		46.5	14.0	7.4	14.8	19352.0	25188.1
		47.5	15.0	8.0	15.1	23074.1	25148.5
		47.0	14.5	7.6	14.7	20135.2	20113.2
		48.0	14.0	7.5	15.1	22285.3	21824.2
		53.0	14.5	6.7	14.5	19966.8	28596.2

Geno	Treatment	TA	Lo	1/2 RT	TPT	-dP/dt	+dP/dt
Min	Control	41.0	14.5	9.1	16.6	18649.3	18754.1
		40.0	14.0	8.8	15.9	10469.5	24772.9
		45.0	14.0	8.3	16.6	16022.1	15937.7
		44	13	15.2	17.6	17445.5	20633.5
		47.5	13.5	8.4	15.2	9274.4	29960.3
		36.0	13.0	9.7	16.6	9091.8	12842.9
		44.5	14.5	8.8	14.9	15343.1	24668.5
		47	14.5	7.0	15.1	11664.6	26941.3
		48	14	6.4	14.6	12838.8	23085.8
		27.0	13.5	12.5	19.2	4576.0	8595.9
Min	Wheel	32.0	15.0	20.2	28.5	1556.0	10377.4
		43.5	14.5	11.3	15.9	14983.3	21026.9
		48.0	14.5	8.6	16.0	13028.6	24308.5
		49.0	14.0	8.6	16.8	10720.7	28287.1
		48.5	14.5	6.8	14.6	23360.1	22856.5
		45.0	15.0	11.2	16.5	13708.2	18251.9
		44.0	14.5	7.1	14.8	13176.1	19037.7
		47.0	14.0	7.5	16.6	13501.5	25049.2
		34.0	13.5	11.7	19.8	14119.8	15440.5
		50	14.5	10.3	16.8	12746.1	25285.2

Table C.45 The effect of free wheel access on body weight, polyp size, and plasma IL-6

Treatment	Geno	11	12	13	14	15	16	17	18	19
Control	B6	22.9	23.8	23.3	23.3	23.5	24.5	25.1	25.8	25.5
		23.7	23.7	23.5	24.0	24.5	24.8	25.1	25.9	25.7
		25.0	25.0	24.5	25.0	24.8	26.3	26.7	27.6	27.3
		24.0	24.0	24.4	24.1	24.6	25.0	25.5	26.8	26.3
		24.0	23.5	23.4	24.1	24.2	24.5	24.3	24.7	26.0
		22.5	23.6	23.6	24.1	24.4	25.0	25.7	25.1	25.7
		24.1	24.1	23.9	24.1	23.8	25.0	25.3	25.8	26.0
		24.4	24.0	23.6	24.3	23.8	24.8	24.9	26.2	25.7
		22.7	22.8	22.2	22.7	22.6	23.6	23.8	24.7	24.3
		21.3	21.5	21.2	21.8	22.0	22.1	22.2	22.9	22.4
Wheel	B6	23.5	23.3	23.7	23.7	24.1	23.7	24.7	25.4	25.0
		24.2	23.5	24.1	24.1	24.0	24.7	25.2	25.1	25.2
		24.6	23.9	24.4	24.5	25.3	25.0	25.4	25.6	26.5
		23.9	24.3	24.5	24.1	26.1	25.1	25.7	25.3	25.3
		21.9	22.5	22.5	22.5	23.4	23.3	23.6	24.3	24.3
		22.8	23.4	23.4	23.7	24.3	24.8	25.4	25.1	25.1
		21.9	22.5	22.5	22.6	23.3	23.2	23.6	24.5	24.4
		24.2	23.5	24.1	24.3	24.1	24.7	24.2	25.9	25.3
		24.6	23.9	24.4	24.5	24.5	25.5	25.7	26.5	26.6

Treatment	Geno	11	12	13	14	15	16	17	18	19
Control	Min	23.5	22.7	22.7	22.7	24.3	24.2	23.4	22.7	22.5
		24.4	24.2	24.4	24.4	24.6	24.8	24.7	23.9	24.5
		21.3	21.7	22.0	22.0	23.5	24.5	25.1	25.5	25.1
		21.9	21.5	21.3	21.3	23.0	23.5	23.7	23.5	23.5
		23.9	24.0	24.4	24.8	25.1	24.8	22.5	25.1	24.5
		25.0	26.0	26.4	26.7	26.4	25.1	23.7	22.7	21.9
		22.5	23.2	22.6	23.1	23.0	23.4	23.8	24.4	24.8
		22.9	23.1	22.9	22.9	23.4	23.9	23.7	24.3	25.1
		23.4	23.1	22.9	22.8	23.1	23.8	24.4	24.2	24.2
		22.4	21.1	20.2	19.6	19.1	19.1	19.1	19.1	19.1
Wheel	Min	23.7	23.2	23.3	23.3	24.6	24.5	21.9	21.2	21.5
		21.0	20.7	21.5	21.5	22.8	23.0	22.5	24.0	23.9
		22.1	21.8	22.1	23.3	23.7	24.1	24.7	25.0	25.8
		22.9	23.5	24.0	24.5	24.7	24.9	25.4	25.9	26.6
		23.0	23.7	24.0	23.9	24.9	24.5	25.1	26.0	26.0
		23.5	23.9	24.0	24.4	25.7	25.4	25.8	26.6	26.2
		22.1	22.8	23.2	23.2	24.2	24.2	24.2	24.2	24.5
		22.5	23.5	23.6	23.7	24.0	25.4	25.3	25.5	25.5
		20.2	20.3	21.0	21.3	21.0	21.9	19.2	20.2	20.4
		22.4	22.4	22.6	23.0	24.0	24.5	24.4	25.6	24.6

Table C.46 The effect of free wheel access on body weight, polyp size, and plasma IL-6

Treatment	Geno	Intestines Total	<1mm Total	1-2mm Total	>2mm Total	Plasma IL-6
Control	Min	103	5	23	75	11.7
		114	5	8	99	61.5
		87	17	25	44	7.8
		93	9	23	61	7.8
		99	0	13	86	7.8
		133	2	19	110	109.0
		55	0	13	42	11.8
		59	0	9	50	23.0
		72	4	11	57	14.6
		96	0	0	95	40.6
Wheel	Min	112	2	10	98	84.4
		101	16	21	64	27.0
		95	27	26	41	7.8
		68	7	8	53	7.8
		87	8	16	62	25.0
		90	4	5	79	37.0
		101	12	11	77	7.8
		94	2	31	60	70.5
		70	0	1	67	40.1
		87	1	26	58	18.3

Table C.47 The effect of free wheel access on body weight, polyp size, and plasma IL-6

		Average Time Per Day Per Week				
Treatment	**Geno**	**1**	**2**	**3**	**4**	**5**
Wheel	B6	141.0	148.8	174.1	147.3	161.3
		142.6	159.0	159.3	139.8	150.1
		125.4	185.2	86.3	101.6	62.9
		106.3	145.3	150.0	235.3	236.8
		43.9	191.6	110.0	105.4	124.4
		101.1	129.7	132.8	153.1	139.4
		134.0	168.5	162.0	130.3	154.6
		156.0	168.0	201.0	139.0	160.6
		121.5	169.5	212.2	197.1	150.7
Wheel	Min	107.0	87.9	71.4	53.1	7.6
		108.0	231.3	281.3	263.3	183.4
		58.3	41.0	67.0	106.9	70.4
		85.2	114.5	112.9	111.3	59.4
		170.6	246.8	183.3	132.0	28.6
		76.0	111.5	160.3	158.4	121.9
		126.4	151.0	134.0	132.0	87.1
		153.7	42.8	55.6	38.7	35.7
		131.0	22.4	150.0	220.8	91.3
		60.9	67.7	132.6	107.1	76.7

Table C.48 The effect of free wheel access on skeletal muscle force production in the male MIN

Geno	Treatment	10	30	50	80	100	120	150	180	200
B6	Control	291	291	428	1008	1287	1443	1508	1504	1477
		311	342	481	1067	1258	1289	1379	1335	1404
		305	330	501	1140	1288	1280	1400	1335	1375
		298	334	472	1140	1481	1613	1649	1631	1621
		330	364	517	1162	1407	1645	1582	1702	1727
		274	288	431	990	1287	1298	1388	1443	1360
		336	416	649	1254	1535	1559	1705	1744	1733
		333	519	492	1156	1411	1510	1528	1654	1655
		256	265	478	1032	1320	1429	1507	1541	1513
		282	261	371	1017	1225	1358	1321	1373	1310
B6	Wheel	279	340	436	1071	1217	1326	1355	1439	1462
		302	385	570	1022	1302	1523	1605	1511	1437
		267	282	375	1082	1353	1449	1522	1404	1538
		376	440	579	1312	1575	1676	1670	1667	1785
		261	322	569	1115	1429	1555	1640	1661	1678
		342	479	645	1166	1388	1573	1666	1733	1781
		199	247	344	920	1211	1452	1526	1545	1554
		273	334	472	974	1238	1330	1456	1649	1676
		305	318	597	1093	1324	1484	1668	1687	1747

Geno	Treatment	10	30	50	80	100	120	150	180	200
Min	Control	298	349	569	1109	1297	1359	1350	1455	1453
		323	312	476	830	882	1197	1270	1294	1306
		204	266	303	728	1180	1252	1289	1360	1221
		346	437	547	981	1193	1308	1389	1410	1354
		321	345	557	1202	1324	1384	1401	1423	1417
		292	298	600	842	896	925	972	961	920
		300	420	655	1195	1369	1499	1492	1583	1606
		294	477	687	1031	1144	1282	1444	1486	1455
		233	352	439	944	1155	1235	1290	1297	1284
		241	364	558	634	662	687	671	635	535
Min	Wheel	302	570	744	788	769	777	744	742	741
		265	311	370	898	1084	1148	1253	1295	1272
		317	356	501	1271	1445	1550	1575	1590	1592
		314	368	538	1152	1345	1425	1494	1524	1508
		295	366	487	1084	1340	1471	1621	1713	1759
		290	255	348	813	1149	1131	1187	1218	1217
		232	263	411	949	1038	1105	1202	1207	1247
		299	328	504	1119	1362	1444	1467	1395	1390
		171	217	345	767	973	1066	1104	1146	1166
		268	358	457	1021	1244	1364	1501	1464	1403

Table C.49 The effect of free wheel access on skeletal muscle force production in the male MIN

Geno	Treatment	10	30	50	80	100	120	150	180	200
B6	Control	54	54	79	187	239	268	280	279	274
		53	58	82	182	215	220	235	228	239
		52	57	86	196	221	220	240	229	236
		52	58	82	198	258	281	287	284	282
		60	67	95	213	257	301	289	311	316
		53	56	83	191	248	250	268	278	262
		64	80	124	240	294	298	326	334	332
		64	100	95	224	273	292	296	320	320
		46	48	86	185	237	256	270	276	271
		57	53	75	205	247	274	266	277	264
B6	Wheel	53	65	83	204	231	252	258	274	278
		58	74	109	196	249	292	307	289	275
		47	50	66	190	238	255	267	247	270
		71	83	109	247	296	315	314	314	336
		50	61	109	213	273	297	313	317	320
		68	96	129	233	278	315	333	347	356
		39	48	67	180	237	284	298	302	304
		50	62	87	180	229	246	269	305	310
		53	55	103	189	230	257	289	292	303

Geno	Treatment	10	30	50	80	100	120	150	180	200
Min	Control	67	78	127	248	291	304	302	326	326
		72	69	106	184	196	266	282	287	290
		40	52	60	144	233	247	254	268	241
		65	82	102	184	223	245	260	264	253
		58	62	100	217	238	249	252	256	255
		67	68	137	193	205	212	222	220	210
		62	87	135	247	283	309	308	327	332
		57	93	134	201	224	251	282	291	284
		43	65	81	174	214	228	238	240	237
		76	115	177	201	210	218	213	201	169
Min	Wheel	90	169	221	234	228	231	221	220	220
		56	66	78	190	229	242	265	273	269
		61	68	96	243	277	297	302	304	305
		57	67	97	209	244	258	271	276	273
		56	69	92	205	254	279	307	324	333
		61	54	73	172	243	239	251	257	257
		48	55	86	198	217	231	251	252	260
		56	62	95	211	257	273	277	263	262
		43	55	87	193	245	268	278	288	293
		49	66	84	188	229	251	276	269	258

Table C.50. The effect of free wheel access on skeletal muscle fatigability in the male MIN

Geno	Treatment	0	5	10	15	20	25	30	35	40	45	50
B6	Control	287	241	292	376	434	401	450	499	528	541	546
		278	252	284	316	377	424	453	481	507	522	526
		392	330	385	481	513	531	551	542	542	536	511
		340	305	346	414	519	587	611	626	640	638	651
		291	260	296	308	353	387	424	460	485	497	501
		330	258	286	327	370	392	452	480	527	551	575
		505	439	482	558	636	648	675	664	689	649	649
		391	337	394	497	591	643	668	683	691	695	687
		326	245	273	296	380	398	424	437	498	555	604
		320	311	354	436	530	589	625	650	672	680	672
B6	Wheel	373	326	363	449	525	563	577	595	605	596	593
		366	305	376	444	489	518	537	557	543	560	552
		373	303	339	403	445	487	520	549	571	588	596
		389	342	392	457	560	625	660	686	709	730	740
		414	337	367	411	485	537	567	590	608	620	627
		417	346	400	490	566	615	658	701	736	751	752
		279	253	277	309	349	394	425	439	443	437	424
		305	262	286	325	396	472	514	550	579	594	624
		344	310	308	322	324	387	366	457	473	477	488

55	60	65	70	75	80	85	90	95	100	105	110
540	527	503	476	444	406	368	339	308	286	263	246
515	499	467	442	416	392	370	353	337	325	315	306
481	476	433	425	403	381	361	345	339	319	316	308
616	593	577	532	518	493	463	454	423	403	398	381
495	487	470	445	427	406	387	370	352	335	323	308
582	577	563	548	528	502	477	451	425	403	387	362
635	638	585	566	545	515	473	447	416	463	385	438
668	633	597	560	526	495	469	449	428	409	390	385
633	635	620	595	557	515	482	447	415	391	365	349
644	605	565	529	500	477	452	436	419	407	396	384
583	555	526	493	463	433	412	391	377	367	354	348
522	505	504	465	403	364	362	364	339	315	313	286
597	593	584	567	548	523	502	482	466	454	443	436
741	730	708	679	643	604	564	526	493	464	440	422
621	608	581	549	510	474	441	418	395	382	367	359
739	715	687	652	614	576	534	497	464	432	405	385
403	376	351	328	308	291	277	259	243	238	225	221
607	588	564	541	517	483	455	424	395	374	354	331
463	462	428	384	393	375	356	344	321	302	286	279

115	120	125	130	135	140	145	150	155	160	165	170	175
237	227	223	217	211	207	204	202	195	194	192	187	187
294	289	277	266	264	251	246	240	233	229	223	218	216
287	288	290	289	269	279	262	258	247	249	248	244	243
373	364	356	351	343	335	333	326	307	304	292	287	284
295	283	274	264	255	246	243	236	231	228	223	219	218
348	328	311	305	292	279	272	266	264	256	259	245	242
375	367	372	354	376	351	348	343	327	339	319	311	310
372	367	362	353	353	341	343	341	337	337	331	330	323
335	324	317	308	300	295	289	281	271	267	259	257	251
374	369	360	353	348	343	337	334	328	327	320	323	318
342	336	331	325	321	317	314	309	306	303	300	298	294
287	274	276	275	269	260	259	247	241	233	229	218	216
425	424	415	410	403	400	395	390	386	381	378	372	367
406	395	380	373	362	355	348	338	333	325	319	311	307
348	340	331	323	315	310	304	297	291	287	281	274	273
365	347	334	318	307	299	289	282	275	267	261	256	251
220	203	196	194	190	182	180	171	170	168	163	161	158
319	302	289	279	270	258	252	245	237	233	225	222	221
269	252	241	216	229	218	233	212	209	198	214	205	184

180	185	190	195	200	205	210	215	220	225	230	235	240
182	180	180	177	178	174	171	169	168	164	165	162	160
215	209	208	210	202	203	205	198	195	197	197	193	189
239	256	234	223	233	226	223	218	218	216	216	214	205
291	276	278	273	266	262	259	249	252	256	252	243	241
216	214	209	207	206	204	201	199	199	194	195	193	189
247	243	240	226	238	227	226	226	219	225	220	213	224
299	297	294	293	286	280	278	275	269	263	255	259	254
321	319	315	310	308	304	300	295	295	292	286	285	283
244	240	236	232	224	220	217	208	208	204	201	198	194
317	311	306	303	300	296	294	287	291	290	286	285	280
294	288	289	285	281	280	275	274	271	269	262	261	258
206	202	199	210	192	194	201	197	198	189	183	180	180
363	361	357	355	348	345	343	339	336	335	327	324	326
299	294	288	282	278	274	267	262	260	254	249	246	240
269	263	257	251	246	242	238	231	229	224	222	216	214
247	241	235	234	232	231	226	226	225	223	223	220	218
191	155	154	151	155	155	145	146	146	141	142	146	138
211	211	209	206	210	202	209	199	201	199	201	198	196
187	239	227	197	236	236	233	229	229	227	211	230	204

245	250	255	260	265	270	275	280	285	290	295	300
158	156	154	155	153	151	148	149	146	149	145	139
192	186	185	186	186	180	178	181	179	179	175	171
211	207	206	202	202	200	198	194	192	192	189	188
232	236	226	236	216	220	217	213	214	227	204	205
191	189	187	183	187	184	183	177	178	175	174	172
210	211	210	206	207	219	206	208	214	200	214	210
264	249	241	244	236	235	231	232	231	236	222	231
276	268	268	266	262	268	264	258	257	250	245	244
191	190	184	184	180	179	174	175	172	171	170	169
281	279	277	273	270	269	266	264	262	258	257	256
257	255	253	258	254	244	243	240	236	236	234	232
180	179	169	177	175	176	175	177	175	169	173	169
316	308	313	310	301	295	303	290	294	280	284	275
237	234	231	226	224	223	223	219	217	217	212	214
215	211	211	211	207	207	207	202	201	201	201	199
217	217	216	217	222	213	212	210	209	210	208	208
138	140	142	137	139	138	135	135	133	133	133	136
197	196	190	190	189	186	188	184	184	183	181	181
228	225	225	220	215	218	216	215	209	209	209	191

300	305	310	315	320	325	330	335	340	345	350	355	360
552	445	428	423	416	412	398	400	396	390	387	382	382
762	697	681	669	653	648	640	635	633	631	623	627	624
625	529	511	510	470	498	497	484	480	470	466	470	462
811	701	689	667	665	653	646	628	623	626	624	604	620
929	889	831	798	782	768	747	739	728	724	719	716	712
895	836	746	713	694	668	664	659	655	656	646	640	636
851	735	692	662	655	634	920	897	877	862	843	815	806
794	685	670	659	645	641	637	627	624	621	618	618	606
795	697	685	677	668	652	646	640	635	632	622	619	615
744	673	666	655	648	637	629	626	615	611	601	602	595
730	646	635	624	611	590	591	588	582	576	584	577	577
690	627	599	594	572	558	556	551	544	537	542	534	535
912	826	793	782	753	739	728	715	710	703	695	689	689
1060	925	893	865	840	815	803	789	780	771	763	756	755
1006	837	804	781	752	738	711	702	694	680	675	669	668
1050	916	871	824	798	777	762	747	743	727	728	722	718
649	562	540	521	501	490	479	474	467	460	454	454	453
973	857	819	784	754	736	721	709	701	695	687	685	677
923	766	731	688	597	728	583	571	548	620	542	613	604

365	370	375	380	385	390	395	400	405	410	415	420	425
373	373	367	375	374	371	363	366	362	338	359	354	355
618	622	616	615	615	611	615	613	606	610	609	607	609
460	461	446	454	459	459	465	440	449	455	458	457	441
617	603	608	599	615	604	602	599	606	602	599	595	580
712	709	703	706	707	707	706	704	704	702	703	702	700
637	635	641	633	633	636	634	634	634	635	636	633	639
773	755	610	632	635	810	621	607	610	611	613	627	658
608	611	616	605	616	610	607	602	615	612	604	606	605
610	609	605	605	596	593	595	592	591	591	587	586	584
590	583	580	578	572	574	574	566	567	564	564	552	560
573	574	564	563	559	569	553	555	556	552	550	551	552
529	529	528	529	529	528	538	522	523	523	523	522	518
683	689	675	674	668	663	661	663	663	663	656	659	656
749	749	744	742	738	738	736	741	735	729	729	728	726
661	663	657	653	651	645	646	643	642	642	635	638	635
712	715	716	715	703	705	705	704	703	703	706	706	706
448	447	449	451	448	446	444	442	439	443	443	435	440
676	677	678	673	673	671	670	665	667	666	664	659	660
595	592	583	581	566	561	564	566	568	555	552	566	553

430	435	440	445	450	455	460	465	470	475	480	485	490
351	359	346	347	347	335	333	331	329	342	326	321	329
597	602	604	600	598	600	598	595	596	596	596	592	594
451	448	450	450	441	436	434	444	434	442	407	436	431
585	588	588	591	577	588	587	598	588	585	587	578	583
698	694	697	695	694	693	692	692	691	690	690	687	688
638	637	631	637	634	640	639	638	634	635	636	637	638
655	656	624	626	634	638	639	620	655	622	634	631	603
604	601	605	601	594	599	602	606	598	603	597	596	595
584	576	577	574	577	578	574	571	571	570	571	569	567
558	563	560	558	559	560	558	558	559	555	554	555	554
550	549	550	549	546	547	542	541	538	540	538	544	542
517	516	516	516	511	517	510	510	514	511	509	510	510
655	657	658	648	646	651	650	649	643	655	640	637	637
725	719	725	722	714	716	715	716	713	714	714	711	715
637	639	634	632	629	629	630	633	631	632	630	633	647
702	702	702	700	700	700	695	697	689	693	696	691	690
443	436	435	443	438	434	439	434	432	432	434	436	430
653	655	656	655	653	652	652	651	651	652	649	646	650
556	549	556	549	539	547	536	541	530	527	526	520	524

495	500	505	510	515	520	525	530	535	540	545	550	555
319	322	322	319	319	318	323	314	316	313	310	307	310
598	588	589	591	593	587	591	592	587	588	590	591	581
439	437	440	434	431	438	437	427	421	416	425	429	430
580	578	584	582	575	582	586	571	584	589	578	587	574
688	694	692	690	690	691	691	688	688	688	686	687	687
638	638	640	637	641	635	632	635	635	633	631	637	632
632	636	638	631	607	639	613	616	610	607	611	599	597
604	600	596	595	600	594	593	598	593	599	586	589	590
569	567	564	566	568	569	563	567	564	564	564	558	564
547	549	551	548	548	547	544	544	543	541	544	544	545
539	540	541	530	531	531	531	532	535	535	532	532	531
509	513	511	508	507	510	506	507	505	501	509	506	503
639	635	634	633	630	629	627	631	626	626	623	625	631
712	708	706	707	707	705	701	707	704	703	701	702	697
632	631	632	643	640	635	631	632	627	628	628	631	631
692	682	692	689	690	687	688	686	686	682	682	682	680
436	430	430	431	431	433	431	432	431	432	432	432	434
647	644	648	646	645	643	644	643	639	640	636	635	634
519	517	522	508	504	512	456	495	505	492	500	482	480

560	565	570	575	580	585	590	595	600
310	309	307	305	305	307	305	305	305
588	582	588	580	581	582	584	579	585
425	315	422	426	433	427	424	432	431
563	574	565	575	570	566	577	568	575
684	683	682	680	681	680	679	680	682
637	638	637	632	634	631	632	635	632
608	769	618	612	615	607	626	615	606
594	581	582	584	587	583	584	589	585
563	559	561	558	557	559	555	558	554
535	539	536	542	543	541	540	540	539
530	520	530	522	525	521	525	525	521
508	503	505	500	504	502	503	504	498
629	627	632	630	631	632	642	635	630
699	696	694	692	696	696	696	690	689
634	631	634	628	635	622	630	629	626
683	679	680	681	680	680	679	677	676
429	434	432	427	429	422	427	436	433
639	638	638	640	640	635	638	639	636
478	495	498	490	477	491	472	475	470

Geno	Treatment	0	5	10	15	20	25	30	35	40	45	50
Min	Control	513	404	504	593	641	670	685	685	685	685	681
		560	490	626	693	704	691	667	632	601	561	531
		313	222	240	264	266	298	305	336	336	338	357
		224	177	195	217	232	255	286	297	308	315	321
		494	442	462	493	503	493	475	442	413	373	352
		443	480	479	449	410	373	342	318	299	282	268
		444	323	356	423	515	576	610	629	644	657	662
		458	387	453	571	617	625	623	604	582	555	527
		376	306	344	410	476	505	515	514	510	499	480
		251	225	204	213	203	195	192	154	161	148	150
Min	Wheel	690	673	658	637	620	587	559	515	475	438	407
		322	273	326	410	473	480	507	512	515	517	504
		394	331	365	455	515	525	551	554	545	531	531
		443	339	401	493	546	563	582	586	580	568	559
		400	307	330	346	362	385	419	448	473	494	503
		382	282	316	386	418	449	461	460	475	467	464
		374	272	298	366	428	466	486	497	504	507	505
		492	346	437	530	576	601	614	619	616	605	586
		329	259	282	343	399	428	443	462	481	495	501
		402	319	346	403	465	472	472	466	461	447	432

55	60	65	70	75	80	85	90	95	100	105	110	115
665	650	629	604	575	545	516	488	471	446	432	422	409
503	482	460	443	424	408	395	383	372	361	352	341	334
354	341	340	343	326	315	320	293	288	270	275	260	258
320	314	312	306	295	288	275	264	253	244	233	226	217
332	320	304	298	281	268	266	256	248	241	242	238	231
256	240	228	218	208	204	203	199	194	188	185	182	178
662	647	627	597	561	523	492	460	432	403	388	368	351
494	473	454	432	417	400	384	375	366	352	344	338	336
468	450	430	414	395	380	362	353	339	329	321	312	304
141	126	130	123	117	106	106	93	82	80	73	63	58
380	359	342	329	313	300	284	270	261	250	240	234	224
471	451	431	404	398	381	360	360	345	345	337	328	341
499	460	440	422	414	385	360	363	351	341	338	336	331
529	546	471	448	431	406	385	379	369	361	356	352	347
496	487	470	447	426	404	386	367	352	336	326	311	298
466	452	444	419	415	385	354	354	326	307	297	274	275
494	484	461	451	443	423	413	401	391	377	367	357	351
560	631	502	474	447	426	410	395	387	381	373	368	364
502	498	488	475	460	442	421	400	384	367	349	333	316
413	398	383	372	362	355	353	346	344	338	339	336	332

120	125	130	135	140	145	150	155	160	165	170	175	180
400	394	389	386	382	376	375	372	369	365	362	356	355
328	320	316	312	307	303	301	297	293	292	289	285	284
235	234	237	224	223	224	223	215	211	202	210	209	194
210	202	188	186	181	171	169	162	159	154	150	148	147
227	224	220	210	208	218	215	206	212	213	205	205	203
174	172	169	163	156	151	154	156	157	157	156	147	142
340	328	316	307	298	290	282	278	269	267	261	258	252
329	325	318	317	313	315	310	305	309	303	307	306	300
298	290	284	280	278	275	270	268	265	262	259	256	253
53	54	46	46	40	39	38	48	38	42	42	40	35
217	208	201	194	188	180	175	167	160	153	146	143	138
327	318	318	311	306	306	300	301	293	292	287	284	281
326	324	318	319	314	314	309	309	306	300	304	298	299
343	339	333	333	329	326	322	320	317	313	313	308	306
285	275	265	254	259	252	248	244	238	236	229	227	226
265	260	270	244	242	245	225	220	219	219	209	227	206
342	335	329	328	317	314	311	308	303	300	298	295	293
359	355	348	347	343	339	335	331	327	326	322	318	314
305	294	291	278	269	264	259	261	250	250	241	241	238
332	328	326	323	320	318	315	314	310	308	304	302	300

185	190	195	200	205	210	215	220	225	230	235	240	245
348	345	339	333	329	324	321	315	310	307	302	297	294
280	279	277	276	274	273	271	267	266	267	264	263	259
192	189	182	191	182	181	177	175	176	172	173	187	171
146	142	139	136	134	131	130	128	126	125	119	120	118
202	204	198	200	195	197	195	189	190	187	187	177	184
147	148	150	151	150	150	144	141	144	145	139	140	142
248	244	237	235	230	226	225	221	220	216	213	210	206
303	296	297	293	292	289	289	300	285	285	282	280	279
251	247	244	241	239	237	234	233	229	227	219	221	219
38	38	37	29	32	31	27	28	27	26	26	28	19
131	130	126	123	123	120	118	116	113	112	109	108	106
277	282	272	269	265	275	272	277	263	252	250	249	248
301	297	299	297	291	293	289	288	291	284	286	284	282
306	302	302	300	295	295	291	289	288	284	283	280	277
222	220	216	216	210	213	205	204	201	204	199	200	199
197	199	200	195	191	189	183	185	185	184	175	177	175
290	289	279	286	279	274	273	270	266	264	266	262	256
311	307	306	304	300	297	292	289	285	283	279	276	273
236	231	227	222	220	215	210	204	200	196	198	192	189
297	294	290	288	285	283	279	276	274	273	272	267	263

250	**255**	**260**	**265**	**270**	**275**	**280**	**285**	**290**	**295**	**300**
291	286	282	280	276	274	271	268	266	264	261
261	260	261	257	256	253	252	253	252	249	247
169	168	167	166	162	162	177	161	157	156	154
119	115	116	113	113	112	110	108	107	106	106
181	193	187	185	186	179	177	178	176	172	175
135	132	134	133	131	134	138	139	138	140	139
204	203	201	197	195	191	188	186	185	182	181
278	279	276	276	273	268	271	264	263	267	269
217	216	212	213	210	207	204	202	201	201	199
21	24	19	24	20	20	18	18	16	16	15
106	103	102	102	101	101	101	102	102	102	102
245	241	243	239	247	235	231	240	231	231	228
278	266	267	276	272	272	270	270	266	269	265
274	265	264	268	264	263	260	258	255	256	252
198	197	194	192	194	192	191	189	186	185	187
181	177	175	172	169	164	171	165	166	166	155
256	252	247	246	250	245	242	240	238	236	238
269	265	262	259	256	253	251	247	244	243	239
184	182	180	183	180	177	173	166	168	164	164
261	259	256	255	251	248	245	245	242	239	237

300	305	310	315	320	325	330	335	340	345	350	355	360
861	743	688	644	611	593	570	563	550	542	539	532	527
576	494	489	476	470	464	457	451	443	439	432	431	428
703	636	636	594	579	566	561	550	538	530	525	536	527
576	498	454	436	431	405	393	396	381	374	373	368	365
415	336	324	329	317	311	311	263	265	262	260	270	271
405	347	334	311	295	302	302	301	301	302	300	299	286
940	754	728	693	664	641	621	601	583	571	565	550	544
597	501	497	489	482	479	474	470	466	468	457	453	454
684	581	570	550	536	524	513	509	502	495	494	484	481
16	16	16	16	16	15	15	15	15	14	14	14	14
147	108	106	105	105	102	102	103	109	109	113	115	114
644	558	549	520	527	510	496	489	497	483	470	470	472
574	518	511	501	502	493	501	479	492	488	449	441	456
589	520	513	501	496	489	489	479	481	478	456	452	459
968	865	808	778	752	733	723	708	703	698	694	695	691
621	551	523	512	491	483	462	474	448	440	463	451	424
758	681	663	637	621	602	591	584	571	563	564	555	564
604	522	515	501	491	486	478	478	469	468	463	463	463
793	700	663	630	593	569	546	533	525	512	507	503	502
638	601	583	583	571	567	568	567	558	556	552	547	551

365	370	375	380	385	390	395	400	405	410	415	420	425
523	521	527	525	515	523	532	518	518	518	514	513	517
424	420	417	413	414	409	405	407	403	402	400	401	396
530	520	520	524	524	517	518	544	516	509	512	499	511
369	351	343	357	335	344	342	355	348	341	326	348	345
261	258	261	260	248	252	251	264	252	250	242	261	243
277	295	298	282	277	287	295	292	294	277	295	295	292
540	538	540	534	536	532	527	522	524	526	522	520	516
451	443	444	438	438	438	435	433	432	431	431	428	429
483	472	473	468	472	469	465	467	464	465	461	461	460
13	13	13	13	13	12	12	12	12	11	11	11	11
120	121	120	123	127	126	127	121	125	128	130	132	134
460	464	467	458	455	454	458	455	458	456	466	446	456
444	458	461	468	465	442	454	452	446	442	450	451	439
452	458	457	461	458	445	450	448	445	441	444	445	439
691	693	690	690	685	687	684	685	687	685	682	686	682
440	426	434	438	430	413	424	426	420	423	416	428	425
550	547	549	544	542	543	547	548	547	545	535	554	537
460	457	454	453	450	448	446	444	444	439	439	439	438
498	501	508	497	497	496	494	493	492	497	497	494	490
545	541	539	634	543	541	542	537	532	529	534	533	531

430	435	440	445	450	455	460	465	470	475	480	485	490
514	512	511	510	515	511	507	506	506	511	508	509	511
398	395	396	395	397	395	396	396	394	395	392	395	393
501	493	505	474	505	501	486	508	468	492	496	473	482
346	323	322	337	317	334	344	344	325	340	341	314	322
258	250	241	263	250	263	255	244	251	247	256	247	246
272	267	283	288	288	286	287	290	278	275	271	283	283
517	521	516	518	513	516	513	510	510	510	510	502	512
431	427	427	427	426	426	424	426	423	420	420	420	419
460	462	459	461	455	460	462	456	458	460	457	454	458
11	10	10	10	10	9	9	9	9	9	8	8	8
134	135	138	138	138	137	135	137	140	137	138	137	138
460	460	460	467	455	458	459	456	453	449	457	458	457
454	453	448	440	413	452	437	436	443	437	442	421	433
446	445	442	437	423	442	434	434	436	433	435	425	431
679	684	680	678	682	676	671	675	680	678	673	672	671
425	419	423	416	422	422	412	409	406	408	414	408	402
538	536	534	535	530	528	525	525	530	529	534	533	534
439	437	437	434	433	433	431	433	429	429	428	429	429
492	492	488	488	488	488	489	495	489	483	484	480	482
543	529	534	538	537	538	535	537	537	533	533	536	529

495	**500**	**505**	**510**	**515**	**520**	**525**	**530**	**535**	**540**	**545**	**550**	**555**
512	510	515	502	502	502	501	513	502	502	505	500	500
390	393	392	389	390	388	387	388	388	388	385	387	387
496	509	485	508	491	497	495	499	504	499	471	481	479
334	340	321	334	336	326	329	329	342	330	334	336	335
242	235	235	237	229	242	235	237	233	241	236	239	231
284	286	284	273	267	274	275	279	279	278	261	272	276
504	502	503	499	501	500	504	499	494	495	494	494	492
416	419	414	416	416	415	413	415	414	415	414	414	413
444	451	453	453	453	457	454	453	452	451	454	453	450
8	7	7	7	7	7	6	6	6	6	5	5	5
135	137	136	134	135	136	136	135	135	138	137	139	141
443	449	447	448	447	456	447	453	461	456	457	454	447
424	439	425	427	431	408	416	434	427	426	418	407	406
425	433	425	426	428	415	420	428	425	424	420	414	413
673	675	668	670	667	665	667	665	668	670	663	669	664
418	416	408	406	409	398	403	406	415	400	405	393	395
529	530	523	525	523	521	521	530	522	520	522	520	518
427	427	426	425	424	423	424	422	422	422	423	420	420
478	481	480	478	480	477	478	478	477	480	477	479	483
530	511	532	531	523	526	518	510	514	514	518	509	518

560	565	570	575	580	585	590	595	600
496	499	498	495	498	497	495	500	495
388	384	387	385	386	387	382	387	383
486	473	489	472	492	476	468	494	486
329	331	330	332	328	326	322	329	326
233	230	226	230	229	241	228	219	233
257	263	268	270	252	242	241	260	264
489	490	492	487	490	491	486	486	485
411	408	413	395	396	402	406	410	406
451	448	450	434	450	446	432	445	444
5	4	4	4	4	4	3	3	3
139	141	140	144	142	144	144	144	140
445	447	457	442	451	457	452	455	458
412	399	406	397	399	396	395	398	395
415	408	412	406	408	407	404	407	405
664	668	667	664	665	664	654	660	655
410	403	393	390	402	402	398	393	404
515	516	510	514	517	516	512	511	514
419	417	417	416	417	417	412	415	414
478	478	474	477	475	483	475	477	476
515	512	508	513	512	510	510	511	516

Table C.51 The effect of free wheel access on skeletal muscle fatigability in the male MIN

Geno	Treatment	Max Force Following Submax Fatigue	Max Force Following Max Fatigue	Max Force Following 5 Minute Recovery
B6	Control	552.49	305.24	836.23
		762.10	585.24	1147.55
		624.54	430.60	868.33
		810.52	574.72	1273.52
		929.07	682.00	1259.63
		895.44	631.79	1167.07
		919.82	606.10	1393.51
		794.42	585.11	1411.95
		795.39	553.95	1152.90
		743.77	539.07	1178.19
B6	Wheel	730.15	520.84	1115.08
		689.67	498.47	1121.65
		911.76	630.17	1355.84
		1059.93	689.32	1572.38
		1006.09	626.08	1409.83
		1049.59	676.24	1470.08
		649.25	432.59	1134.33
		973.17	636.39	1333.95
		923.43	469.77	1119.74

Geno	Treatment	Max Force Following Submax Fatigue	Max Force Following Max Fatigue	Max Force Following 5 Minute Recovery
Min	Control	861.16	495.33	1153.65
		576.28	382.86	923.54
		703.31	486.47	1011.98
		576.14	325.64	721.79
		415.12	233.32	643.82
		404.65	264.37	559.15
		939.92	484.73	1389.07
		596.73	406.21	1058.49
		684.21	444.31	1071.63
		16.40	2.90	16.67
Min	Wheel	147.08	140.42	582.52
		643.73	458.17	1050.29
		573.75	395.02	871.31
		588.66	404.63	954.02
		967.72	654.52	1249.10
		620.79	403.62	871.03
		757.87	513.70	1006.68
		603.57	414.25	1036.73
		792.78	476.33	990.90
		638.20	515.69	1158.58

Table C.52 The effect of wheel access on skeletal muscle mitochondrial content in isolated skeletal muscle mitochondria in the male MIN.

					Mitochondrial Complex				
Treatment	**Geno**	**State 3**	**State 4**	**RCR**	**I**	**II**	**III**	**IV**	**V**
Control	B6	7.14	2.00	3.57	0.86	0.80	0.87	0.74	1.03
		10.13	1.81	5.59	0.93	0.67	0.84	0.70	0.79
		9.12	2.26	4.04	1.41	1.94	1.22	1.49	1.15
		9.29	2.06	4.51	1.27	1.43	1.14	1.05	1.05
		10.57	2.03	5.22	0.83	0.63	0.98	1.20	0.97
		6.75	1.16	5.82	0.69	0.54	0.95	0.83	1.01
Wheel	B6	8.22	1.52	5.41	1.21	2.09	1.49	1.27	1.20
		9.48	2.09	4.54	1.26	1.85	1.45	1.31	1.26
		8.23	1.62	5.07	1.39	1.94	1.37	1.20	1.20
		10.16	1.95	5.22	1.32	2.12	1.38	1.24	1.21
		9.68	2.01	4.82	1.37	2.39	1.53	1.34	1.34
		7.12	1.78	4.00	1.37	1.68	1.31	1.09	1.29
Control	Min	9.00	1.47	6.14	0.95	0.55	0.81	0.69	1.02
		7.54	1.16	6.52	0.57	0.30	0.64	0.51	0.92
		7.71	1.75	4.40	0.89	0.66	0.86	0.60	1.05
		8.54	1.32	6.49	1.33	0.95	1.05	0.83	1.16
		5.38	2.22	2.43	1.17	0.54	0.76	0.54	1.05
		9.47	2.18	4.35	1.32	0.80	0.92	0.68	1.21
Wheel	Min	8.25	2.23	3.70	1.33	0.74	0.94	0.62	1.25
		9.84	1.91	5.15	1.41	1.01	1.06	0.66	1.18
		8.52	1.29	6.61	1.39	1.25	0.98	0.68	1.10
		10.97	2.79	3.93	1.32	1.19	0.96	0.63	1.10
		7.10	1.98	3.59	1.37	1.56	1.02	0.70	1.15
		10.47	2.02	5.18	1.27	1.37	0.94	0.71	1.22